



<https://theses.gla.ac.uk/>

Theses Digitisation:

<https://www.gla.ac.uk/myglasgow/research/enlighten/theses/digitisation/>

This is a digitised version of the original print thesis.

Copyright and moral rights for this work are retained by the author

A copy can be downloaded for personal non-commercial research or study,  
without prior permission or charge

This work cannot be reproduced or quoted extensively from without first  
obtaining permission in writing from the author

The content must not be changed in any way or sold commercially in any  
format or medium without the formal permission of the author

When referring to this work, full bibliographic details including the author,  
title, awarding institution and date of the thesis must be given

Enlighten: Theses

<https://theses.gla.ac.uk/>  
[research-enlighten@glasgow.ac.uk](mailto:research-enlighten@glasgow.ac.uk)

OBSERVATIONS OF  
LINE PROFILE VARIATIONS  
IN EARLY-TYPE STARS

Thesis  
submitted to the  
University of Glasgow  
for the degree of  
Ph.D.  
by  
T. H. ALAN WYLLIE

Department of Astronomy,  
University of Glasgow.

March 1976.

ProQuest Number: 10984470

All rights reserved

INFORMATION TO ALL USERS

The quality of this reproduction is dependent upon the quality of the copy submitted.

In the unlikely event that the author did not send a complete manuscript and there are missing pages, these will be noted. Also, if material had to be removed, a note will indicate the deletion.



ProQuest 10984470

Published by ProQuest LLC (2018). Copyright of the Dissertation is held by the Author.

All rights reserved.

This work is protected against unauthorized copying under Title 17, United States Code  
Microform Edition © ProQuest LLC.

ProQuest LLC.  
789 East Eisenhower Parkway  
P.O. Box 1346  
Ann Arbor, MI 48106 – 1346

## C O N T E N T S

Summary	i
Preface	v
1. <u>Introduction</u>	
1.1 Rapid Balmer Line Variability of the Be and Shell Stars	1
1.2 Rapid Balmer Line Variability of the Ap Stars	13
1.3 Other Stars Reported as Showing Rapid Line Profile Variations	23
1.4 Summary	29
2. <u>Properties of Narrow Band Interference Filters Relating to Tilt-Scanning</u>	
2.1 Introduction	31
2.2 Throughput of the Optical System	32
2.3 Filter Performance in Parallel Light	40
2.4 Wavelength Calibration and Filter Profiles	42
2.5 Variations of Filter Passbands with Tilt	47
2.6 Purity of Recorded Line Profiles	65
3. <u>Instrumentation and Data Handling</u>	
3.1 Introduction	69
3.2 The Photometer Head	70
3.3 Electronics	76
3.4 Data Reduction	84
4. <u>Photometric Accuracy with the Interference Filter Scanner</u>	
4.1 Introduction	89
4.2 Pulse Counting Photometry	90
4.3 Noise Introduced by the Atmosphere	96

4.4	Instrumental Errors	104
4.4.1	Errors due to Seeing Conditions	106
4.4.2	Errors due to Poor Telescope Guidance	112
4.5	$\beta$ -Index Photometry	120
5.	<u>Astronomical Observations</u>	
5.1	Introduction	124
5.2	Observations of Be and Shell Stars	129
5.3	Observations of $\epsilon$ UMa and $\gamma^2$ Vel	157
5.4	Conclusions	166
	Appendix I Control Electronics - Logic Diagrams	171
	Appendix II Data Format - Fortran Programme	181
	References	189

S U M M A R Y

During the past few years the literature has contained several reports concerning rapid line profile variations of some Be, Ap, Wolf-Rayet and other early-type stars. In some cases the time-scales of the variations have been reported to be as short as minutes or even seconds and clearly, if such variations are intrinsic to the stars, the processes giving rise to them must be accounted for by any future theories regarding the stellar structures and atmospheres.

However, some of the earlier observations are open to criticism and the reported variations may, in some cases, be the result of various instrumental errors which have not been fully appreciated. The work reported in this thesis was undertaken in order to investigate further the variations reported for the  $H\beta$  line in some of these stars.

A considerable amount of the work has been concerned with developing a novel stellar line profile scanner. By tilting a narrow band ( $\sim 2 \text{ \AA}$  half-width) interference filter in a collimated beam, a moderate resolution wavelength-scanning monochromator is achieved. The tilt-scanning technique has been explored in some depth and it is believed that this work is the first intensive application of the technique to the measurement of stellar line profiles at this wavelength resolution.

The indications are that the scanning range of one filter may be of the order of  $200 \text{ \AA}$ . Although there is a degree of distortion of the recorded profiles caused by the filter's transmittance decreasing and its pass-band broadening with tilt, the application for this study was concerned only with detecting line profile variations rather than making absolute measurements. However, over the smaller wavelength range normally scanned ( $\sim 30 \text{ \AA}$ ), the distortions of the recorded line profiles are sufficiently small as to be neglected.

More important, however, are the changes of the filter passband, and hence of the recorded profiles, brought about by variations in the angular size and movement of the stellar seeing disc in the telescope's focal plane due to unsteady seeing conditions and telescope tracking errors. Both of these topics have been considered as sources of photometric noise and it is felt that some of the variations of the Be stars reported previously by others may be the result of similar effects, especially since the extent of the noise becomes greater as the spectral gradients increase.

A special purpose double-beam photometer has been designed and built. One beam passes through a narrow band scanning filter while the other beam passes through a broader band ( $\sim 50 \text{ \AA}$ ) fixed interference filter whose passband is centred on the continuum adjacent to the scanned line. This second beam acts as a reference and after subtracting sky and dark contributions, the ratio of the signal in the two beams is largely free of atmospheric noise. The scanning filter is moved automatically along a series of discrete wavelength points by a stepping motor and both the step-size and the number of spectral points can be set on the electronic control. Pulse counting photometry is employed; the signals in both beams are recorded simultaneously and, after preset integration times, are punched on paper tape together with a record of the filter position and the Universal Time. Wavelength/tilt calibration is performed by piping light from laboratory lamps into the photometer by a fibre optic tube.

Observationally, the main emphasis of the work has been on measurements of the  $H\beta$  line in Be stars, several of which have been found to show night-to-night profile variations. Although variations of this type have been reported previously for some of the stars observed (e.g.  $\gamma$  Cas,  $\zeta$  Tau), it is believed that there are no previous reports of night-to-night variations for several of the others ( $\alpha$  Ara,  $\delta$  Cen,  $\mu$  Cen,  $\zeta^1$  Sco). No evidence of very rapid variability was found.

Other observations were made of the Ap star  $\epsilon$  UMa but these showed no signs of any of the variations reported earlier. The Wolf-Rayet star and spectroscopic binary  $\gamma^2$  Vel was also observed and in addition to the known variations of the H $\beta$  line with phase, night-to-night variations were also indicated.

The main advantages of the tilting-filter scanner over other line scanners with comparable resolution are its simplicity of design and its small physical size which, together with a high overall transmittance of the optical components, allows it to be used with small telescopes. Although the spectral purity of the recorded profiles is not as good as can be achieved with more sophisticated scanners, the technique clearly has a useful application for the detection of line profile variations.



P R E F A C E

The aims of the work presented in this thesis were: a) to explore the technique of tilt-scanning narrow band interference filters to obtain moderate wavelength resolution stellar line profiles and b) to apply the technique to observations of line profile variations of the H $\beta$  line ( $\lambda$  4861 Å) in some early-type stars (Be, Ap and Wolf-Rayet stars). Both of these aims have been fulfilled.

A special line profile scanner employing the tilting-filter technique has been built. The photometer head is of my own design and was constructed in the Observatory's workshop; the electronic data acquisition and control system is again of my own design and was assembled by myself.

Some previous reports of rapid line profile variations in Be, Ap, Wolf-Rayet and other stars are discussed in Chapter 1 where a very critical examination highlights several weaknesses in the observations and in the analysis and presentation of the data. It is suggested that some of the rapid variations reported in these earlier studies are possibly not intrinsic to the stars but might be attributed to observational errors due to instrumental and atmospheric effects and to over-optimistic accuracy levels which have not been properly related to the basic photon shot noise.

Chapter 2 discusses the technique of tilt-scanning with narrow band interference filters and describes how the filter passbands are affected by tilting of the filters and by illumination with non-collimated light which may be polarized. The quality of the recorded profiles is assessed by comparison with scans simulated from high resolution spectrum atlases.

A description of the optical and mechanical components of the scanner and the electronic control and data recording system is presented in Chapter 3.

Chapter 4 discusses observational errors due to photon noise, and atmospheric and instrumental effects. In particular, the effects of broadening and wavelength shifts of the filter passbands by variations of the size of the seeing disc and its movement are discussed. Some of the conclusions regarding these instrumental effects are applicable in considering the accuracy of  $\beta$ -index photometry.

The scanner has been used at Glasgow University Observatory, at the Royal Greenwich Observatory (Herstmonceux) and at the South African Astronomical Observatory (Sutherland, R.S.A.) where telescope time was allocated by the Large Telescope Users Panel. Some astronomical observations are presented and discussed in Chapter 5.

The original work of the thesis is contained in Chapters 2, 3, 4 and 5.

The scanner and its electronic control were built and developed in the Department of Astronomy at Glasgow University Observatory and it is a pleasure to thank Professor P. A. Sweet for the facilities and help provided in his department.

The research topic was suggested by Dr. David Clarke and I am extremely grateful to him for his advice and encouragement and for the many stimulating discussions which we have had together.

Further thanks are also due to Dr. Clarke and his family for their assistance and co-operation in making many of the observations, especially those in South Africa; to Mr. W. Edgar for assembling the photometer head, with the help of only our conversations and of his own technical drawings; to the Director of the Royal Greenwich Observatory for the allocation of observing time on the Yapp telescope and to the Director and staff of the South African Astronomical Observatory for the facilities and assistance provided during the visit of Dr. Clarke and myself to Cape Town and Sutherland.

Finally, I would like to thank Mrs. M. I. Morris for her very careful preparation of the typescript and diagrams.

This work was carried out while the author was in receipt of a Science Research Council Postgraduate Studentship.

T. H. Alan Wyllie.

1. INTRODUCTION

Variability of stellar line profiles is a phenomenon which has been observed for many years. Indeed, there are so many groups of stars which exhibit some degree of line profile variability that a comprehensive description is far beyond the scope of this introduction.

The particular aspect of line profile variability which stimulated this work was the appearance in the literature of reports of rapid profile variations of the Balmer lines in particular groups of stars, notably the Be and shell stars and the Ap stars.

A brief and critical account is given below of some of the variability which has been observed previously among these classes of stars. Attention is drawn to certain observational hazards which lead to the possibility of some of the reported variations being due to instrumental effects and not intrinsic to the stars.

1.1 Rapid Balmer Line Variability of the Be and Shell Stars.

The Be stars have been known for a considerable time to be variable on time-scales of months and years. The famous "Catalogue and Bibliography of Stars of Classes B and A Whose Spectra Have Bright Hydrogen Lines" and its Supplements, compiled by Merrill and Burwell (1933, 1943, 1949 and 1950) contains in the notes and bibliography many references concerning observations prior to 1950 of emission line stars which have shown spectral variations. In fact, Merrill and Burwell (1933) note that, "The spectra of many, possibly all, of the stars in Tables I and II are variable to a greater or lesser extent." Other more recent catalogues of Be stars (e.g. Wackerling 1970; Jaschek, Ferrer and Jaschek 1971) also give references in the bibliographies to observations of long-term variability among this class of star.

From surveys of stellar rotational velocities it has been found that those stars which have the fastest rotation belong to the spectral types O,

B, A and F. Of this group, the Be stars rotate most rapidly with values of  $v \sin i$  (the projected rotational velocity) often in excess of  $250 \text{ km s}^{-1}$ . Such high rotational velocities almost certainly result in centrifugally forced ejection of material from the equatorial regions of the stellar surface to form a circumstellar gaseous envelope. The hydrogen emission lines are formed within this envelope, probably by excitation and recombination mechanisms. The shape of the emission lines is strongly dependent on the angle of inclination to the line of sight of the axis of rotation of the envelope and also on the density and motion of the material within the envelope. This simple model of a Be star was first suggested by Struve (1931) although subsequent developments have led to much more complicated models.

Briefly, when a Be star is viewed equator-on, the main features of the optical spectrum are the strong hydrogen emission lines, decreasing in strength from  $H\alpha$  to higher members of the Balmer Series. The emission lines are superimposed on Doppler broadened photospheric absorption lines which, because of the high rotational velocity, are very broad and very shallow. The emission itself often consists of a violet and a red (Doppler displaced) component known as the V and R components. These two emission peaks are produced in the two lobes of the rotating envelope and are separated by a central absorption which is produced by those parts of the envelope which are seen against the stellar disc. If the central absorption is strong and is accompanied by other strong, metallic absorption lines, usually characteristic of a later spectral type, the star is classified as a shell star.

Since the circumstellar envelope is often thought to be in the form of an equatorial disc or toroid, when the Be stars are seen nearly pole-on the absorption and the single-peaked emission lines appear much narrower and the shell absorption features are no longer visible.

Spectrum variability of the Be stars generally affects the separation

of the V and R emission peaks, the relative intensity of the peaks (known as the V/R ratio), the intensity of the emission above the continuum level (known as the E/C ratio) and the depth and wavelength of the shell absorption core if this is present. Such variations are likely to be produced by changes in the amount of material within the envelope as well as expansion or contraction of the shell. For example, an expanding envelope will produce a blue shifted absorption core which will reduce the strength of the V emission peak and vice versa.

Many Be stars have been observed to show some, if not all, of the above variations of their emission line profiles. For example, McLaughlin (1957), Lacoarret (1965) and Hubert (1973) have each observed such changes in a number of Be stars over periods of years. In some cases, the strength of the emission lines shows a cyclic behaviour (Hubert 1973) with periods of less than twenty years.

Shell stars also show irregular variations in their line profiles. The famous period of activity of the shell star  $\gamma$  Cas during the 1930's is described by Beer (1956) and summaries of the longer term spectral variations of the shell stars 48 Lib and  $\zeta$  Tau are given by Underhill (1960a, 1966). Peters (1972) gives a detailed description of the day to day changes, chiefly at  $H\beta$ ,  $H\gamma$  and  $H\delta$ , observed in the spectrum of the shell variable HR2142 during the period 1969 to 1971. These are just a few of the many reports that can be found in the literature.

It is apparent that changes in the spectra of the Be stars are not uncommon. However, the structure of the extended atmospheres of the Be stars is not yet fully understood, and clearly the observed variations are indications of changes which are occurring within and around these stars. Further observations of the line profiles and their variations should contribute towards a better understanding of the nature of the extended shells and the processes associated with them.

Various models have been suggested for the Be stars and their atmospheres. Of particular interest is the method by which the circumstellar material is supported. For example, Limber and Marlborough (Limber 1965, 1967, 1969; Limber and Marlborough 1968) have suggested centrifugal force as a support mechanism while Hutchings (1970a) has proposed that radiation pressure could be supporting the envelope surrounding  $\gamma$  Cas. The latter mechanism has also been suggested by Hutchings (1970b) for the support of the extended atmospheres of the O-B supergiants.

It is common practice to develop the various models by changing those parameters of the models which determine the shape and structure of the emission lines so that computed line profiles derived from the models will closely fit the observed profiles (e.g. see Marlborough 1969, 1970; Hutchings 1968a, 1970a, 1971). The final models developed yield values for the density, temperature, distribution, etc. of the shell material in addition to the surface temperature, surface gravity, etc. of the star itself. A method for obtaining the size of the extended atmosphere from the shape of the line profiles has been developed by Kitchin (1970). The variations of the line profiles which are observed must obviously be accounted for in terms of variations of at least some of the model parameters which, in turn, must be compatible with known physical processes.

A further recently developed method of obtaining information regarding the structure of the Be stars is provided by spectropolarimetry. In order to explain the peculiar wavelength dependence of polarization for the shell star  $\zeta$  Tau, determined by broad band spectropolarimetry, Capps, Coyne and Dyck (1973) proposed a model for this star in which the photospheric radiation is polarized by electron scattering in an asymmetric circumstellar envelope. This model accounted for the decrease in the degree of polarization observed at the Paschen and Balmer limits since any emission produced within the circumstellar envelope (principally hydrogen line-emission)

should be less polarized because it undergoes less scattering than the photospheric radiation. The model also predicted that there should be a decrease in the degree of polarization (for the same reason) across any particular emission line.

By means of high resolution spectropolarimetry, Clarke and McLean (1974b) have detected a reduced polarization in the  $H\beta$  emission line of  $\gamma$  Cas. This depolarization effect has since been observed in the  $H\alpha$ ,  $H\beta$  and  $H\gamma$  emission lines in a number of other Be stars (see Clarke and McLean 1975; Coyne and McLean 1975; Hayes 1975; Hayes and Illing 1974; McLean and Clarke 1975; Poeckert 1975). The above polarization effects are almost certainly related to the circumstellar envelopes of the Be stars and it is to be expected that time variations in the structure of the envelopes will be accompanied by variations of the intrinsic polarization of these stars. Broad band measures of the continuum polarization have shown slow variability for a number of Be stars (Serkowski 1970) and more rapid changes in the continuum polarization in  $\zeta$  Tau have been suggested by Clarke and McLean (1975) and by Poeckert (1975). However, the only evidence of variability of the emission line depolarization is an unconfirmed report by Clarke and McLean (1974b).

Changes in the degree of polarization across the emission lines of the Be stars not only indicate that the observed polarization is intrinsic to these stars but also provide an alternative means of monitoring changes in the envelope structure in addition to yielding information on the levels within the envelope at which the emission and shell absorption are being produced. Although some of the polarimetric observations cited above have been obtained at moderate wavelength resolution ( $\sim 1.5 \text{ \AA}$ ), only a limited number of discrete points across the profile have been measured and it is desirable to increase the number of points, especially in the case of shell stars such as  $\zeta$  Tau and 48 Lib which show sharp and deep shell absorption cores in addition to the emission features.

If the depolarization effect is related to the strength of the (unpolarized) emission as proposed by Clarke and McLean (1974b) and Poeckert (1975), simultaneous polarimetric measurements and line profile measurements would confirm the expected correlation between their time variability. Such a study has not yet been carried out.

Most of the line profile measurements prior to the later part of the last decade were obtained, usually photographically, with low time resolution. More recent observations have, however, seen increasing application of photoelectric spectrum scanners. Many different varieties of spectrum scanner have been constructed (see Code and Liller 1962) most of which rely on diffraction gratings to achieve their wavelength dispersion. Scanning in wavelength is normally obtained either by moving an exit slit and detector (usually a photomultiplier tube) along the spectrum or by rotating the diffraction grating and having a fixed exit slit and detector. More recently, image Isocon tubes have been used in conjunction with grating spectrographs and have the effect of a multi-element storage device enabling many wavelength elements to be measured simultaneously. (See Walker, Auman, Buchholz, Goldberg and Isherwood 1971).

For the work presented in this thesis, it was decided to explore the technique of obtaining a particular stellar line profile ( $H\beta$ ) by tilt-scanning a narrow band interference filter. The method is simple and the overall transmittance of the optical system is high. In addition, because of the small physical size of the scanner in relation to the spectral resolution which can be achieved, the technique has potential for measurements with small telescopes; an important consideration if prolonged observing runs are required as in the case of searching for irregular line profile variability. Although the technique does not yield line profiles of high spectral purity it was felt that this is of little consequence if the aim is to detect intrinsic profile variations. The technique of tilt-scanning with

narrow band filters and some preliminary results have been published elsewhere (Clarke, McLean and Wyllie 1975).

As a result of their extremely good linearity of response and high quantum efficiency, photoelectric spectrum scanners have the potential of yielding a higher photometric accuracy and a much higher time resolution than photographic spectrographs. Observations made at high time resolution with these scanners have revealed rapid, hour to hour and perhaps minute to minute variations of the Be emission line profiles.

The reported variations occur in particular parts of the profiles and can only be monitored in detail with high time resolution and high spectral resolution. Unfortunately, as higher time and spectral resolution are achieved it is usually found (except perhaps with multi-channel devices) that the photometric accuracy of single profile scans is reduced because of the higher level of photon shot-noise. Because of the statistical uncertainties involved, single scans will reveal only large scale profile variations, however if time-averages of an increasing number of scans are formed, slower and smaller amplitude variations are more likely to be seen. Variations of the Be profiles have been reported on individual scans and also on time-averaged mean scans.

The earliest reference found concerning rapid Balmer line variability among the Be stars is a report by Hutchings (1967) of rapid profile changes of the H $\gamma$  line in the shell star  $\gamma$  Cas. Hutchings (1967) presents profiles of H $\gamma$  obtained over  $\sim 5 \text{ \AA}$  of spectrum at a resolution of  $\sim 0.3 \text{ \AA}$ ; the scans consisting of a series of measurements at wavelength intervals of  $0.25 \text{ \AA}$ .

A photometric accuracy of  $\sim 1$  per cent of the continuum level was achieved with a time resolution of  $\sim 1$  hour and the scans obtained show variations of H $\gamma$  from hour to hour and on longer time-scales. Further profile measurements at H $\beta$  and H $\alpha$  for this star, obtained with a different scanner, apparently show even more rapid variations on a time-scale of minutes (Hutchings 1968b, 1970a).

Similar rapid variations (from scan to scan) have also been reported for the H $\beta$  and H $\gamma$  lines in the Be stars  $\kappa$  Dra and HD142926 (Hutchings 1968b, 1971) and for the H $\alpha$  line in these two Be stars and in the shell star 48 Lib (Hutchings, Auman, Gower and Walker 1971a; Hutchings, Walker and Auman 1971b).

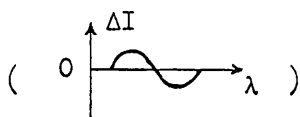
The H $\alpha$  observations (Hutchings et al 1971a, 1971b) were obtained with an Isocon television camera and seem to indicate variability on time-scales of minutes or even less. However, as a result of the experience gained during the work leading to this thesis, it is suspected that some of the rapid variability reported by Hutchings et al (1971a, 1971b) might be due to low photometric accuracy of individual scans. In addition to photon shot-noise, there may also be noise on the scans due to instrumental effects possibly related to seeing conditions and telescope guidance errors.

For example, H $\alpha$  profiles for HD142926 ( $m_v = 5.6$ ) were obtained with an Isocon camera (Hutchings et al 1971b). Although the integration time (on a single "scan") per spectral element was 40 seconds, the linear wavelength dispersion of the grating spectrometer and the resolution of the Isocon tube were such that the wavelength range covered by each spectral element was only  $\sim 0.2 \text{ \AA}$ . It would seem likely therefore that the integrated photon count in a single spectral element would be subject to a photon shot-noise of at least several per cent. Hutchings et al do not give details of either the photometric accuracy achieved for single profiles or of the theoretical accuracy based on photon-counting statistics. Furthermore, they do not present any observations of comparison stars.

However, the order of magnitude of the noise on individual profiles can be seen in the continuum on either side of the H $\alpha$  line. On the mean of a large number of profiles, the continuum is seen to be flat and smooth while considerable "structure" (produced by photon noise) is seen on the individual profiles. The fluctuations suggested by Hutchings to occur in the emission feature are no larger than this level of noise.

A similar explanation might also apply to the reported rapid variability of the shell star 48 Lib ( $m_v = 4.7$ ) (Hutchings et al 1971b). Again the noise level on the individual profiles is not commented on by Hutchings but is probably partly due to photon shot-noise perhaps combined with other effects. As with HD142926, the order of magnitude of the noise can be assessed by inspection of the continuum regions of the profiles and again the noise would seem to be large enough to be responsible for the variations reported in the emission line.

Hutchings et al (1971a, 1971b) also present data for HD142926,  $\kappa$  Dra and 48 Lib in the form of differences of individual profiles from the mean profiles. These differences often show systematic effects which take the form of a sinusoidal variation of the differences with wavelength



which are called "S-shapes" by Hutchings. As Hutchings remarks, the "S-shapes" are almost certainly due to wavelength shifts of individual profiles by up to  $2 \text{ \AA}$  from the mean. The problem is to determine if such wavelength shifts are intrinsic to the stars or if they are of instrumental origin.

Although Hutchings et al (1971a) claim that the shifts are too large to be produced by instrumental effects or guidance errors, it has been found that the interference filter scanner used in this work can be subject to wavelength shifts as the result of guidance errors. Similar effects are possible with most angular dispersive spectrometers and the effect is usually larger at higher dispersions. In addition, Griffin (1970) has drawn attention to the fact that image movement along a spectrograph slit, as well as across it, is a possible, although often overlooked, source of error due to wavelength shifts. Image movement along the slit is likely to be due to telescope guidance errors although fluctuations in the size of the seeing disc might also result in wavelength shifts or passband broadening due to this effect.

Of course, the design of any particular instrument will determine the extent of the wavelength shifts resulting from image movement or changes in its size. However, the effect must be considered as a possible alternative to rapid radial velocity variations within the circumstellar envelopes. Some of the observed profile variations would require rapid pulsation of the envelopes on time-scales of less than 1 minute and these are very difficult to explain in terms of known physical processes.

Further observations of rapid H $\beta$  profile variability among the Be stars have been reported by Bahng. The observations were made with a rapid spectrum scanner (Bahng 1971a) and consisted of a series of discrete measures at wavelength intervals of 10 Å with a spectral resolution of  $\sim 20$  Å (the resolution was dependent on the size of the seeing disc but was limited by the entrance aperture to a worst case of  $\sim 35$  Å).

Because of the low spectral resolution, the structure within the emission lines was not observed and the data is presented in the form of measures of the integrated H $\beta$  equivalent width. By making similar measures of the H $\beta$  equivalent width in a standard star, Bahng (1971a) determined the rms. (root-mean-square) deviation of the equivalent width of the standard star to be  $\sim 3$  per cent and adopted a figure of 6 per cent as a  $2\sigma$  statistical significance level for variability of the Be stars (i.e., those stars which showed an rms. deviation greater than 6 per cent in the H $\beta$  equivalent width were taken as showing real variations). However, the large scatter in the equivalent width measures of the Be stars  $\phi$  Per, HR985 and  $\pi$  Aqr can perhaps once again be explained by seeing and guidance effects producing changes in instrumental resolution and wavelength shifts. It is unlikely that these effects would have been apparent on examination of the scans, since the wavelength step-size was too large and the spectral resolution was not sufficiently high to show them, hence the effects would have appeared merely as intensity fluctuations at those discrete wavelength positions close to

the H $\beta$  line. The reason for the rms. deviation being greater for the Be stars than for the comparison star HR801 (B3V) could simply be because of the steeper gradients of the emission line profiles of the Be stars in which case a given shift in wavelength would have resulted in a larger change in the measured intensity.

Rapid variations of the H $\beta$  equivalent width for the shell star  $\zeta$  Tau are also reported by Bahng (1971b). Once again, the scans were not of sufficiently high spectral resolution to reveal the true shape of the emission feature but it is reported that within a 13 minute interval, the integrated H $\beta$  equivalent width changed from net absorption to net emission and then back to absorption once more. It is possible again, however, that these changes might be instrumentally produced. The H $\beta$  line profile of  $\zeta$  Tau measured with the interference filter scanner during the winter of 1974/75 showed a very asymmetrical shape with one strong, sharp emission peak (the R peak) and a deep shell absorption feature (see Chapter 5). Although the profile at the time of Bahng's observations (December 1970) was probably different, since long-term changes are known for this star, it is likely that the profile still contained sharp emission peaks and absorption cores. With an emission feature of this shape and with a 10  $\text{\AA}$  wavelength step-size it is vital to know precisely where the instrumental passband is centred and it is even more important to ensure that the positioning of the passband relative to the emission feature remains the same on successive scans. However, guidance errors might easily produce sufficient wavelength shifts to move the centre of the passband on one scan from an emission peak into an absorption core with a resulting variation in the equivalent width which would be obtained from that scan. Moreover, Bahng reports that with his scanner, a change in the size of the seeing disc from 3.8 arc seconds to 6.75 arc seconds (see Bahng 1971a) would cause the spectral bandpass to change from 20  $\text{\AA}$  to 35  $\text{\AA}$  since the slit width was usually greater than the seeing disc diameter. Obviously, if such changes occur rapidly within a

single scan, a considerable distortion of the measured profile is likely to occur. Once again the comparison stars have vastly different (absorption) line shapes and hence are not so sensitive to these effects. In addition, the figures given by Bahng (see above) show that the wavelength shifts that will result from image movement in the entrance aperture are likely to be as large as several Angströms and such shifts when not on a flat spectrum might produce large variations in signal from scan to scan. Again the effect on the recorded signal is very dependent on the shape of the line being scanned.

To summarise the reports concerning the Be and shell stars, it can be said that slow variations of the hydrogen emission lines, on time-scales of the order of one hour or longer, are almost certainly real. However, it is felt that considerable doubt is still associated with the reported rapid variations on time-scales of seconds to minutes. It would appear that sufficient consideration has not been given in the reports cited to the possible sources of noise and errors (e.g. photon, instrumental, atmospheric) and that the quality of the data has not been fully assessed. Observations of comparison stars are too few in number, and even when they are obtained, the conditions of observation for the reference stars and the stars of interest are very different. For example, it has frequently been implied in the preceding discussions that the instrumental response to and the photometric accuracy attainable for the broad absorption lines of normal B and A type stars will be quite different from the response and accuracy for the very sharp emission lines found in most Be stars, because of the marked differences in the gradients of the spectral features. In any case, both the instrumental response and the photometric accuracy attainable are liable to be dependent on the sky conditions at the time of the observations.

For the above reasons, and independent of whether the stars have intrinsic short-term fluctuations or not, the photometric accuracy of line

profiles of Be stars is expected to be less than for standard, normal B type stars (all other factors being equal).

In the cited reports of rapid Balmer line variability, the theoretical photometric accuracies which might have been expected are not discussed for the programme stars or for the comparison stars. It is difficult, therefore, to assess the quality of the measurements and to determine the extent of any sources of noise other than photon noise.

Clearly further observations of these stars are required at high time and spectral resolution. However, it is important to know the expected and the observed accuracies of the observations and to be aware of the differences likely to exist between the accuracy attainable for the Be stars and for the comparison stars, whether or not they are measured under the same seeing conditions.

## 1.2 Rapid Balmer Line Variability of the Ap Stars

The peculiar A or Ap stars are a group of stars whose spectra show either unusually great strength or weakness of the lines of certain elements (e.g. strong lines of the Eu - Cr - Sr group). The Ap stars share their peculiar line intensities with the metallic-line A stars or Am stars.

In addition, many of the Ap and Am stars whose spectral lines are sharp enough, have shown evidence of Zeeman splitting of the lines, indicating the presence of magnetic fields. Many of these stars which show spectral peculiarities or strong magnetic fields also show periodic or nearly periodic changes in their line intensities, light and colour and in their magnetic field. Ledoux and Renson (1966) give a table of magnetic stars listing various parameters (e.g. spectrum, light, line strength, etc.) which are variable or periodic, the periods being in the range of less than one day to several hundred days and with the amplitude of the light variability usually less than 0.1 magnitudes.

The periodic variations are probably related to the rotation periods of the stars and might be due to non-uniform chemical abundances or a "spottiness" of the stellar surfaces (see Preston 1971).

Continuum light variations with amplitudes of  $\sim 0.01$  magnitudes and on time-scales as short as 30 minutes to 2 hours have been reported by Rakos (1963), Maitzen and Moffat (1972), Stępień and Romaniuk (1973) and Percy (1973). These short period variations may be due to pulsation in the Ap stars (Breger 1969) in which case they may also be apparent as radial velocity and line profile variations.

Even more rapid variations in the profiles and equivalent widths of the hydrogen and calcium lines on time-scales of minutes have been reported for a number of Ap stars. Some of these reports will now be commented on briefly. The observations have, in general, been performed by the techniques of spectrum scanning and, for the hydrogen lines, by  $\beta$ -index photometry (also  $\gamma$  and  $\delta$ ) in the system of Crawford (1958, 1960); some photographic studies are also described.

Wood (1964) reports observations of  $\epsilon$  Ursae Majoris ( $\epsilon$  UMa) made at Lowell Observatory with a low resolution spectrum scanner ( $20 \text{ \AA}$  exit slit). The equivalent width of  $H\beta$  is reported to have changed by 10 per cent over a 4 minute interval, the variations in the line profile seemingly being restricted to the line wings about 15 to  $20 \text{ \AA}$  from the line centre.

When individual line profile scans are to be compared in order to detect variations from scan to scan, it is very important that any systematic effects due to changes of the signal level, either from scan to scan or across a single scan, should be completely removed. Such changes in signal level might be, for example, due to transparency changes, differential atmospheric extinction, photomultiplier gain changes, etc. Removal of the effects of these changes is normally performed by various methods of rectification and normalisation of the line profiles and after such corrections

have been made, it is to be expected (because of the procedures normally adopted) that the continuum levels on the corrected profiles should be in good agreement with each other.

However, the scans presented by Wood for the H $\beta$  profile in  $\epsilon$  UMa reveal that the levels of the continuum,  $\sim 150 \text{ \AA}$  from the line centre and therefore well out of the wings of the broad H $\beta$  line, do not coincide when successive scans are superimposed. This would imply that the method adopted by Wood for normalising the scans has been inadequate and has not removed all of the effects mentioned above. If re-normalisation of the scans were to be performed so as to match the levels of the continuum, it would be found that the variations would then occur in the H $\beta$  line core. In addition, the profile variations that would then be apparent would be in the form of filling-in of the line core accompanied by an increase of the line half-width. Variability such as this could be caused by broadening of the instrumental transmission profile as the result of a change in the size of the seeing disc in the entrance aperture of the spectrograph.

The quality of the line profile measurements is further in doubt, since it has been deduced from the dates and times of the observations (given by Wood) that the altitude of  $\epsilon$  UMa was less than  $10^\circ$  when the reported H $\beta$  variations occurred. Wood bases the accuracy of his measurements on a comparison with an H $\beta$  standard star,  $\alpha$  Lacertae, which was near the zenith when observed. It is very unlikely that the seeing conditions would have been the same for these two stars and it is also unlikely that the photometric accuracies of the line profiles would be comparable to one another. Although a nearby comparison star was also observed and was reported as showing no line variations, Wood does not say how frequently the comparison star was observed and he does not state the accuracy achieved for the line profiles of this star.

Furthermore, the very low altitude of  $\epsilon$  UMa during these observations

in conjunction with the spectral range of the scans ( $\sim 400 \text{ \AA}$ ) means that the effects of differential atmospheric extinction cannot be ignored. The differential extinction between the extreme ends of the scans can be calculated to have been  $\sim 0.4$  magnitudes and could be ignored if it remained constant with time. However, because of the rapid rate of change of sec Z and because of the wavelength dependence of the extinction coefficient, calculations show that not only was the amount of extinction increasing at the rate of 0.013 magnitude/minute but that the differential extinction between opposite ends of the scans was increasing at the rate of 0.003 magnitude/minute (i.e. an intensity variation of  $\sim 0.3$  per cent/minute) at the time of the observations. (The figures are based on the position of  $\epsilon$  UMa at the time of observation supplied by Wood and on a plot of the variation of the extinction coefficient with wavelength given by Hardie (1962)). Since the scanning rate was  $\sim 200 \text{ \AA}/\text{minute}$ , these effects are certainly not negligible.

However, the effects of extinction are apparently ignored by Wood and, in addition, no mention is made by him of the effects of sky transparency fluctuations at such low altitudes, or of attempts to compensate for them by double-beam techniques. It must be concluded therefore that these will be additional sources of noise which have not been evaluated and removed from the data.

Other observations of Balmer line variability in  $\epsilon$  UMa, detected by means of interference filter  $H\beta$  photometry, have also been reported by Wood (1965, 1968) but seem to be inconclusive. Measurements are first made in a natural filter system in which  $\beta'$ -indices are determined and these are converted into the standard  $\beta$ -index system by means of transformation coefficients determined from observations of  $H\beta$  standard stars. Wood defines the "scatter" of the observations as the average deviation (not the rms. deviation) of individual measures from the mean and states that the "scatter" of

the comparison star measurements is usually less than 0.007 magnitude and sometimes as small as 0.002 magnitude in  $\beta'$ .

Wood claims that his observations of  $\epsilon$  UMa show rapid and irregular real variations of the  $\beta'$ -index. However, values of  $\beta'$  for  $\epsilon$  UMa on December 25, 1963, may be obtained from a plot of  $\beta'$  against time presented by Wood (1965). It is found that these values have a "scatter" of 0.004 magnitude, identical to the scatter quoted by Wood for the comparison star. (The rms. deviation in  $\beta'$  is found to be  $\pm 0.006$  magnitude ( $\sim 0.6$  per cent photometry)). The equivalent "scatter" in the equivalent width determined from the  $\beta$ -index is in fact  $0.18 \text{ \AA}$  or 1.36 per cent. The variations of the  $\beta$ -index for  $\epsilon$  UMa reported for this occasion would seem, therefore, not to be significant in relation to the accuracy of the comparison star measurements.

In addition, the spectrum scanner observations of July 1963 (see Wood 1964) gave the equivalent width of the  $H\beta$  line as  $\sim 18 \text{ \AA}$  while the  $\beta$ -index measurements of December 1963 (see Wood 1968) showed the equivalent width to be  $\sim 13 \text{ \AA}$ . The implication of these results is that either the scanner or the interference filter observations (or both) had systematic errors associated with them, or alternatively the intrinsic equivalent width of the  $H\beta$  line in  $\epsilon$  UMa decreased by 27 per cent over a five month interval. Such a variation in the strength of the  $H\beta$  line in this star could be occurring on this longer time-scale, however the very rapid variations reported by Wood might simply be over-resolved noise on the observations.

Rapid spectrum scanner observations of  $\epsilon$  UMa have been made more recently by Breger (1974). The equivalent width of the  $H\alpha$  line was measured from the line profiles which were obtained at 45 second intervals over a period of  $2\frac{1}{2}$  hours and it was found that the observed and the photon predicted standard deviations of a single observation were both 0.2 per cent. Breger concluded that his observations showed no significant rapid variations of

the equivalent width of  $H\alpha$  over this period and he further proposed that many of the earlier rapid variability observations by others could be challenged on the grounds that insufficient account had been taken of the observational errors. Moreover, the statements which are made concerning the accuracy of the  $\beta$ -index measurements of  $\epsilon$  UMa, and other stars still to be described, are based on less frequent observations of comparison stars and no attempt has been made by anyone other than Breger to compare the observed errors with the errors that might be expected from photon statistics. The validity of the comparison star observations is also in doubt since, as with the Be stars, it is virtually impossible to find a comparison star which shows exactly the same spectral features as the Ap stars and which does not belong to that spectral type itself. The broad, featureless Balmer lines found in the normal A type stars contrast sharply with the very many blended metallic lines superimposed on the wings of the Balmer lines in the Ap stars. The effect on the B-index produced by seeing fluctuations and guidance drifts could perhaps be more pronounced when there is contamination of the  $H\beta$  line by the metallic lines found in the Ap spectra. If changes in the  $\beta$ -indices are due to seeing conditions or guidance errors, it is because the narrow band and the broad band filters respond differently to these effects. However, the time-scales of instrumental and atmospheric effects would be much more able to account for the observed variability than any physical processes occurring in the stars. For instance, Wood (1967) reported a 30 per cent change in the equivalent width of  $H\beta$  for the magnetic star HD215441 (Babcock's star) in a time interval of 90 seconds!

The Ap star 73 Draconis has also been reported to show rapid variations of the Balmer and calcium lines in addition to a 20-day periodic variation in the strength of many metallic lines. The long period variations were first reported by Morgan (1933) and confirmed later by Durham (1943) while, more recently, Berg (1967) has shown the period to be constant

at 20.2755 days. Babcock (1958) found that 73 Draconis had an irregularly varying magnetic field.

Rapid variations (over several minutes) of the hydrogen lines were observed by Wood (1964, 1965, 1968) by means of interference filter photoelectric photometry. The  $\beta$ -index in the Crawford system was determined from measurements in Wood's  $\beta'$  system together with similar  $\gamma$ - and  $\delta$ -indices for the H $\gamma$  and H $\delta$  lines. All three indices were found to show small amplitude 10-minute fluctuations which were sometimes in phase with each other and sometimes in anti-phase. The fluctuations, suspected of being confined mainly to the line wings as for  $\epsilon$  UMa, were not always observed and it was proposed that their appearance was an irregular variation in the line strength superimposed on the longer 20-day period.

The rapid variations of the H $\beta$ , H $\gamma$  and H $\delta$  lines were confirmed, photographically, by Bonsack and Markowitz (1967) who also reported that the activity was apparently confined to the line wings and was not found in the core. More will be said of Bonsack and Markowitz's observations later. Similar rapid variations (on a time-scale of about 1 hour) in the strength of the calcium K line have been detected photographically for this star by Honeycutt (1966).

Breger (1974) has also observed 73 Draconis with the result that a series of rapid profile scans of the H $\beta$ , H $\gamma$  and Ca K lines were found to show no statistically significant short period variations of the equivalent widths of these lines. Breger showed that the error in a single observation of the equivalent width due to photon statistics is not negligible but is predicted for his observations of this star to be of the order of 1 per cent for the hydrogen lines and 5 per cent for the calcium K line depending on the photon count, the strength of the line, etc. The observed errors in the equivalent widths were  $\sim 2$  per cent for the H $\beta$  and H $\gamma$  lines and  $\sim 8$  per cent for the calcium line. The observed errors are larger than the photon

predicted errors by a factor of about 2 and this is explained by Breger as being due to wavelength shifts produced by unavoidable guiding errors allowing image movement within the entrance slit of the scanner.

Breger (1974) states further that his observations of 73 Dra were made at the same phase of the 20-day period as Wood's observations (Wood 1964, 1968) and that the lack of variability cannot be explained by phase differences. It is of course possible that the rapid variability is a transient phenomenon and that the stars  $\epsilon$  UMa and 73 Dra were both inactive when observed by Breger. It is worth noting also that Breger states that the constancy of 2 per cent (i.e. the standard deviation of a single measurement) in the equivalent widths of  $H\beta$  and  $H\gamma$  for 73 Dra on three different nights indicated that no intrinsic rapid variations occurred on these occasions while, if the variations of the  $\beta$ -indices reported by Wood (1964, 1965) for 73 Dra are expressed in terms of equivalent widths according to the conversion coefficients given by him, it is found that for 73 Dra on August 19, 1963 (one of the nights showing the apparent 10-minute fluctuations of the  $\beta$ -index for 73 Dra), the standard deviation of a single observation was 0.01 magnitude in  $\beta'$  and only  $\sim 4$  per cent (i.e.  $0.48 \text{ \AA}$ ) in the equivalent width of  $H\beta$ . The standard error of the mean of the equivalent width was 1 per cent ( $0.13 \text{ \AA}$ ).

Wood does not state what errors were to be expected on the basis of the (unquoted) integration times, the brightness of the star ( $m_v = 5.2$ ) and the size of the collecting aperture (16 inches), etc. However, the error of 4 per cent in equivalent width does not seem to be excessively large and, like Breger, it is felt that some of the reported variability might simply be noise mistaken for intrinsic fluctuations. If the variations of the various photometric indices are found to be larger than the theoretical errors expected, it is suggested here that this could be partly due to changes in the size of the stellar seeing disc together with guidance

errors having an effect on the filter passbands (see Chapter 4). Similar arguments can be applied to Wood's observations of rapid variability in HR9080.

The comparison star observations are not reliable since, in a plot of the time variations of the  $\beta'$ ,  $\gamma'$  and  $\delta'$ -indices, it appears that the comparison star is the more stable (see Wood 1968). However, this is largely due to there being fewer measurements made of the comparison star and so the variations seem less rapid. The range of values in the comparison star measures is in fact almost as large as that in HR9080.

Returning to the observations by Bonsack and Markowitz (1967), the report of rapid Balmer line variability in 73 Dra is based on a series of plates which have a dispersion of  $42 \text{ \AA mm}^{-1}$  and which were exposed over a 3 hour interval. Bonsack and Markowitz made the mistake, however, of comparing the absolute variations of the equivalent widths of a number of lines when, in fact, they should have considered the fractional variations of the equivalent widths. When the data is examined in terms of fractional changes, it is found that all of the lines measured are showing "rapid variations" of their equivalent widths over the 3 hour interval! In fact, the standard deviations of single measurements of the equivalent widths are in the range 4.5 — 18.7 per cent with a mean of 9.8 per cent; the values for the Balmer lines are 8.4, 7.6 and 6.1 per cent for  $H\beta$ ,  $H\gamma$  and  $H\delta$  respectively. It is most probable that these variations are of the same order of magnitude as the limit of the accuracy of equivalent width measurements that can be achieved by photographic spectrophotometry which, according to Wright (1962), is likely to have errors in a single observation of equivalent width of 10 - 20 per cent. Gulliver and Winzer (1973), in a report of spectrum and light variations of the A0p star HD51418 measured photographically with a dispersion of  $12 \text{ \AA mm}^{-1}$ , state that the spectrum in that star is very crowded with lines and that there is considerable blending of the lines with

the result that the errors in the equivalent widths of individual lines are about 20 per cent. This might therefore be a reasonable figure to adopt for Bonsack and Markowitz's observations of the A2p star 73 Dra in which case the reported variations are not statistically significant.

Gulliver and Winzer (1973) also measured photoelectric  $\beta$ -indices for HD51418 and found variations of  $\beta$  with phase (HD51418 is a spectrum variable Ap star with a period of  $\sim 5.4$  days) and also, on one occasion, on a shorter time scale of minutes. It is suggested again that the rapid variations in  $\beta$  (in the form of a step) could be caused by changing seeing conditions (perhaps due to undetected thin cirrus cloud) affecting the illumination of the interference filters.

Further strengthening the belief that many of the reported variations are instrumentally produced is the fact that observations by Wood (1968) of six magnetic and spectrum variable stars and six comparison stars revealed that five of the suspected variables and five of the comparison stars showed Balmer line variations. In view of the high percentage of normal (i.e. comparison) stars which showed variability, it seems possible that the observed fluctuations in the  $\beta$ -indices are not intrinsic to these stars but are probably due to some source of instrumental noise. In contrast to Wood's observations, Williams, Frantz and Breger (1974) have obtained rapid photoelectric scans of the  $H\beta$  line in a further three Ap stars, one Am star and one  $\delta$  Del star. None of these stars was found to show any rapid variability of the  $H\beta$  equivalent width which was statistically significant in relation to the level of the predicted photon noise.

The question of rapid Balmer line variability in the Ap stars seems to be highly debatable and further observations are essential. Whatever technique is employed to measure the shapes or equivalent widths of the lines, it is important to know the extent of any fluctuations in relation to the statistical accuracy of the photometry. It is equally important to know

the photometric accuracy that is expected from theoretical considerations, since it is only by comparison of the expected and the observed accuracies with the amplitude of the variations that it is possible to determine if the variations are significant or merely noise. Determination of the expected photometric accuracy must always, in the first instance, consider the level of photon noise. In addition, although often neglected, consideration should also be given to the way in which the instrumental response may be affected by guidance errors, changing seeing conditions and the type of spectral detail being measured. Comparison of programme stars and reference stars can therefore be made more meaningful if the expected accuracies are evaluated in this way.

In the reports cited above, the possibility of a variable instrumental response has never been considered, and even the photon noise has only been evaluated in one or two cases.

### 1.3 Other Stars Reported as Showing Rapid Line Profile Variations

In addition to the types of star already discussed, many early-type supergiants are also known to exhibit line profile variations. Irregular radial velocity changes have been observed for these stars and are thought to be due to mass motions of the atmosphere (e.g. see Underhill 1960b). Rosendhal (1973) found that out of twenty early-type supergiants studied, thirteen showed large long-term changes in the strength or structure of the  $H\alpha$  line. Rapid variations of the Balmer line profiles among several early-type supergiants on time-scales similar to those of the variations of the Be stars have been reported by Hutchings (1967, 1968b, 1973) and, like the Be stars, these variations are interpreted in terms of changes within the extended atmospheres of these stars.

The accuracy of the long-term observations is sufficiently high and the variations are sufficiently large as to put a high confidence in their reality. However, the short-term changes are again questionable since the line

profiles (often in emission at  $H\alpha$  and sometimes at  $H\beta$ ) have steep gradients (even for the absorption lines), as in the case of the Be stars, and will be subject to the same sources of instrumental errors as have already been discussed for those stars.

Observations by Wood and Hollis (1971) with a rapid profile scanner have been made for the (normal) A1 IV star Beta Carinae. They have reported that the core of the  $H\beta$  line in this star occasionally shows variations with a quasi-period of  $\sim 35$  minutes, however they stress that the amplitude of the variation is small compared to the statistical fluctuations determined by observations of a comparison star. Again this report is somewhat lacking in that the statistical uncertainties based on photon counting are not presented for comparison with the observations. However, based on the photon count presented, the standard deviation of the count in one channel should have been of the order of 1.4 - 2 per cent. A core ratio was formed by taking  $7/6$  times the ratio of the sum of six continuum channels to the sum of seven core channels. It was reported by Wood and Hollis that this ratio showed a sinusoidal variation with an amplitude of  $\sim 2$  per cent. However, the data presented shows that the mean square residuals of the core ratios from sine curves were only marginally less than the mean square residuals from straight lines. They also state that the noise on the comparison star measurements was only about half of that on the  $\beta$  Car measurements. Night to night variations in the  $\beta$ -index of  $\beta$  Car are also reported by Wood and Hollis and support a similar earlier observation of  $H\beta$  variability for this star by Wood.

Rapid variations in the emission lines of Wolf-Rayet stars and Of stars have also been found. Brucato (1971) reported variations on a time-scale of 10 minutes in the emission line strengths of some Of stars. Jeffers, Weller and Sanyal (1973) have reported a 200-second periodic variation in the emission line-strength of the He II ( $\lambda 4686 \text{ \AA}$ ) and C III-IV ( $\lambda 4650 \text{ \AA}$ ) complex

in the spectrum of  $\gamma^2$  Velorum, a spectroscopic binary with a Wolf-Rayet component (WC7+09). A critical examination of these results leads to the following conclusions. It would appear that the periodic variation only occurred during one short 10 minute run on  $\gamma^2$  Vel. Since the scanner used was a single-beam instrument and provided no means of compensation for atmospheric effects, it is possible that rapid variations in sky transparency could go unnoticed. It is also possible that the variations could be due to the size of the seeing disc, and hence the instrumental resolution, changing on a time-scale of 2 - 3 minutes and resulting in the measured equivalent widths also changing. The observations of the comparison star and the sky brightness were made before and after the  $\gamma^2$  Vel observations and the sky condition would be different at those times. The sky brightness probably would not be affected by seeing, and the comparison star ( $\alpha$  Carinae, Sp: F0 Ib) would be affected by seeing conditions differently from  $\gamma^2$  Vel since the lines in the comparison star would be very weak in comparison to the strong emission in  $\gamma^2$  Vel.

Further observations of  $\gamma^2$  Vel by Sanyal, Weller and Jeffers (1974) are reported as showing a 154-second periodic variation of the same emission line complex. These observations were made with a photon counting photometer using an interference filter with a half-width of  $75 \text{ \AA}$  centred at  $\lambda 4686 \text{ \AA}$ . The photometer was a single channel instrument and for a star as bright as  $\gamma^2$  Vel ( $m_V = 1.8$ ) the accuracy of the observations would be sky transparency and scintillation limited. In a plot of the photon count in 20-second integrations against time, presented by Sanyal et al, the peak-to-peak variation of the photon count is typically less than 1 per cent. This amplitude of variation is considerably greater than the expected photon noise ( $< 0.1$  per cent) but could easily be accounted for by noise due to rapid transparency changes and scintillation. A frequency power-spectrum of the  $\gamma^2$  Vel data is compared by Sanyal et al with a power-spectrum of normally distributed random data having the same mean and standard deviation as the star data. Although the power-spectra are different, with a

peak at 154 seconds in the  $\gamma^2$  Vel power-spectrum, this does not rule out the possibility that the reported variations in the  $\gamma^2$  Vel data could have been due to pseudo-periodic sky transparency changes, perhaps caused by "ribbed" cirrus cloud.

The comparison star observed was  $\gamma^1$  Vel (Sp: B3) and it and  $\gamma^2$  Vel were observed alternately for  $\sim 10$ -minute intervals giving a total integration time of 30 minutes for  $\gamma^1$  Vel and 35 minutes for  $\gamma^2$  Vel. However,  $\gamma^1$  Vel is  $\sim 2.6$  magnitudes fainter than  $\gamma^2$  Vel and in addition the spectrum of  $\gamma^1$  Vel has no strong emission around  $\lambda 4686 \text{ \AA}$ . Sanyal et al (1974) do not quote the photon counts for  $\gamma^1$  Vel, however the net result of the previous two facts is that the photon counting rate for  $\gamma^1$  Vel might be a factor of 30 - 40 down on the counting rate for  $\gamma^2$  Vel. A factor of 10 is due to the magnitude difference between the two stars and a further factor of at least 3 can be attributed to the difference in their line strengths (Bahng (1975a) presents profiles for  $\gamma^2$  Vel of the region  $\lambda\lambda 4600 - 4720 \text{ \AA}$  in which the peak intensities of the lines  $\lambda 4650$  and  $\lambda 4686$  relative to the continuum are  $\sim 3.5$  and  $\sim 1.5$  respectively). Since the photon count in a 20 second integration of  $\gamma^2$  Vel was quoted as  $\sim 2.3 \cdot 10^6$ , the count in a similar integration of  $\gamma^1$  Vel would be of the order of  $7 \cdot 10^4$  and the photon error on this count (i.e.  $\pm \sqrt{7 \cdot 10^4}$ ) would be  $\sim \pm 0.4$  per cent. Thus, the photon noise on the  $\gamma^1$  Vel data is comparable with a sky transparency noise of  $\pm 0.5$  per cent which it is suggested here might be the source of the observed variability. Thus the pseudo-periodic transparency noise in the  $\gamma^1$  Vel data would be combined with a random photon noise of the same amplitude and power-spectra of the  $\gamma^1$  Vel data would therefore compare more favourably with power-spectra of random data, as reported by Sanyal et al.

The observed variations could also be accounted for by a "periodic" variation in the size of the seeing disc which would again be more evident on the  $\gamma^2$  Vel data than on the  $\gamma^1$  Vel data because of the different line strengths and shapes and the resulting different instrumental response.

Bahng (1975a) has also observed the same spectral region of  $\gamma^2$  Vel as Sanyal, Weller and Jeffers in an attempt to detect short term variability. Bahng reports that he found the observed rms. (root-mean-square) variations in the equivalent widths of the  $\lambda$  4650 and  $\lambda$  4686 lines were at least three times larger than the errors predicted by photon statistics and concludes that this is due to there being real variations in these lines on short time-scales. Comparison with the errors found for standard stars was not possible since the latter showed no structure in that region of their spectra. Bahng also reports longer-term (i.e. night to night) changes in the equivalent widths of these lines.

As a means of expressing brightnesses, various "magnitudes"  $m$  are defined by Bahng for different parts of the emission lines as

$$m = 2.5 \log \left\{ \frac{\sum_{\lambda_1}^{\lambda_2} F_o(\lambda)}{\sum_{\lambda_1}^{\lambda_2} F(\lambda)} \right\}$$

where  $F_o(\lambda)$  and  $F(\lambda)$  are the mean count and the actual count of an individual scan at each wavelength point  $\lambda$  ( $\sim 30$  in all), and  $\lambda_1$  and  $\lambda_2$  are chosen to select the particular region of the spectral feature. Bahng reports that the observed rms. variations of these magnitudes (including continuum regions) are substantially larger than the theoretical rms. variations based on photon statistics. However, since the actual counts are used without normalising, this is to be expected, since no compensation is made for sky transparency changes. The photometer (scanner) used for the observations contained two diaphragms, one to isolate the star plus sky and the other to isolate a portion of nearby sky. Such a system cannot provide any compensation for sky transparency changes or scintillation and, for the reported observations, the second channel is virtually useless and the instrument is essentially operating in a single-beam mode. It is also noted by Bahng that the value of the rms. variations changes from night to night but this

might simply be due to the sky transparency being more stable on some nights than on others. Bahng, however, interprets the larger observed rms. variations as indicating real variability in  $\gamma^2$  Vel in the form of changes of the underlying continuum which affect all parts of the scans.

Power-spectrum analyses were performed by Bahng on the equivalent width measurements and the magnitude measurements with the result that no significant periodicities were found for the equivalent width variations. However a strong periodicity at  $\sim 119.6$  seconds period with an amplitude of  $\sim 0.003$  magnitude (i.e.  $\sim 0.3$  per cent) was found for the magnitude variations. Bahng finally traced this periodicity to being due to a periodic error of 2 sidereal minutes (i.e. 119.7 seconds) in the sidereal drive of the telescope. Apart from this, no other significant periodicities were found in the data and the observations of Sanyal et al were not confirmed. It is worth noting that the periodic variation did not appear on the comparison star ( $\epsilon$  Cen) data and this could partly account for the observed rms. variations in the comparison star magnitudes being closer to their photon predicted values, as Bahng found.

Since it is conceded by Bahng that there was a periodic error in the sidereal drive during the observations of  $\gamma^2$  Vel, this suggests that there would have been a resulting wandering of the star image in the entrance aperture of the scanner. Such a wandering would almost certainly result in uncontrolled wavelength shifts of the instrumental profile and these in turn might be partly responsible for the large observed rms. variations in the equivalent widths (the scans were made with a slit width of  $10 \text{ \AA}$  at  $4 \text{ \AA}$  intervals). The periodic drive error appeared on the  $\gamma^2$  Vel data on two separate observing runs (March 1973 and February 1974) and must place considerable doubt on the other variations reported on these occasions for this star. This example serves to show how dangerous it can be to compare programme star data with comparison star data without first determining if the observation parameters and conditions are identical for the two stars.

Bahng (1975b) has made similar observations of the same emission lines in five other Wolf-Rayet stars and concludes that none of these stars shows any short-term variations of their equivalent widths or brightness of the emission lines. There are however indications that there are night to night variations of the equivalent widths in some cases but further observations are required before these variations can be confirmed or refuted.

#### 1.4 Summary

From the observations by others which have just been described it would seem that the reported line profile variations on time-scales of hours to days are almost certainly real and intrinsic to the stars.

However, certain weaknesses in the reports of more rapid variations have been pointed out here. In some cases it seems doubtful that the reported variations are even real and not merely statistical noise on the data. In other cases the observed variations may be real to the data but can perhaps be attributed to instrumental effects and varying seeing conditions. In the reports cited, these sources of error have not been considered in sufficient depth, or at all, and the preceding discussions have attempted to consider the validity of the reported rapid variations in the light of these errors.

The amount of data obtained for comparison stars is usually less than for the programme stars and in addition it has been indicated here that too much reliance should not be placed on the comparison star observations. The importance of the differences between the spectral features of the comparison and programme stars has also been mentioned in relation to the errors resulting from instrumental and seeing effects.

It is necessary either to confirm or refute the reports of rapid variability among the various types of star described here since such phenomena are astrophysically very important. However, future observations must be examined carefully to determine the significance of any observed "variations."

In the chapters which follow, a novel approach to obtaining moderate time and spectral resolution stellar line profiles by tilt-scanning narrow band interference filters is presented. The behaviour of the interference filters and the resulting instrumental errors are considered in some detail along with the errors due to photon statistics and atmospheric noise sources.

## 2. PROPERTIES OF NARROW BAND INTERFERENCE FILTERS RELATING TO TILT-SCANNING

### 2.1 Introduction

Interference filters are commonly used in astronomical photometry as a means of isolating selected regions of spectrum in order that colour magnitudes may be determined. Such applications use narrow and intermediate band filters having half-widths (half-width (HBW)  $\equiv$  full-width at half maximum transmittance (FWHM)  $\equiv \Delta\lambda$ ) of 30 - 150 Å. Much narrower band interference filters are, however, now readily obtainable commercially.

By placing a narrow band filter in a collimated beam and tilting it, a simple wavelength scanning monochromator is achieved; a bandwidth of about 2 Å is easily possible with a potential scan range of almost 200 Å. The technique of tilt-scanning has been used before to obtain spectral detail of extended objects. Eather and Reasoner (1969) have measured line profiles in aurorae and airglow while de Vaucouleurs (1967) has determined radial velocities of galaxies and nebulae from line profiles obtained by tilt-scanning. De Vaucouleurs (1967) also measured calcium H and K line profiles of a few late type stars by tilting filters having bandwidths of 8 - 10 Å in parallel light but which were broadened to 15 - 20 Å as a result of the convergent beam of the photometer. Barbieri et al (1974) have measured line intensities in cometary spectra by tilt-scanning a solid Fabry-Pérot. The technique has also been used at Glasgow University Observatory by Clarke and McLean (1974a, 1974b) as a means of isolating portions of a spectrum line (e.g. the line core or one wing) in order to perform spectropolarimetry at those wavelengths.

It is believed that the work reported here is the first intensive study of the application of an interference filter scanner with a resolution of 2 - 3 Å to the measurement of stellar line profiles.

The remainder of this chapter will be devoted to describing the principles of tilt-scanning with interference filters and will discuss some of

the properties of these filters in relation to astronomical spectrophotometry. In the last section some measured line profiles are presented for comparison with simulated profiles. The latter were obtained by numerically convoluting Airy functions with digitised portions of spectra derived from high resolution spectrum atlases.

## 2.2 Throughput of the Optical System

In order to obtain stellar line profiles with moderate wavelength resolution and good time resolution some form of wavelength scanning monochromator which can accept all of the star's seeing disc (i.e. has a high throughput) is required. The throughput or luminosity ( $L$ ) of an optical component is given by

$$L = \epsilon A \Omega ,$$

where  $A$  is the collecting area and  $\Omega$  is the collecting solid angle;  $\epsilon$  is a transmission coefficient and is often taken as unity. The throughputs of prisms, gratings and Fabry-Pérot's having equal resolving powers and equal areas have been compared by Jacquinet (1954) with the now famous conclusion that the grating is much superior to the prism and the Fabry-Pérot is in turn much superior to the grating; "higher throughput" is sometimes referred to as "Jacquinet advantage."

The effective throughput of an entire optical system is determined by that optical component with the smallest individual throughput. In astronomical spectrophotometry it is obviously desirable that the system should only be limited by the telescope. In other words, the throughput of all the other optical pieces must be at least as great as that of the telescope.

Figure 2.1 illustrates some simple telescope/spectrometer systems for which the throughput may easily be evaluated. In order to accept all of the stellar seeing disc, the prism and grating are considered slitless and the star's seeing disc in the focal plane of the telescope acts as a circular

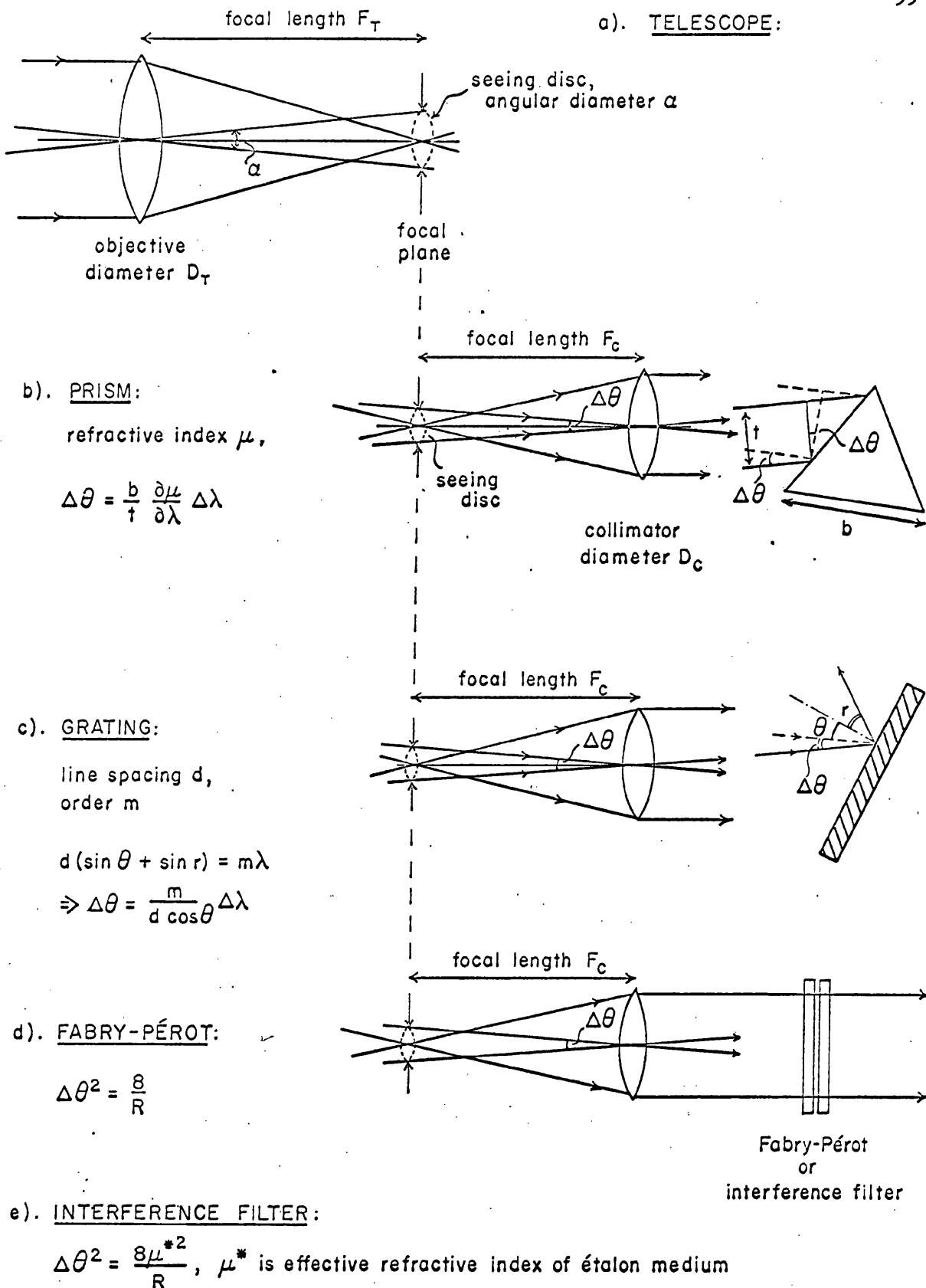


Figure 2.1

Luminosity is the product of collecting area and collecting solid angle.

$$\text{Telescope : } L = \frac{\pi D_T^2}{4} \cdot \frac{\pi \alpha^2}{4}, \quad \text{Spectrometers : } L = \frac{\pi D_C^2}{4} \cdot \frac{\pi \Delta\theta^2}{4}$$

The spread in angle ( $\Delta\theta$ ) produces a spread in wavelength ( $\Delta\lambda$ ) which determines an effective resolving power ( $\lambda/\Delta\lambda$ ).

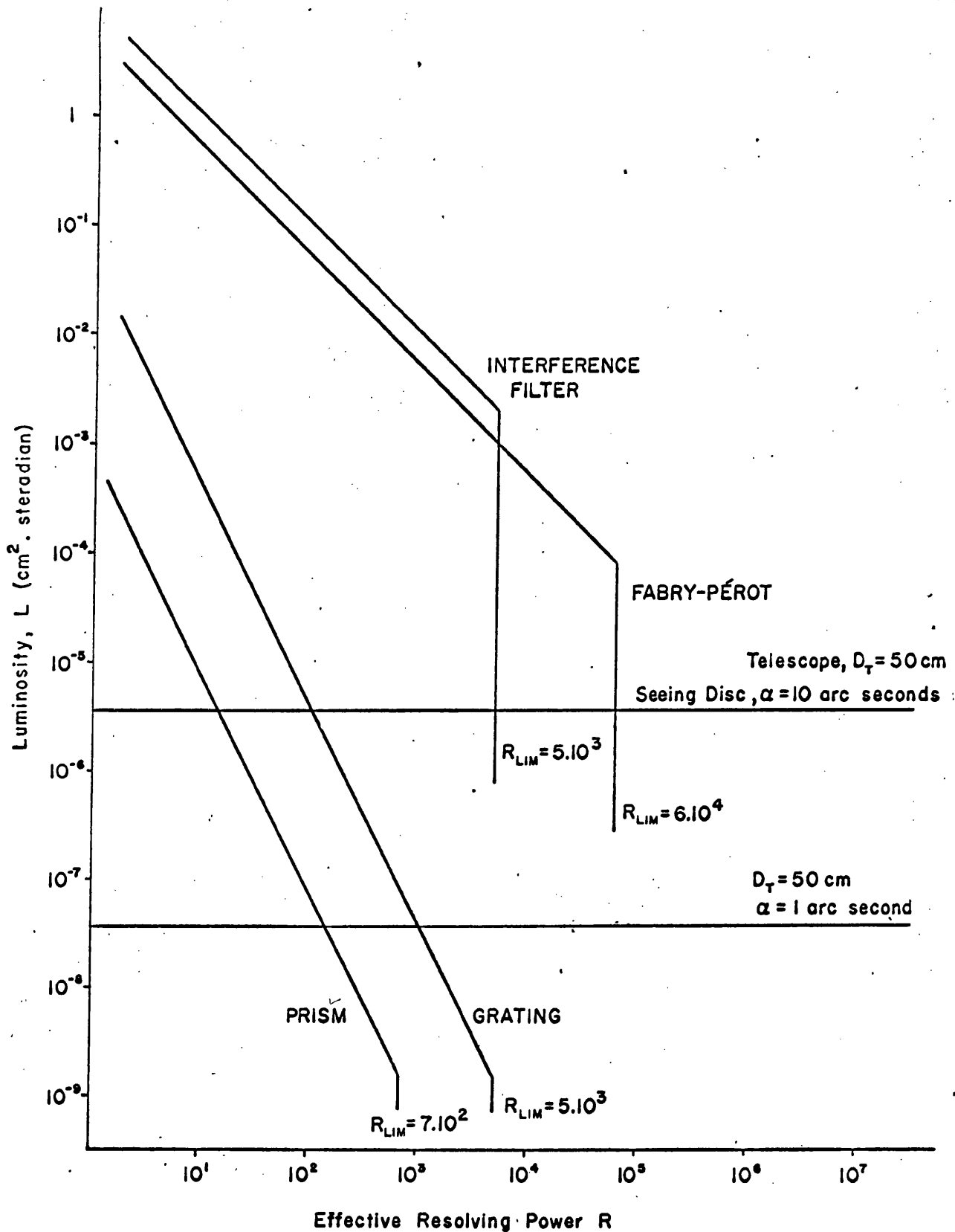


Figure 2.2 Luminosity as a function of effective resolving power (see Table 2.1) for the spectrometer systems shown in Figure 2.1. The spectrometric elements have illuminated areas of  $\sim 1 \text{ cm}^2$ .

$D_T = 50 \text{ cm}$ ,  $F_T/F_C = 50$ ,  $\lambda = 5000 \text{ \AA}$ . Prism:  $b \approx t$ ,  $\frac{\partial \mu}{\partial \lambda} = 7 \cdot 10^2 \text{ cm}^{-1}$ ;

Grating:  $\theta = 0$ ,  $m = 1$ ,  $d = 2 \cdot 10^{-4} \text{ cm}$ ; Filter:  $\mu^* = \sqrt{2}$ .

entrance aperture. The wavelength dispersive element is assumed always to be fully illuminated.

In each case, the spread in angle,  $\Delta\theta$ , produced by the finite size of the seeing disc results in a spread in wavelength,  $\Delta\lambda$ , which in turn gives an effective resolution  $R_{\text{eff}}$ , where  $R_{\text{eff}} = \frac{\lambda}{\Delta\lambda} \leq R_{\text{lim}}$ , the theoretical resolution of the system;  $\Delta\theta$  is related to the angular diameter,  $\alpha$ , of the star's seeing disc on the sky by

$$\Delta\theta = \frac{F_T}{F_C} \alpha$$

where  $F_T$  and  $F_C$  are the respective focal lengths of the telescope and collimator. Since  $R_{\text{eff}}$  and  $L$  both depend on  $\Delta\theta$ , it is possible to relate  $L$  to  $R_{\text{eff}}$ .

Figure 2.2 shows the luminosity  $L$  of the various spectrometer systems displayed in Figure 2.1 as a function of the effective resolving power,  $R_{\text{eff}}$ . The illuminated areas of the prism, grating, etc., are all assumed to be equal and are given by

$$\frac{\pi D_T^2 F_C^2}{4 F_T^2}$$

where  $D_T$  is the diameter of the telescope aperture and  $F_T$  and  $F_C$  are the focal lengths of the telescope and collimator lens. The values shown in Figure 2.2 are for  $D_T = 50$  cm (the Glasgow University telescope) and  $F_T/F_C = 50$ . Such a system requires that the spectrometric element has an illuminated area of  $\sim 1$  cm<sup>2</sup>. Interference filters of this size and with a resolving power of  $5.10^3$  are readily available commercially.

The expressions relating  $L$  and  $R$  for the various systems are given in Table 2.1 and the theoretical resolving powers,  $R_{\text{lim}}$ , are listed in Table 2.2. In each case  $\lambda$  is taken as 5000 Å. Typical working values have been taken;

Table 2.1 Luminosities of the telescope and simple spectrometers shown in Figure 2.1.

	<u>COLLECTING AREA</u>	<u>COLLECTING SOLID ANGLE</u>	<u>LUMINOSITY</u>
<u>Telescope:</u> Diameter $D_T$ Focal length $F_T$ Angular diameter of seeing disc $\alpha$	$\frac{\pi D_T^2}{4}$	$\frac{\pi \alpha^2}{4}$	$\frac{\pi^2 D_T^2 \alpha^2}{16}$
<u>Prism:</u> Base length $b \approx t$ Refractive index $\mu$ Resolution $R_{\text{eff}} = \frac{\lambda}{\Delta\lambda}$ Focal length of collimator $F_C$	$\frac{\pi D_C^2}{4} = \frac{\pi D_T^2 F_C^2}{4 F_T^2}$	$\frac{\pi \Delta\theta^2}{4} = \frac{\pi b^2 \lambda^2}{4 t^2 R_{\text{eff}}^2} \left( \frac{\partial \mu}{\partial \lambda} \right)^2$	$\frac{\pi^2 D_T^2 F_C^2 \lambda^2}{16 F_T^2 R_{\text{eff}}^2} \left( \frac{\partial \mu}{\partial \lambda} \right)^2$
<u>Grating:</u> Grating equation $d(\sin \theta + \sin r) = m\lambda$ Line spacing $d$ Order $m = 1$ $\cos \theta \approx 1$	$\frac{\pi D_T^2 F_C^2}{4 F_T^2}$	$\frac{\pi \Delta\theta^2}{4} = \frac{\pi m^2 \lambda^2}{4 d^2 \cos^2 \theta R_{\text{eff}}^2}$	$\frac{\pi^2 D_T^2 F_C^2 \lambda^2}{16 F_T^2 d^2 R_{\text{eff}}^2}$
<u>Fabry-Pérot:</u> Air spaced	$\frac{\pi D_T^2 F_C^2}{4 F_T^2}$	$\frac{\pi \Delta\theta^2}{4} = \frac{2\pi}{R_{\text{eff}}}$	$\frac{\pi^2 D_T^2 F_C^2}{2 F_T^2 R_{\text{eff}}}$
<u>Interference Filter:</u> Effective refractive index of étalon medium $\mu^*$	$\frac{\pi D_T^2 F_C^2}{4 F_T^2}$	$\frac{\pi \Delta\theta^2}{4} = \frac{2\pi \mu^*}{R_{\text{eff}}}$	$\frac{\pi^2 D_T^2 F_C^2 \mu^*}{2 F_T^2 R_{\text{eff}}}$

Table 2.2

Prism:  $R_{LIM} = b \frac{\partial \mu}{\partial \lambda}$  ,  $b$  is base length of prism  
 $\frac{\partial \mu}{\partial \lambda}$  is dispersion of refractive index with wavelength

for  $b = 1$  cm,  $\frac{\partial \mu}{\partial \lambda} = 7 \cdot 10^2$  cm<sup>-1</sup>

$$R_{LIM} = 7 \cdot 10^2$$

Grating:  $R_{LIM} = mN$  ,  $m$  is the order of interference  
 $N$  is the total number of grating lines

If grating spacing,  $d = 2 \cdot 10^{-4}$  cm (i.e.  $5 \cdot 10^3$  lines/cm)

and  $m = 1$  ,

then for a 1 cm grating

$$R_{LIM} = 5 \cdot 10^3$$

Fabry-Pérot:  $R_{LIM} = nN_r$  ,  $n$  is the order of interference,  
 $n \gg 1$ ,

$N_r$  is the number of recombining beams.

$N_r = \pi(1 - r)^{-1} r^{\frac{1}{2}}$  where  
 $r$  is the reflection coefficient of the reflecting layers.

For  $n = 10^3$ ,  $N_r = 60$  ,

$$R_{LIM} = 6 \cdot 10^4$$

Interference Filter:  $R_{LIM} = nN_r$  ,

For  $n = 2$ ,  $N_r = 2 \cdot 5 \cdot 10^3$  ,

$$R_{LIM} = 5 \cdot 10^3$$

Theoretical limiting resolving powers of the spectrometric elements shown in Figure 2.1 and with the same dimensions as in Figure 2.2.

the dispersion of refractive index with wavelength for the prism ( $\frac{\partial\mu}{\partial\lambda}$ ) is taken as  $7 \cdot 10^2 \text{ cm}^{-1}$ , the line spacing of the grating ( $d$ ) is  $2 \cdot 10^{-4} \text{ cm}$  (i.e.  $5 \cdot 10^3 \text{ lines cm}^{-1}$ ) and the effective refractive index of the interference filter ( $\mu^*$ ) is  $\sqrt{2}$ .

The telescope, diameter  $D_T$  and focal length  $F_T$ , provides the spectrometer system with a luminosity of

$$\frac{\pi^2 D_T^2 \alpha^2}{16}$$

where  $\alpha$  is the angular size (in radians) of the stellar seeing disc. This is shown in Figure 2.2 as a line of constant luminosity.

It can be seen from Figure 2.2 that if the prism or grating systems are to accept all of the light even from a 1 arc second seeing disc (i.e. have a luminosity at least equal to that of the telescope), they are forced to work at much reduced effective resolving power. It should be noted that the luminosity of any of the systems can be increased by increasing the focal length of the collimator,  $F_C$ , thus increasing the illuminated area of the spectrometer. However, even if  $F_C$  is increased by a factor of 10, thus requiring an increase of a factor of 100 in the area of the spectrometric element, both the prism and the grating still cannot achieve an effective resolving power of  $5 \cdot 10^3$  while accepting all of a 1 arc second seeing disc.

On the other hand, both the Fabry-Pérot and the interference filter are capable of achieving their theoretical resolving power while accepting a seeing disc in excess of 10 arc seconds diameter. They have the additional advantage of small physical size enabling easy use on small telescopes. A grating having an area of  $100 \text{ cm}^2$  and requiring a system in which  $F_T/F_C = 5$  (assuming  $D_T = 50 \text{ cm}$ ) results in a very large spectrometer which would be liable to mounting difficulties and might suffer from flexure. In addition,

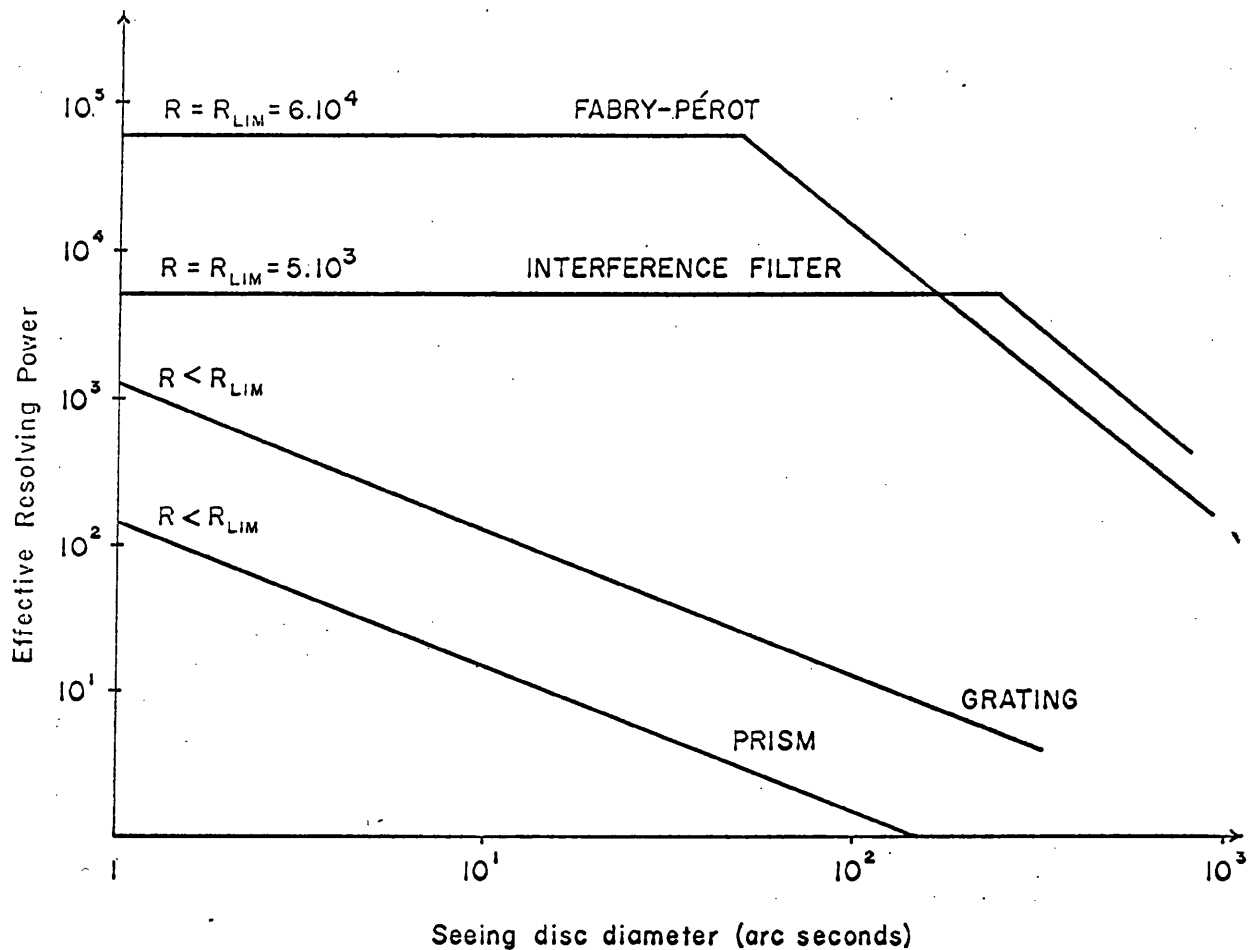


Figure 2.3

Variation of effective resolving power ( $R_{\text{eff}}$ ) with diameter of seeing disc accepted ( $\alpha$ ) for the spectrometer systems shown in Figure 2.1, with

$$\Delta\theta = \frac{F_T}{F_C} \alpha, \quad \Delta\lambda = \frac{\lambda}{R_{\text{eff}}}$$

and using the same dimensions as Figure 2.2. Expressions for  $R_{\text{LIM}}$  are given in Table 2.2.

the filter may be used directly on the optical axis of the telescope, so enabling a simple spectrometer shape. Optical aberrations in such a system should not cause problems as they usually do in angular dispersive instruments.

The effective resolving power of the various systems is shown in Figure 2.3 as a function of the seeing disc diameter.

In conclusion, it is felt that for observations for which a spectral resolution of  $\sim 5 \cdot 10^3$  is adequate and which require the maximum amount of transmitted light in order to achieve good time resolution, the interference filter has application as a very compact spectrometer which is far superior to a grating or prism spectrometer of equivalent size.

### 2.3 Filter Performance in Parallel Light

An interference filter may be considered as a Fabry-Pérot étalon with a solid dielectric spacer. The spacer thickness is given by  $\frac{n\lambda}{2}$ , where  $n$  is the order of interference. Unlike the Fabry-Pérot, the interference filter works at low order, usually 1 or 2, and achieves its resolution by virtue of the large number of interfering beams resulting from the high reflectivity of the reflecting stack. This stack consists of a number of quarter-wave layers of dielectric materials of alternate high and low refractive indices. Cryolite and zinc sulphide are the most commonly used materials.

The normalised transmitted intensity  $I_\lambda$  at wavelength  $\lambda$  is given by the Airy function

$$I_\lambda = \frac{1}{1 + \frac{4r}{(1-r)^2} \sin^2\left(\frac{\delta}{2}\right)}$$

where  $r$  is the reflection coefficient of the dielectric layers and  $\delta$  is the phase difference between successive reflected beams emerging from the interfering gap.

The phase difference  $\delta$  is given by

$$\delta = \frac{2\pi}{\lambda} \times \text{optical path difference}$$

$$\text{i.e. } \delta = \frac{2\pi \mu^* 2d \cos \beta}{\lambda}$$

where  $\mu^*$  is the effective refractive index of the gap,  $d$  is the thickness of the gap and  $\beta$  is the angle of incidence of the beam within the gap.

It can be seen that  $I_\lambda$  is a maximum when  $\sin^2 \left(\frac{\delta}{2}\right) = 0$ , i.e.  $\frac{\delta}{2} = n\pi$ , again  $n$  is the order of interference. Thus maxima occur when

$$n\pi = \frac{2\pi d \mu^* \cos \beta}{\lambda}$$

$$\text{or } \lambda = \frac{2d \mu^*}{n} \cos \beta$$

If  $\lambda_0$  is the wavelength transmitted by the filter at normal incidence, then  $\lambda_0 = \frac{2d \mu^*}{n}$  and  $\lambda_\theta = \lambda_0 \cos \beta$ . By Snell's law,  $\mu^* \sin \beta = \sin \theta$ , where  $\theta$  is the external angle of incidence of the beam. Thus,

$$\lambda_\theta = \lambda_0 \left(1 - \frac{\sin^2 \theta}{\mu^{*2}}\right)^{\frac{1}{2}} \quad (2.1)$$

where  $\lambda_\theta$  is the wavelength transmitted when a collimated beam is incident at an angle  $\theta$  to the filter.

Equation (2.1) may be written in an approximate form as

$$\lambda_\theta = \lambda_0 \left(1 - \frac{\sin^2 \theta}{2\mu^{*2}}\right) \quad (2.2)$$

$$\text{or as } \lambda_\theta = \lambda_0 \left(1 - \frac{\theta^2}{2\mu^{*2}}\right) \quad (2.3)$$

Any one of Equations (2.1) to (2.3) may be considered when expressing  $\lambda$  as a function of  $\theta$ .

The relationship between  $\lambda$  and  $\theta$  forms the basis of the interference

filter scanner. By tilting a filter in a collimated beam it is possible to shift the filter's passband towards shorter wavelengths in an easily controlled way. Obviously some form of wavelength/tilt calibration is required, since the relationship is non-linear. This can be achieved by measuring the tilts required to transmit emission lines of known wavelengths from laboratory spectrum lamps and hence determining the constants  $\lambda_0$  and  $\mu^*$ .

#### 2.4 Wavelength Calibration and Filter Profiles

The spectrum line of interest for this study was chosen to be the Balmer H $\beta$  line at 4861.3 Å. In order to obtain profiles of this line by the tilting-filter technique, it is necessary to have filters whose wavelength of peak transmittance at normal incidence is longer than H $\beta$ . For most of the work reported, two narrow band filters were used (the filters were manufactured by Thin Film Products Inc.), both of which have their normal incidence wavelength at about 4874 Å and have half-widths (FWHM) of 1.9 Å and 2.2 Å at normal incidence.

Wavelength calibration of these two filters can be easily performed with hydrogen and zinc spectrum lamps. The hydrogen lamp provides a line at H $\beta$  and the zinc lamp has lines at 4810.5 Å, 4722.2 Å and 4680.1 Å.

In addition to finding the constants  $\lambda_0$  and  $\mu^*$ , calibration of the filters also requires determining the zero-point ( $\phi_0$ ) on the scale which registers tilt, since  $\theta = \phi - \phi_0$  where  $\phi$  is the scale reading corresponding to an angle of incidence  $\theta$  and  $\phi_0$  corresponds to normal incidence. The fiducial,  $\phi_0$ , can be found by tilting the filter to both sides of normal incidence and noting the position on each side of normal incidence at which any line, H $\beta$  say, is transmitted. Normal incidence occurs mid-way between these positions. Further tilting of the filter in one direction will cause it to transmit each of the zinc lines in turn. The values of tilt thus obtained may be used in a least squares solution of one of Equations (2.1) to (2.3) to determine  $\lambda_0$  and  $\mu^*$ . Examples of calibration curves for the two filters mentioned above are shown in Figure 2.4.

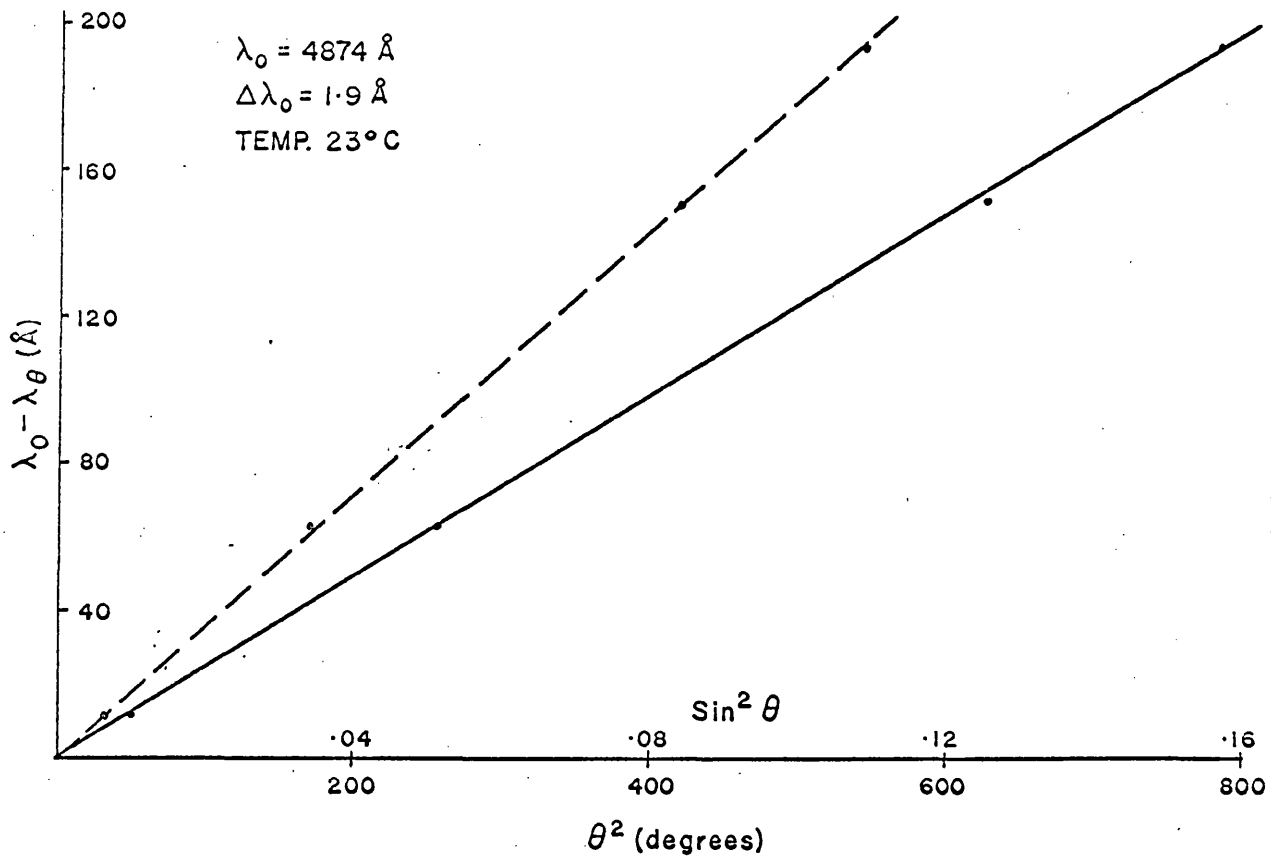
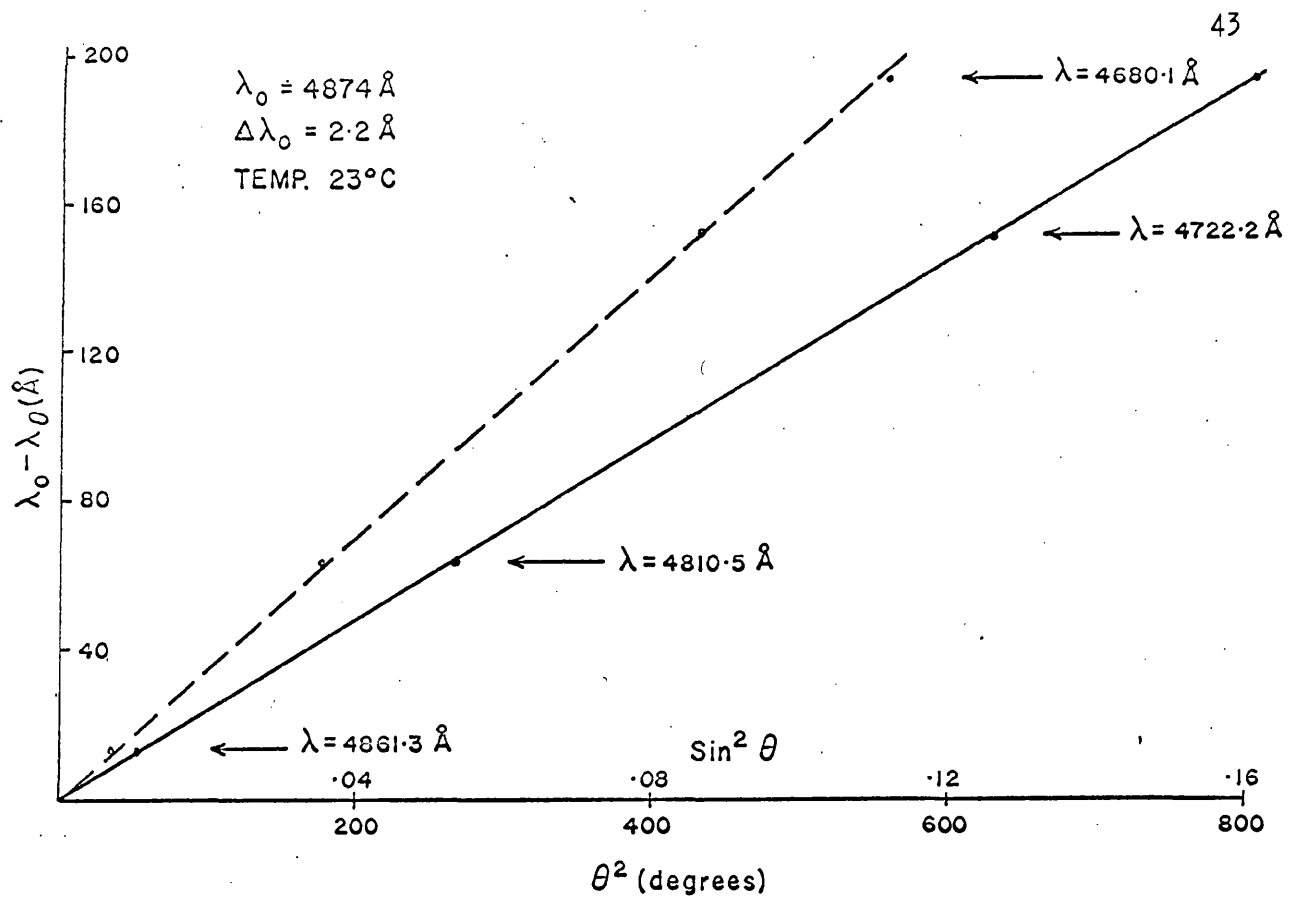


Figure 2.4

Variation of the wavelength of peak transmittance with tilt for the two narrow band filters used to scan H $\beta$ . Solid lines:  $\sin^2 \theta$  (Equation 2.2); Dashed lines:  $\theta^2$  (Equation 2.3). Half-width (FWHM) at normal incidence is  $\Delta\lambda_0$ .

The ability of these two filters to transmit the zinc line at  $4680 \text{ \AA}$  would seem to indicate that they have a potential scanning range of at least  $200 \text{ \AA}$ . However, the line profiles thus obtained would be subject to a certain degree of distortion due to changes in the filter passband and in most cases on the telescope scanning has been restricted to about  $40 \text{ \AA}$  from normal incidence. For most studies, this range of scan is sufficient but may easily be extended to  $70 \text{ \AA}$  without serious deterioration of the instrumental profile.

The effects of tilt on the filter passband will be discussed in the next section.

Wavelength calibration was done with the filters in situ in the photometer while it was attached to the telescope. Light from the calibration lamps was piped into the photometer by a fibre optic tube, the end of which was held on a slide enabling it to be positioned on the optic axis prior to the telescope/collimator focal plane. A diaphragm matching the size of a typical stellar seeing disc was mounted in the focal plane so as to limit the size of light source and thus prevent broadening of the filter passband (see later for explanation). The subsequent optics were unchanged from those used when measuring stellar sources.

If an emission line in the spectrum of a laboratory lamp is assumed to be of negligible width compared with the instrumental profile, then the recorded profile obtained by scanning this line is simply that of the instrument. In this way it was possible to measure the instrumental profile at the wavelength of each of the calibration lines.

An example of such an instrumental profile is presented in Figure 2.5 and is compared with an Airy function of the same half-width. Table 2.3 lists manufacturer's specifications and some measured parameters for the two narrow filters used for scanning  $H\beta$  and for two other broader filters used

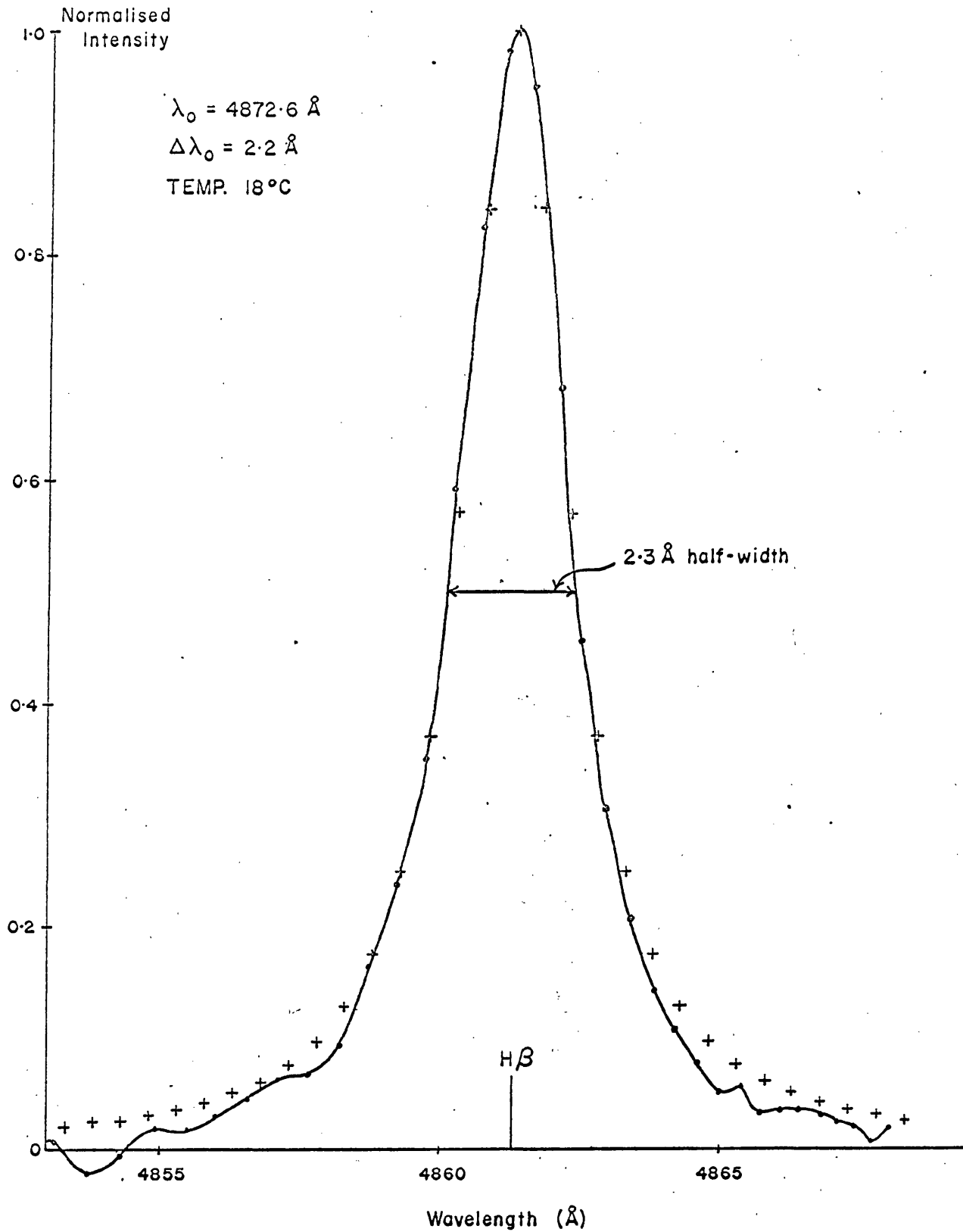


Figure 2.5

Transmission profile (dots and solid line) for one of the narrow band filters, measured by scanning an intrinsically narrow laboratory spectrum line (H $\beta$ ). An Airy function (crosses) with a half-width of 2.3 Å is shown for comparison.

in a second beam of the photometer to measure the intensity of a fixed region of continuum adjacent to H $\beta$  so that compensation for atmospheric effects could be obtained.

As can be seen from Table 2.3, the filter half-widths increase with tilt, the effect being most severe for the narrow filters. There are several factors which can contribute to the increase in half-width some of which will be briefly discussed here.

Manufacturer's Specifications (Thin Film Products Division of Infra Red Industries Inc.)				Measured Parameters with filters in situ within the photometer				
FWHM ( $\Delta\lambda$ , $\text{\AA}$ )	Temp ( $^{\circ}\text{C}$ )	Transmittance (%)	Centre of Passband ( $\lambda_0$ , $\text{\AA}$ )	Centre of Passband ( $\lambda_0'$ , $\text{\AA}$ )	FWHM ( $\Delta\lambda$ , $\text{\AA}$ ) Wavelengths ( $\text{\AA}$ )			
					4861.3	4810.5	4722.2	4680.1
1.9	26	38	4874.9	4873.6	2.0	2.5	3.2	3.5
2.2	26	36	4876.7	4874.0	2.3	3.2	3.7	4.1
10	24	51	4872.4	4871.8	9.9	9.9	—	—
12	25	58	4877	4877.3	12.8	13.4	—	—

Table 2.3. Manufacturer's specifications for bandwidth (FWHM), wavelength of peak transmittance, at normal incidence and the filter transmittance together with measurements of the bandwidths at various wavelengths for the filters which have been used to obtain stellar line profiles. The differences between the measured wavelengths of normal incidence ( $\lambda_0'$ ) and the manufacturer's values ( $\lambda_0$ ) are most likely due to a combination of temperature differences and ageing effects of the filters.

## 2.5 Variations of Filter Passbands with Tilt

Figure 2.6 shows a simple optical arrangement which may be used to illuminate an interference filter with collimated light. In this arrangement, the filter is located at the position at which the collimator forms an image of the telescope aperture. This ensures that any movement of the star image in the telescope focal plane does not result in movement of the collimated beam on the surface of the filter. Any such movement would be a possible source of noise, since the wavelength and half-width of a filter passband are often not constant across its diameter (see Meaburn, 1970).

It can be seen from Figure 2.6 that the stellar seeing disc as seen by the filter has a finite angular size. Because of this, the filter is illuminated with a cone of light, even after collimation. The effect on the wavelength of peak transmittance and the half-width of the instrumental profile produced by the convergent beam from an extended source as opposed to the collimated beam from a point source can be assessed by first considering the filter's response to a single ray and then considering the integrated effect for all rays, resulting in an effective instrumental profile.

In order to determine the angle of incidence on the filter of an arbitrary ray from a point within the extended image of the seeing disc in the focal plane, consider the co-ordinate system shown in Figure 2.7. Suppose that  $O$  represents any point on the filter surface and that  $OZ$  is parallel to the optical axis of the telescope. Every point on the filter will be illuminated by a cone of light (as shown in Figure 2.6) and suppose that  $PO$  represents an arbitrary ray within the cone which has its apex at  $O$ . The wavelength of the filter passband corresponding to this ray is determined by the angle,  $\beta$ , between  $PO$  and the normal to the filter at the point  $O$ .

As the filter is tilted, its surface, except for points along the axis

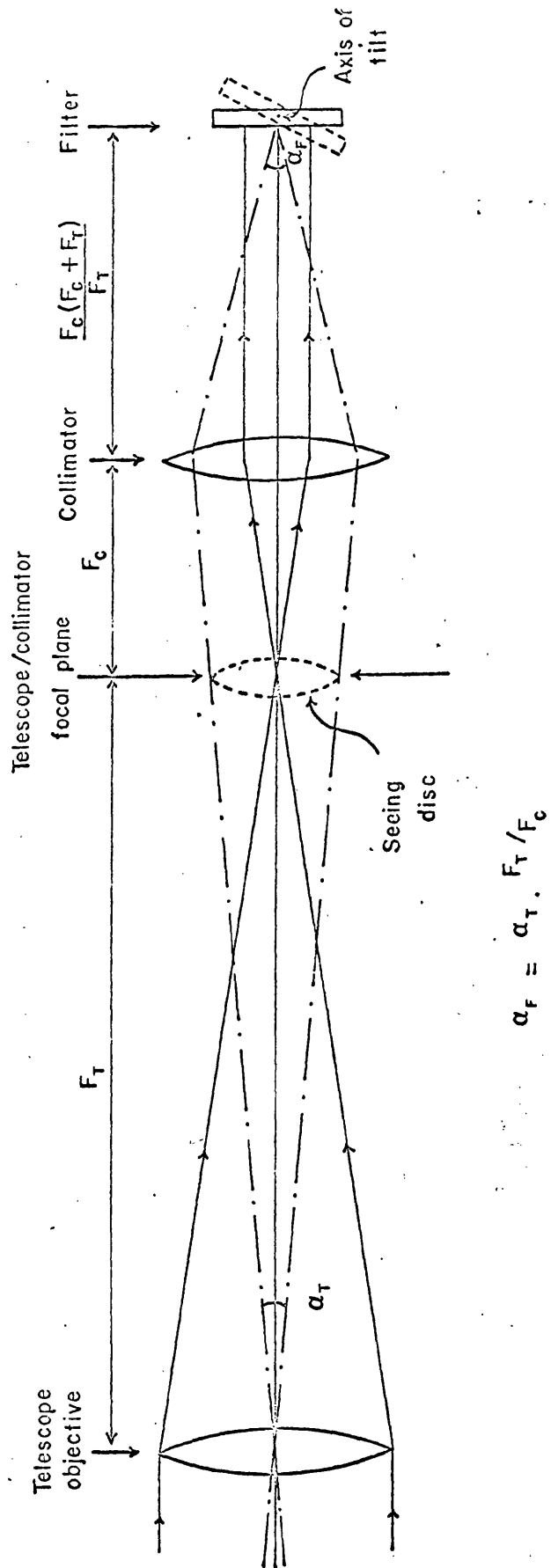


Figure 2.6

Basic optical layout of the tilting-filter scanner. The filter is at the position where the collimator images the telescope aperture, but even after collimation it is illuminated by a coned beam due to the finite angular diameter of a star's seeing disc.

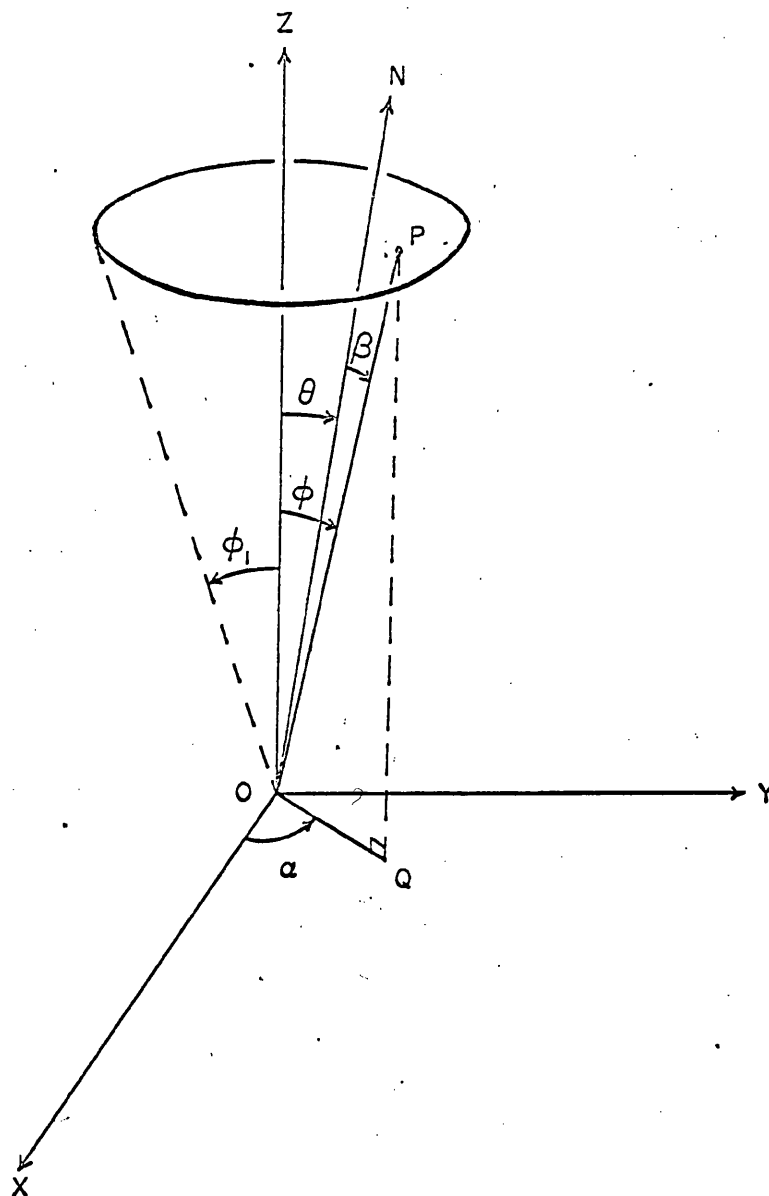


Figure 2.7

Any point  $O$  on the filter is illuminated by a cone of light of semi-angle  $\phi_1$ . The wavelength of peak transmittance for an arbitrary ray  $PO$  (defined by  $\phi$  and  $\alpha$ ) within the seeing cone is determined by the angle  $\beta$  between  $PO$  and the normal to the filter  $ON$ . The filter is tilted through an angle  $\theta$  about  $OX$  and the telescope's optical axis is parallel to  $OZ$ .

of tilt, will be shifted out of the plane in which the image of the telescope aperture is formed (see Figure 2.6). As a result, the original illuminating cones at any point on the surface of the filter will become truncated. However, rays from other parts of the telescope aperture, parallel to the original rays, will converge to form new cones of identical shape to the cones which were truncated. It will be assumed that the intensity distribution with angle within the new illuminating cones is the same as it was within the original ones.

Suppose that when it is perpendicular to the optical axis, the filter lies in the plane OXY (see Figure 2.7) and suppose also that the axis of tilt of the filter is parallel to OX and in the plane OXY. It follows that the normal to the filter at the point O will always lie in the plane ZOY. When the filter is perpendicular to the optical axis, the normal at point O lies along OZ, and when the filter is tilted through an angle  $\theta$ , the direction of the normal is given by ON, where  $\hat{ZON} = \theta$ . The direction of any ray PO within the illuminating cone is defined by the angles ZOP ( $= \phi$ ) and XOQ ( $= \alpha$ ) where OQ is the projection of OP on the plane OXY.

Suppose that  $\underline{p}$  and  $\underline{n}$  are unit vectors along  $\overrightarrow{OP}$  and  $\overrightarrow{ON}$ . In component form,  $\underline{p}$  and  $\underline{n}$  are given by

$$\underline{p} = (\sin \phi \cos \alpha, \sin \phi \sin \alpha, \cos \phi)$$

and

$$\underline{n} = (0, \sin \theta, \cos \theta).$$

(The components lie along the X, Y and Z axes respectively).

If the angle between OP and ON is  $\beta$  (i.e. the angle of incidence of the ray PO when the normal to the filter at point O lies along ON), then  $\beta$  is given by the scalar product of the vectors  $\underline{p}$  and  $\underline{n}$ .

Thus,

$$\underline{p} \cdot \underline{n} = |\underline{p}| |\underline{n}| \cos \beta,$$

and since  $\underline{p}$  and  $\underline{n}$  are unit vectors,  $|\underline{p}|$  and  $|\underline{n}|$  are both unity. Therefore,

$$\cos \beta = \underline{p} \cdot \underline{n} = p_X n_X + p_Y n_Y + p_Z n_Z \quad ,$$

where  $p_X, n_X$ , etc., are the components of the vectors  $\underline{p}$  and  $\underline{n}$ .

It follows that,  $\cos \beta = \sin \theta \sin \phi \sin \alpha + \cos \theta \cos \phi$ .

The wavelength transmitted by the filter,  $\lambda_\beta$ , corresponding to the angle of incidence  $\beta$  is given by Equation 2.2 as

$$\lambda_\beta = \lambda_0 \left( 1 - \frac{\sin^2 \beta}{2\mu^2} \right)$$

or, since  $\sin^2 \beta = 1 - \cos^2 \beta$ , then

$$\lambda_\beta = \frac{\lambda_0}{2\mu^2} (2\mu^2 - 1 + \cos^2 \beta) \quad ,$$

$$\text{i.e.} \quad \lambda_\beta = \frac{\lambda_0}{2\mu^2} \left( 2\mu^2 - 1 + [\sin \theta \sin \phi \sin \alpha + \cos \theta \cos \phi]^2 \right) \quad (2.4)$$

Equation 2.4 gives an expression for the wavelength transmitted at the point O on the filter for an arbitrary ray PO ( $\phi, \alpha$ ) when the filter is tilted at an angle  $\theta$  to the optical axis. If the filter is assumed to be uniform across its surface, its behaviour at any other point will be identical to that at the point O.

For the ray PO, the transmitted light will not be monochromatic, the filter having a spread of transmittance with wavelength  $T_\beta(\lambda)$ , similar to the transmission profile of the filter when used at normal incidence but with its peak transmittance centred on the wavelength  $\lambda_\beta$  ( $\phi, \alpha, \theta$ ). To a good approximation the filter profile can be considered as being Gaussian and, over the small range of angles of the rays contained in the seeing cone, the form of the Gaussian can be considered as constant. Thus the transmittance as a

function of wavelength for the ray PO may be written as

$$T_{\beta}(\lambda) = T_0 e^{-k(\lambda - \lambda_{\beta})^2}$$

where  $k$  and  $T_0$  are independent of wavelength;  $k$  is a constant related to the theoretical instrumental half-width for a point source illuminating the filter at normal incidence. The quantity  $T_0$  is the transmitted intensity at the wavelength of the centre of the passband ( $\lambda_{\beta}$ ) and assuming that there are no variations of filter transmittance with angle of incidence or across its surface,  $T_0$  will be a function of the intensity distribution  $I$  across the extended image of the seeing disc. If  $I$  is assumed to be independent of the angle  $\alpha$  and only varies with  $\phi$ , then  $T_0$  will be a function of  $\phi$ . For example, if the intensity distribution across the seeing disc has a Gaussian shape, then the transmitted intensity at the passband centre will be given by

$$T_0 = T e^{-c\phi^2}$$

where  $T$  is the transmitted intensity corresponding to rays from the centre of the seeing disc (i.e.  $\phi = 0$ ) and  $c$  is a constant.

Thus the transmittance of the filter as a function of wavelength for the ray PO will be given by

$$T_{\beta}(\lambda) = T e^{-c\phi^2} e^{-k(\lambda - \lambda_{\beta})^2}$$

All of the rays within the illuminating cone will be transmitted with a similar wavelength distribution, but each ray will have its own values of  $T_0$  and  $\lambda_{\beta}$  corresponding to the angles  $\phi$  and  $\alpha$  which define the position of the ray within the cone. The effect of combining the transmission profiles of all of the rays within the cone is to produce an effective instrumental transmission profile,  $T(\lambda)$ , which is obtained by integrating  $T_{\beta}(\lambda)$  over the angular extent of the seeing cone.

Thus

$$T(\lambda) = \int_{\alpha=0}^{2\pi} \int_{\phi=0}^{\phi_1} T e^{-c\phi^2} e^{-k(\lambda - \lambda_\beta)^2} \phi \, d\phi \, d\alpha \quad (2.5)$$

where  $\phi_1$  is the semi-angle of the illuminating cone (see Figure 2.7) and  $\lambda_\beta$  is a function of  $\phi$ ,  $\alpha$  and  $\theta$  as given in Equation 2.4.

If the filter is uniform across its surface, then the cones of light passing through each point on the surface of the filter will produce identical effective instrumental transmission profiles and the integrated effect over the illuminated area of the filter will also have this effective transmission profile.

Clearly, the wavelength of peak transmittance and the half-width of the effective instrumental profile will not be the same as those produced by a point source and both will vary with the angle of tilt of the filter ( $\theta$ ) and with the angular extent of the seeing disc seen by the filter. Both of these topics will now be considered.

It is possible to estimate from Equation 2.4 the shift in the wavelength of peak transmittance brought about by illuminating the filter with a cone of light as opposed to parallel light. Suppose that an effective wavelength of peak transmittance,  $\lambda_{\text{eff}}$ , can be defined for the effective instrumental profile by integrating over the seeing cone the wavelength of peak transmittance for an arbitrary ray PO, given in Equation 2.4, assuming that the intensity across the seeing disc is constant. Thus the effective wavelength is defined as

$$\lambda_{\text{eff}} = \frac{\int_{\phi=0}^{\phi_1} \int_{\alpha=0}^{2\pi} \lambda_\beta \phi \, d\phi \, d\alpha}{\int_{\phi=0}^{\phi_1} \int_{\alpha=0}^{2\pi} \phi \, d\phi \, d\alpha}$$

By substituting for  $\lambda_\beta$  from Equation 2.4, then

$$\lambda_{\text{eff}} = \frac{\int_0^{\phi_1} \int_0^{2\pi} \frac{\lambda_0}{2\mu^{*2}} \left( 2\mu^{*2} - 1 + [\sin \theta \sin \phi \sin \alpha + \cos \theta \cos \phi]^2 \right) \phi \, d\phi \, d\alpha}{\pi \phi_1^2}$$

and by evaluating the double integral, it can be shown that

$$\begin{aligned} \lambda_{\text{eff}} = & \frac{\lambda_0}{2\mu^{*2}} \left\{ 2\mu^{*2} - 1 \right\} + \frac{\lambda_0}{2\mu^{*2}} \cos^2 \theta \left\{ \frac{\sin \phi_1 \cos \phi_1}{\phi_1} - \frac{1}{2} \left( \frac{\sin \phi_1}{\phi_1} \right)^2 + \frac{1}{2} \right\} \\ & + \frac{\lambda_0}{2\mu^{*2}} \sin^2 \theta \left\{ \frac{1}{4} \left( \frac{\sin \phi_1}{\phi_1} \right)^2 - \frac{\sin \phi_1 \cos \phi_1}{2\phi_1} + \frac{1}{4} \right\} \end{aligned} \quad (2.6)$$

Equation 2.6 gives the wavelength of peak transmittance of the effective instrumental profile when the filter is tilted through an angle  $\theta$  from normal incidence and is illuminated by a cone of semi-angle  $\phi_1$ . The wavelength of peak transmittance when the filter is tilted through an angle  $\theta'$ , but is illuminated with collimated light from a point source, is given in Equation 2.2 and may be written as

$$\lambda_\theta = \frac{\lambda_0}{2\mu^{*2}} \left( 2\mu^{*2} - 1 + \cos^2 \theta \right) \quad (2.7)$$

If the semi-angle of the seeing cone,  $\phi_1$  radians, is assumed to be small, and if  $\sin \phi_1$  and  $\cos \phi_1$  are expanded in Maclaurin Series and terms of order greater than  $\phi_1^2$  are neglected, then Equation 2.6 may be written as

$$\begin{aligned} \lambda_{\text{eff}} = & \lambda_0 - \frac{\lambda_0}{2\mu^{*2}} \left\{ 1 - \cos^2 \theta \left[ 1 - \frac{5\phi_1^2}{12} - \frac{1}{2} \left( 1 - \frac{4\phi_1^2}{12} \right) + \frac{1}{2} \right] \right. \\ & \left. - \sin^2 \theta \left[ \frac{1}{4} - \frac{\phi_1^2}{12} - \frac{1}{2} + \frac{5\phi_1^2}{24} + \frac{1}{4} \right] \right\} \end{aligned}$$

i.e.,

$$\lambda_{\text{eff}} = \lambda_0 - \frac{\lambda_0}{2\mu^{*2}} \left\{ 1 - \cos^2 \theta \left( 1 - \frac{\phi_1^2}{4} \right) - \sin^2 \theta \cdot \frac{\phi_1^2}{8} \right\} \quad (2.8)$$

where  $\phi_1$  is in radians.

Equations 2.7 and 2.8 show that the wavelength/tilt calibration will be dependent on the cone semi-angle and the wavelength shift produced by illuminating the filter at a fixed angle of tilt with a cone of light is given by

$$\lambda_{\theta} - \lambda_{\text{eff}} = \frac{\lambda_0 \phi_1^2}{16\mu^{*2}} [3 \cos^2 \theta - 1] \quad (2.9)$$

Table 2.4 lists  $(\lambda_{\theta} - \lambda_{\text{eff}})$  for various combinations of  $\phi_1$  and  $\theta$ , taking  $\lambda_0 = 4874 \text{ \AA}$  and  $\mu^* = \sqrt{2}$ . It can be seen that the wavelength shift of the passband produced by a cone of light is very small, even at tilts as large as  $20^\circ$ . If the ratio of the focal lengths of the telescope and collimator is taken as 60 : 1, then the values of  $\phi_1$  in Table 2.4 correspond to seeing discs with angular diameters on the sky of 2, 4, 8, 16 and 32 arc seconds. (If  $\alpha_T$  is the angular diameter on the sky of the seeing disc, then

$$2 \phi_1 = \alpha_T \frac{F_T}{F_C}$$

where  $F_T$  and  $F_C$  are the focal lengths of the telescope and the collimator as before).

When the filter is at normal incidence (i.e.  $\theta = 0$ ) in a converging beam of semi-angle  $\phi_1$ , Equation 2.9 reduces to

$$\lambda_{\theta} - \lambda_{\text{eff}} = \lambda_0 - \lambda_{\text{eff}} = \frac{\lambda_0 \phi_1^2}{8\mu^{*2}} \quad (2.10)$$

while, if  $\theta$  is set equal to  $\phi_1$  when the filter is illuminated with collimated light, Equation 2.7 gives

$$\lambda_{\phi_1} = \frac{\lambda_0}{2\mu^{*2}} (2\mu^{*2} - 1 + \cos^2 \phi_1)$$

i.e.  $\lambda_0 - \lambda_{\phi_1} = \frac{\lambda_0}{2\mu^{*2}} (1 - \cos^2 \phi_1)$

or  $\lambda_0 - \lambda_{\phi_1} = \frac{\lambda_0 \phi_1^2}{2\mu^{*2}} \quad (2.11)$

since  $\phi_1$  is small ( $\phi_1$  in radians).

VALUES OF  $\lambda_{\theta} - \lambda_{\text{eff}}$

$\theta$	$\phi_1$	1 arc minute	2'	4'	8'	16'
0°		$2.58 \cdot 10^{-5} \text{ \AA}$	$1.03 \cdot 10^{-4} \text{ \AA}$	$4.12 \cdot 10^{-4} \text{ \AA}$	$1.65 \cdot 10^{-3} \text{ \AA}$	$6.60 \cdot 10^{-3} \text{ \AA}$
2°		"	1.03	4.12	"	6.59
4°		"	1.02	4.09	"	6.55
8°		"	1.00	4.00	"	6.41
12°		"	$9.64 \cdot 10^{-5} \text{ \AA}$	3.86	"	6.17
16°		"	9.14	3.65	"	5.85
20°		"	8.50	3.40	"	5.44

Table 2.4 Estimated differences between the wavelengths of peak transmittance ( $\lambda_{\theta}, \lambda_{\text{eff}}$ ) of an interference filter when illuminated by collimated and coned (semi-angle  $\phi_1$ ) beams of light incident at an angle  $\theta$ .

$$\lambda_{\theta} - \lambda_{\text{eff}} = \frac{\lambda_0 \phi_1^2}{16\mu} (3 \cos^2 \theta - 1), \quad \phi_1 \text{ in radians.}$$

$$\lambda_0 = 4874 \text{ \AA}, \quad \mu^* = \sqrt{2}.$$

Equations 2.10 and 2.11 show that when an interference filter is illuminated by a cone of light of semi-angle  $\phi_1$  with axis normal to the filter, the resulting wavelength shift of the effective passband is one quarter of the wavelength shift produced by illuminating the filter with parallel light from a point source incident at an angle  $\phi_1$  to the filter.

Determination of the exact increase in the half-width of the effective instrumental profile after broadening due to the spread in angle within the seeing cone requires the double integral in Equation 2.5 to be evaluated. As an alternative, an order of magnitude for the effect may be obtained by adopting a simplified approach. Consider, for example, the broadening of the passband which would be brought about if the seeing disc was extended in only one direction.

Suppose, in Equation 2.4, that  $\alpha = \pi/2$  (and  $3\pi/2$ ) and suppose further that an upper limit for the increase in bandwidth of the filter can be estimated by the difference between the wavelengths of peak transmittance for the two extreme rays of the cone given by  $\phi = \phi_1$  ( $\alpha = \pi/2$  and  $3\pi/2$ ). If these wavelengths are  $\lambda_1$  and  $\lambda_2$ , then they are given by Equation 2.4 as

$$\begin{aligned}\lambda_1 &= \lambda_0 - \frac{\lambda_0}{2\mu^*2} \left\{ 1 - \left[ \sin \theta \sin \phi_1 + \cos \theta \cos \phi_1 \right]^2 \right\} \\ &= \lambda_0 - \frac{\lambda_0}{2\mu^*2} \left\{ 1 - \cos^2 (\theta - \phi_1) \right\}\end{aligned}$$

$$\begin{aligned}\text{and } \lambda_2 &= \lambda_0 - \frac{\lambda_0}{2\mu^*2} \left\{ 1 - \left[ -\sin \theta \sin \phi_1 + \cos \theta \cos \phi_1 \right]^2 \right\} \\ &= \lambda_0 - \frac{\lambda_0}{2\mu^*2} \left\{ 1 - \cos^2 (\theta + \phi_1) \right\}\end{aligned}$$

The above expressions for  $\lambda_1$  and  $\lambda_2$  apply for cases where  $\theta > \phi_1$ . For small

amounts of tilt where  $\theta < \phi_1$ , the long wavelength limit of the filter pass-band is merely  $\lambda_1 = \lambda_0$ . The increase in bandwidth,  $\Delta\lambda$ , can therefore be estimated by

$$\begin{aligned} \Delta\lambda &= \lambda_1 - \lambda_2 \\ \text{i.e. } \Delta\lambda &= \frac{\lambda_0}{2\mu^*2} \left( \sin^2 (\theta + \phi_1) - \sin^2 (\theta - \phi_1) \right), \text{ where } \theta > \phi_1 \\ &= \frac{\lambda_0}{2\mu^*2} 2 \sin \theta \cos \phi_1 \cdot 2 \cos \theta \sin \phi_1 \\ \text{i.e. } \Delta\lambda &= \frac{\lambda_0}{2\mu^*2} \sin 2\theta \sin 2\phi_1, \quad \theta \geq \phi_1 \\ \text{or } \Delta\lambda &= \frac{\lambda_0}{2\mu^*2} \sin^2 (\theta + \phi_1), \quad \theta \leq \phi_1 \end{aligned} \quad \left. \vphantom{\begin{aligned} \Delta\lambda &= \lambda_1 - \lambda_2 \\ \text{i.e. } \Delta\lambda &= \frac{\lambda_0}{2\mu^*2} \left( \sin^2 (\theta + \phi_1) - \sin^2 (\theta - \phi_1) \right), \text{ where } \theta > \phi_1 \\ &= \frac{\lambda_0}{2\mu^*2} 2 \sin \theta \cos \phi_1 \cdot 2 \cos \theta \sin \phi_1 \\ \text{i.e. } \Delta\lambda &= \frac{\lambda_0}{2\mu^*2} \sin 2\theta \sin 2\phi_1, \quad \theta \geq \phi_1 \\ \text{or } \Delta\lambda &= \frac{\lambda_0}{2\mu^*2} \sin^2 (\theta + \phi_1), \quad \theta \leq \phi_1 \end{aligned}} \right\} \quad (2.12)$$

Equation 2.12 expresses the increase in filter bandwidth,  $\Delta\lambda$ , as a function of the angle of inclination of the filter to the optical axis,  $\theta$ , and of the semi-angle of the illuminating cone,  $\phi_1$ , and  $\Delta\lambda$  is plotted as a function of  $\theta$  in Figure 2.8. It should be noted that this approach neglects the intensity distribution with angle within the seeing cone and that the values of  $\Delta\lambda$  obtained are an upper limit since the effect is largest for rays for which  $\alpha = \pi/2$  or  $3\pi/2$ . Clearly, as seen in Figure 2.8, the effect is an important one and changes of a filter's bandwidth due to seeing effects will result in changes in the transmitted signal. This topic will be discussed more fully in Chapter 4.

The statement made earlier in Section 2.2 regarding the ability of an interference filter to accept entirely a seeing disc whose diameter is in excess of 10 arc seconds must now be modified to state that this is only valid if the angle of tilt of the filter is small. When the filter is at normal

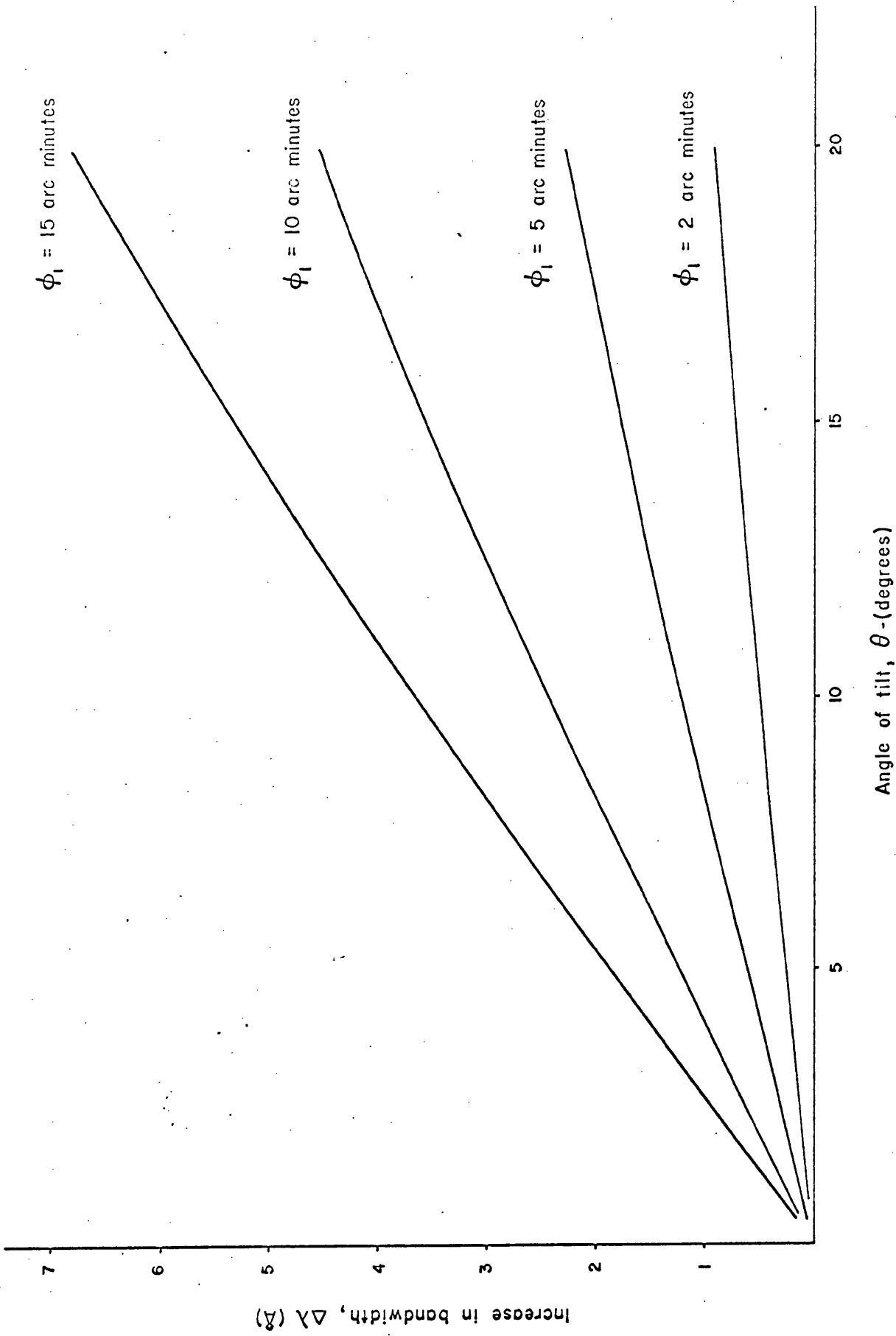


Figure 2.8 Estimated variation of bandwidth when a filter is tilted in a coned beam of semi-angle  $\phi_1$ .

incidence ( $\theta = 0$ ), the amount of broadening of the passband is given by

$$\Delta\lambda = \frac{\lambda_0}{2\mu^2} \sin^2 \phi_1$$

and  $\Delta\lambda < 0.1 \text{ \AA}$  for  $\phi_1 = 30$  arc minutes (i.e. a seeing disc  $\sim 60$  arc seconds in diameter).

As an illustration of the effect, the instrumental profile of the  $2.2 \text{ \AA}$  filter (see Table 2.3) was measured at various angles of tilt as before, except that a larger diaphragm was placed in the focal plane of the telescope (the diameter was 10 times that of the smaller diaphragm normally used for wavelength calibrations and was equivalent to 50 arc seconds on the sky for the 50 cm f/8 telescope at Glasgow ( $F_T/F_C = 80$  and  $\phi_1 = 33$  arc minutes)). It was found that the instrumental half-widths had increased to  $5.1 \text{ \AA}$  at  $4861.3 \text{ \AA}$  (H $\beta$ ) ( $\theta \simeq 6^\circ$ ) and  $9.9 \text{ \AA}$  at  $4810.5 \text{ \AA}$  (Zn) ( $\theta \simeq 13^\circ$ ). It must be remembered that the cone of light from the fibre optic pipe will not be the same as the cone from a stellar seeing disc but this example shows that the effect does exist in practice. By performing normal wavelength calibrations with a very small focal plane diaphragm, it is hoped that the above effects produced by the convergent light from the fibre optic pipe will be reduced to a minimum.

Another complication in the broadening of the filter passband is apparent when polarization is considered. Calibrations have been performed with linearly polarized light whose azimuth of vibration was first set parallel to the tilt axis and then normal to it. It was found that each plane of vibration gave its own calibration curve, as shown in Figure 2.9, and that the rate of change of wavelength with tilt was greater when the plane of vibration was parallel to the tilt axis. The different rates of change of wavelength with tilt are the result of the reflection coefficients of the

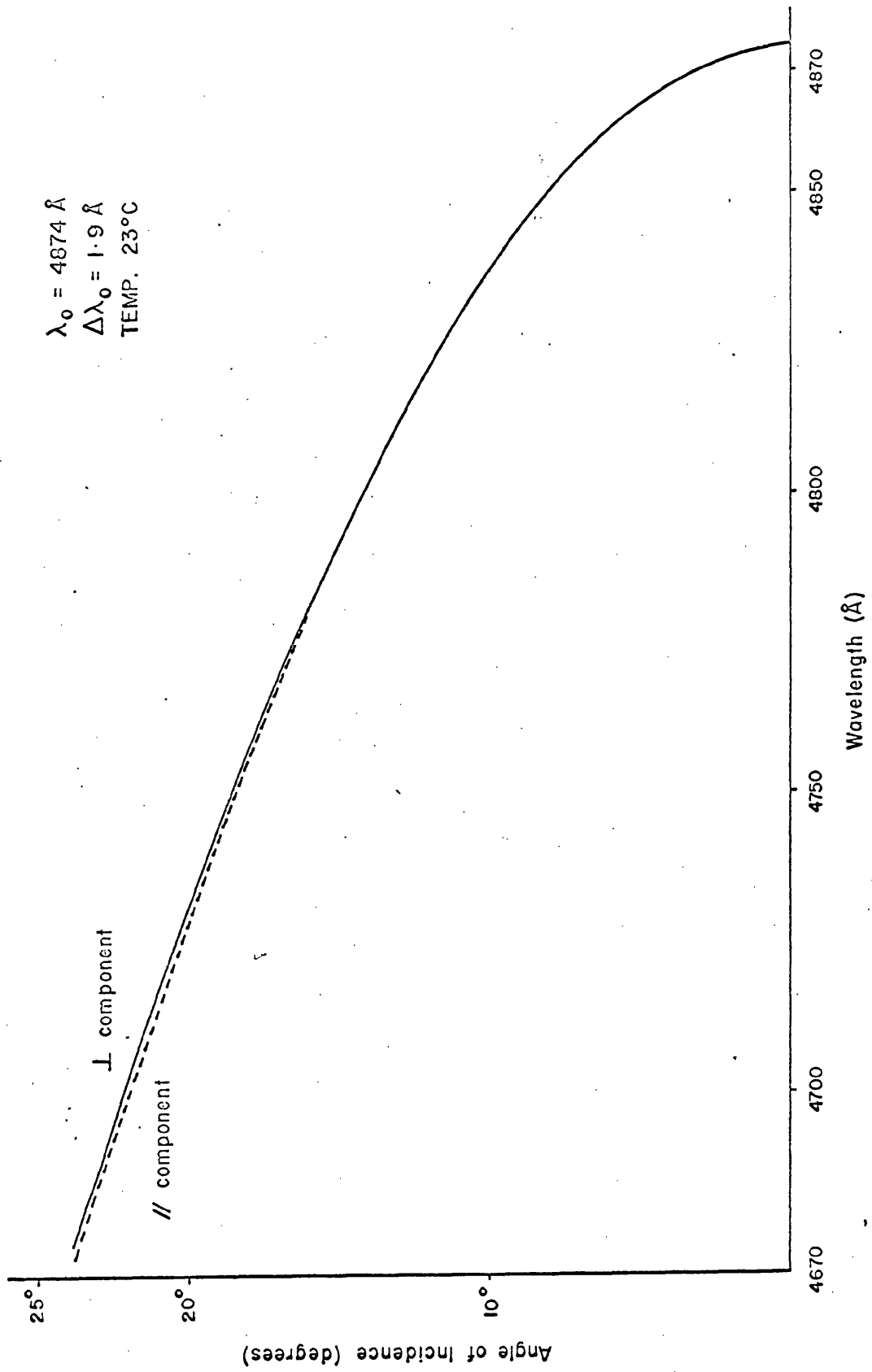


Figure 2.9 Wavelength/tilt calibrations for one of the narrow band filters measured for two orthogonal directions of vibration of polarized light. The separation of the passbands is  $\sim 2 \text{ \AA}$  when the angle of incidence is  $\sim 22^\circ$ .

dielectric layers, and hence  $\mu^*$ , being dependent on the direction of vibration and the angle of incidence of the incident light. Additionally, the phase change introduced on internal reflection at the boundary between the spacer and the dielectric layers is not exactly equal to  $\pi$  and the departure from  $\pi$  is also dependent on the direction of vibration and the angle of incidence of the incident light.

The effect that this has on unpolarized light is to split the passband into two parts, the separation of which increases with tilt and is about  $2 \text{ \AA}$  at a tilt of  $22^\circ$ . Broadening by this means can largely be avoided by placing a polarizer in the optical system, prior to the filter, so ensuring that the filter is only illuminated with light having one fixed plane of vibration. If the polarizer also serves as a beamsplitter so as to provide a sky transparency monitor channel, very little additional light is lost in this system as opposed to one using a non-polarizing beamsplitter.

Finally, line profiles recorded by the tilt-scanning technique might be affected by changes in the filter's transmittance with tilt. It might also be thought that the increase in filter half-width would cause an increase in signal level, however, due to the decrease of transmittance with tilt, this effect is partly compensated for. Scans of a white light source have been performed to investigate the variation of signal level with tilt that might be expected when scanning a stellar continuum.

The white light source consisted of a Ferranti GRD 7 diode, operated at a heater current of 1.8 amp. According to the manufacturer this gives the filament an operating temperature of  $2,200^\circ\text{K}$ . If the heater is assumed to behave like a black body, then the intensity as a function of wavelength can be determined from the Planck formula. Figure 2.10 shows the ratio of the relative intensity recorded to that predicted from the black body curve,

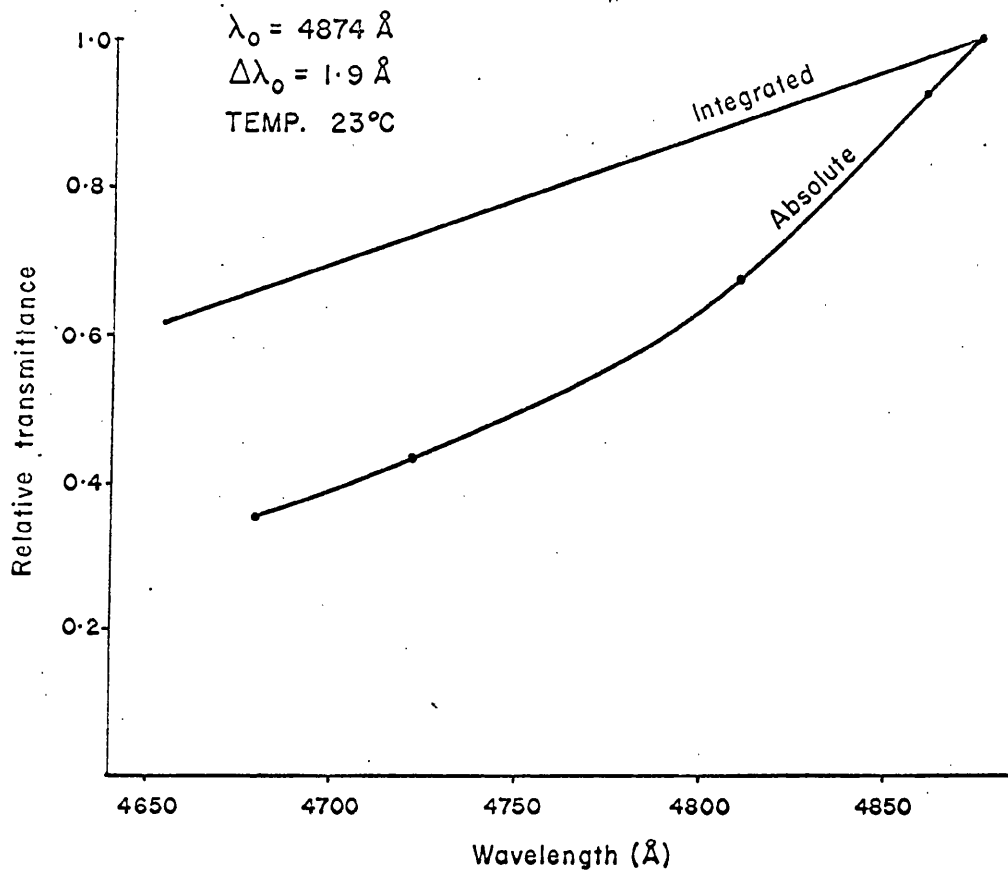


Figure 2.10

Variation of integrated filter transmittance with wavelength ( $\equiv$  tilt) derived by scanning a black body source and rectifying to a flat spectrum. If allowance is made for the increase of filter bandwidth with tilt, the absolute transmittance can be estimated at the wavelength of each of the calibration lines.

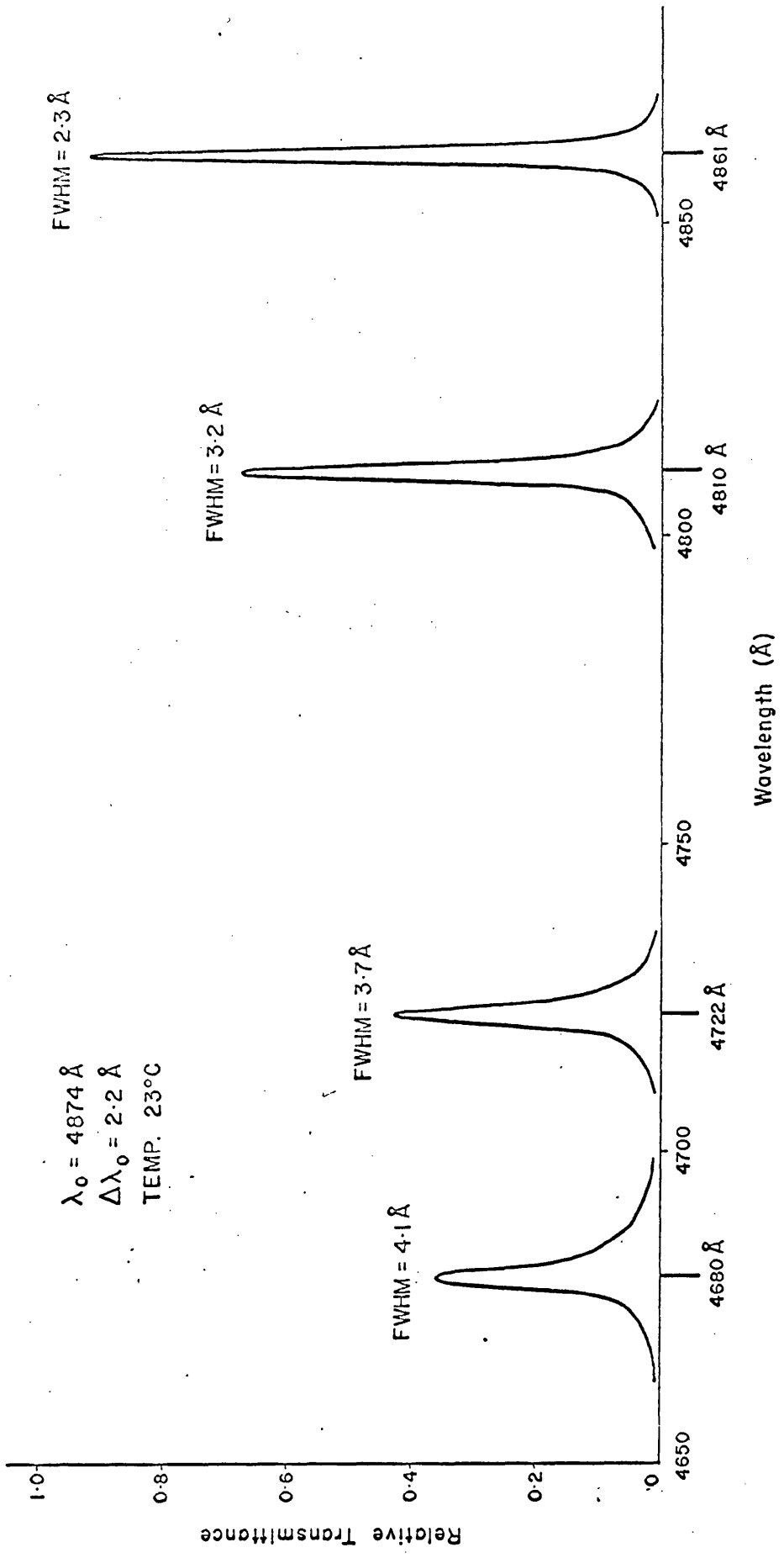


Figure 2.11

Variation of a filter transmission profile with wavelength ( $\equiv$  tilt) obtained by scanning laboratory spectrum lines. The intensities are scaled according to the variation of the filter's absolute transmittance with wavelength (see Figure 2.10).

that is, the true variation of signal with tilt after removing the slope of the Planck function. This may also be interpreted as a relative integrated transmittance and if allowance is made for the increasing half-width in scanning from  $4874 \text{ \AA}$  to  $4680 \text{ \AA}$ , the absolute transmittance can be estimated at each of the wavelengths at which the half-width is known. This is also shown in Figure 2.10.

If the measured instrumental profiles at each of the four calibration lines are scaled according to the absolute relative transmittance as given in Figure 2.10, then the profiles may be drawn on the one intensity scale as in Figure 2.11.

## 2.6 Purity of Recorded Line Profiles

Line profiles of  $H\beta$  have been measured for several stars for comparison with simulated scans in order to assess their quality.

Appropriate sections of the solar spectrum (Minnaert et al., 1940) and the Arcturus ( $\alpha$  Boo) spectrum (Griffin, 1968) were first digitised and then scanned numerically with various Airy functions having half-widths equal to those of the interference filters. The simulated spectra obtained in this way are presented in Figures 2.12 and 2.13 along with recorded  $H\beta$  profiles for  $\alpha$  Aur (G0),  $\alpha$  Boo (K2 III p) and  $\beta$  Gem (K0 III).

It is fair to say that the recorded profiles match the simulated ones reasonably well. The only reduction procedures used on the recorded profiles have been the conversion to a linear wavelength scale and normalisation to some arbitrary position on the blue continuum.

Clearly, over the wavelength range of these scans, the effects of changes of filter transmittance and half-width are relatively unimportant.

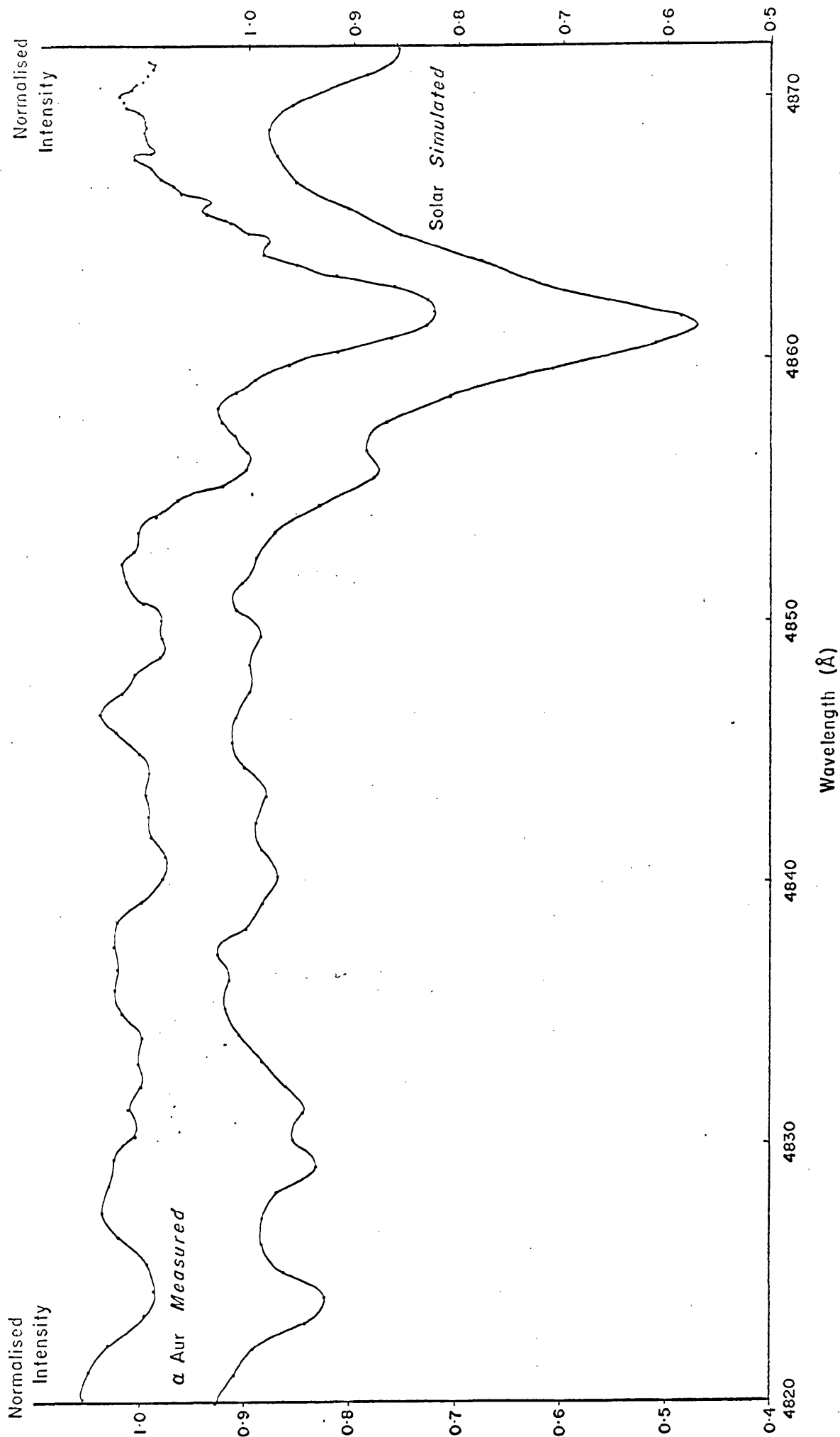


Figure 2.12 H $\beta$  profile for  $\alpha$  Aur (GO), measured with 4874/2.2 Å ( $\lambda_0/\Delta\lambda_0$ ) filter, compared with a convolution of an Airy function (2 Å half-width) with a digitised solar H $\beta$  profile.

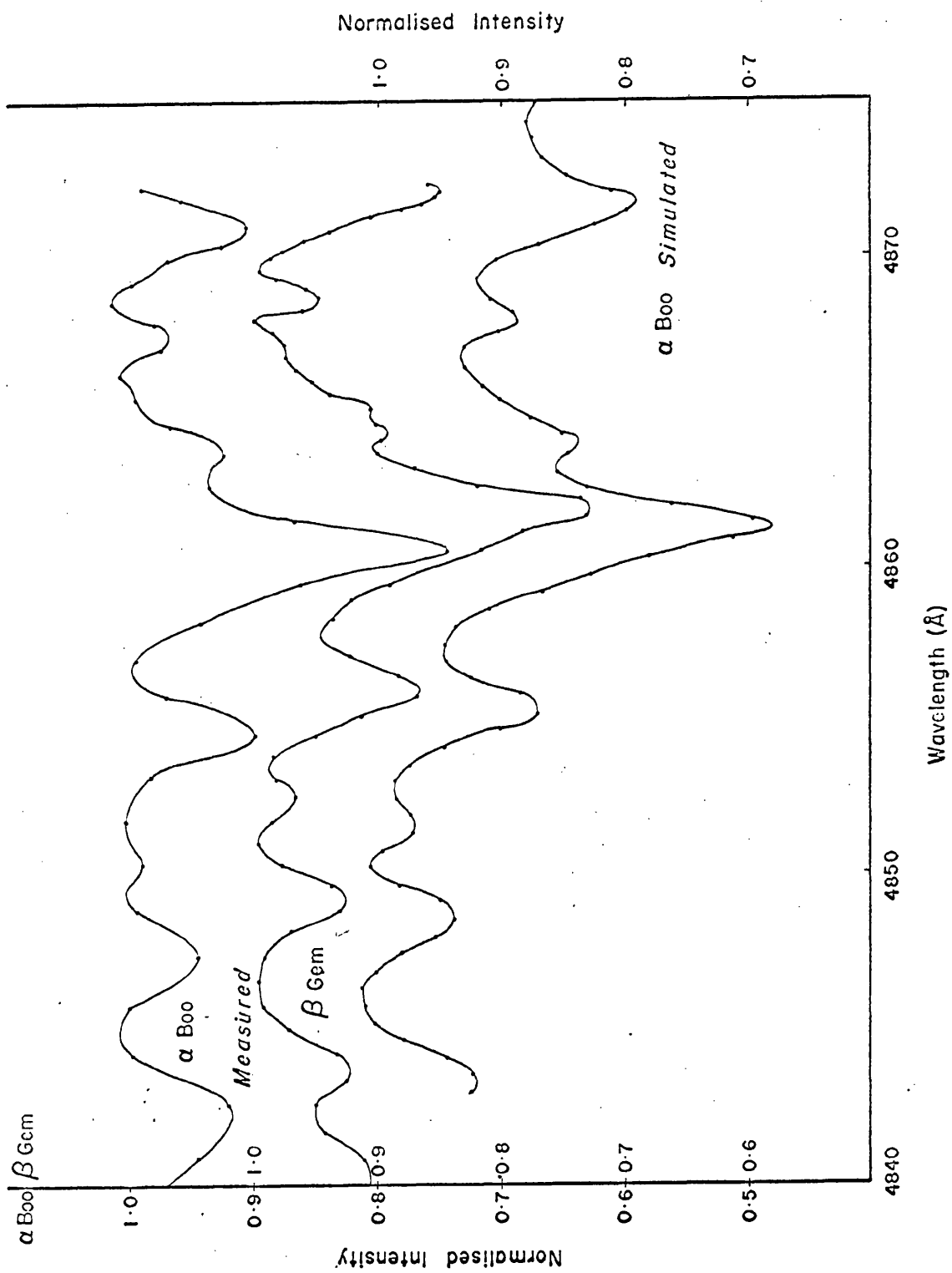


Figure 2.13 H $\beta$  profiles for  $\alpha$  Boo (K 2 III p) and  $\beta$  Gem (K 0 III), measured with 4874/1.9  $\text{\AA}$  filter, compared with a convolution of an Airy function with a digitised H $\beta$  profile for  $\alpha$  Boo.

The quality of these records supports the belief that line profiles obtained by tilt-scanning narrow band interference filters are sufficiently well recorded as to provide a possible means of detecting rapid intrinsic variations of  $H\beta$  in certain classes of stars. Moreover, the resolution obtained while accepting the entire seeing disc can only be matched by a large grating spectrometer and even then, the overall transmittance of the latter is so low as to require a large collecting telescope and suffers a loss of time resolution.

### 3. INSTRUMENTATION AND DATA HANDLING

#### 3.1 Introduction

At the start of this study in October, 1972, the application of tilt-scanning with narrow band interference filters to obtain stellar line profiles was already being explored at Glasgow University Observatory. The instrument that was then attached to the telescope was a double-beam polarimeter in which interference filters were being tilt-tuned to isolate particular regions of the hydrogen H $\beta$  line in stellar spectra in order to measure differential polarization across the spectrum line. The filters were tilted by a micrometer and lever arm system which could either be turned by hand or could be rotated continuously by a small synchronous motor. This polarimeter/photometer used pulse counting when measuring polarization but the electronic system was not constructed to provide digital control of the wavelength scan and the profiles that were obtained were usually measured by a D.C. amplifier and recorded on a pen chart recorder. No compensation was made for atmospheric effects and, as expected, the profiles were very noisy due to atmospheric scintillation. It was decided, therefore, to design and build a completely new photometer head with the aim of measuring stellar line profiles by the tilt-scanning technique. An electronic control and data recording system was also designed and built with this particular photometer in mind.

The photometer head and much of the electronics chassis were machined entirely by Mr. W. Edgar of the University Observatory. The control electronics are based on TTL Integrated Circuits (I.C.'s; TTL = Transistor-Transistor Logic) and were designed and built by the author. Because of unavoidable delay in the supply of components, the photometer did not become operational until April, 1974. Since that date, the photometer has been used on most clear nights in Glasgow.

The entire system was taken by car from Glasgow to the Royal Greenwich Observatory (RGO) in October 1974 when it was used on 14 nights with the 91 cm

Yapp reflector. During the period April 1974 - March 1975, the photometer and electronics underwent numerous modifications as regular observations revealed further areas for improvement.

In April 1975, the photometer was shipped to South Africa for use with the telescopes on the South African Astronomical Observatory (SAAO) site at Sutherland. The photometer was attached to the 76 cm reflector for 3 nights in April and was attached to the 50 cm reflector for 6 nights in April and 7 nights in May. In all of the above-mentioned telescope changes, the photometer was mounted and the telescope balanced in less than 2 hours. The electronics can be cabled-up in 30 minutes and have always worked immediately except on first arrival in South Africa when there was some minor damage caused by a transformer breaking loose of its mountings during shipping.

The simplicity of design together with small size and low weight while having a working resolution of  $2 \text{ \AA}$  are among the main attractions of the interference filter scanner.

### 3.2 The Photometer Head

A simple double-beam photometer has been designed and constructed for the application of measuring stellar line profiles by tilt-scanning narrow band interference filters. Among the design considerations were size and weight, since the photometer was to be attached in the first instance to the 50 cm Grubb Parsons reflector at Glasgow.

The basic optical and mechanical arrangements are shown in Figures 3.1 and 3.2. The waveplate wheel shown in Figure 3.2 was added in October 1974, before visiting the RGO, to allow differential polarimetry across spectrum lines to be studied. The wheel has 6 apertures at click-stop positions. Three of the apertures contain  $\lambda/2$  (half-wave) retarders mounted such that when they are in the beam their axes are at  $0^\circ$ ,  $30^\circ$  and  $60^\circ$  to the polarization axis of the polarizing prism. Another two apertures contain  $\lambda/4$  (quarter-wave) retarders mounted with their axes at  $45^\circ$  and  $135^\circ$  to the axis of the

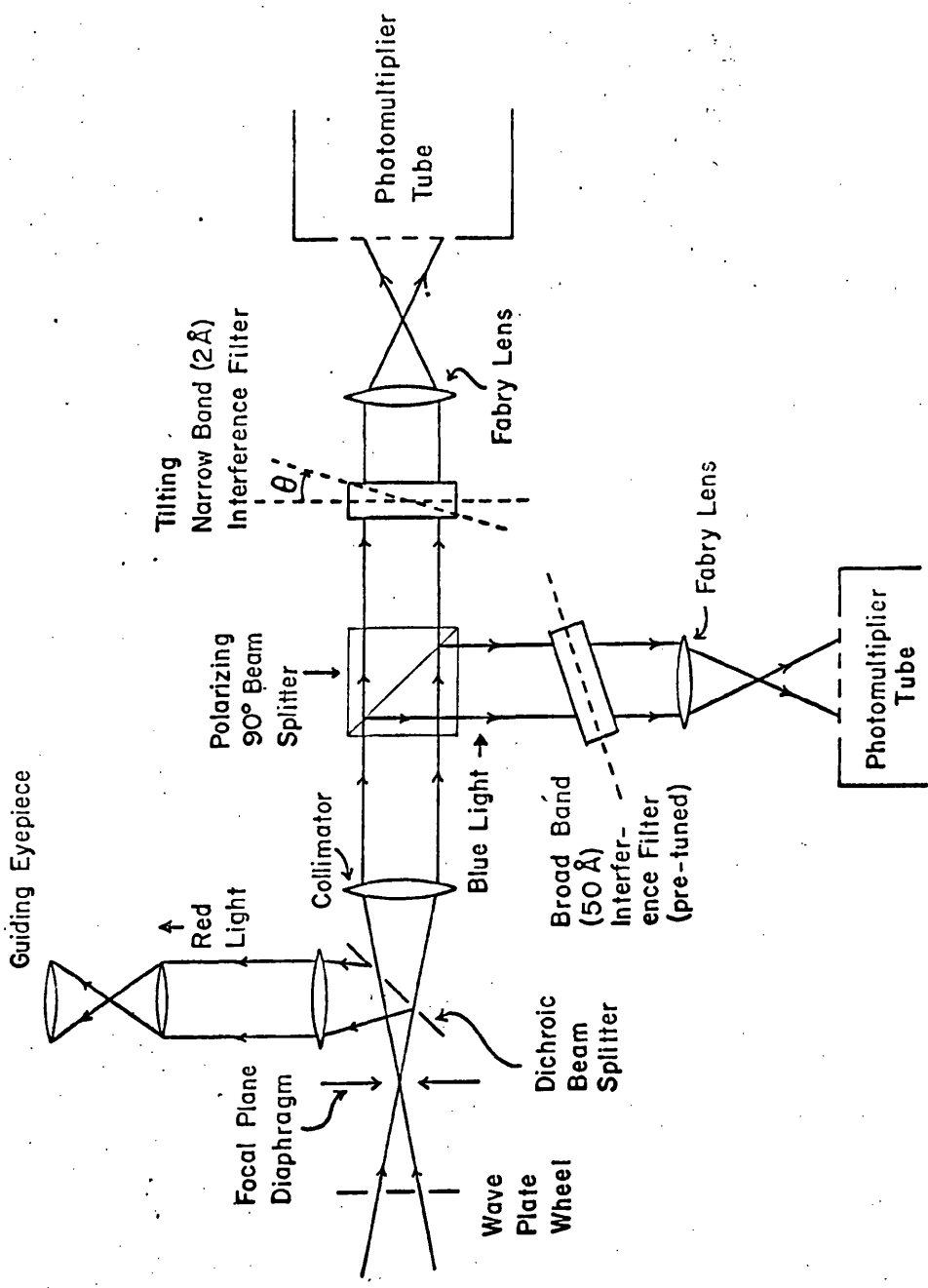


Figure 3.1.

Schematic optical layout of the tilting-filter scanner. The wave-plate wheel was normally positioned at a clear aperture. Both filters, positioned as close as possible to where the collimator images the telescope aperture, are imaged on the photomultipliers by the Fabry lenses.

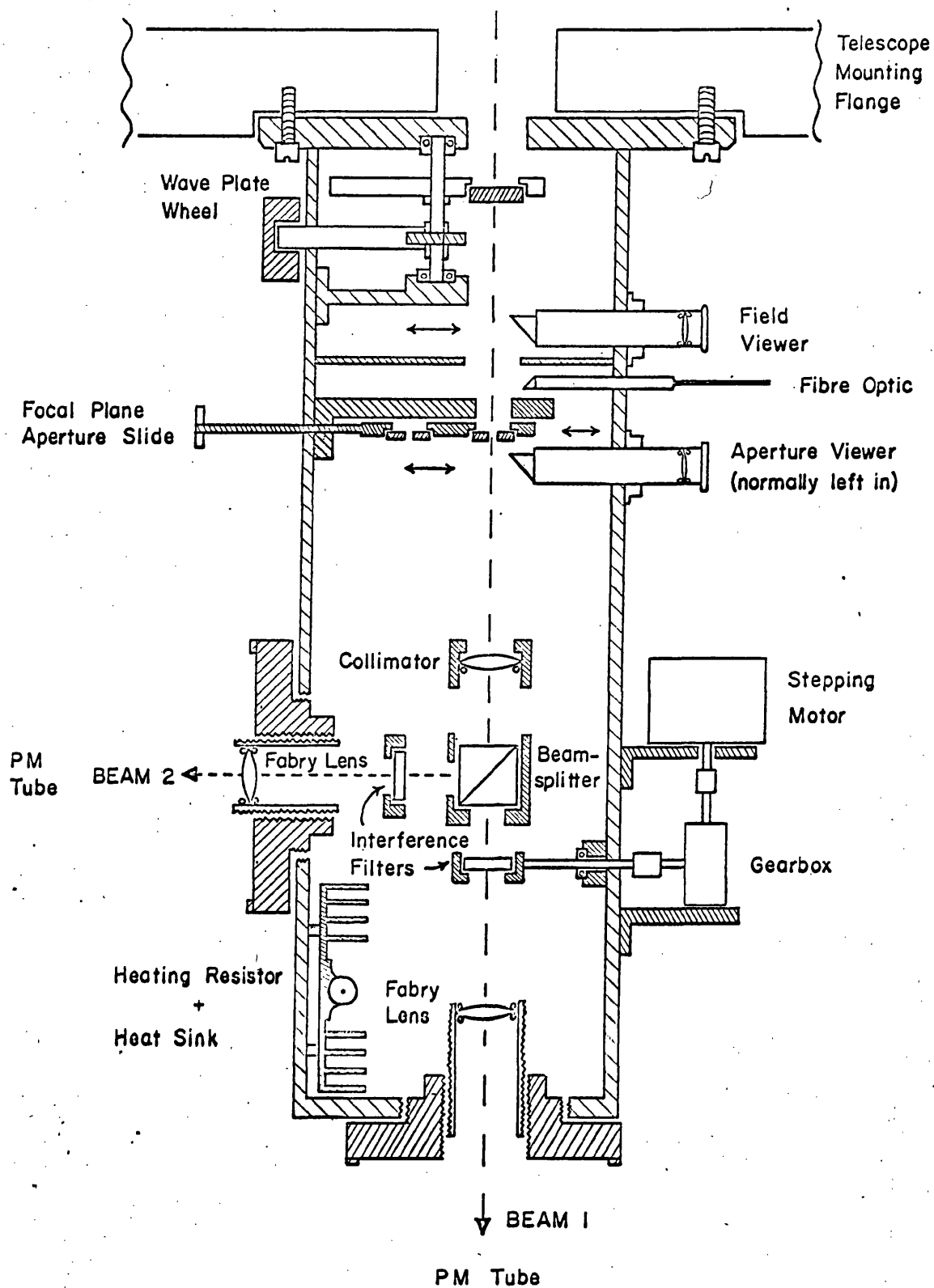


Figure 3.2 Cross-sectional diagram of the tilting-filter scanner.

prism. The sixth aperture is clear and is the one normally in the beam when measuring intensity line profiles. The wave-plate wheel is rotated to click-stop positions by hand with a knob, external to the photometer, attached to the wheel via a set of helical gears.

Mounted in the focal plane of the telescope is a slide containing two diaphragms whose diameters are equivalent to 50 arc seconds and 5 arc seconds on the sky. (These figures are for the 50 cm, f/8 telescope at Glasgow). In Glasgow, the larger diaphragm is normally chosen for stellar measurements since the diameter of the seeing disc is often  $\sim 10$  arc seconds and the telescope tracking is rather poor. The smaller diaphragm always replaces the large one for wavelength calibration.

On either side of the diaphragm are two viewers. The pre-viewer consists of a roof-prism which can be pushed into the beam and serves to locate the desired star in the field. The post-viewer enables the star to be centred in the diaphragm. Originally the second viewer was also a roof-prism mounted on a draw-tube. When this was the case, guiding on the star was done by a small auxiliary guiding telescope attached to the side of the main telescope. Ideally some sort of off-set acquisition and guiding head should have been provided but this would have considerably increased the size and weight of the photometer and was felt to be unnecessary.

It was found by October 1974, however, that due to a lack of collimation between most main and guiding telescopes, a star could be kept central in the diaphragm only for several minutes before the cross-wires of the guider needed resetting. This was apparent with the 50 cm telescope at Glasgow and the 91 cm telescope at the RGO. The effect of guiding errors on the line profiles will be discussed in Chapter 4.

In order to overcome this problem it was decided to replace the prism of the post-viewer with a dichroic filter. A filter was obtained such that, when

inserted in the beam at  $45^\circ$  to the optic axis, it would reflect red light for guiding while blue light which still contained  $H\beta$  would be transmitted. This filter is now left in the beam permanently, even for wavelength calibrations, and results in a drop in transmission at  $H\beta$  of about 10%.

Beyond the dichroic filter is a collimator lens, mounted in a sliding tube so as to allow focussing. The positioning of the collimator can be checked by ensuring that the light reflected from either filter is brought to a focus on the surface of the diaphragm. The collimator has a focal length of 4.8 cm giving a value of  $F_T/F_C$  of  $\sim 80$  for the Glasgow telescope. The resulting collimated beam is 0.6 cm in diameter.

Following the collimator, the beam is divided into two linearly polarized components by a 2.5 cm cube polarizing beam-splitter. Light of one plane of vibration is transmitted while the orthogonally polarized component is reflected at  $90^\circ$  to the telescope optic axis. The reflected beam passes through a relatively broad band interference filter ( $\sim 50 \text{ \AA}$ ) and provides a fixed wavelength monitor channel so as to allow compensation for atmospheric effects.

The transmitted beam passes through the scanning narrow band filter. Tilting of this filter is done by a stepping motor linked to the filter cell through an anti-backlash gearbox. The stepping motor has a single step movement of  $7.5^\circ$  and the reduction ratio of the gearbox is 60:1 giving a rotation of  $0.125^\circ/\text{step}$  at the filter. This corresponds to about  $0.5 \text{ \AA}/\text{step}$  at  $H\beta$  and  $1 \text{ \AA}/\text{step}$  at  $4800 \text{ \AA}$  for the narrow band filters used. Scales and moving pointers are provided externally on both the stepping motor shaft and the filter driving shaft so that the mechanical positioning of the filter may be checked against an electronic position indicator.

Both filters are 2.5 cm in diameter and each is mounted as close as possible to a position at which the collimator forms an image of the telescope aperture. These images and the collimated beams are then imaged on the photo-

cathodes of the photomultiplier tubes by means of Fabry lenses. In this way, the beams should not move across the surface of either the filters or the photocathodes if the star image moves in the focal plane of the telescope. The focal lengths of the Fabry lenses are  $\sim 4$  cm and give illuminated spots of 0.6 cm diameter on the 1 cm diameter photocathodes.

Light for wavelength calibration, as stated previously in Chapter 2, is fed into the photometer by a fibre optic pipe mounted on a push-pull tube which is inserted into the beam prior to the focal plane diaphragm.

The interior of the photometer is maintained at a constant temperature by a proportional temperature controller. This device, housed in the electronics crate, was obtained commercially and operates by having a duty cycle which automatically decreases as the set temperature is neared. Heating of the air within the photometer is done by a 30 Watt resistor mounted on a heatsink and thermally insulated from the photometer wall. The air temperature is monitored by a small thermistor which forms a remote part of the temperature controller circuit. In order to achieve a uniform temperature independent of telescope orientation, the air inside the photometer is mixed continuously by a small model boat propellor driven by a low voltage D.C. motor.

The exterior of the photometer has been covered with foam polystyrene to reduce heat loss to the external air. Even without insulation, the photometer could reach its operating temperature and stabilise within 20 to 30 minutes. Because of the rapid warm-up time, the temperature controller was switched off during daylight and was normally switched on about 1 hour before starting observations.

The original home-made photomultiplier housings have been replaced with commercial units (Products for Research Inc.). The new housings have magnetic, electrostatic and R.F. shielding but are uncooled. They were chosen in preference to cooled housings for reasons of cost, weight and size, and perform

adequately without cooling for the bright stars studied so far. Additional magnetic shielding of the stepping motor is provided by mu-metal foil.

The photometer head, without photomultiplier housings, measures approximately 30 x 15 x 10 cm, and weighs only 12 kg complete with photomultipliers and pre-amplifiers.

### 3.3 Electronics

The electronic system consists of two main parts; signal detection, including data recording, and wavelength scanning control. These two functions are synchronised and accurately timed by further logic circuits. A block diagram of the electronic system is shown in Figure 3.3.

The detectors of the data recording system consist of two photomultiplier tubes (EMI types 9502B and 9789B) with dynode chains wired for pulse counting. Both photomultiplier tubes obtain their EHT from the same stabilised power supply. One EHT line, however, contains an additional potentiometer so that a limited but independent voltage adjustment is possible for that line. By running both photomultiplier tubes off the same EHT supply differential changes in the gains of the tubes due to EHT voltage fluctuations can largely be avoided. This is an important point if the ratio between the two signals is to be formed. The photocathodes are run at a negative potential ensuring that the anodes are close to ground potential thus eliminating the need for coupling capacitors. The output pulses are negative going and about 20 nS (nano-seconds) wide.

The pre-amplifiers/discriminators are a variation of a circuit developed by the staff of the Royal Observatory, Edinburgh (ROE). Thanks are due to Mr. W. Parker and Mr. I. Sheffield of the ROE for the printed circuit layout from which the circuits were developed.

Photomultiplier pulses are fed directly to one input of a Signetics NE527K integrated circuit with a 1 k $\Omega$  leakage resistor connected to ground.

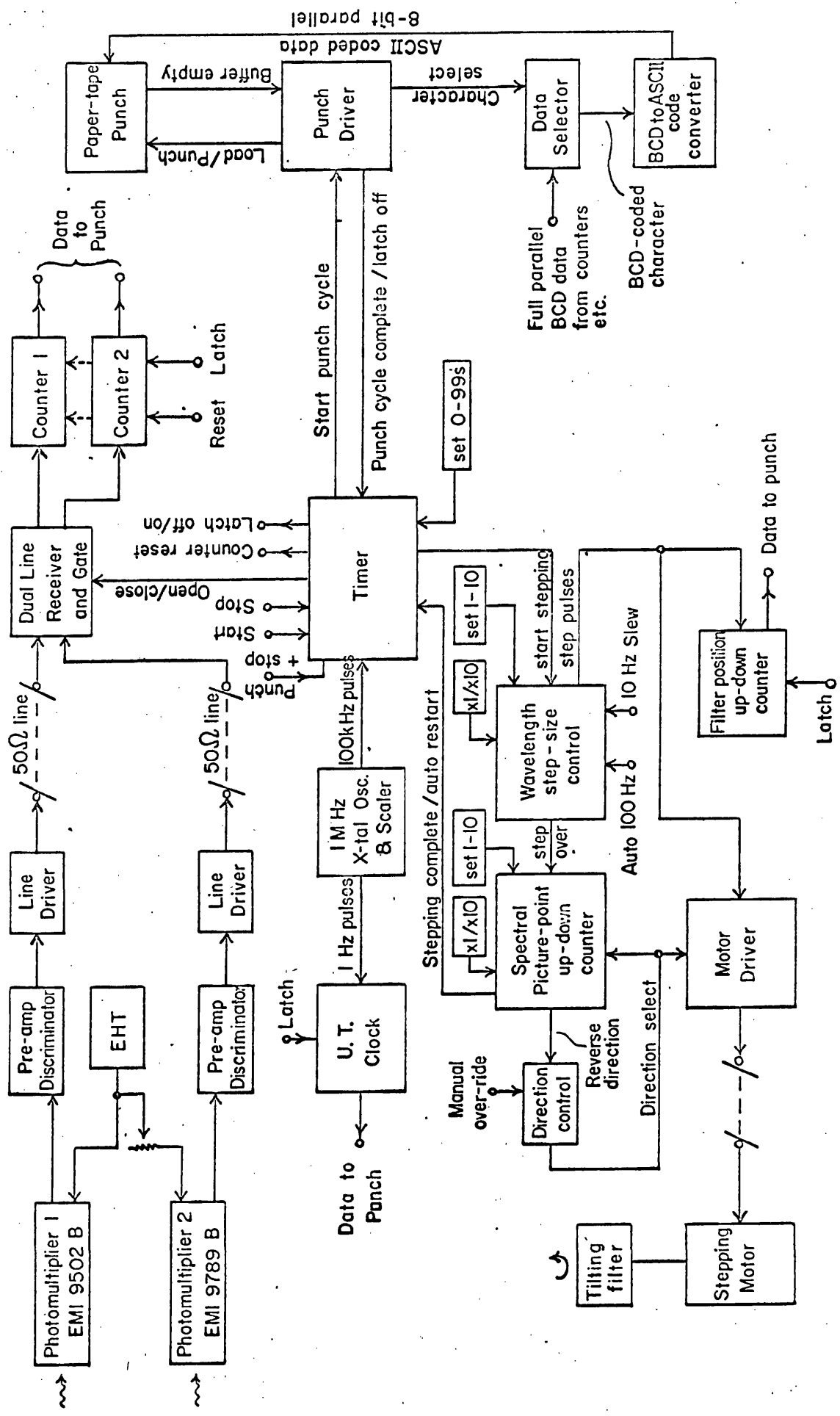


Figure 3.3 Block diagram of the electronic control and data recording system

The other input is connected to a multi-turn potentiometer which forms part of a voltage divider chain and serves to set the discriminator threshold. Pulses exceeding the discriminator voltage appear at the output of the NE527K as TTL level pulses which are fed to a dual TTL monostable (SN74123). One half of the monostable defines a dead-time of 400 nS (resulting in a maximum count rate of 2.5 MHz) while the other half produces pulses of constant width ( $\sim 150$  nS) which are then fed to a line-driver integrated circuit (SN75110). This is a constant current type driver and is capable of driving twisted-pair lines up to 3000 metres long. The signal cables are, in fact, 50-ohm co-axial cable for which the driving capabilities are less than for twisted-pair but are still well in excess of the 20 metres required between the photometer and the electronics crate.

At the receiving end, each line is fed to one of the inputs of a dual line receiver (SN75107). The lines are suitably terminated with resistors to prevent pulse overshoot. The other inputs of the line receivers are connected to variable voltage dividers so as to allow discrimination against any noise on the lines. The dual line receiver also gates the signals to the pulse counters and both channels are strobed simultaneously and for the same duration by the integration timer.

The signal in each channel is recorded on a separate 6-decade counter. A hard copy of the data is produced on punched paper tape but only the five most significant digits in each counter channel are recorded. These digits are also displayed on cold-cathode number tubes. The Universal Time (U.T.), filter position and spectral picture-point are displayed on miniature seven-segment LED (Light Emitting Diode) displays.

The control electronics, counters and stepping motor drive together with appropriate power supplies are housed in one cabinet measuring 52 x 40 x

30 cm. The punch interface is contained in another case measuring 20 x 30 x 15 cm. The operation of the main logic circuitry is described below.

The time-base for the timer, U.T. clock and wavelength stepping is derived from a 1 MHz crystal oscillator (Heath EU 800-Kc). The oscillator has an accuracy of  $\pm 2$  Hz, a temperature stability of  $\pm 10$  ppm (parts per million) from 10 - 40°C and an ageing rate of less than 10 ppm/year. Outputs from a seven decade scaler allow frequencies of 1 MHz to 0.1 Hz to be obtained simultaneously from the oscillator.

The integration timer runs at a frequency of 100 kHz to ensure that gating errors will be small. The 100 kHz frequency is divided down to 1 Hz pulses which are counted by a two decade counter allowing integration times of 1 - 99 seconds. On pressing the manual start button, the line receiver gates are opened and the timer commences counting 1 Hz pulses. When the number of elapsed seconds is equal to the value preset from the front panel, the signal gates are closed and the timer is stopped. At the same time, the data to be punched on paper tape is latched, allowing counting to restart before the punching cycle is complete. In this way, the dead-time between integration periods is  $\sim 250$  mS depending on the wavelength scanning requirements. (The Data Dynamics paper-tape punch operates at 46 characters/sec and requires about 700 mS to punch the 32 characters in each punch cycle).

A delay of 7  $\mu$ S is allowed after latching the data before the punch cycle is activated. After a further 70 mS delay, and while punching is taking place, both timer and signal counters are reset to zero and wavelength scanning is initiated. The wavelength step-size is set by a front panel switch at 1 - 10 steps with an optional x10 multiplier. Pulses at a frequency of 100 Hz from the crystal oscillator are counted and passed to the stepping motor drive and the filter position indicator circuits. The filter position display is

latched at its previous setting while punching is taking place. Its value is recorded on the paper tape and serves to identify each wavelength position at which the filter is set. The counter has a range of 0 - 199 (originally 0 - 99, but this gave too limited a scan range) and covers a tilt range of  $25^{\circ}$  (equivalent to more than 200 Å for the narrow filters used for tilt-scanning). The counter will count up or down according to the scan direction control.

When the number of pulses counted in any one wavelength change is equal to the value preset on the front panel, stepping is ceased and the step size counter is reset. A single pulse is also sent to the spectral picture-point counter to indicate that the new wavelength position has been reached.

The number of picture-points in a scan is also set via front panel switches at 1 - 10 points with a x10 option. The picture-point counter is also of the up-down type and when the count becomes equal to either that set on the switches or zero, a pulse is generated to reverse the scan direction. The pulse from the wavelength step-size control to the picture-point counter is delayed by 150 mS and also serves to restart the integration timer after the new wavelength position has been reached. The delay of 150 mS allows any stepping motor jitter to subside before the signal gates are re-opened.

Various functions exist to allow initial setting of the filter position. The scan direction can be changed manually and may be latched in either direction thus over-riding the direction control of the picture-point counter. The stepping motor can be slewed to any starting position at a rate of 10 steps/second and it can also be single stepped. In addition, the wavelength scan can be completely inhibited so that repetitive measures may be made at the same wavelength. Alternatively, the stepping motor may be inhibited by itself so as to allow the initial correspondence between the mechanical filter position and that indicated by the electronic filter position counter to be set as desired.

The main electronics cabinet also houses a 24-hour digital clock which is run from 1 Hz pulses from the 1 MHz oscillator. Switching of the 1 Hz pulses allows the hours or minutes to be slewed separately at 1 count/second so as to preset the clock to the correct U.T. The clock display also is latched at the end of each integration interval to allow the U.T. to be punched on the paper tape.

The punch interface is contained in a free standing case complete with its own 5 V power supply. It is linked by multi-core cables to the main electronics chassis and to the paper-tape punch. Its function is to serialise, code and format the data for punching.

Each complete punch cycle results in the punching of 32 characters. These include 5 leading digits, set by thumbwheel switches on the interface, which are used as codes to allow programmed data reduction. The data which is punched includes the counts in each channel (5 digits for each), the Universal Time (6 digits) and the filter position (3 digits). The remaining characters are taken up by spaces, carriage return and line-feed characters.

When a punch cycle is initiated by the control logic, certain starting conditions within the interface are set up. Among these conditions is the resetting to zero of a hexa-decimal counter (i.e. one which counts 0 - 15, 0 - 15, etc.). The output of this counter is in BCD form (Binary Coded Decimal) and is fed together with the output from a divide-by-2 bi-stable (counts 0 - 1 - 0 - 1, etc.) to the address lines of the data selectors. These devices select one of sixteen lines according to the 4-bit BCD address code given to them. The data selectors are arranged in two banks of four, each bank receiving the data for sixteen characters (addressed as decimal 0 - 15, or binary 0000 - 1111). The bank which is addressed is determined by the divide-

by-2 circuit. Each bank contains four data selectors since the data is also in BCD code at this point and is made up of four bits which must be selected simultaneously and presented to the code converter to be changed into an 8-bit ASCII code (American Standard Code for Information Interchange).

With the hexa-decimal counter and the divide-by-2 both reset to zero, the first character is thus selected. It is then coded in 8-bit ASCII code and presented on the data lines to the punch. The interface generates a voltage level change which causes the punch to load this character into a buffer to await punching. Before punching takes place, the character in the first punch buffer is transferred to a second buffer and the first buffer is cleared. The act of clearing the first buffer is indicated by the punch as a voltage level change on the Buffer Empty output. The level change is detected by the interface and results in the hexa-decimal counter being incremented by one. The next character is thus selected, after which another load pulse is produced and returned to the punch. The mode of punch operation just described is called asynchronous since the punch determines its own operating speed and requests characters as it is able to accept them.

The supply of characters to the punch continues until sixteen characters have been punched at which stage the output of the hexa-decimal counter will be 1111 (in binary) and the next clocking of the counter will return it to 0000. At the same time, however, the divide-by-2 will also be clocked and so the second bank of data selectors will be addressed as the hexa-decimal counter increments from 0000 to 1111 again. On reaching 1111 for the second time, the subsequent request for the next character is diverted back to the main control logic where it is used to release the data latches thus completing a punch cycle.

If a failure occurs in either the punch or punch interface, a 21-column

## BCD CODE

## GENERATED ASCII CODE

Decimal Character	Bit				ASCII Character	Bit							
	4	3	2	1		8	7	6	5	4	3	2	1
0	0	0	0	0	0	0	0	1	1	0	0	0	0
1	0	0	0	1	1	1	0	1	1	0	0	0	1
2	0	0	1	0	2	1	0	1	1	0	0	1	0
3	0	0	1	1	3	0	0	1	1	0	0	1	1
4	0	1	0	0	4	1	0	1	1	0	1	0	0
5	0	1	0	1	5	0	0	1	1	0	1	0	1
6	0	1	1	0	6	0	0	1	1	0	1	1	0
7	0	1	1	1	7	1	0	1	1	0	1	1	1
8	1	0	0	0	8	1	0	1	1	1	0	0	0
9	1	0	0	1	9	0	0	1	1	1	0	0	1
10	1	0	1	0	Line feed	0	0	0	0	1	0	1	0
11	1	0	1	1	Vert. Tab	1	0	0	0	1	0	1	1
12	1	1	0	0	Form Feed	0	0	0	0	1	1	0	0
13	1	1	0	1	Carriage Return	1	0	0	0	1	1	0	1
14	1	1	1	0	Shift Out	1	0	0	0	1	1	1	0
15	1	1	1	1	Space	1	0	1	0	0	0	0	0

Table 3.1

4-bit BCD codes are converted to 8-bit ASCII codes before punching on paper tape.

digital printer can be used to record the data. The printer accepts full parallel data (i.e. bit parallel and character parallel) and uses the same output connectors and driving commands as the punch interface. The formatting of the data is similar to that produced by the punch interface, although no leading code digits are printed.

The layout and assembly of the electronics cases has been designed for ease of access for servicing and fault finding. Power supplies, circuit boards, etc., can all be removed from the main chassis, without de-soldering, in about 30 minutes leaving only wiring in place. The control logic is mounted on four plug-in I.C. Vero-boards measuring 11 x 15 cm. The integrated circuits are themselves mounted in I.C. sockets enabling replacement in a matter of seconds.

The pre-amplifier/discriminator/line-driver circuit is shown in Appendix I together with logic diagrams of the timer, step-size control, picture-point/direction control, U.T. clock, punch driver, data selector and code converter. Table 3.1 gives the ASCII characters and codes that are produced by the code converter from the BCD codes 0000 - 1111 (Decimal 0 to 15).

In conclusion it can be said that the electronic system just described forms a compact and reliable unit which, with some precautions, is undisturbed by the electrically noisy environment of a telescope dome. Occasional faults have developed in the integrated circuits but replacement of the faulty circuit is simple. The cost of the entire optical, electronic and mechanical system is estimated to be just in excess of £2000 inclusive of photomultipliers, interference filters, paper-tape punch and workshop time.

#### 3.4 Data Reduction

Initial data reduction is done either on the University's KDF9 computer

or on a Hewlett Packard programmable desk calculator. The punched paper tape can be read directly by either of these machines. It is possible to have the Hewlett Packard calculator reading the data tape in a pseudo on-line mode. This is done by including a small non-functional loop in the programme and arranging the number of times this is cycled so that the time taken to do so is about the same as the integration time of the counters. In this way, the paper tape can be read at the same rate as it is being punched and the dead-time between punching and reading is determined by the length of tape required between the tape punch and the tape reader.

Because of its limited memory size, the Hewlett Packard calculator is restricted in the number of wavelength positions which it can analyse at one run of the data tape. The programme can, however, separate star and background signals and can handle up to 21 wavelength positions. The programme averages the data and calculates the errors at each of the specified wavelengths. It can also normalise the data to any one of these wavelengths. The mean values and their errors are printed out when the end of the data tape is reached.

The KDF9 programme for obtaining line-profiles is much more powerful. However, it should be noted that the programme described here only carries out simple averaging of the data so that the line profiles can be plotted and the accuracy of the data can be assessed. Other special purpose programmes can be applied to the data if required (e.g. to evaluate equivalent widths). The only data required in addition to that on the paper tape is the wavelength position to which the intensities are to be normalised. Basically, the programme interprets the data according to the codes set by the thumbwheel switches on the punch interface. The functions of the codes used so far are listed in Table 3.2.

SWITCH SETTINGS

Action

5

4

3

2

1

Switch No:

Switch No:	1	2	3	4	5	Action
Tape I.D.	0	4 digit tape identification no.				Other data on this line is ignored
Date	1	Day	Month			Other data on this line is ignored
Star Signal	4	wave-plate number	3 digit star identification number			Other data on this line is valid star signal
Background Signal	5		Any setting			Other data on this line is valid background signal
End of Tape	9		Any setting			Other data on this line is ignored

Table 3.2

Functions of the codes set on the thumbwheel switches of the punch interface. Each block of data is preceded by a 5-digit code which determines how the data is interpreted by the reduction programmes.

A punch cycle produces a block of 32 characters, the last two being carriage return and line feed, and this is printed on a Teletype or interpreted by the computer as one line of data. Each data tape starts with a line giving a tape identification number. The next line usually gives the date of the observation. These numbers are set on the interface thumbwheel switches (see Table 3.2) and a manual punch command given. Subsequent lines contain background signal and star signal. Each tape has a terminating line, with a code recognised by the programmes, so that reading of the tape will stop automatically.

After printing the tape number and the date of the observation, the programme averages any background signal which is present. If at any later stage more background signal measurements are encountered, these will be averaged separately and their mean values will replace the previous means.

The data at the normalising wavelength is averaged first. The intensities are found from

$$\frac{N_1 - D_1}{N_2 - D_2}$$

where  $N_1$ ,  $N_2$  are the star counts in beam 1 (scanning) and beam 2 (monitor) and  $D_1$ ,  $D_2$  are average background counts (if any) in the two beams. The ratios thus obtained should be largely free of atmospheric effects.

Having thus found the mean ratio at the normalising wavelength, the data at every other wavelength, in ascending order of filter position, is normalised and averaged in a similar way. The corrected standard deviation of a single observation ( $\sigma$ ) and the standard error of the mean ( $s$ ) are also calculated. The former is given by

$$\sigma = \sqrt{\frac{\sum_{i=1}^N (x_i - \bar{x})^2}{(N - 1)}}$$

i.e. 
$$\sigma = \sqrt{\frac{\left(\sum_{i=1}^N (x_i^2)\right) - N(\bar{x})^2}{(N - 1)}}$$

where  $N$  is the number of observations,

$x_i$  ( $i = 1, \dots, N$ ) are the individual observations  
and  $\bar{x}$  is the mean of the  $x_i$ 's.

The standard error of the mean is given by

$$s = \frac{\sigma}{\sqrt{N}}$$

Both of these quantities can be compared with the values expected from photon statistics (see Chapter 4) as a means of judging the quality of the data.

The mean values and their errors are calculated for each wavelength for any other positions of the wave-plate wheel, as indicated by the setting of one of the code switches.

Appendix II contains a sample Teletype listing of a data tape and a listing of the KDF9 FORTRAN programme used for initial reduction of the data.

#### 4. PHOTOMETRIC ACCURACY WITH THE INTERFERENCE FILTER SCANNER

##### 4.1 Introduction

All photometric measurements, no matter how they are made, are subject to various uncertainties. For example, the measured intensities ultimately carry photon noise, the equivalent wavelength of the system may not be what the observer thinks it is and the widths of the passbands may be assumed wrongly. In this study, it was intended to investigate the application of an interference filter scanner to the detection of rapid line profile variability. Depending on the time resolution required in conjunction with the brightness of the star being measured, it may be necessary to examine individual line profile scans for variation or it may be possible to combine a number of scans to obtain a mean line profile. Both techniques have been used to interpret the observations which are presented in Chapter 5. Obviously, there will be "noise" present on the line profiles and the amplitude of the noise across a profile must be known before any statements can be made about intrinsic variability of the profiles.

Three main sources of noise exist and each will be dealt with separately in this chapter. Briefly, they are Poissonian noise associated with the photon counting process, noise introduced by the atmosphere and instrumental noise.

The discussions presented later in this chapter relating to both Poissonian and atmospheric noise are quite general while the discussions on the instrumental noise are chiefly concerned with the use of the narrow band ( $\sim 2 \text{ \AA}$  FWHM) interference filters which have already been discussed in Chapters 2 and 3 although many of the conclusions are quite valid for broader band interference filters and have a possible bearing on the accuracy of  $\beta$ -index photometry.

The method of obtaining line profiles by forming the ratio of the signal

in a wavelength scanning beam with that in a fixed wavelength monitor beam yields only relative photometry and is incapable of detecting any large scale changes within the stellar spectra which might affect both beams simultaneously and to the same extent.

However, the technique has the benefit that due to the narrow bandwidths of the filters and the small wavelength separation of their passbands, no corrections are required for differential atmospheric extinction; a common source of error in photometric measurements.

#### 4.2 Pulse Counting Photometry

A convenient method of making photometric measurements and at the same time obtaining information on the accuracy of those measurements is provided by the pulse counting technique. In most cases, measurements made by pulse counting methods will have a greater precision than those obtained by techniques involving current integrators and pen recorders. An additional attraction of digital data recording is that data reduction can be performed without further measurements being required and the data is in a form which can be analysed immediately by computer. Hybrid techniques employing analogue to digital converters also exist and these methods compare favourably with pulse counting. Since digital electronics formed the control system described in Chapter 3, it was decided for this work to employ pulse counting as the means of signal measurement.

Under ideal observing conditions and assuming there to be no other sources of noise present, the accuracy of pulse counting photometry should only be limited by Poisson statistics; sometimes called photon statistics or photon noise. The error of a single measurement due to photon noise is merely a function of the number of pulses counted.

In an integration time  $t$  the number of pulses counted  $N$  will be given by

$$N = \frac{\pi D_T^2 t}{4} \int_{\lambda_a}^{\lambda_b} \tau(\lambda) Q(\lambda) T(\lambda) n_m(\lambda) d\lambda \quad (4.1)$$

where  $D_T$  is the diameter of the collecting aperture,  $\tau(\lambda)$  is the combined transmittance of the Earth's atmosphere and the telescope/photometer optics at wavelength  $\lambda$ ,  $Q(\lambda)$  is the quantum efficiency of the detector at wavelength  $\lambda$ ,  $T(\lambda)$  is the transmittance of the spectrometric element (e.g. a filter) at wavelength  $\lambda$ ,  $n_m(\lambda)$  is the number of photons per unit area per unit time per unit wavelength interval at wavelength  $\lambda$  above the Earth's atmosphere from a star of magnitude  $m$  and  $\lambda_a$  and  $\lambda_b$  are the limits of the wavelength interval over which the light is measured.

If it is assumed that Poisson statistics apply, the number of photons counted,  $N$ , will be subject to an absolute error of  $\pm (N)^{\frac{1}{2}}$ . This error is sometimes called the standard deviation of a single observation ( $\sigma$ ). The fractional error  $\epsilon$  which is associated with a count of  $N$  photons will therefore be given by

$$\pm \sigma/N \quad \text{or} \quad \pm (1/\sqrt{N})$$

and the percentage error will be  $\epsilon \cdot 10^2$ .

A typical value of  $n_m(\lambda)$  for Equation 4.1 may be obtained from the value of the flux density for the B passband given by Johnson (1966) for a zero magnitude star of spectral type A0V. The value derived is

$$n_0(\lambda) = 1.6 \cdot 10^3 \text{ photons cm}^{-2} \text{ sec}^{-1} \text{ \AA}^{-1}$$

and the value of  $n_m(\lambda)$  for a star of magnitude  $m$  may be obtained from

$$n_m(\lambda) = n_0(\lambda) (2.512)^{-m}$$

There will of course be variations of  $n_m(\lambda)$  due to different spectral types and luminosity classes and the values obtained in practice will correspond to wavelengths around  $4861 \text{ \AA}$  although the effective wavelength and the bandwidth of the B passband are  $\sim 4400 \text{ \AA}$  and  $\sim 960 \text{ \AA}$ . However, the figure given should be correct to an order of magnitude.

If it is assumed that  $(\lambda_b - \lambda_a)$  is small and if over a small range in wavelength  $\tau(\lambda)$ ,  $Q(\lambda)$  and  $n_m(\lambda)$  can be taken as constant, then Equation 4.1 reduces to

$$N = \frac{\pi D_T^2 t}{4} \tau(\bar{\lambda}) Q(\bar{\lambda}) n_m(\bar{\lambda}) \int_{\lambda_a}^{\lambda_b} T(\lambda) d\lambda$$

$$\text{where } \bar{\lambda} = \frac{\lambda_b + \lambda_a}{2} .$$

Further, if the filter is assumed to have a rectangular transmission profile,

$$\begin{aligned} \text{i.e. } T(\lambda) &= 0, \quad \lambda < a \text{ or } \lambda > b \\ \text{and } T(\lambda) &= 1, \quad a \leq \lambda \leq b \end{aligned}$$

then

$$N = \frac{\pi D_T^2 t}{4} \tau(\bar{\lambda}) Q(\bar{\lambda}) n_m(\bar{\lambda}) \Delta\lambda \quad (4.2)$$

$$\text{where } \Delta\lambda = \lambda_b - \lambda_a .$$

For example, if typical values are taken for the interference filter scanner attached to the 50 cm telescope at Glasgow ( $\tau(\bar{\lambda}) = 0.06$ ,  $Q(\bar{\lambda}) = 0.15$ ,  $\bar{\lambda} = 4860 \text{ \AA}$  and  $\Delta\lambda = 2 \text{ \AA}$ ) the predicted photon count in  $t$  seconds for a zero magnitude AOV star is given by

$$N \simeq 5.6 \cdot 10^4 t$$

and for a star of magnitude  $m$ ,

$$N \simeq 5.6 \cdot 10^4 t (2.512)^{-m} \quad (4.3)$$

For a star of magnitude 1.8 and spectral type A 1 IV ( $\beta$  Carinae) measured at H $\beta$  with a 2 Å passband when the scanner was attached to the 50 cm telescope at Sutherland (the SAAO site) the observed count rate was  $7.10^3$  counts/second while the count rate predicted by Equation 4.3 is  $\sim 10^4$  counts/second. The difference between these two values will be due to a combination of several factors. In addition to the different spectral type and luminosity class of the star involved, there might also be a substantial variation in the atmospheric transparency at the two sites and it is unlikely that the two telescopes will have the same overall reflectivity. Furthermore, a small number of photon produced pulses will not be counted due to the action of the pulse height discriminator of the pre-amplifier. The discriminator level is set so as to reject a large number of the many small, thermally produced pulses from the photomultiplier tube (the dark count) but it will inevitably also reject some signal pulses.

Assuming a pulse counting rate of  $10^4$  counts/second, a photometric accuracy of 1 per cent should be achieved in an integration time of one second. If the integration time or the size of the collecting aperture is increased so that the count rate is  $10^6$  counts/second, the photometric accuracy obtained in one second will be 0.1 per cent. Since the fractional error  $\epsilon$  is given by  $\pm (1/\sqrt{N})$ , the expression relating  $\epsilon$  to  $m$  and  $t$  derived from Equation 4.3 is

$$\epsilon^2 \simeq 1.8 \cdot 10^{-5} (2.512)^m t^{-1}$$

where the values of  $D_{\eta}$ ,  $\tau(\lambda)$ , etc. have been taken for the Glasgow telescope as before. Table 4.1 lists some expected percentage errors, based on photon statistics, for various combinations of stellar magnitude and integration time.

Obviously, as the pulse counting rate varies across a stellar line profile so too will the photometric accuracy that can be achieved in a given time.

Table 4.1

## Percentage Error

t \ m	0	1	2	3	4	5
1 <sup>s</sup>	0.42%	0.67	1.06	1.69	2.67	4.24
10 <sup>s</sup>	0.13	0.21	0.34	0.53	0.84	1.33
100 <sup>s</sup>	0.04	0.07	0.11	0.17	0.27	0.42

Percentage error ( $\epsilon \times 10^2$ ) for stars of various magnitudes ( $m$ ) and for various integration times ( $t$ ).

The fractional error,  $\epsilon$ , is obtained from

$$\epsilon^2 = \frac{4(2.512)^m}{\pi D_T^2 \tau(\bar{\lambda}) Q(\bar{\lambda}) n_o(\bar{\lambda}) \Delta \lambda t}$$

$$D_T = 50 \text{ cm}, \tau(\bar{\lambda}) = 0.06, Q(\bar{\lambda}) = 0.15$$

$$n_o(\bar{\lambda}) = 1.6 \times 10^3 \text{ cm}^{-2} \text{ sec}^{-1} \text{ \AA}^{-1},$$

$$\Delta \lambda = 2 \text{ \AA}, \bar{\lambda} = 4860 \text{ \AA}.$$

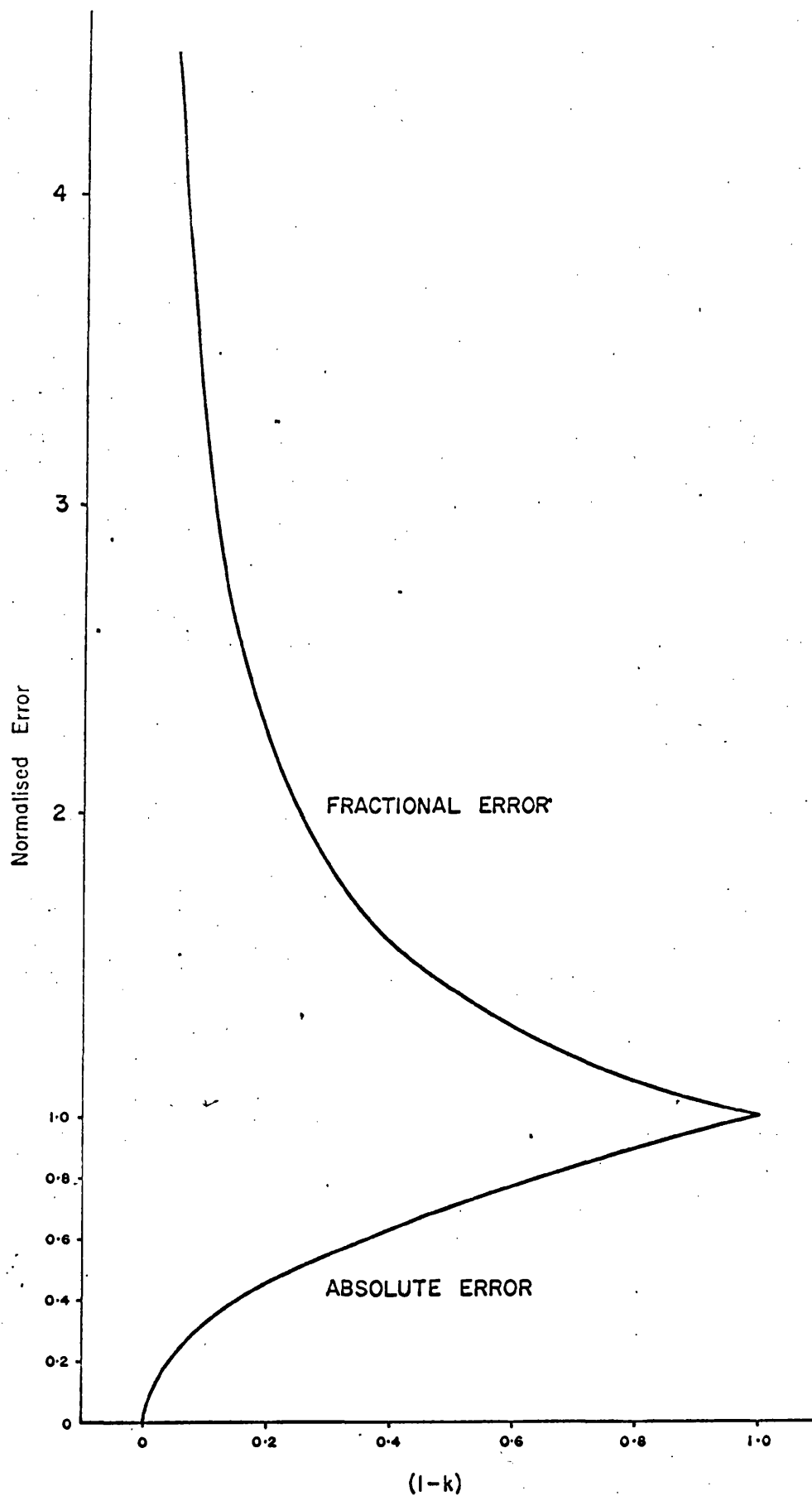


Figure 4.1

Variation of the absolute and fractional photon errors with line depth  $(1 - k)$  relative to the errors for the continuum  $(1 - k = 1)$ .

For example, the absolute photon error will be less for the centre of an absorption line than for the adjacent continuum since the value of  $N$  will be smaller at the line core. However, the fractional error  $\epsilon$  will be greatest at the line centre, due entirely to photon statistics. If in an integration time  $t$ , there are  $N$  pulses counted for the continuum or line wings and  $(1 - k)N$  pulses counted for the line centre, the absolute errors will be  $\pm (N)^{\frac{1}{2}}$  and  $\pm (1 - k)^{\frac{1}{2}} (N)^{\frac{1}{2}}$  respectively ( $0 \leq k \leq 1$ ). The fractional errors will be  $\pm (N)^{-\frac{1}{2}}$  and  $\pm (1 - k)^{-\frac{1}{2}} (N)^{-\frac{1}{2}}$ . Figure 4.1 shows the absolute and fractional errors that are associated with various values of  $(1 - k)$  relative to the errors for  $(1 - k)$  equal to unity (i.e., continuum) and shows how the noise level due to photon statistics might be expected to vary across an absorption feature.

#### 4.3 Noise Introduced by the Atmosphere

Ideal photometric conditions are seldom experienced, however, and atmospheric scintillation and transparency changes are other sources of noise which can affect the recorded signal. Scintillation noise can vary considerably with time in both frequency and amplitude, and in addition it is often wavelength dependent. Fortunately, the wavelength dependence can be neglected as explained in Section 4.1. Over a limited area of sky (the size of which is variable and dependent on many factors) the rms. (root-mean-square) value of the scintillation noise can be represented simply as a fraction of the photon count and is independent of the brightness of the star. A typical value might be 5 per cent; obviously this figure will vary from one part of the sky to another and with time, and will also be related to the quality of the observing site.

Figure 4.2 shows the expected number of photons counted in one second as a function of the apparent stellar magnitude (based on the values given in

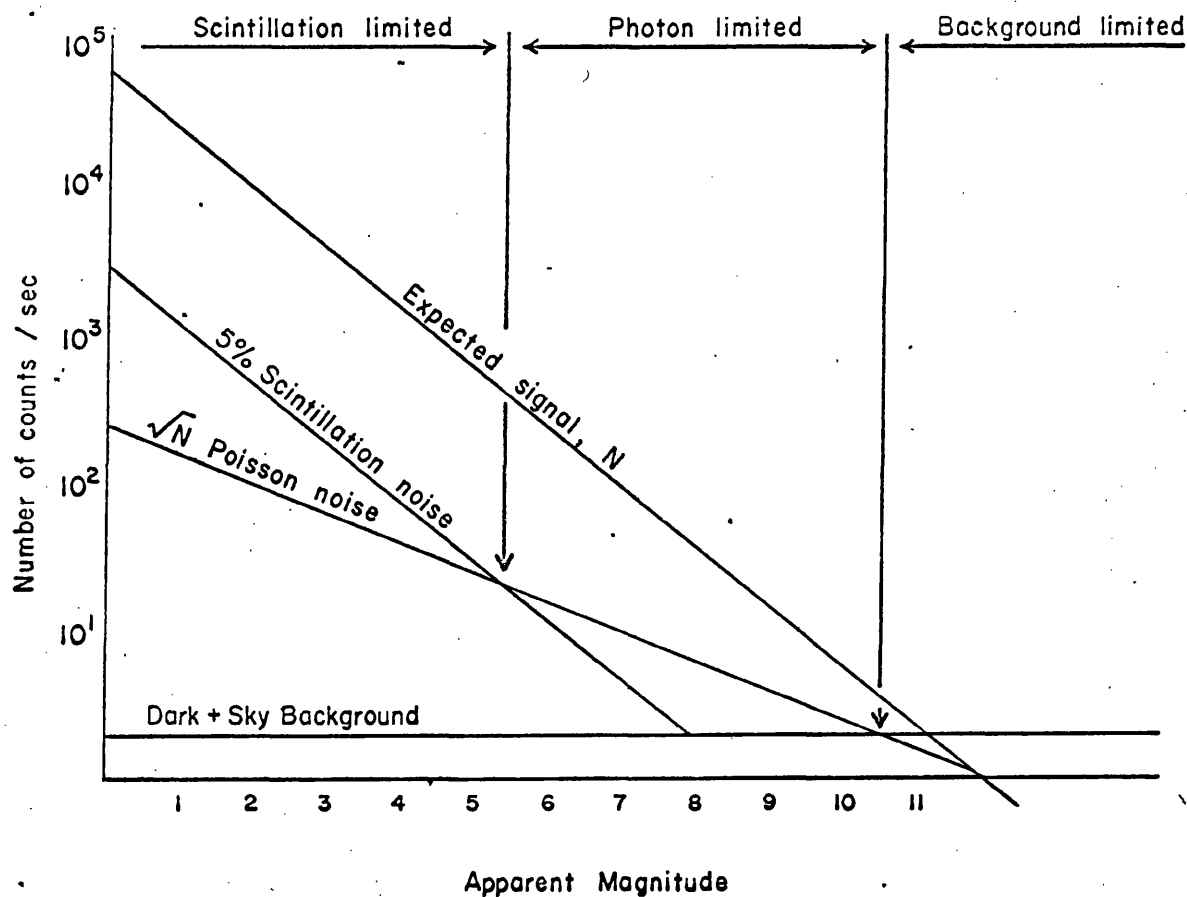


Figure 4.2

Expected photon count as a function of apparent magnitude  $m$ , given by

$$N = \frac{\pi D_T^2 \tau(\bar{\lambda}) Q(\bar{\lambda}) n_o(\bar{\lambda}) \Delta \lambda t}{4 (2.512)^m}$$

with working values;  $D_T = 50 \text{ cm}$ ,  $\bar{\lambda} = 5000 \text{ \AA}$ ,  $\tau(\bar{\lambda}) = 0.06$   
 $Q(\bar{\lambda}) = 0.15$ ,  $n_o(\bar{\lambda}) = 1.6 \cdot 10^3 \text{ cm}^{-2} \text{ sec}^{-1} \text{ \AA}^{-1}$ ,  $\Delta \lambda = 2 \text{ \AA}$ ,  
 $t = 1 \text{ sec}$ .

The zones are indicated in which the dominant source of noise is scintillation noise (5%), photon shot-noise ( $\sqrt{N}$ ) or background noise.

Section 4.2) together with the errors expected due to photon statistics and scintillation noise.

It can be seen from Figure 4.2 that with the Glasgow telescope the limiting source of noise for stars brighter than magnitude 5.4 approximately will be scintillation while for fainter objects, the dominant source of noise will be photon noise. It can also be seen that if the measurements are made with a simple single channel photometer, the limit of the photometric accuracy which can be expected is likely to be several per cent. In order to detect rapid small amplitude intrinsic intensity changes it is necessary to improve this degree of accuracy by at least a factor of ten.

It is well known that a considerable improvement in photometric accuracy can be achieved with a double beam photometer. If the signals in two beams are measured simultaneously, the ratio of the signals will, to a great extent, be free of scintillation noise, since the latter will be coherent in both beams. A double beam instrument has the additional advantage (for the same reason) of being able to work under conditions of severe transparency changes due to fairly thick cloud or mist. Figure 4.3 shows the signal recorded over a 5 minute interval in one beam of the double beam interference filter scanner described in Chapter 3, together with the ratio formed between this and the second beam. In this example, the beam for which the signal is shown contained a filter of  $\sim 1.9 \text{ \AA}$  half-width, normally used for tilt-scanning but maintained at a constant wavelength for this demonstration of double beam compensation. The other beam contained a fixed filter of  $51 \text{ \AA}$  half-width. Figure 4.4 shows a further example of the ability of the double beam photometer to compensate for large scale transparency changes by means of forming the ratio of the two signals.

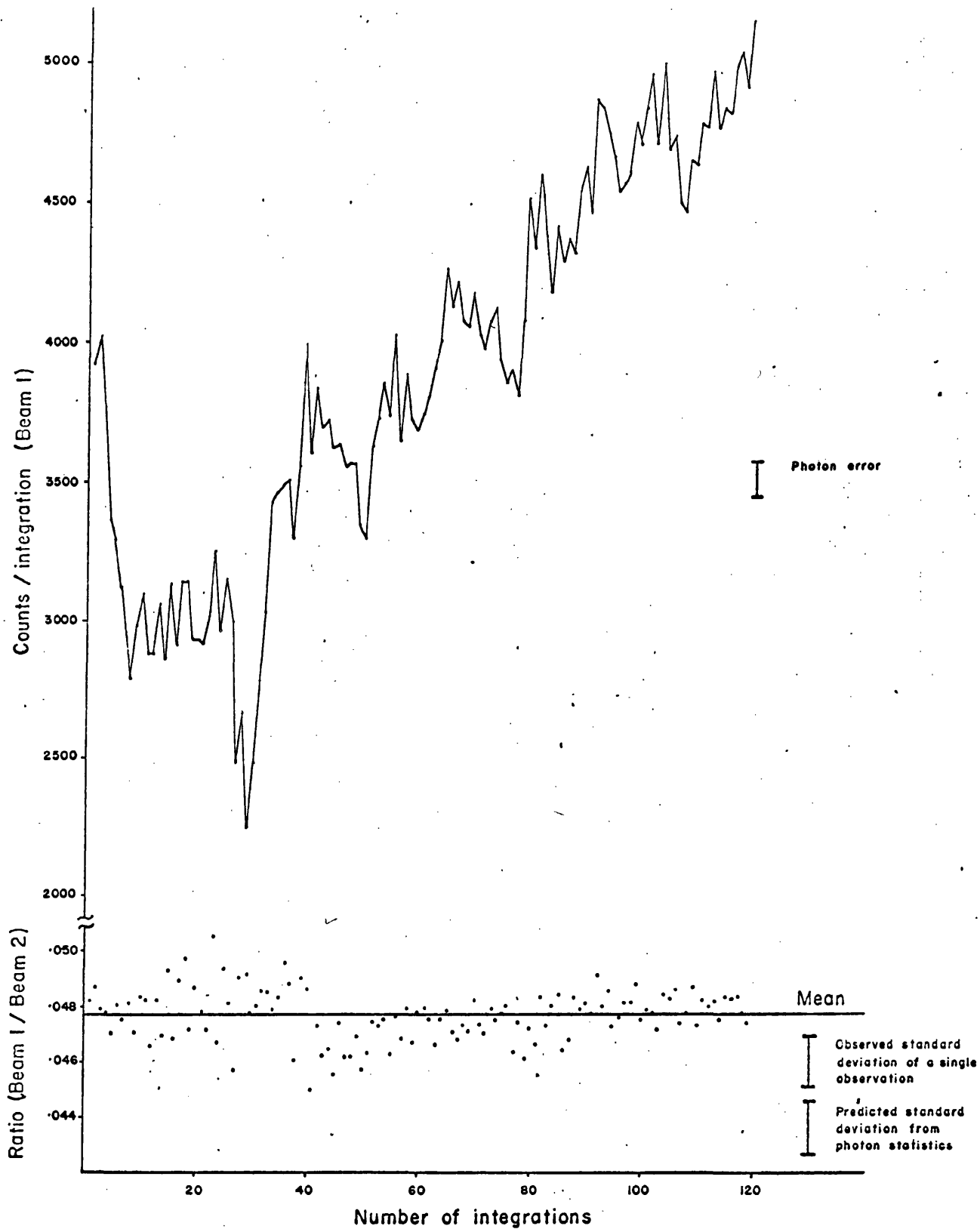


Figure 4.3

The effects of scintillation and sky transparency changes for a single channel photometer (upper) are removed by forming the ratio with the photon count in a second beam (lower). ( $\Delta\lambda = 1.9 \text{ \AA}, 51 \text{ \AA}$ ).

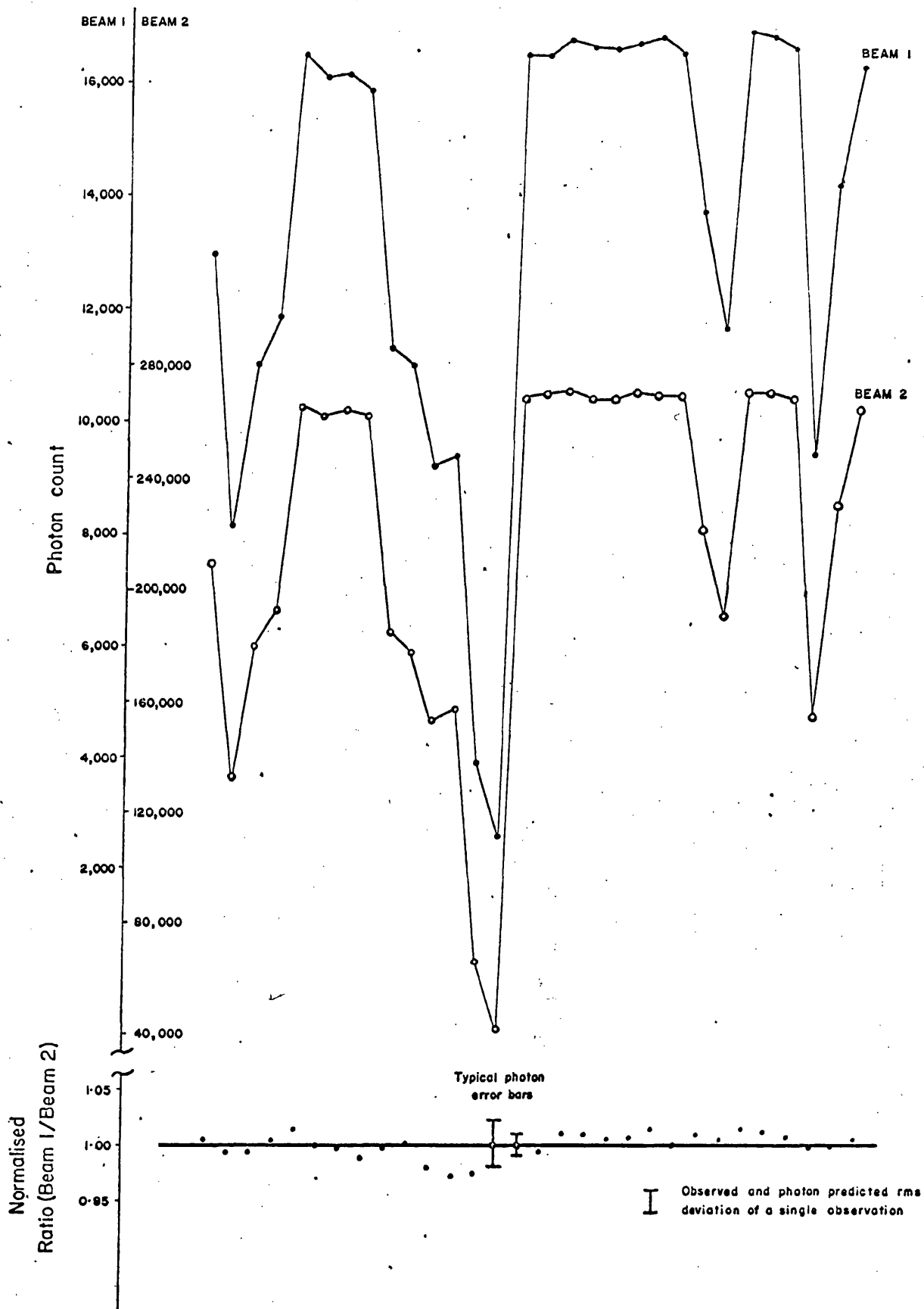


Figure 4.4

Large variations of the photon count at fixed wavelength for two beams ( $\Delta\lambda = 1.9 \text{ \AA}$ ,  $51 \text{ \AA}$ ) (upper) are removed by taking the ratio of the counts (lower).

Suppose that the atmospheric noise is completely coherent in the two beams and let  $N_1$ ,  $xN_1$ ,  $N_2$  and  $xN_2$  be two successive counts in each beam. The fractional change in signal due to scintillation and transparency fluctuations is given by  $x$ . Due to photon shot noise, which is still present, each of these counts will have an error given by the square root of the count. If the ratios of the signals in the two beams,  $R_1$  and  $R_2$ , are formed, then

$$R_1 = \frac{N_1 \pm (N_1)^{\frac{1}{2}}}{N_2 \pm (N_2)^{\frac{1}{2}}} = \frac{N_1}{N_2} \pm \Delta R_1$$

$$\text{and } R_2 = \frac{xN_1 \pm (xN_1)^{\frac{1}{2}}}{xN_2 \pm (xN_2)^{\frac{1}{2}}} = \frac{N_1}{N_2} \pm \Delta R_2$$

where the uncertainties in  $R_1$  and  $R_2$  are  $\Delta R_1$  and  $\Delta R_2$  respectively. If, in general,

$$R = \frac{A \pm \Delta A}{B \pm \Delta B} = \frac{A}{B} \pm \Delta R, \quad \text{then}$$

$$\Delta R = \sqrt{\left(\frac{\partial R}{\partial A}\right)^2 (\Delta A)^2 + \left(\frac{\partial R}{\partial B}\right)^2 (\Delta B)^2}$$

$$\text{thus, } \Delta R_1 = \frac{N_1}{N_2} \sqrt{\frac{1}{N_1} + \frac{1}{N_2}}$$

$$\text{and } \Delta R_2 = \frac{N_1}{N_2} \sqrt{\frac{1}{x} \left(\frac{1}{N_1} + \frac{1}{N_2}\right)}$$

The fractional errors,  $\epsilon_1$  and  $\epsilon_2$ , are given by

$$\epsilon_1 = \frac{\Delta R_1}{R_1}$$

$$\text{i.e. } \epsilon_1 = \left(\frac{1}{N_1} + \frac{1}{N_2}\right)^{\frac{1}{2}}$$

$$\text{and } \epsilon_2 = \frac{\Delta R_2}{R_2}$$

$$\text{i.e. } \epsilon_2 = \left\{ \frac{1}{x} \left( \frac{1}{N_1} + \frac{1}{N_2} \right) \right\}^{\frac{1}{2}} = \left( \frac{1}{x} \right)^{\frac{1}{2}} \epsilon_1$$

It can be seen from the expressions for  $\epsilon_1$  and  $\epsilon_2$  that:

- (i) Although combining the two counts  $N_1$  and  $N_2$  results in a ratio which has an uncertainty greater than that in either of the original quantities, if the system is designed such that  $N_2 \gg N_1$ , then the uncertainty in the ratio can be made almost equal to the uncertainty in  $N_1$  by itself. Thus,  $\epsilon_1 \simeq N_1^{-\frac{1}{2}}$ ; i.e. the same as the photon error for one beam. In fact, if  $N_2 = 10 N_1$ ,  $\epsilon_1 = 1.049 (N_1)^{-\frac{1}{2}}$ ; only five per cent greater than the photon predicted error associated with  $N_1$ .
- (ii) If  $x$  represents a fractional change in signal, coherent in both beams, then the ratio of the signals is unaltered by the signal variation. In addition, the fractional uncertainty of the ratio is modified by a factor of  $\left(\frac{1}{x}\right)^{\frac{1}{2}}$ . For example, if  $x = 0.25$  (corresponding to a drop in signal of a factor of 4), the uncertainty of the ratio is only twice (i.e.  $1/\sqrt{0.25}$ ) what it was before the drop in signal.

If a series of  $n$  measurements of the ratio of the signals in the two beams each have a standard deviation of a single observation of  $\sigma$ , then the standard error of the mean of the  $n$  measures,  $S_n$ , will be given by  $\sigma/\sqrt{n}$ . Figure 4.5 shows the standard error of the mean of a sample of ratios as a function of  $n$ . The observed error curve ( $S_{\text{obs}}$ ) matches reasonably well the curve expected from photon statistics ( $S_{\text{exp}}$ ).

The implication is that a double beam photometer can perform accurate relative photometry by the ratio technique and, except for very faint stars, is limited in accuracy only by photon statistics. Under ideal observing conditions, or for stars for which photon noise is dominant, the process of

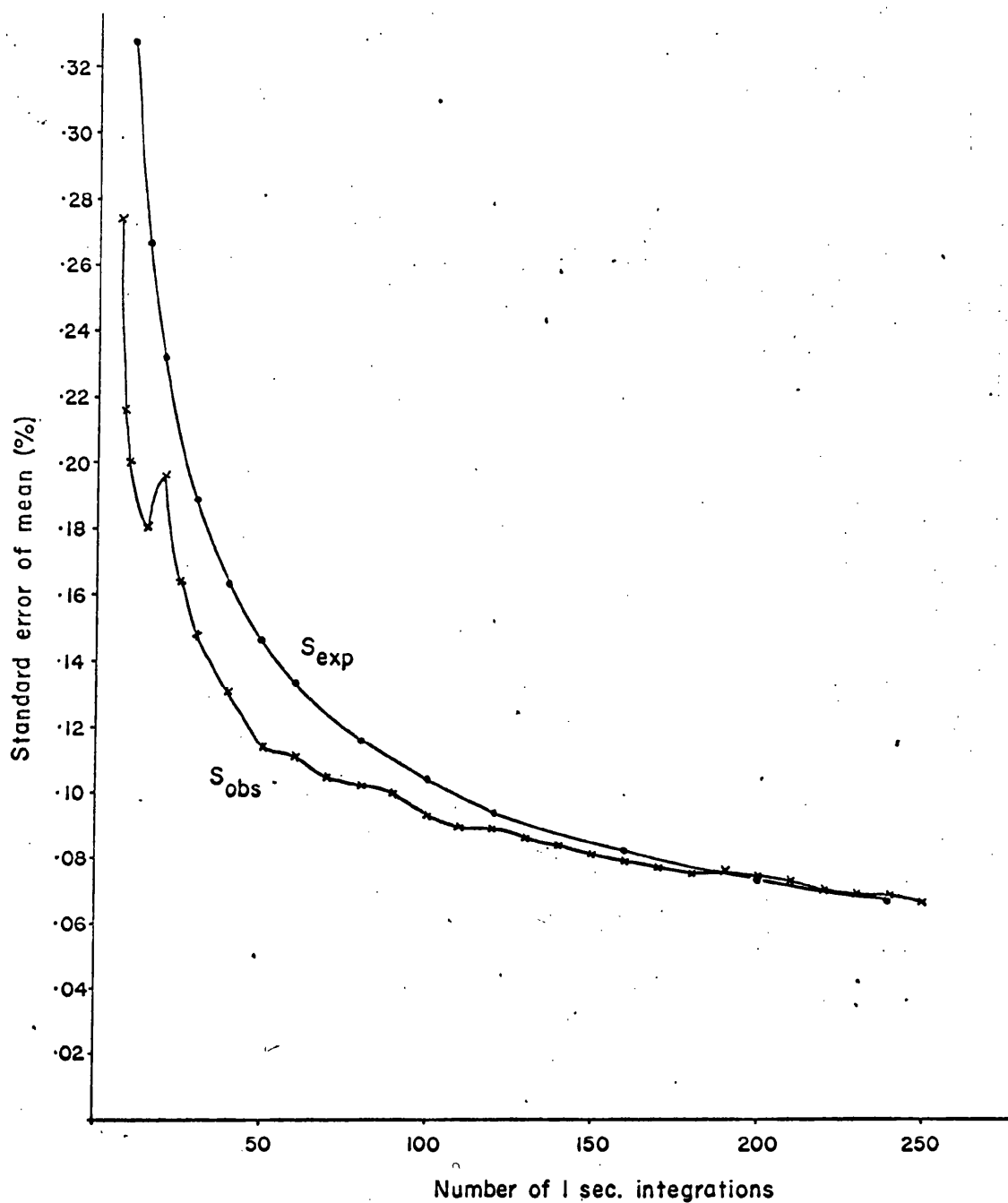


Figure 4.5

Variation of the observed and expected standard errors ( $S_{obs}$  and  $S_{exp}$ ) with the number of measurements of the ratio of the counts at fixed wavelengths for the two beams of the scanner. The expected error decreases as  $1/\sqrt{n}$  where  $n$  is the number of measurements.

forming ratios causes a slight increase in the uncertainty of the observations but, with a suitable choice of bandwidths in the two beams, the increase can be reduced to a minimum. When sky transparency and scintillation noise are dominant, the ratio technique is essential for high photometric accuracy.

#### 4.4 Instrumental Errors

In addition to the sources of noise already considered, allowance has to be made for any errors introduced by the photometer itself. Some causes of possible distortion of the recorded line profiles have already been considered in Chapter 2. It was seen there that under reasonable observing conditions the recorded profiles compared favourably with simulated profiles obtained from high resolution spectrum atlases.

Although there are liable to be distortions of the line profiles due to changes with tilt of the filter's half-width and transmittance, the distortions are not serious and for many purposes can normally be neglected. The application of interference filters to the measurement of stellar line profiles was not, however, intended as a means of obtaining profiles of high spectral purity but as a means of detecting rapid profile variations.

The distortions of the line profiles discussed in Chapter 2 should not, provided they remain constant, affect the ability to detect intrinsic line profile variability. This section will examine some instrumental effects which are themselves liable to be variable and which may produce spurious line profile variations. The main emphasis of the discussions will be on effects relating to the interference filters although, of course, effects relating to other parts of the instrumentation are possible.

For example, when the photometer was first constructed it was found that the gain of one of the photomultipliers was very sensitive to the position at

which the stepping motor on the wavelength scanner was stopped. This effect was due to the magnetic field of the coils within the motor interacting with the field of the photomultiplier dynodes and was removed completely by shielding the motor and the photomultipliers with mu-metal foil. A similar effect, dependent on the orientation of the telescope, can sometimes be produced by the Earth's magnetic field. Again, when the photometer was in its initial stages, it was found that the air temperature within the filter cavity was sensitive to the telescope orientation. Any temperature variation will produce a wavelength shift of the filter passbands, the shift being to longer wavelengths at higher temperatures. This problem was overcome by installing the small propellor and D.C. motor mentioned in Chapter 3, so ensuring a good circulation of the warm air within the photometer.

Another instrumental effect sometimes encountered with pulse counting techniques is counting losses due to high counting rates resulting in pulses piling up and overlapping one another. Such an effect results in the response of the system being non-linear with respect to intensity changes and this could give rise to serious distortions of the line profiles. By design of the pre-amplifiers, the maximum count rate which can be accepted is  $\sim 2.5 \cdot 10^6$  counts/second although a pre-amplifier bandwidth of 0 - 20 MHz could be achieved by changing the time constants which define the pulse width and dead-time. In practice, due to the narrow spectral bandwidth of the filters and the small telescopes to which the photometer has been attached, counting rates greater than  $10^4$  counts/second have rarely been experienced and counting losses can be neglected as a source of error. Profile variation might also appear as the result of differential gain changes between the two beams, although, as well as running both photomultipliers from the same EHT supply, the two pre-amplifiers use a common, stabilised power supply in an effort to avoid this possibility.

If the preceding instrumental sources of error can be assumed to have been removed there still remain errors produced by the interference filters and brought about by seeing conditions and inadequate telescope guidance. Both of these topics, in relation to the half-width and wavelength of the instrumental profiles and how the recorded line profiles are affected by them, will be considered separately. The difficulty regarding the detection of line profile variability is that both of these effects are variable, often on a time scale less than that required to complete one line profile scan and it is possible that these instrumental effects may be mistaken for intrinsic profile changes.

#### 4.4.1 Errors due to Seeing Conditions.

In the following simplified but analytical treatments of the effects of seeing conditions and guidance errors, the instrumental transmission profile will be considered as a Gaussian function. Consider now the convolution of the instrumental profile with the stellar spectrum.

Suppose that a stellar absorption line can also be taken as Gaussian in shape. Figure 4.6 shows such an absorption line. The line centre is at wavelength  $\lambda_0$ , the line depth is  $k$  ( $0 \leq k \leq 1$ ) and the half-width of the line is  $\Delta_L$ . An instrumental transmission profile is also shown in Figure 4.6 with its wavelength of peak transmittance at  $\ell$  and with a half-width of  $\Delta_F$ . Suppose that the intensity distributions with wavelength for the stellar and the instrumental lines are given by  $I_L(\lambda)$  and  $I_F(\lambda)$  respectively. Thus

$$I_L(\lambda) = 1 - k \cdot \exp \left\{ \frac{-(\lambda - \lambda_0)^2 \cdot 4 \log_e 2}{\Delta_L^2} \right\} \quad \text{and}$$

$$I_F(\lambda) = \left( \frac{4 \cdot \log_e 2}{\pi} \right)^{\frac{1}{2}} \cdot \frac{1}{\Delta_F} \cdot \exp \left\{ \frac{-(\lambda - \ell)^2 \cdot 4 \log_e 2}{\Delta_F^2} \right\}$$

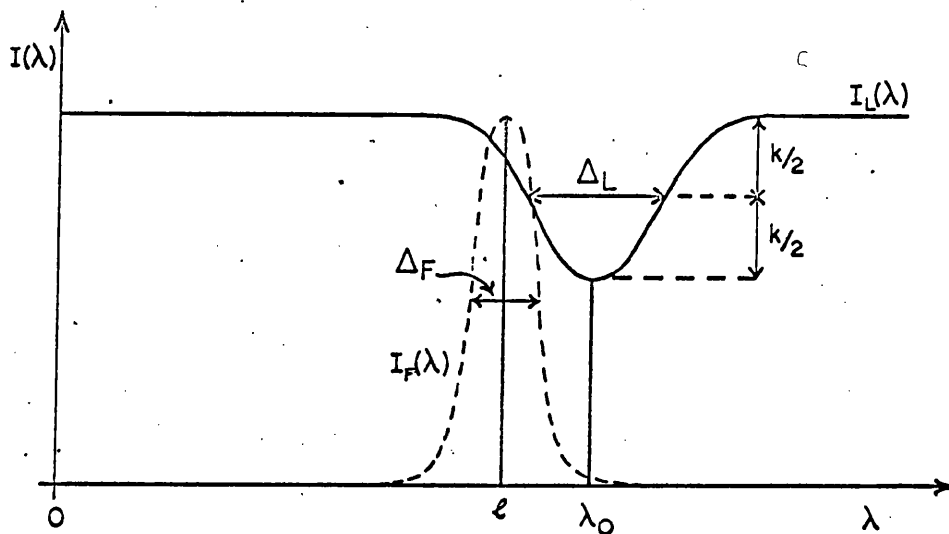


Figure 4.6

Representation of a Gaussian absorption line ( $I_L(\lambda)$ ) with central wavelength  $\lambda_0$ , half-width  $\Delta_L$  and depth  $k$  and of a Gaussian filter profile ( $I_F(\lambda)$ ) with wavelength of peak transmittance  $\ell$  and half-width  $\Delta_F$ . The recorded intensity at wavelength  $\ell$  is given by

$$S(\ell) = \int_0^{\infty} I_F(\lambda) I_L(\lambda) d\lambda.$$

The recorded signal  $S(\ell)$  obtained when the filter is centred on wavelength  $\ell$  is given by

$$S(\ell) = \int_0^{\infty} I_F(\lambda) \cdot I_L(\lambda) d\lambda$$

$$\text{or } S(\ell) \approx \int_{-\infty}^{\infty} I_F(\lambda) \cdot I_L(\lambda) d\lambda \quad ,$$

since  $\Delta_L$  and  $\Delta_F \ll \lambda_0$  and  $\ell$ .  $I_L(\lambda)$  and  $I_F(\lambda)$  are not defined for  $-\infty < \lambda < 0$ , but since  $I_F(\lambda) \approx 0$  for  $|\ell - \lambda| \gg \Delta_F$ , it is assumed that  $\int_{-\infty}^0 I_F(\lambda) \cdot I_L(\lambda) d\lambda = 0$ .

Indeed, by evaluating the above integral it can be shown that

$$S(\ell) \approx 1 - \frac{k \Delta_L}{(\Delta_L^2 + \Delta_F^2)^{\frac{1}{2}}} \cdot \exp \left\{ \frac{-(\ell - \lambda_0)^2 \cdot 4 \log_e 2}{(\Delta_L^2 + \Delta_F^2)} \right\} \quad (4.4)$$

If the instrumental profile is now scanned in wavelength (i.e. by varying  $\ell$ ), Equation 4.4 yields another Gaussian absorption line with a depth given by

$$\frac{k \Delta_L}{(\Delta_L^2 + \Delta_F^2)^{\frac{1}{2}}}$$

and a half-width given by  $(\Delta_L^2 + \Delta_F^2)^{\frac{1}{2}}$ , the pythagorean sum of the half-widths of  $I_L$  and  $I_F$ . Equation 4.4 shows that the recorded absorption profile will be partly filled-in and will also be broadened. In fact, it is well known that if  $\Delta_L \gg \Delta_F$  then the recorded profile will only be slightly distorted, but if  $\Delta_F \gg \Delta_L$  the recorded profile will closely match the shape of the instrumental profile. Equation 4.4 also shows that the signal recorded at any wavelength  $\ell$  is dependent on both  $\Delta_F$  and  $\ell$  and will vary with either of these quantities.

The effects on  $\Delta_F$  and  $\ell$  produced by a seeing disc of finite angular size as seen by the interference filter at various amounts of tilt have already been derived in detail in Chapter 2. It was seen there that, provided the

seeing disc was symmetrical about the optical axis, the effect on the wavelength of peak transmittance of the filter passband ( $\ell$ ) was very small (the shift in wavelength of the passband was less than  $10^{-2}$  Å). However, the effect on the half-width of the instrumental profile is not negligible, particularly in the case of very narrow band filters.

If the ratio of the focal lengths of the telescope and the collimator is taken for convenience as 60 : 1, the curves shown in Figure 2.8 correspond to stellar seeing discs with angular diameters of 4, 10, 20 and 30 arc seconds. It can be seen from Figure 2.8 that when seeing discs of the above angular diameters are seen by an interference filter at a tilt of  $6^\circ$  (this tilt corresponds approximately to  $\lambda = 4861$  Å (i.e. H $\beta$ ) for the 1.9 Å and 2.2 Å filters discussed before), the resulting increase in the filter half-width from its nominal value for a point source at normal incidence will be 0.3, 0.7, 1.4 and 2.2 Å respectively.

Such large changes in the instrumental half-width must obviously be accompanied by corresponding changes in the recorded signal hence leading to distorted profiles. The magnitude of the variations produced in the signal will be related to the structure of the stellar spectrum and to the nominal half-width and wavelength of the filter passband. In addition the time scale of the variations can be very short if seeing conditions are very bad.

As the diameter of the stellar seeing disc in the focal plane of the telescope increases, in order that the total light flux passing through the focal plane remains constant, the intensity per unit area within the image of the seeing disc must decrease. Thus the intensity of light from a given area of the seeing disc, and hence the intensity transmitted at the wavelength corresponding to the angle of incidence for this area, will decrease as the

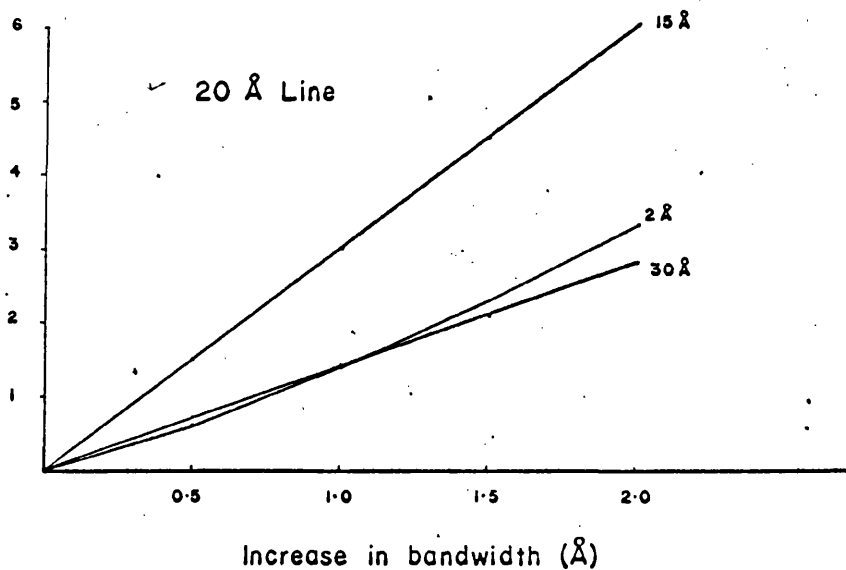
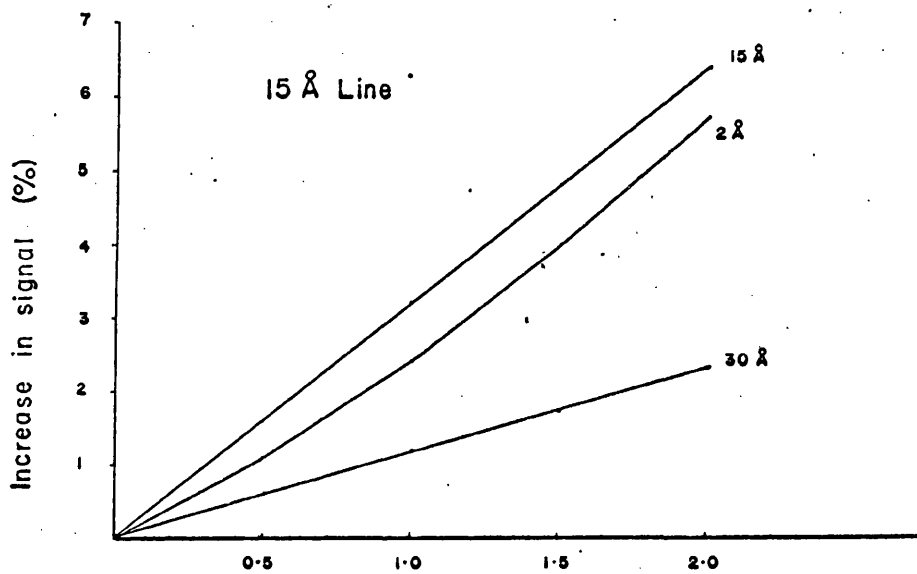
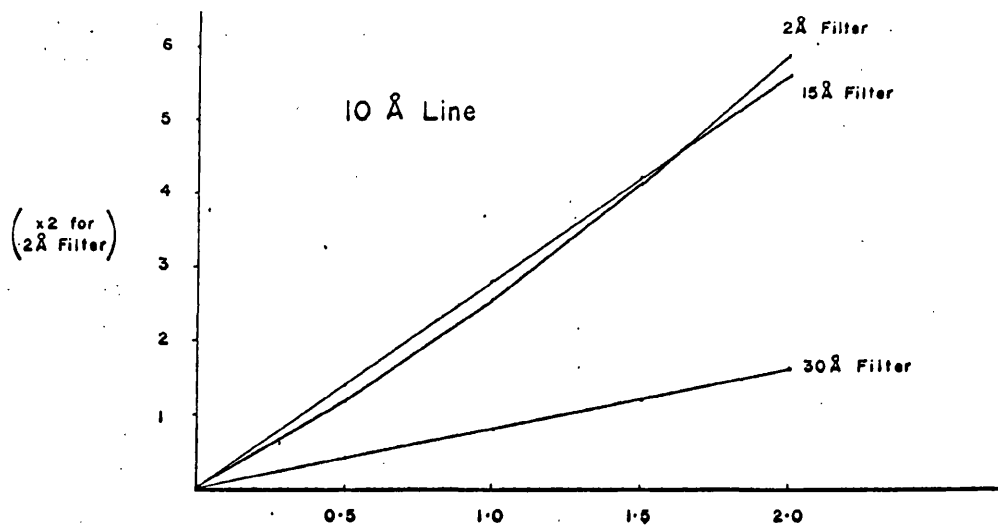


**Figure 4.7** Variation of recorded signal with increase of filter bandwidth plotted for various combinations of absorption line and nominal filter half-widths. In each case, the filter passband is centred on the line, which has a depth ( $k$ ) of 0.7

seeing disc expands. However, due to the increased wavelength range now transmitted as a result of the larger angular size of the seeing disc, it will be assumed that the integral of the instrumental profile, i.e.

$$\int_{-\infty}^{\infty} I_F(\lambda) d\lambda \quad ,$$

will remain constant. In fact,  $I_F(\lambda)$  has been defined such that

$$\int_{-\infty}^{\infty} I_F(\lambda) d\lambda = 1 \quad .$$

Shown in Figure 4.7 are some expected percentage increases in signal derived from Equation 4.4 and plotted as functions of the increase in filter bandwidth for various combinations of filter and line half-widths. In these simplified illustrations of the effect of changes of the filter half-width, the instrumental profile is exactly centred on the absorption line and the line depth  $k$  has been taken as 0.7 in each case.

From Figure 4.7 it can be seen for example that if the filter bandwidth increases from its nominal value by  $0.7 \text{ \AA}$  as a result of the seeing disc increasing from a point source to a diameter of 10 arc seconds (see Figure 2.8;  $\phi_1 = 5$  arc minutes,  $\theta = 6^\circ$ ,  $F_T/F_C = 60$ ), there will, for those filter half-widths considered, be a corresponding increase in signal  $\sim 1 - 2$  per cent.

As explained in Chapter 2, the inability of a narrow band interference filter to accept seeing discs of the order of 10 arc seconds diameter without loss of resolution only arises when the filter is tilted away from its normal incidence position so as to obtain a wavelength scan. Clearly, this is a

serious source of noise and there is little that can be done to overcome the problem. Unless the seeing conditions are very stable, errors due to this effect are likely to set the limit of photometric accuracy at one or two per cent. In addition, it is likely that night to night differences in the size of the seeing discs will result in variable instrumental resolution with corresponding changes in the measured line profiles.

The same problem will be present with any angular dispersive spectrometer, however most prism or grating spectrometers limit the size of the seeing disc accepted by employing a narrow entrance slit. Such a solution to the problem will usually result in a loss of light accepted and may even introduce an additional source of noise in the form of slit-jaw noise. This approach has not been attempted with the interference filter scanner since, because of the design of the photometer head, guidance would be very difficult if only part of the seeing disc was accepted. Also, with the reduction in signal that would occur, time resolution would have to be sacrificed if a particular photon error is to be maintained. Clearly, it is very much a question of what time resolution and photometric accuracy are required of the observations. It was decided for this study that all of the stellar seeing disc should be accepted.

#### 4.4.2 Errors due to Poor Telescope Guidance

The discussions in Section 4.4.1 of this chapter and some of those in Section 5 of Chapter 2 were concerned with the effect an extended image of the seeing disc would have on the instrumental transmission profile of an interference filter. For the purposes of this section it will be assumed that both the star and its image in the focal plane of the telescope are point sources and the effect on the instrumental profile as this point source is allowed to move in the focal plane due to a lack of telescope guidance accuracy will be considered.

The same approach to the problem of the filter's response to an arbitrary ray as developed in Section 2.5 can be applied here, with the simplification that only one ray need be considered. Using the same notation as Section 2.5 and the co-ordinate system shown in Figure 2.7, the wavelength of peak transmittance of the filter passband corresponding to an arbitrary ray PO incident at an angle  $\beta$  to the normal to the filter (see Figure 2.7) when the filter is tilted through an angle  $\theta$  will again be given by

$$\lambda_{\beta} = \lambda_0 - \frac{\lambda_0}{2\mu^2} \left\{ 1 - (\sin \theta \sin \phi \sin \alpha + \cos \theta \cos \phi)^2 \right\} \quad (4.5)$$

where  $\theta$  is the angle of inclination of the filter to the optical axis, and  $\phi$  and  $\alpha$  define the direction of the ray PO relative to the directions of the optical axis and the axis of tilt of the filter. All other rays from the point source will be parallel to the ray PO and hence they will all be transmitted at the same wavelength,  $\lambda_{\beta}$ .

If the image of the star is kept central in the focal plane diaphragm (i.e. on the optical axis) then the wavelength of peak transmittance of the filter passband,  $\lambda_{\theta}$ , will be given by Equation 4.5 with  $\phi = 0$ ;

$$\text{i.e.} \quad \lambda_{\theta} = \lambda_0 - \frac{\lambda_0}{2\mu^2} \left\{ 1 - \cos^2 \theta \right\} \quad (4.6)$$

This is, as expected, the same as the expression for  $\lambda_{\theta}$  given by Equation 2.2.

As the image of the star is allowed to deviate from the optical axis (either due to poor guidance or perhaps due to seeing conditions) there will be a resulting shift in the wavelength of the filter passband. The shift in wavelength,  $\delta\lambda$ , will be given by

$$\delta\lambda = \lambda_{\theta} - \lambda_{\beta}$$

$$\delta\lambda = \lambda_\theta - \lambda_\beta (\bar{\lambda})$$

$\alpha$	$\phi = 1'$			$\phi = 5'$			$\phi = 10'$			$\phi = 15'$						
	$\theta = 1^\circ$	$5^\circ$	$15^\circ$													
	$90^\circ$	-.01	-.06	-.12	-.18	-.06	-.31	-.60	-.88	-.11	-.61	-1.20	-1.76	-.16	-.90	-1.80
$120^\circ$	-.01	-.05	-.11	-.15	-.05	-.26	-.52	-.77	-.10	-.52	-1.04	-1.53	-.14	-.78	-1.55	-2.28
$150^\circ$	-.01	-.03	-.06	-.09	-.03	-.15	-.30	-.44	-.05	-.30	-.60	-.88	-.07	-.44	-.89	-1.31
$180^\circ$	.00	.00	.00	.00	.00	.00	.00	.00	.01	.01	.01	.01	.02	.02	.02	.02
$210^\circ$	.01	.03	.06	.09	.03	.16	.31	.44	.07	.32	.62	.90	.12	.48	.93	1.35
$240^\circ$	.01	.05	.11	.15	.05	.27	.53	.77	.12	.54	1.06	1.54	.18	.82	1.60	2.32
$270^\circ$	.01	.06	.12	.18	.06	.31	.61	.89	.13	.63	1.22	1.78	.21	.95	1.84	2.68

Table 4.2

Differences between the wavelengths of peak transmittance ( $\lambda_\theta, \lambda_\beta$ ) of an interference filter at various angles of tilt ( $\theta$ ) when illuminated by a point source on the optical axis and by a point source at an angular displacement of  $\phi$  (as seen by the filter) from the optical axis. The azimuth of the displaced source relative to the filter's tilt axis is  $\alpha$  (see Figure 2.7) and the angular displacement of the point source on the sky is given by  $\phi^* C/F_T$ .

$$\lambda_\theta - \lambda_\beta = \frac{\lambda_0}{2\mu} (\cos^2 \theta - (\sin \theta \sin \phi \sin \alpha + \cos \theta \cos \phi)^2) : \lambda_0 = 4874 \text{ \AA}, \quad \mu^* = \sqrt{2}.$$

$$\text{i.e. } \delta\lambda = \frac{\lambda_0}{2\mu^2} \left\{ \cos^2 \theta - (\sin \theta \sin \phi \sin \alpha + \cos \theta \cos \phi)^2 \right\} \quad (4.7)$$

The angle  $\phi$  is in fact the angular deviation of the point source from the optical axis, as seen by the filter. As before, the angle on the sky is given by  $\phi \cdot F_C/F_T$ , where  $F_C$  and  $F_T$  are once again the focal lengths of the collimator and the telescope. Table 4.2 lists values of  $\delta\lambda$  calculated from Equation 4.7 for various values of  $\theta$  and  $\phi$ . The values of  $\phi$  are given in arc minutes, but if  $F_T/F_C = 60$  (for convenience) the values shown also represent the guidance errors in arc seconds on the sky.

The difficulty regarding the recorded line profiles is that the wavelength/tilt calibration associates a particular wavelength with a particular click-stop filter position or tilt. If there are guidance errors, however, the correspondence will no longer hold since offsetting the star image from the optical axis is equivalent to changing the fiduciary point on the scale which registers the tilt of the filter (see Section 2.4). In other words, even if the filter is set at a fixed angle of tilt, guidance errors will cause the wavelength which corresponds to this tilt to change from the nominal wavelength when the star is on the optical axis. As can be seen from Equation 4.7 and Table 4.2, the shift in wavelength is dependent on  $\theta$ ,  $\phi$  and  $\alpha$  and in some cases the shift can be as large as plus or minus several Angströms.

If the guidance error remains constant for the duration of a complete wavelength scan, the recorded line profile will maintain the same basic shape but it will be shifted in wavelength. The recorded profile will also be either stretched or compressed in wavelength depending on the sign of the wavelength shift (determined by the direction of the guidance offset) since the extent of the shift varies across the profile as  $\theta$  varies. An example of this situation is presented in Figure 4.8.

The observations on which the figure is based were made on the 50 cm telescope at Glasgow ( $F_T/F_C = 80$ ) and profiles of the  $H\beta$  line in  $\alpha$  Aur were obtained with the star centred in the focal plane diaphragm and then deliberately offset. In Figure 4.8, curve A shows the mean profile obtained from ten consecutive scans with the star central in the diaphragm. The standard error of the mean for each point is  $\sim \pm 0.003$  (i.e.  $\pm 0.3$  per cent). Curves B and C (standard errors  $\sim \pm 0.007$ ) are each the average of just two profile scans and are therefore more noisy (due to photon noise) than curve A. The latter two curves were obtained with the star offset in the diaphragm in the directions of positive and negative declination, corresponding to  $\alpha = 270^\circ$  and  $90^\circ$  respectively in Equation 4.7. The amount of offset was  $\sim \pm 15$  arc seconds on the sky, which with  $F_T/F_C = 80$  gives  $\phi$  as  $\pm 20$  arc minutes as seen by the filter. The filter was tilted from  $\sim 2^\circ$  ( $\sim 4870 \text{ \AA}$ ) to  $\sim 10^\circ$  ( $\sim 4840 \text{ \AA}$ ) with the line centre occurring at a tilt of  $\sim 6^\circ$  from normal incidence. The wavelength scale shown in Figure 4.8 corresponds to curve A while the scale giving the angle of tilt of the filter is the same for all of the curves. It was found that the wavelength shifts of profiles B and C were  $\sim \pm 1.5 \text{ \AA}$ , a value which is in good agreement with the value predicted by Equation 4.7.

The wavelength shift of the filter passband, while the angle of tilt of the filter remains constant, is easily detected when the offset of the star image is constant during a scan, as in the previous example. In practice, however, this will seldom be the case, especially if the star image is moving rapidly in the focal plane of the telescope due to poor seeing conditions. In such a situation, the wavelength shifts will simply appear as variations in the signal levels at each filter position and the variations will be both random in time and variable across the profile, since the structure within the intrinsic spectrum is also important. For example, suppose that the

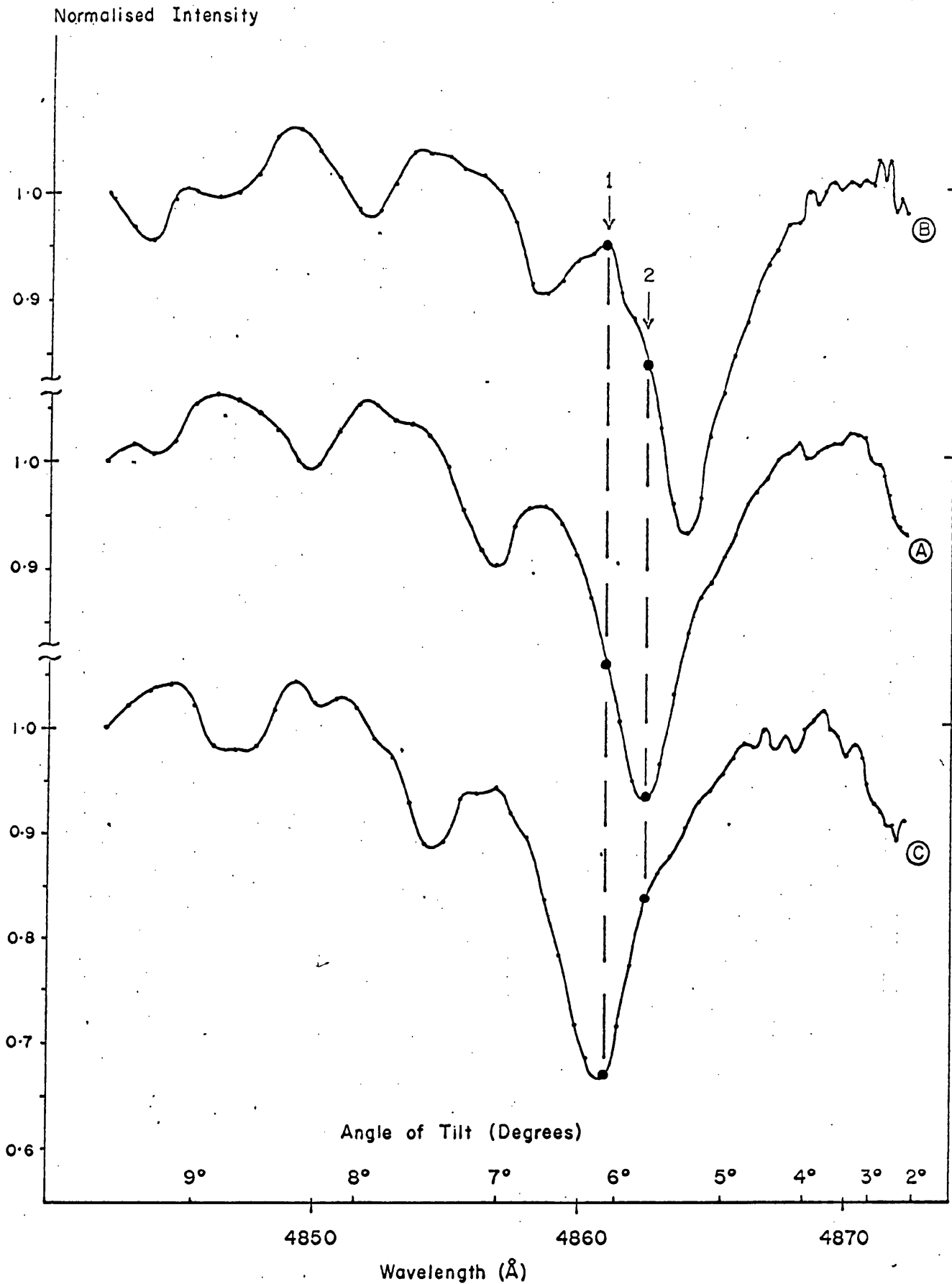


**Figure 4.8** Apparent wavelength shifts caused by image movement can be seen in these H $\beta$  profiles for  $\alpha$  Aur obtained with the image on the optical axis (A) and deliberately displaced off-axis by  $\pm 15$  arc second in declination (B and C). The wavelength/tilt calibration is correct for profile A only.

guidance error in declination is within the range  $- 20$  arc seconds to  $+ 20$  arc seconds. It can be seen from Figure 4.8 that the resulting wavelength shifts of the filter passband corresponding to the amounts of tilt marked by the Points 1 and 2 will cause the passband either to move up and down the blue wing of the line, as for Point 1, or to move from one wing of the line to the other, as for Point 2. In this particular example the normalised intensity at Point 1 will therefore be in the range  $\sim 0.67$  to  $\sim 0.95$  while that at Point 2 will be in the range  $\sim 0.68$  to  $\sim 0.84$  thus giving less noise on the signal recorded at the line centre than on one of the line wings.

It is difficult in a practical situation to assess the exact amount of noise which will be introduced at any particular point of the stellar spectrum because of poor telescope guidance. However, even with accurate telescope guidance ( $\sim \pm 1$  arc second) the wavelength shifts introduced are still likely to be of the order of a few tenths of an Ångström. The resulting variation in signal level produced by wavelength shifts of this order could amount to several per cent. Clearly, the gradient of the intrinsic spectrum will determine the change in signal which is produced by a given shift in the wavelength of the filter passband and the effect will be greatest for those stars which show the steepest line profile gradients (e.g. some of the Be stars and shell stars).

Consider, for example, a much simplified case in which the spectrum being measured consists merely of a featureless slope. If it is assumed that the filter half-width and transmittance are not affected by tilt, the recorded slope, obtained by tilt-scanning the filter, will have the same gradient as the intrinsic spectrum. Suppose that the recorded spectrum is normalised to a flat continuum of unity at some wavelength and suppose further that the gradient is  $0.05$  intensity units/Å, i.e. the normalised intensity drops from

a value of 1.0 to 0.5 over a wavelength interval of  $10 \text{ \AA}$  (this is typical of a fairly broad spectrum line and much steeper gradients are found in many stars). Since the two slopes are identical, it follows that a shift of  $0.2 \text{ \AA}$  in the wavelength of the filter passband will produce a change of 0.01 units in the recorded normalised intensity. The resulting fractional change or fractional error  $\epsilon$  produced in the recorded intensity will be dependent on the actual value of the intensity; e.g. if the normalised intensity is 0.5, the fractional error will be 0.02 (or 2 per cent photometric accuracy) while it will be 0.01 (i.e. 1 per cent photometric accuracy) at the continuum level.

The effect of guidance errors is therefore another source of noise which by itself is liable to limit the accuracy of photometric measurements made with narrow band interference filters to at least one per cent. Normally, both effects, seeing and guidance, will be combined in some complex fashion.

In the discussions concerning these effects, the ratio of focal lengths ( $F_T/F_C$ ) frequently appears in relating what happens to the star on the sky to what happens to its image at the filter. The angular size of the seeing disc and the angular displacement of the image from the optical axis are both magnified by the factor  $F_T/F_C$ . Obviously, the errors due to seeing and guidance effects could be reduced by making the ratio  $F_T/F_C$  smaller by, for example, increasing the focal length of the collimator lens. However, if the focal length of the collimator is increased the diameter of the collimated beam produced will also be increased. Unfortunately, because of manufacturing difficulties, interference filters having half-widths of  $\sim 2 \text{ \AA}$  cannot be made accurately or uniformly over diameters much larger than a few centimetres, setting an upper limit to the beam diameter which can be used without loss of light.

It would seem, therefore, that the sources of error described in this

section and Section 4.4.1 might seriously reduce the usefulness of the interference filter scanner for detecting rapid line profile variations of small amplitude. However, it will be seen later that such observations are possible although all instrumental effects must first be considered when source variability is suspected.

#### 4.5 $\beta$ -index Photometry

The discussions presented in the preceding sections have been primarily concerned with the effects of seeing conditions and telescope guidance on the accuracy of photometry attainable with very narrow band interference filters (FWHM  $\sim 2 \text{ \AA}$ ). However, the amount of broadening of the filter passband and the extent of the wavelength shifts are not dependent on the half-width of the passband and are equally present with broader band interference filters.

Such broader band interference filters having half-widths of  $15 \text{ \AA}$  to  $30 \text{ \AA}$  are commonly applied to the measurement of  $\beta$ -indices in the system developed by Crawford (1958, 1960). Filters having bandwidths of this order are sometimes not manufactured to a high degree of accuracy and different filter sets commonly have different half-widths and wavelengths of peak transmittance. As a result, corrections have frequently to be made to convert measurements made with a particular set of filters to a standard system of  $\beta$ -indices. In addition, other corrections, known as star corrections and night corrections which are derived from observations of "standard stars", have often to be applied (e.g. see Crawford and Mander, 1966).

Even after the above corrections have been applied to the  $\beta$ -index measurements, a number of reports have been made by others concerning stars which exhibit variability of their  $\beta$ -indices on very short time scales (e.g. Wood, 1968). Indeed, the appearance of these reports in the literature was partly

responsible for the initiation of the H $\beta$  scanner project forming the topic of this thesis.

The  $\beta$ -index is a measure of the H $\beta$  line strength and can be used as a classification parameter. It is defined as the ratio of the fluxes (expressed in magnitudes) measured through two filters with half-widths of  $\sim 30 \text{ \AA}$  and  $\sim 150 \text{ \AA}$  and both centred on the hydrogen  $\beta$  line. A summary of H $\beta$  photometry and the usefulness of the  $\beta$ -index is given by Golay (1974).

If  $F_N$  and  $F_W$  are the fluxes measured through the narrow band and the broad band filters, the  $\beta$ -index is defined by

$$\beta = -2.5 \log_{10} \left( \frac{F_N}{F_W} \right) .$$

In some cases there are differences in the gains  $g_N$  and  $g_W$  of the detectors with which the two fluxes are measured, in which case

$$\beta = -2.5 \log_{10} \left( \frac{g_W F_N}{g_N F_W} \right)$$

i.e.  $\beta = -2.5 \log_{10} \left( \frac{F_N}{F_W} \right) + 2.5 \log_{10} \left( \frac{g_N}{g_W} \right) .$

In either case, variations of  $\Delta F_N$  and  $\Delta F_W$  in the two fluxes  $F_N$  and  $F_W$  will result in a change in the  $\beta$ -index of  $\Delta\beta$  given by

$$(\Delta\beta)^2 = \left( \frac{\partial\beta}{\partial F_N} \right)^2 (\Delta F_N)^2 + \left( \frac{\partial\beta}{\partial F_W} \right)^2 (\Delta F_W)^2$$

where  $\frac{\partial\beta}{\partial F_N} = -\frac{2.5}{\log_e 10} \cdot \frac{1}{F_N}$

and  $\frac{\partial\beta}{\partial F_W} = \frac{2.5}{\log_e 10} \cdot \frac{1}{F_W} .$

Thus

$$(\Delta\beta)^2 = 1.086^2 \left( \frac{\Delta F_N}{F_N} \right)^2 + 1.086^2 \left( \frac{\Delta F_W}{F_W} \right)^2 .$$

If the variations in the fluxes are due to the effects described in Sections 4.4.1 and 4.4.2, it is likely that

$$\left( \frac{\Delta F_W}{F_W} \right)^2 \ll \left( \frac{\Delta F_N}{F_N} \right)^2$$

Therefore,

$$\Delta\beta \approx 1.086 \frac{\Delta F_N}{F_N}$$

where  $\Delta F_N/F_N$  is the fractional change in flux (or signal) measured through the narrow band filter. Thus the uncertainty associated with a single measurement of the  $\beta$ -index will be  $\sim 1.086$  times the uncertainty in the photometry attainable with the narrow band filter. However, it can be seen from Figure 4.7 that for a filter with a half-width of  $30 \text{ \AA}$  centred on a stellar absorption line, an increase in bandwidth of  $1 \text{ \AA}$  will typically result in an increase of  $\sim 1$  per cent in the measured signal. The exact increase will depend on the half-width of the absorption line. Thus, if  $\Delta F_N/F_N = 0.01$ , then  $\Delta\beta$  will be  $\sim 0.01$ .

Many  $\beta$ -index measurements are made with photometers which were designed to perform broad band measurements but which have had narrow band filters added to them. It is common with such instruments for the interference filters to be placed in converging or diverging beams and this will immediately broaden the passbands of the filters. In addition, when the filters are in coned beams they will be more likely to suffer from the effects of seeing and guidance drifts. Another complication is that filter manufacturers will sometimes mount a filter in a cell and will have the filter pre-tilted relative to the axis of the cell so as to tune the wavelength of the passband to the desired

value. Care must also be taken to ensure that there is no flexure of the photometer or misalignment of it with the optical axis of the telescope since these will also increase the tilt of the filter.

The net result of these hazards together with the errors due to photon noise and scintillation might be to limit the accuracy of the photometry and hence of the  $\beta$ -index to  $\sim 1$  per cent (i.e.  $\sim 0.01$  magnitudes in  $\beta$ ). Such a possibility should be borne in mind when discussing observations of stars which exhibit variable  $\beta$ -indices, although some examples of intrinsic variability almost certainly exist.

## 5. ASTRONOMICAL OBSERVATIONS

### 5.1 Introduction

The observations which have been made with the interference filter scanner since April 1974 can be divided into those obtained during a development phase and during an application phase.

During the development phase, the scanner was used with the 50 cm telescope at Glasgow and with the 91 cm telescope at the RGO. The profiles were initially measured with the  $4874/2.2 \text{ \AA}$  ( $\lambda/\Delta\lambda$ ) filter (see Table 2.3) and later with the  $4874/1.9 \text{ \AA}$  filter; the monitor beam contained a  $5100/51 \text{ \AA}$  filter. The latter two filters were used exclusively during the application phase.

The measurements made during the development revealed several instrumental difficulties which have been mentioned already; they were associated with the magnetic shielding of the photomultipliers, with temperature variations of the filters and, most seriously, with variations of the filter passbands mainly due to telescope tracking errors but also due to unsteady seeing conditions. As a result of these instrumental difficulties, none of the observations made during the development phase were of astronomical significance. However, the potential of the scanner was immediately apparent and its ability, under good observing conditions, to record accurately spectral detail has already been demonstrated by Figures 2.12 and 2.13.

Two of the most significant modifications which were made to the instrumentation during this phase, and which essentially brought the development phase to an end, were (i) fitting the dichroic filter to the post-viewer (see Chapter 3) allowing the exact position of the seeing disc in the diaphragm to be seen continuously while performing wavelength scanning, and (ii) providing electronic times-ten multipliers to both the step-size control and the spectral point counter, enabling maximum wavelength resolution scans

(i.e. at single step intervals) to be made over a spectral range ( $\sim 30 \text{ \AA}$ ) sufficiently large to encompass a complete line profile with a single scan.

The application phase began around December 1974, after which time the scanner and the recorded profiles could be kept sufficiently stable as to allow reliable astronomical observations to be made. During this second phase, observations were made at Glasgow and at the SAAO and some of these observations will be described and discussed in the following sections of this chapter.

Details of the various telescopes used during the development and application phases are given in Table 5.1. The effects of movements of the stellar seeing discs in the telescopes' focal planes are also listed.

Table 5.1. Details of the telescopes with which the observations were made.

Telescope	Focal Ratio	$F_T/F_C$	Change in angle of incidence at filter produced by image movement off axis	
			$\alpha_T = 1$ arc second	$\alpha_T = 5$ arc second
50 cm (20-inch), Glasgow	f/8	85	1.4 arc minute	6.8 arc minute
91 cm (36-inch), RGO	f/15	286	4.8 " "	24.0 " "
50 cm (20-inch), SAAO	f/18	190	3.2 " "	15.8 " "
76 cm (30-inch), SAAO	f/15	238	4.0 " "	19.5 " "

In order to assess the extent of the wavelength shifts resulting from image movement, a single step of the stepping motor produces a change in the angle of incidence of the beam on the filter of 7.5 arc minutes (i.e. 0.125 degrees/step) and this produces a wavelength shift of the filter passband of  $\sim 0.02 \text{ \AA}$  near normal incidence,  $\sim 0.5 \text{ \AA}$  at a tilt of approximately six degrees (i.e. near  $H\beta$ ) and  $\sim 0.9 \text{ \AA}$  at a tilt of about ten degrees (i.e.  $\sim \lambda 4840 \text{ \AA}$ ). It can be seen from the table that guidance errors even as small as  $\pm 1$  arc second will result in wavelength shifts of up to  $\pm 0.3 \text{ \AA}$  at  $H\beta$  and these shifts can be a very serious source of photometric noise, especially when the spectral gradients are steep. Even with very accurate telescope tracking, rapid

image movements as large as 1 arc second are commonly produced by non-ideal seeing conditions and the resulting wavelength shifts of the instrumental passband almost certainly limit the degree of photometric accuracy which can be achieved. Clearly, the limit will vary according to the spectral features but may be larger than  $\pm 1$  per cent for very steep gradients.

During both of the observing phases, the sequence of operations when making the measurements was typically as follows:

- (i) Locate and centre the star in the field of the pre-viewer, then withdraw the pre-viewer and centre the star in the focal plane diaphragm by using the post-viewer.
- (ii) Sample the signal in both beams and set the integration time (per spectral point per scan) accordingly. The integration time was usually less than ten seconds and was chosen as a compromise between photometric accuracy and time resolution.
- (iii) Set the scanning filter to its starting wavelength position by use of the motor slew, single step and step direction functions (see Chapter 3).
- (iv) Select the wavelength step-size and the number of spectral points per scan. The scans were usually standardised and the starting wavelength, the step-size and the number of spectral points were kept the same for most stars. Before the times-ten multipliers were added, the scans normally consisted of only eleven spectral points at intervals of six steps. Later the scans consisted of sixty-one points at single step intervals and in both cases the spectral range of the scans was  $\sim \lambda 4840 \text{ \AA}$  to  $\sim \lambda 4870 \text{ \AA}$ .
- (v) By using a manual punch command and by setting the thumbwheel code-switches appropriately, punch the tape identification number and the date of observation on the leader of the paper tape.
- (vi) Record the dark background signal or off-set the telescope and

record the sky brightness (and then re-centre the star). Normally, because of the narrow bandwidths of the filters, the sky brightness contribution was much less than the dark background, even when working close to the full Moon.

- (vii) Initiate line profile measurements and continue scanning under automatic control. When scanning is stopped (manually), punch data termination code on the paper tape.

An observation of a star consisted of a series of scans in alternate directions. As a result of the anti-backlash property of the gearbox linking the tilting filter to the stepping motor, no systematic difference could be found between the profiles measured in the two scan directions and therefore no distinction was made between them when reducing the data. A single scan comprised pairs of intensity measurements (scanning beam and fixed monitor beam) at each of the spectral points (i.e. filter positions) determined by the scan control.

The line profiles have been derived from the data by first subtracting the appropriate background signal (dark or sky) from each integrated count for the two beams. After forming the ratios of the residual counts (scanning beam to monitor beam) so as to remove the effects of atmospheric transparency changes and of scintillation noise, the ratios for each spectral point were averaged and the mean line profile finally normalised to the level of the blue continuum. All of the profiles have been normalised to approximately the same wavelength but none has been rectified to a flat continuum, although the transmittances of the two narrow band filters were  $\sim 5$  per cent greater at  $\lambda 4870 \text{ \AA}$  than at  $\lambda 4840 \text{ \AA}$  (see Figure 2.10).

Wavelength/tilt calibrations were performed by the method described in Chapter 2. If the scanner and the interference filters were not disturbed, and by virtue of the temperature stabilisation of the filter chamber, one calibration could be applied to several nights of observations. However,

after time intervals of more than a few days, new calibrations were performed so as to allow for any ageing of the filters.

In the introduction to this thesis, the recent discovery of variations of intrinsic linear polarization across the emission lines of some Be stars was briefly discussed. Although the line profile scanner constructed for this project was not designed as a polarimeter, some polarizing optics (described in Chapter 3) were subsequently added and a few attempts were made during the development and application phases to measure the reduced polarization phenomenon reported for these stars.

Briefly, the linear polarization measurements were made by a variation of Fessenkov's method (see Clarke and Grainger 1971). Three independent half-wave plates with their fast axes oriented (for convenience) at  $0^\circ$ ,  $30^\circ$  and  $60^\circ$  to the axis of the polarizing beam-splitter were placed sequentially in the cone of light, prior to the diaphragm in the telescope's focal plane (see Chapter 3). The first half-wave plate was placed in the beam and a single scan of the line profile was obtained with the thumbwheel code-switches of the punch interface set appropriately. On completion of each scan, the automatic scanning sequence was interrupted to allow a different half-wave plate to be placed in the beam and to reset the thumbwheel code-switches, after which scanning was resumed. This cycle was repeated until a number of scans had been obtained for each half-wave plate.

By combining the three measured (mean) profiles in the appropriate way, it should (in principle) be possible to obtain differential polarization measurements across a spectral line. However, because of the effects of residual guidance errors and of unsteady seeing conditions, together with small wavelength shifts introduced by prismatic effects of the waveplates, it was found that the photometric accuracy which could be achieved was insufficient to allow reliable polarization measurements to be obtained. A

photometric accuracy of  $\pm 0.5$  per cent could be achieved fairly easily, but an accuracy of  $\pm 0.1$  per cent could not be achieved simply by using longer integration times since the other (instrumental) sources of noise which were present prevented this. A photometric accuracy of better than  $\pm 0.1$  per cent is required to detect the expected reduced polarizations. Due to the relatively large and random photometric noise, very inconsistent differential polarization measurements were obtained and it was concluded that the technique was unsuitable for these observations. No further discussion of these measurements will be given and none of the polarimetric observations will be presented.

## 5.2 Observations of Be and Shell Stars

Reliable observations of a number of bright Be and shell stars were carried out at Glasgow and at the SAAO. The Glasgow observations were limited to two of the brightest Be stars ( $\gamma$  Cas and  $\zeta$  Tau) because industrial atmospheric pollution in Glasgow results in poor sky transparency and also causes rapid deterioration of the aluminium coating of the primary mirror of the 50 cm telescope. A further eleven bright Be stars were observed at the SAAO. All of these stars are listed in Table 5.2.

Most of the observations of a star were of short duration ( $\sim 30$  minutes) and were intended merely to investigate night-to-night variations of the  $H\beta$  line. Of the ten Be stars which were observed on more than one occasion (see Table 5.2) only two ( $\omega$  Car and  $\eta$  Cen) failed to show any change in the  $H\beta$  line. However, because measurements of the Be stars have been made on only a relatively small number of nights, the observations reported in this section should be regarded as merely giving an indication of the type of variations which are occurring in these stars.

Rapid profile variations taking place during the observations might be detected by comparing the scatter of the observations (i.e. the rms. deviation or standard deviation of a single measurement,  $\sigma_{\text{Obs}}$ ) with the

Name	HD Number	MWC * Number	Spectral Type †	$m_v$ †	Number of Observations	Remarks
$\gamma$ Cas	5394	9	B0 IV ? e	2.7	14	1, 4, 5
$\zeta$ Tau	37202	115	B 2 IV p	3.0	2	1, 4, 5
$\zeta$ Pup	62623		A 3 II ep	4.0	1	2
$\omega$ Car	89080		B 7 IV	3.3	2	3
—	91465	208	B 5 V e	3.6	1	3
—	102776	218	B 3 V ne	4.3	1	2
$\delta$ Cen	105435	219	B 2 ? V ? pe	2.9	8	2, 3, 5
$\lambda$ Cru	112078		B 5 ? V n	4.6	1	2
$\mu$ Cen	120324	229	B 2 V ? pne	3.5	3	2, 3, 5
$\eta$ Cen	127972	232	B 1.5 V ? ne	2.4	4	3
48 Lib	142983	239	B p	4.8	8	2, 3, 4, 5
$\chi$ Oph	148184	241	B 2 V e	4.3	5	2, 3, 5
$\zeta^1$ Sco	152236	243	B 1 I ae	4.8	3	2, 3, 5
$\alpha$ Ara	158427	261	B 2.5 V	2.9	9	2, 3, 5

\* Mount Wilson Catalogue (Merrill & Burwell 1933 etc.)..

† Spectral types and visual magnitudes are from Hoffleit (1964).

Remarks: (Telescopes) 1) 50 cm Glasgow, 2) 76 cm SAAO, 3) 50 cm SAAO,  
4) Shell star (Underhill 1966),  
5) Changes in H $\beta$  line profile observed.

scatter expected from photon-statistics ( $\sigma_{\text{Phot}}$ ). If the ratio of  $\sigma_{\text{Obs}}$  to  $\sigma_{\text{Phot}}$  is found to be larger than two, it is possible that the observations show variations (or a scatter) which are too large to be accounted for merely by photon shot-noise. Bahng (1975b) has examined his data in this way and has adopted this approach as a means of detecting rapid profile variations of Be and Wolf-Rayet stars. However, although a necessary condition to the detection of rapid intrinsic variability is that  $\sigma_{\text{Obs}}$  be significantly greater than  $\sigma_{\text{Phot}}$ , this is not sufficient to prove conclusively that the differences between the  $\sigma$ 's are due to variability of the star and are not caused by other (instrumental) effects. Also, since most of the observations reported here consist of a small number of scans ( $< 10$ ), it is possible, with such a small data sample, that the observed statistics may depart quite significantly from the idealised photon values. In these cases it is not possible to determine if rapid variations are occurring unless the amplitudes of the variations are many times greater than the photon-shot noise, which was typically  $\pm 1 - 2$  per cent. A few observations of longer duration ( $1 - 1\frac{1}{2}$  hours), consisting of  $\sim 30$  scans, were also obtained for  $\gamma$  Cas. It will be seen later that in these cases the observed statistics are very nearly the same as the photon-statistics, an indication that no rapid variations with amplitudes greater than photon shot-noise were occurring during the observations.

Regular observations of comparison stars have not been made, partly because the usefulness of observations of stars having different spectral features to the Be stars is perhaps doubtful (as discussed in Chapter 1) and also because the observations of the Be stars were concerned only with relative photometry and were aimed at detecting changes in the structure of the H $\beta$  line rather than making absolute photometric measurements.

Some results for individual stars will now be presented and discussed in more detail.

$\gamma$  Cas The observations of  $\gamma$  Cas can be divided into two groups. The first includes the observations made with the 50 cm telescope at Glasgow between December 1974 and February 1975. In these observations the profile of the  $H\beta$  line was measured in two stages, firstly with a moderate wavelength interval (6 motor steps =  $0.75^\circ = \sim 5.5 \text{ \AA}$  at  $\lambda 4840 \text{ \AA}$  or  $\sim 3 \text{ \AA}$  at  $\lambda 4861 \text{ \AA}$ ) between spectral points, with a spectral range from  $\sim \lambda 4841 \text{ \AA}$  to  $\sim \lambda 4872 \text{ \AA}$ , and secondly with the minimum wavelength interval (1 step) over the spectral range  $\sim \lambda 4855 \text{ \AA}$  to  $\sim \lambda 4866 \text{ \AA}$ ; in both stages, eleven spectral points were measured.

The second group of observations of  $\gamma$  Cas was obtained with the Glasgow telescope between September 1975 and November 1975. These profiles were all measured with the minimum wavelength step-size (single step) (i.e. maximum spectral resolution). Each wavelength scan covered the spectral range  $\sim \lambda 4841 \text{ \AA}$  to  $\sim \lambda 4872 \text{ \AA}$  by making use of the times-ten option on the spectral point counter so that each scan consisted of 61 spectral points. Both groups of observations are summarised in Table 5.3.

The mean  $H\beta$  line profiles derived from the first group of observations are shown in Figure 5.1. The standard errors of the mean intensities are typically less than  $\pm 1$  per cent for all spectral points and the spectral points which were measured on the large and small step-size scans are represented by squares ( $\blacksquare$ ) and dots ( $\bullet$ ) respectively while those spectral points which were measured on both types of scans are represented by triangles ( $\blacktriangle$ ).

Variations of the emission line are evident in several respects. For example, it is apparent that the shoulder found on the long wavelength side of the emission feature ( $\sim \lambda 4863 \text{ \AA}$ ) varies in both shape and width from one profile to another. Since  $\gamma$  Cas is known to be a shell star (Underhill 1966), it is likely that this shoulder represents the red component (R component) of a double-peaked emission line, partly obscured by an

Table 5.3 Details of Observations of  $\gamma$  Cas

Date	Mid-time (UT)	T * (seconds)	Number of Scans				Number of Spectral Points	$\sigma_{\text{Phot}}$ (continuum) $\approx \sigma_{\text{Obs}}$
			4841 Å - 4872 Å	4855 Å - 4866 Å	4858 Å - 4864 Å			
1974 Dec 12	23 <sup>h</sup> :21	6	20	-	20	20	$\pm 1.1\%$	
1975 Jan 15	21 <sup>h</sup> :11	8	10	-	10	20	$\pm 1.2\%$	
Feb 2	19 <sup>h</sup> :28	6	16	10	-	28	$\pm 1.5\%$	
Feb 18	19 <sup>h</sup> :24	5	18	12	-	29	$\pm 1.7\%$	
Feb 25	19 <sup>h</sup> :33	5	14	8	-	29	$\pm 1.9\%$	
1975 Sept 14	01 <sup>h</sup> :08	2	31	-	-	61	$\pm 1.8\%$	
Sept 14	02 <sup>h</sup> :42	2	28	-	-	61	$\pm 1.9\%$	
Nov 8	21 <sup>h</sup> :22	3	9	-	-	61	$\pm 1.7\%$	
Nov 8	22 <sup>h</sup> :39	3	30	-	-	61	$\pm 1.7\%$	
Nov 21	18 <sup>h</sup> :03	3	8	-	-	61	$\pm 1.7\%$	

\* T is the integration time per spectral point per scan.

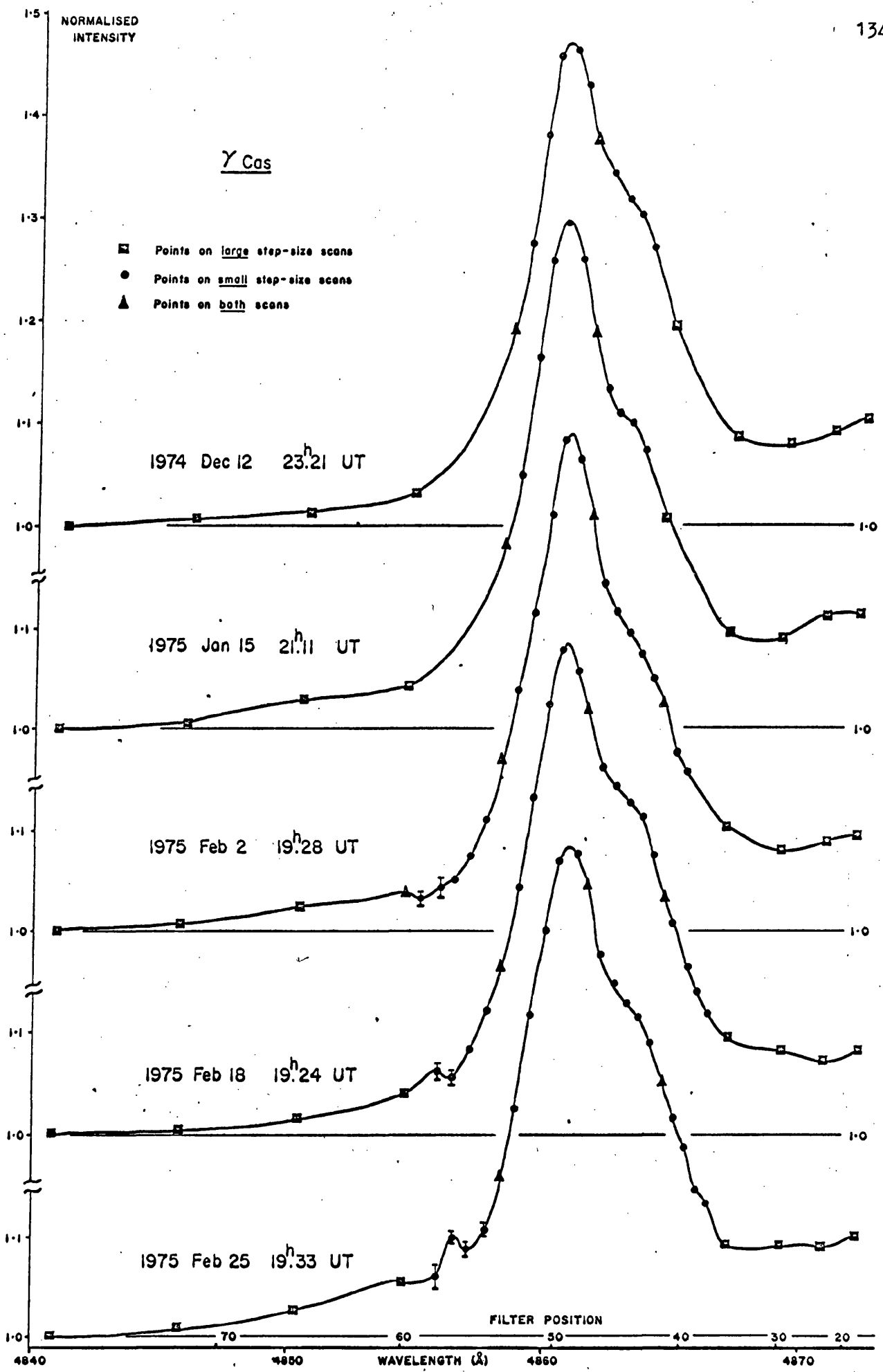


Figure 5.1 H $\beta$  profiles for  $\gamma$  Cas showing changes of the red wing and the appearance of a small emission peak at  $\lambda$  4856 Å.

asymmetric shell absorption feature. Variations of the R component might arise either from changes in the emission strength or from changes of the depth or wavelength of the shell absorption.

A small, blue-shifted, secondary emission peak can be seen developing around  $\lambda$  4856 Å on the profiles measured on 1975 Feb 2, 18 and 25. Unfortunately this region was not scanned with sufficient resolution on 1974 Dec 12 and 1975 Jan 15. As well as increasing in intensity, the small peak also systematically shifted towards longer wavelength, from  $\sim \lambda$  4854.5 Å on 1975 Feb 2 through  $\sim \lambda$  4855.5 Å on Feb 18 to  $\sim \lambda$  4856.5 Å on Feb 25. The error bars shown at this feature in Figure 5.1 represent the standard errors of the mean intensities at those spectral points. Although the error bars at the spectral points making up this feature actually overlap, the fact that the peak occurs on three separate occasions, at approximately (but not precisely) the same wavelength, makes the feature more significant. In addition, it can be seen that on Feb 25 the small peak was contained entirely within the range of the small step-size scans and therefore its presence is unlikely to be a result of combining the data from the two types of scan.

Other less obvious variations of the profiles are seen at the "edges" of the emission line and may be due to either changes in the emission strength or in the underlying photospheric absorption upon which the emission is superimposed. These variations can be seen as a filling-in effect around  $\lambda$  4869 Å on 1975 Feb 18 and Feb 25 relative to the other dates. Also, the blue wing between  $\lambda$  4840 Å and  $\lambda$  4855 Å is least steep on 1974 Dec 12.

The observed scatter of the data ( $\sigma_{\text{Obs}}$ ) has also been evaluated at each spectral point for each of these profiles. The ratios of  $\sigma_{\text{Obs}}$  to  $\sigma_{\text{Phot}}$  are shown in Figure 5.2. Values of  $\sigma_{\text{Phot}}$  are given for the emission peak and for the blue and red wings of the line.

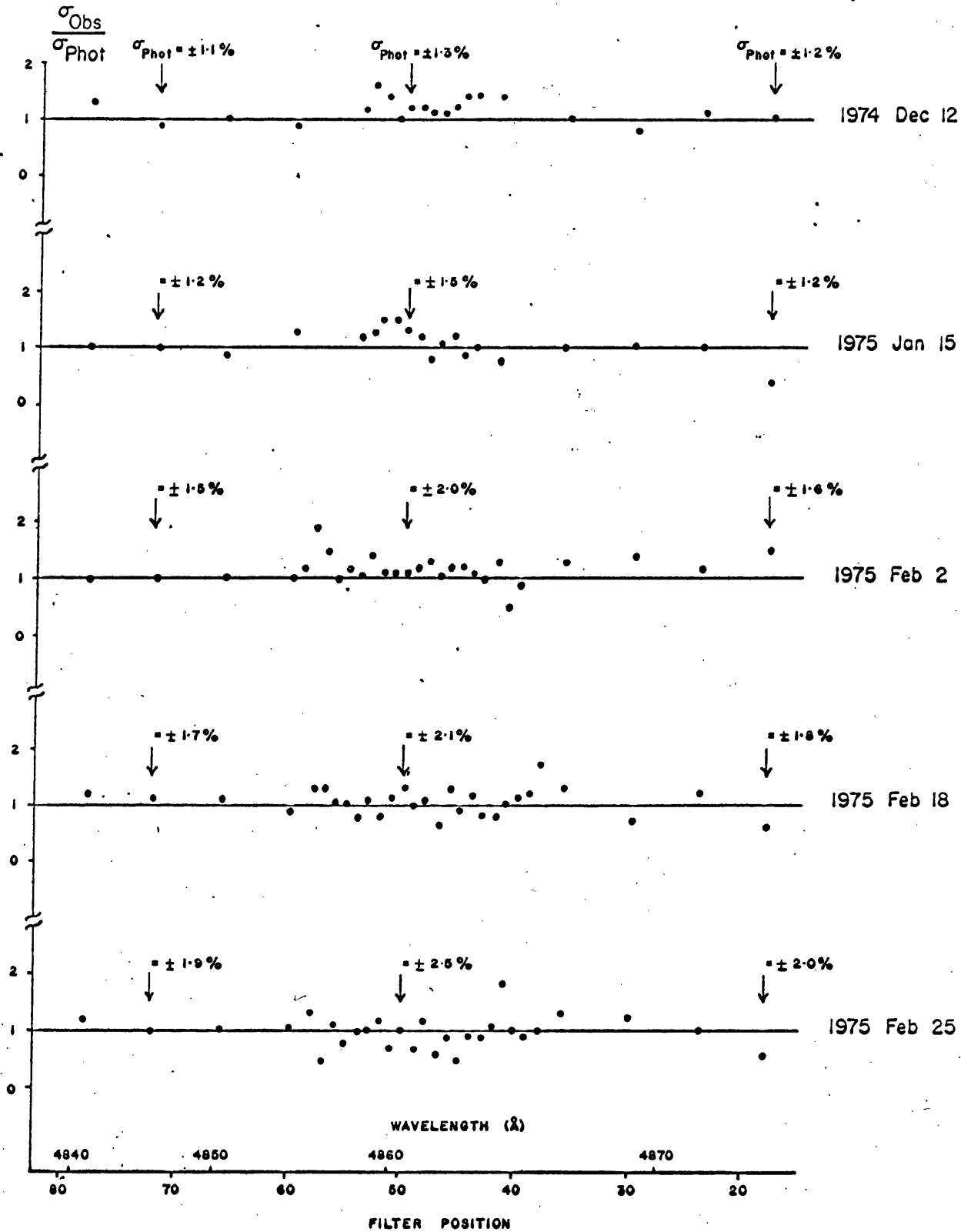


Figure 5.2

Comparison of the observed rms. deviations ( $\sigma_{\text{Obs}}$ ) with the values expected from photon statistics ( $\sigma_{\text{Phot}}$ ) for the observations of  $\gamma$  Cas presented in Figure 5.1

It can be seen from Figure 5.2 that the observed scatter is close to that expected from photon statistics and the largest value of  $\sigma_{\text{Obs}}/\sigma_{\text{Phot}}$  is only 1.8. The values of  $\sigma_{\text{Obs}}/\sigma_{\text{Phot}}$  tend to be slightly larger across the emission feature than on the flatter parts of the spectrum and this might be an indication of residual image movement due to unsteady seeing conditions. However, the size of the data samples are too small to allow reliable statistical parameters to be evaluated. This is evident since  $\sigma_{\text{Obs}}/\sigma_{\text{Phot}}$  is often less than unity when the number of samples (scans) is small, despite the fact that  $\sigma_{\text{Obs}}$  should always be at least as great as  $\sigma_{\text{Phot}}$ . The values of  $\sigma_{\text{Obs}}/\sigma_{\text{Phot}}$  are sufficiently close to unity, however, as to conclude that there were no rapid variations with amplitudes greater than  $\sim \pm 2$  per cent of the continuum intensity occurring during these observations.

The mean profiles obtained from the observations made after September 1975 are shown in Figure 5.3. Again the standard errors of the mean intensities are mostly less than  $\pm 1$  per cent and the profiles have been normalised to approximately the same wavelength as those shown in Figure 5.1.

The emission shoulder at  $\lambda 4863 \text{ \AA}$  is again seen on the profiles for 1975 Sept 14 and its subsequent development into a true double emission peak is seen in the profiles for Nov 8 and Nov 21. In addition, the overall strength of the emission decreased from  $\sim 1.35$  to  $\sim 1.30$  between Sept 14 and Nov 8 and then increased to  $\sim 1.32$  again between Nov 8 and Nov 21. It can also be seen from the profiles in Figure 5.3 that the V/R ratio (i.e. the comparative strength of the V and R emission peaks) not only changed with the development of the R peak but also underwent a significant variation between 1975 Nov 8 21<sup>h</sup>.22 UT and 22<sup>h</sup>.39 UT. The mean profiles for these two sets of observations were obtained from 9 scans and 30 scans respectively (see Table 5.3). However, when the series of 30 scans obtained at 22<sup>h</sup>.39 UT is divided into three groups of ten scans and each group averaged separately, no statistically significant variations of the profile can be found

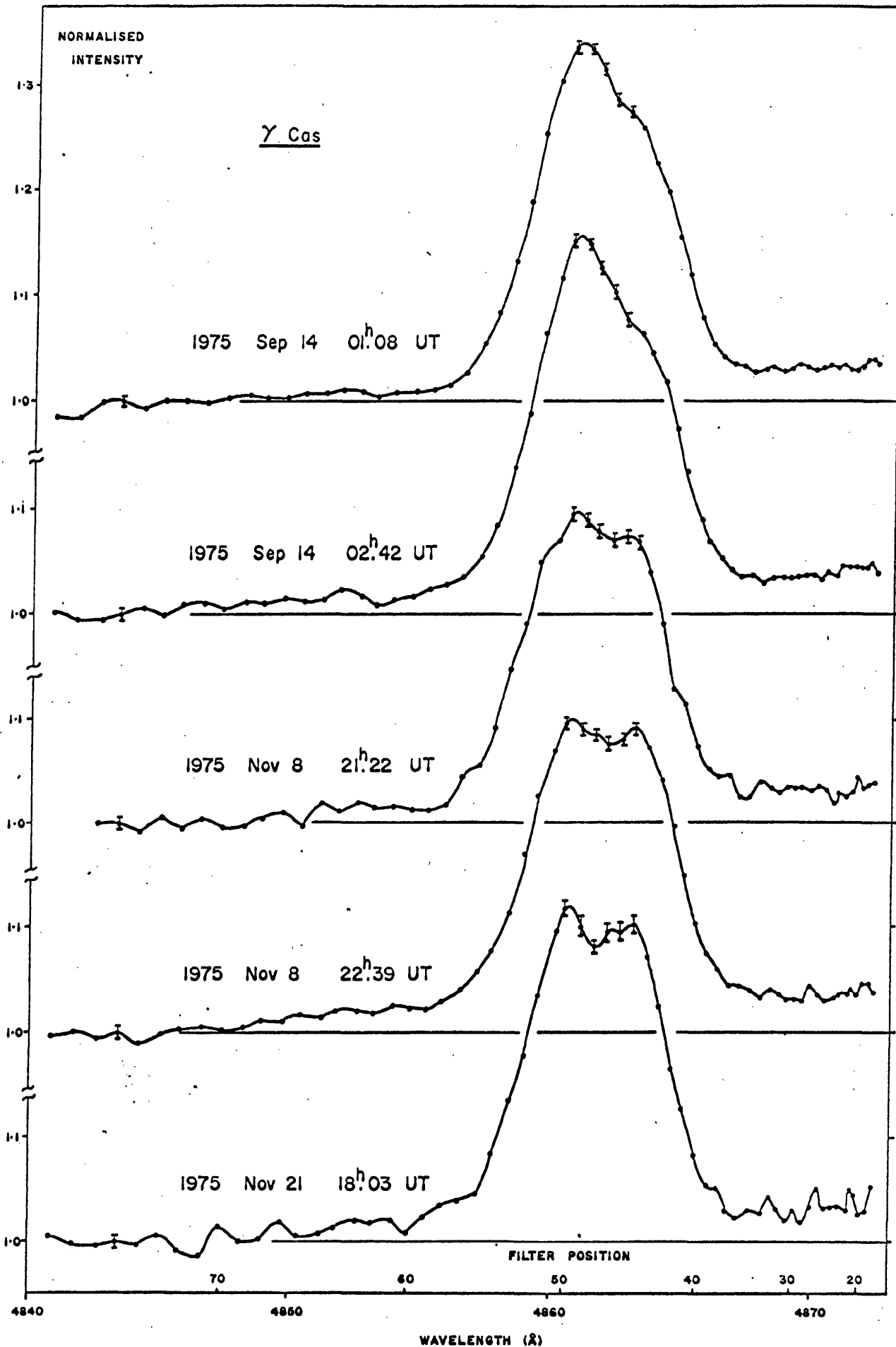


Figure 5.3  $H\beta$  profiles for  $\gamma$  Cas showing variations of the emission strength and the development of a double peaked emission feature.

from one group to another although each group shows the V/R ratio is less than that given by the mean profile for 21.<sup>h</sup>22 UT.

Further comparison of Figure 5.3 with Figure 5.1 reveals that there was also a longer term variation in the emission strength from  $\sim 1.5$  on 1975 Jan 15 to  $\sim 1.3$  on 1975 Nov. 8. Table 5.4 lists the strength of the emission relative to the blue continuum for each of the observations.

The observed and the expected scatter of the data for the observations of  $\gamma$  Cas made since September 1975 have again been compared. It can be seen in Figure 5.4 that the values of  $\sigma_{\text{Obs}}$  are again very nearly equal to the values expected from photon shot-noise and in this case there is no systematic variation of  $\sigma_{\text{Obs}}/\sigma_{\text{Phot}}$  across the emission line.

It can also be seen from Figure 5.4 by comparing the plots of  $\sigma_{\text{Obs}}/\sigma_{\text{Phot}}$  for 1975 Sept 14 and Nov 8 (22.<sup>h</sup>39 UT) with those for Nov 8 (21.<sup>h</sup>22 UT) and Nov 21, that when there are a greater number of scans ( $\sim 30$ ) making up the mean profile, the range of values of  $\sigma_{\text{Obs}}/\sigma_{\text{Phot}}$  is smaller and also there are fewer spectral points for which  $\sigma_{\text{Obs}}$  is less than  $\sigma_{\text{Phot}}$  (i.e.  $\sigma_{\text{Obs}}/\sigma_{\text{Phot}} < 1$ ). This indicates that although there may be some values of  $\sigma_{\text{Obs}}$  which, for a small data sample, do not agree with the expected photon values, when the data sample becomes larger the observed statistics more closely approach the expected photon statistics.

Nevertheless, the conclusion drawn from Figure 5.4 is that, once again, there were no rapid variations of the H $\beta$  line with amplitudes greater than photon noise ( $\sim \pm 2$  per cent) occurring during these observations. The variation in the strength of the R peak over an interval of  $\sim 1$  hour on 1975 Nov 8 (see Figure 5.3 and Table 5.4) is only apparent after several scans are averaged so as to reduce the extent of the photon noise; any rapid variations of this amplitude would be lost in the photon noise on a single scan. Observations of  $\gamma$  Cas are at present being continued at Glasgow.

Table 5.4 Variations of the H $\beta$  Emission Strength for  $\gamma$  Cas

UT - Date			Emission Strength
1974	Dec 12	23 <sup>h</sup> :21	1.475 $\pm$ .004
1975	Jan 15	21 <sup>h</sup> :11	1.500 $\pm$ .007
	Feb 2	19 <sup>h</sup> :28	1.490 $\pm$ .007
	Feb 18	19 <sup>h</sup> :24	1.485 $\pm$ .008
	Feb 25	19 <sup>h</sup> :33	1.485 $\pm$ .008
1975	Sept 14	01 <sup>h</sup> :08	1.340 $\pm$ .004
	Sept 14	02 <sup>h</sup> :42	1.355 $\pm$ .004
	Nov 8	21 <sup>h</sup> :22	(V) 1.295 $\pm$ .006
			(R) 1.275 $\pm$ .006
	Nov 8	22 <sup>h</sup> :39	(V) 1.300 $\pm$ .004
			(R) 1.295 $\pm$ .004
Nov 21	18 <sup>h</sup> :03	(V) 1.320 $\pm$ .007	
		(R) 1.305 $\pm$ .007	

V  $\equiv$  Violet peak

R  $\equiv$  Red peak

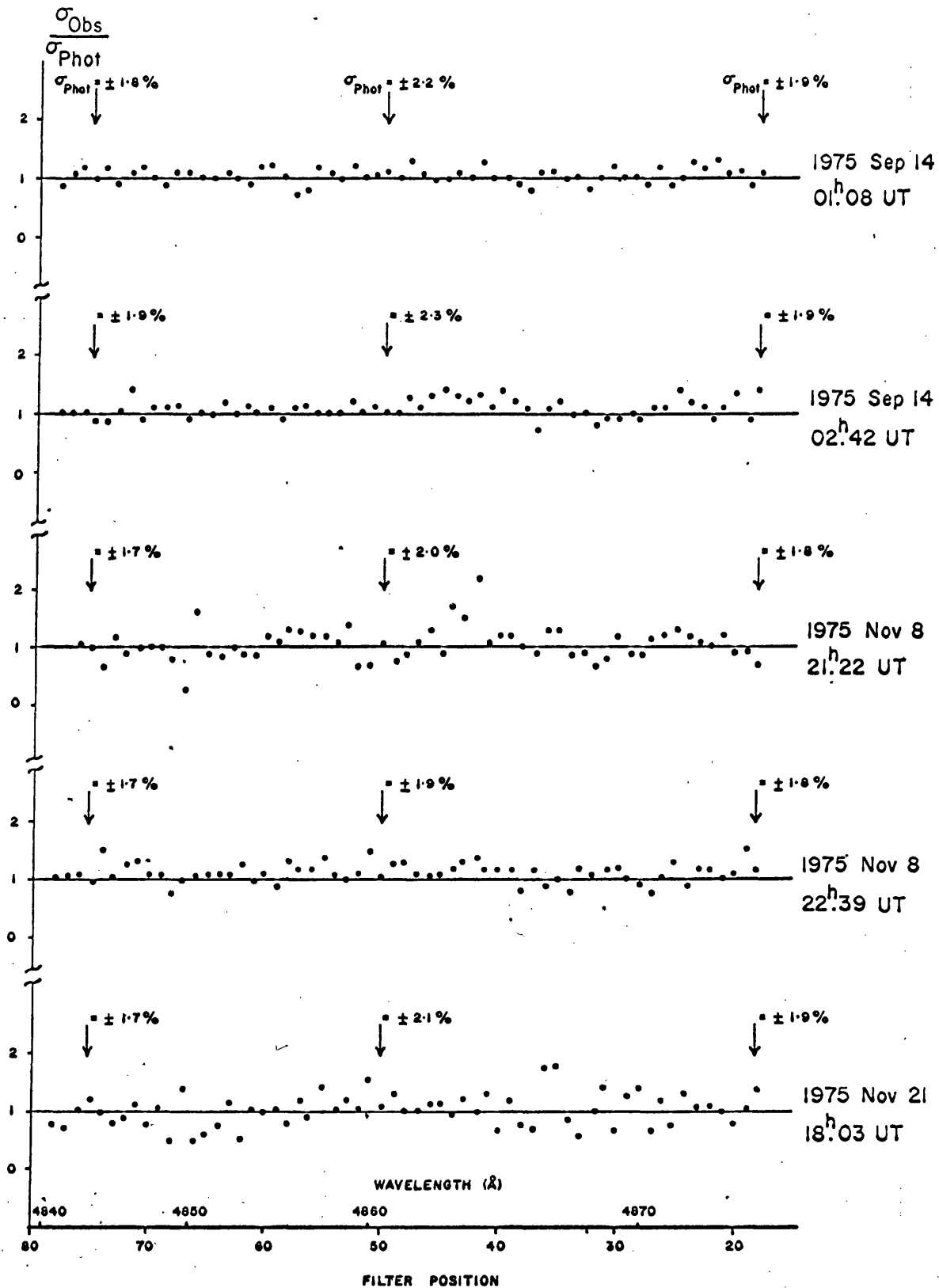


Figure 5.4

Comparison of the observed statistics with the expected photon statistics for the observations of  $\gamma$  Cas presented in Figure 5.3

ζ Tau Despite having an altitude at transit of  $\sim 55^\circ$ , very severe extinction due to smog and haze above the city prevented observations of ζ Tau with the Glasgow telescope on all but a few nights. However, the measurements of the Hβ line profile which were obtained give an indication of variability on a time-scale of days.

For the reasons just mentioned, the observations were only of short duration ( $\sim 30$  minutes) and were at best only obtained at intervals of days. Such day-to-day variations of the Hβ line in ζ Tau have previously been reported by Hack and Struve (1970). No conclusions can be drawn from these observations regarding shorter term variations in this star.

Mean profiles of the Hβ line in ζ Tau are shown in Figure 5.5 (a) for 1975 January 27-28 and February 18-19; details of the observations are given in Table 5.5. These are the two best profiles obtained and the standard errors of the mean intensities are  $\sim \pm 0.6$  per cent. The profiles were again measured by combining large and small step-size scans in the same way as with some of the earlier observations of γ Cas. However, the small step-size scans in this case consisted of 21 spectral points ( $\sim \lambda 4856 \text{ \AA} - \lambda 4866 \text{ \AA}$ ), since the optional times-ten multipliers had been added but were not used over the entire scan range.

Table 5.5 Summary of Observations of ζ Tau

UT Date	T (secs)	Number of scans		Total number of spectral points	$\sigma_{\text{Phot}}$ (continuum) $\approx \sigma_{\text{Obs}}$
		4841 $\text{\AA}$ - 4872 $\text{\AA}$	4856 $\text{\AA}$ - 4866 $\text{\AA}$		
1975 Jan 27-28	8	12	6	28	$\pm 1.5\%$
1975 Feb 18-19	6	10	12	29	$\pm 2.0\%$

It is clear from Figure 5.5 (a) that definite changes in the line profile took place between Jan 27-28 and Feb 18-19. It appears that the strengths of both the V and R peaks increased and the central absorption became less deep. However, there was very little or no shift in the

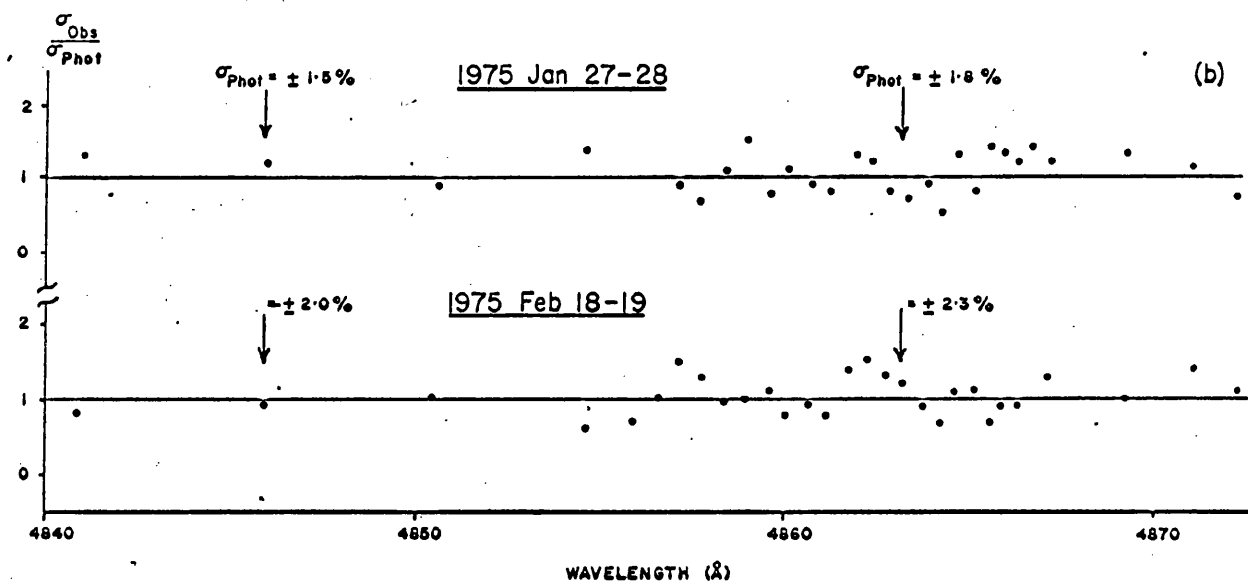
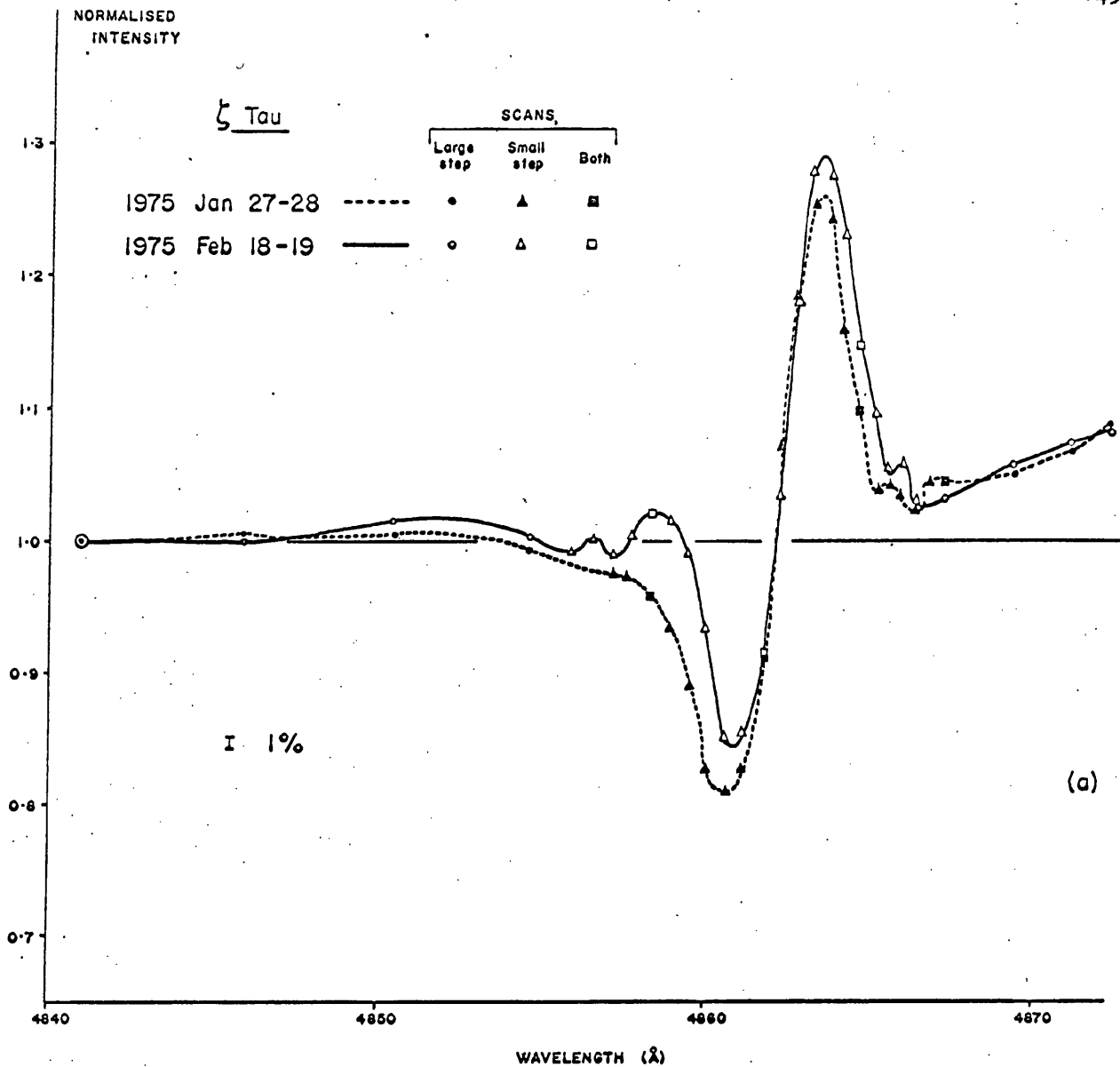


Figure 5.5 a).  $H\beta$  profiles for  $\zeta$  Tau showing changes in the V and R components and in the shell absorption. b). Comparison of the observed and expected statistics for the observations presented in a).

wavelength of either the R peak or the absorption core. Because of the method of normalising the scans, it is inevitable that there is agreement between the levels of the blue continua, however, there is also very good agreement of the levels on the long wavelength side of the line.

The ratios of the observed standard deviations to the deviations predicted by photon statistics are shown in Figure 5.5 (b) for the two dates in question. In all cases,  $\sigma_{\text{Obs}}$  is less than 1.5 times  $\sigma_{\text{Phot}}$  and it is likely that those values of  $\sigma_{\text{Obs}}$  greater than  $\sigma_{\text{Phot}}$  are again the result of the small data sample, since there are also a number of spectral points for which  $\sigma_{\text{Obs}}$  is less than the expected  $\sigma_{\text{Phot}}$ .

The remaining observations which are presented in this section were all obtained at the SAAO during April and May 1975. The profiles all consist of 61 spectral points measured sequentially at single step intervals over the entire spectral range ( $\sim \lambda 4838 \text{ \AA}$  to  $\sim \lambda 4871 \text{ \AA}$ ).

$\alpha$  Ara Line profile measurements of  $\alpha$  Ara were made on two nights with the 76 cm telescope and on 7 nights with the 50 cm telescope at the SAAO. Details of the observations are listed in Table 5.6.

The mean H $\beta$  line profiles derived from these observations are presented in Figure 5.6. The standard errors of the mean intensities of these profiles are all in the range  $\pm 0.2$  per cent to  $\pm 0.5$  per cent.

Systematic variations of the V/R ratio are immediately obvious in these profiles and the interpolated mean intensities of the V and R components for each of the dates are listed in Table 5.7. It would seem that most of the variations are due to the R component increasing in strength, although there are also smaller variations in the strength of the V component. It can be easily seen from the profiles that  $V > R$  on 1975 April 23-24,  $V \approx R$  on April 29-30 and  $V < R$  on May 25-26.

Table 5.6 Details of Observations of  $\alpha$  Ara

UT Date		T (seconds)*	Number of Scans	$\sigma_{\text{Phot}}$ (continuum) $\approx \sigma_{\text{Obs}}$
1975	April 23-24	1	4	$\pm 1.1 \%$
	April 24-25	2	6	$\pm 0.8 \%$
	April 28-29	2	16	$\pm 1.1 \%$
	April 29-30	2	6	$\pm 1.1 \%$
	April 30- May 1	3	4	$\pm 0.9 \%$
	May 20-21	3	14	$\pm 1.1 \%$
	May 21-22	3	6	$\pm 1.1 \%$
	May 24-25	4	8	$\pm 1.0 \%$
	May 25-26	3	6	$\pm 1.2 \%$

\* T is the integration time per spectral point per scan.

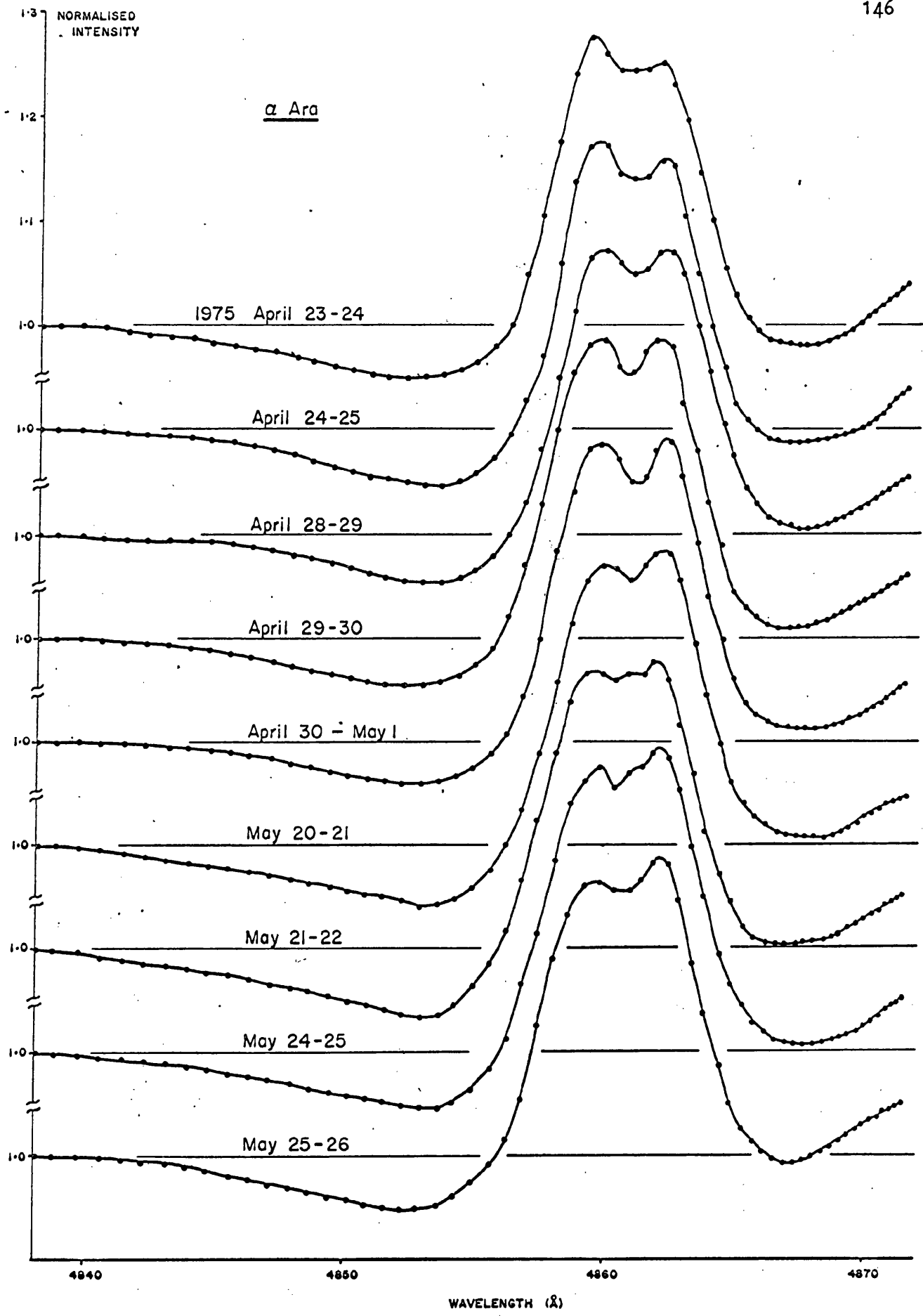


Figure 5.6

A series of H $\beta$  profiles for  $\alpha$  Ara showing systematic V/R variations.

Table 5.7 Variations of the H $\beta$  Emission Strength for  $\alpha$  Ara,  $\delta$  Cen and  $\chi$  Oph

Star	Date (1975)	Emission Strength	
$\alpha$ Ara	April 23-24	(V) $1.278 \pm .008$	(R) $1.255 \pm .009$
	" 24-25	$1.275 \pm .003$	$1.260 \pm .005$
	" 28-29	$1.272 \pm .004$	$1.270 \pm .004$
	" 29-30	$1.285 \pm .007$	$1.285 \pm .006$
	Apr 30-May 1	$1.286 \pm .005$	$1.290 \pm .003$
	May 20-21	$1.273 \pm .003$	$1.285 \pm .003$
	" 21-22	$1.270 \pm .003$	$1.280 \pm .004$
	" 24-25	$1.280 \pm .005$	$1.295 \pm .005$
	" 25-26	$1.265 \pm .005$	$1.285 \pm .006$
$\delta$ Cen	April 22-23		$1.455 \pm .005$
	" 22-23		$1.455 \pm .005$
	" 24-25		$1.492 \pm .005$
	" 29-30	(V) $1.542 \pm .003$	(R) $1.550 \pm .002$
	Apr 30-May 1		$1.538 \pm .005$
	May 20-21		$1.525 \pm .005$
	" 25-26		$1.532 \pm .010$
	" 25-26		$1.532 \pm .007$
$\chi$ Oph	April 22-23		$2.22 \pm .02$
	" 23-24		$2.29 \pm .01$
	Apr 30-May 1		$2.34 \pm .03$
	May 20-21		$2.26 \pm .02$
	" 25-26		$2.37 \pm .02$

V  $\equiv$  Violet peak

R  $\equiv$  Red peak

In addition to the V/R variations, the strength of the central (shell) absorption can also be seen to change from night to night. For example, the absorption core was much deeper ( $\sim 5$  per cent below the intensity of the V and R peaks) on April 30 - May 1 than on May 21-22, when the central absorption was barely visible.

On two occasions (April 28-29 and May 20-21) a larger number of scans (16 and 14 respectively) were obtained. However, no rapid variations (from scan to scan) which were larger than the statistical uncertainties were found.

$\mu$  Cen The emission at  $H\beta$  in  $\mu$  Cen is somewhat weaker than in the Be stars discussed so far and takes the form of slight filling in of the core of the photospheric  $H\beta$  absorption line.

Three profiles of  $H\beta$  in  $\mu$  Cen were obtained and are presented in Figure 5.7; the standard errors of the mean intensities are  $\sim \pm 0.5$  per cent. Very slight variations of the weak emission can be seen in these profiles. On 1975 April 23-24 the emission was slightly asymmetrical and appears to be blue shifted relative to the absorption feature. On April 30 - May 1 the emission was almost centrally placed in the absorption line while on May 20-21 it was closer to the red side of the absorption. There also seems to be an indication that on April 23-24 and April 30 - May 1 the emission consisted of small V and R components separated by a central absorption but there is little or no evidence of this on May 20-21.

48 Lib,  $\zeta^1$  Sco,  $\delta$  Cen and  $\chi$  Oph

Two mean profiles of the  $H\beta$  line for each of these stars are shown in Figures 5.8 and 5.9. The profiles have been selected as showing the largest variations observed and in each case the standard errors of the mean intensities are typically in the range  $\pm 0.5$  per cent to  $\pm 2$  per cent of the continuum.

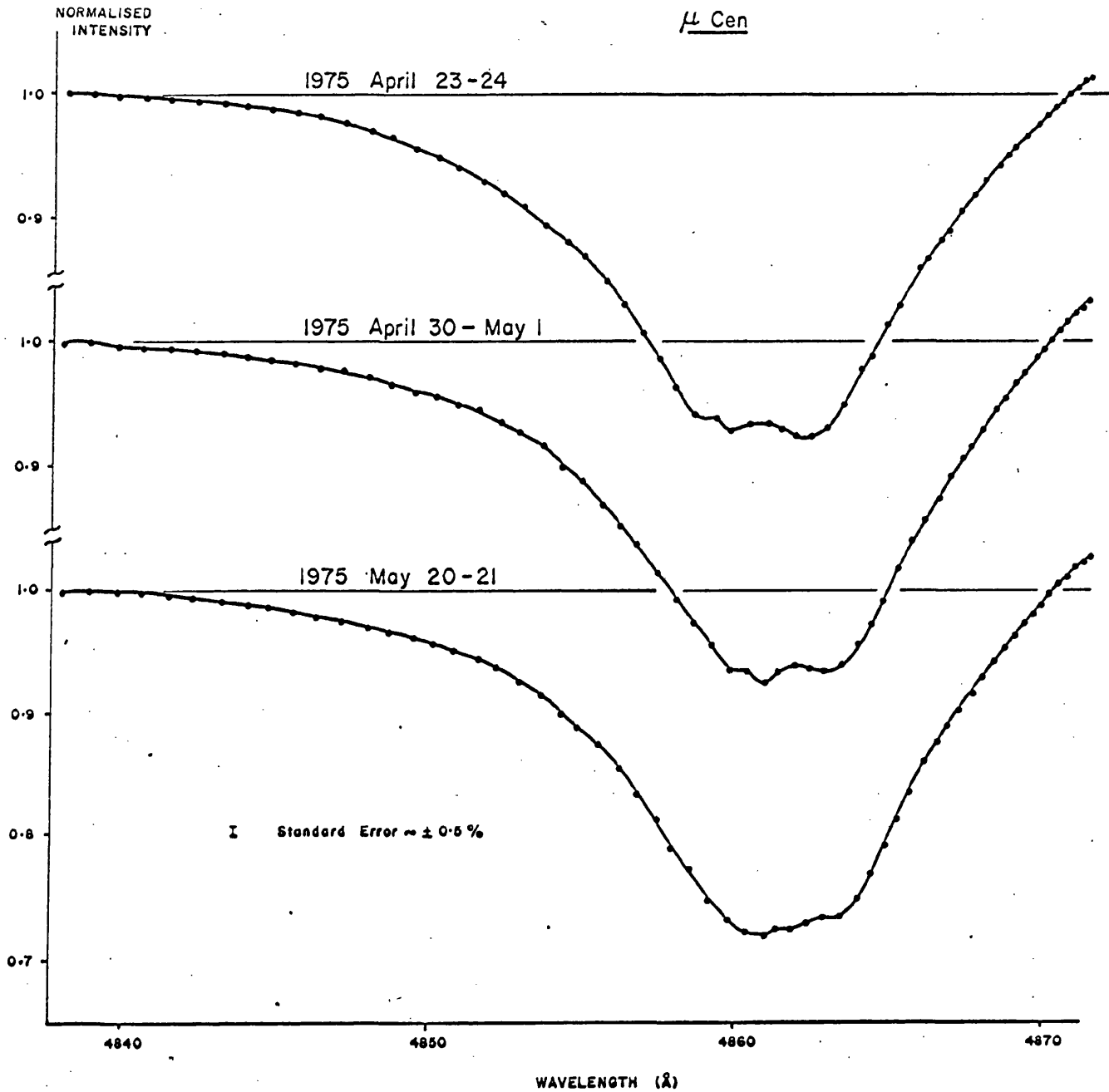


Figure 5.7

H $\beta$  profiles for  $\mu$  Cen. The core of the absorption line is partly filled-in due to weak emission which appears to be variable and may consist of V and R components.

48 Lib The profiles for 48 Lib, shown in Figure 5.8 (a), show clearly the characteristics of a shell star; the underlying photospheric absorption, the double peaked emission line and the sharp shell absorption core are all evident.

A total of eight mean H $\beta$  profiles were obtained for 48 Lib on six nights. Variations, mainly confined to the V component, were found between the profiles for most nights, although the extent of the variations was only one or two per cent. For the profiles shown in Figure 5.8 (a), however, there is a difference of  $\sim 5$  per cent in the strength of the V component between April 22-23 and April 23-24 while the strength of the R component and the depth of the shell absorption are almost unchanged.

It is worth noting that in all of the observations of 48 Lib, it was found that the V component was clearly stronger than the R component. If the relative strength of the V and R components is interpreted as being entirely due to a variable Doppler displaced shell absorption, then at the time of these observations the shell absorption must have been red shifted (i.e. positive radial velocity) relative to the emission line.

A similar result for the H $\alpha$  line in 48 Lib was found by Poeckert (1975) from observations made in April 1974. However, in April 1972, Gray and Marlborough (1974) found that the R components of the H $\alpha$  and H $\beta$  lines were both stronger than their respective V components, indicating that the shell absorption at that time was blue shifted relative to the emission line and the photospheric stellar line.

The radial velocity variations of the shell of 48 Lib between 1935 and 1962 have been shown by Underhill (1966) and Faraggiana (1969) to have a period of about ten years. In addition, a correlation was found between the shapes of the line profiles and the radial velocity; when the radial velocity of the shell absorption was negative (i.e. blue shifted), the R emission component was stronger than the V component and vice versa.

It was later found, however, (Underhill and Geuverink 1969, Geuverink 1970) that radial velocities measured in 1967 and 1968 did not fit the periodic change found earlier. Further studies by Faraggiana (1971) of spectra obtained between 1962 and 1970 revealed that the period of the radial velocity oscillations had become longer than ten years and that the last minimum of the radial velocity had occurred in 1967-68, about two years later than expected. The observations of Gray and Marlborough and those of Poeckert would seem to indicate that the radial velocity crossed through zero (from negative to positive) between 1972 and 1974 while the observations reported here show that the radial velocity was still positive in April 1975. Since the last reversals of the radial velocity took place in 1960 (negative to positive) and in 1964 (positive to negative), all of these observations are in agreement with Faraggiana's conclusion that the period has become longer than ten years and perhaps show that the period may still be lengthening.

$\zeta^1$  Sco Although  $\zeta^1$  Sco is an early-type supergiant and is not a true Be star, it has been included in this section since it shows emission at  $H\beta$ . Variations in the strength and appearance of the Balmer lines (including  $H\beta$ ) have been reported previously for this star to be occurring on a time-scale of years (Jaschek and Jaschek 1973).

Measurements of the  $H\beta$  line were obtained on three nights and the profiles for two of these nights are shown in Figure 5.8 (b). The  $H\beta$  line has a P-Cygni type profile and shows emission at  $H\beta$  together with a blue displaced absorption line.

Obvious differences between the profiles for April 23-24 and May 25-26 can be seen in Figure 5.8 (b). The strength of the emission relative to the blue continuum increased from  $\sim 1.25 \pm 0.01$  on April 22-23 to  $\sim 1.37 \pm 0.01$  on May 25-26. In addition, and possibly due to the increased emission, the absorption depth changed from  $\sim 0.89 \pm 0.01$  to  $\sim 0.96 \pm 0.01$  and the intensity

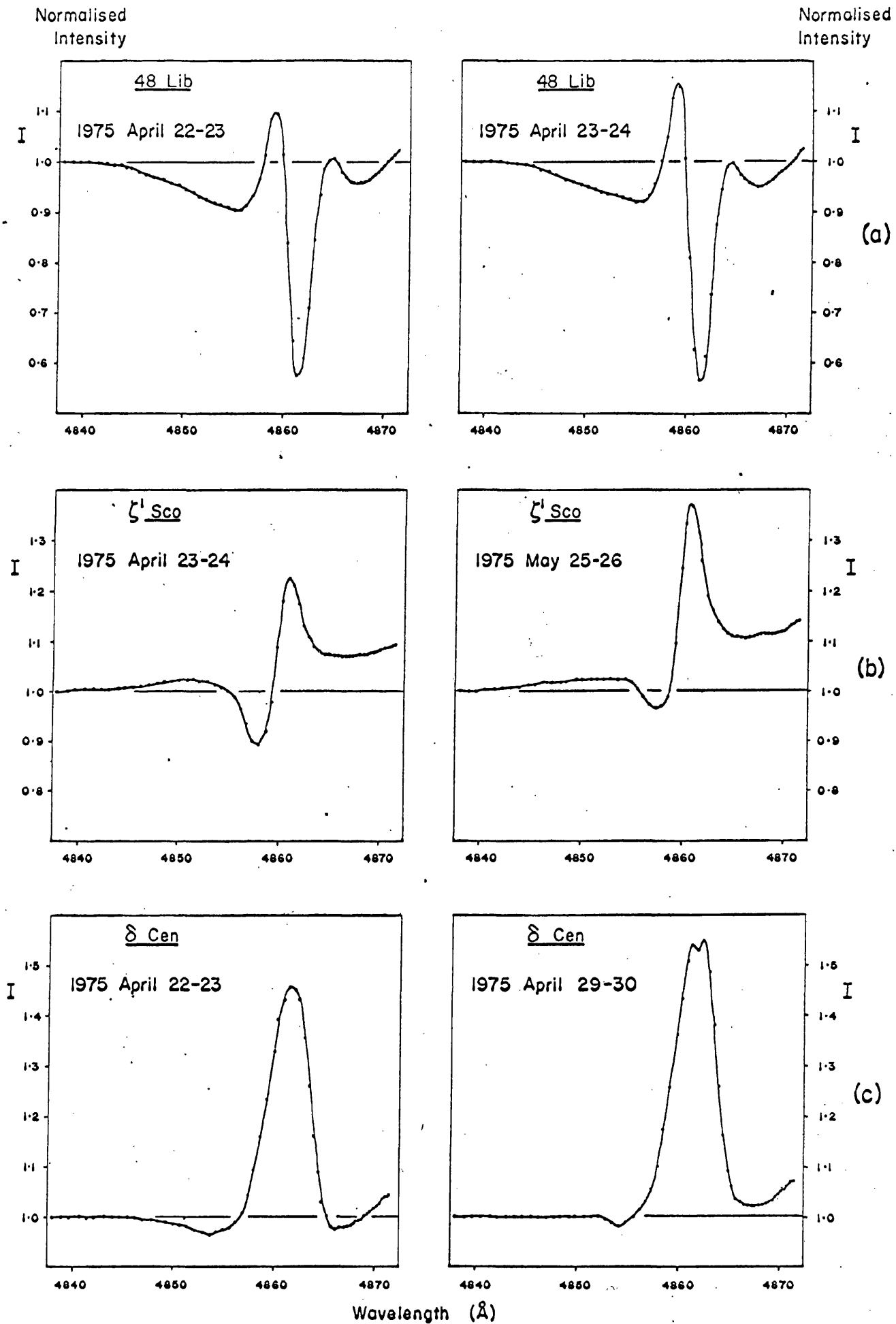


Figure 5.8 Changes of the H $\beta$  profile for a). 48 Lib, b).  $\zeta^1$  Sco, c).  $\delta$  Cen.

on the long wavelength side of the emission also increased slightly over the same time interval. However, the shape and strength of the blue continuum between  $\lambda$  4838 Å and  $\lambda$  4852 Å was hardly different for the two dates. The profile was also measured on May 20-21 and was found to have emission intermediate in strength between that of the profiles shown in Figure 5.8 (b).

The P-Cygni profiles of an early-type supergiant are generally interpreted as arising from emission in an extended atmosphere, the outer and cooler layers of which are in a state of expansion, thus producing the blue shifted absorption lines. Hutchings (1968c) has formulated a model of the atmosphere of  $\zeta^1$  Sco from a study based on radial velocity measurements of different lines formed at various levels within the extended envelope and concludes that the atmosphere is expanding and that the star is losing mass. Although Jaschek and Jaschek (1973) found spectral variations, they only obtained one spectrogram per year and were unable to put a lower limit on the time-scale of the variations. However, the observations reported here show that significant variations of the H $\beta$  line in  $\zeta^1$  Sco can occur on a time-scale as short as one month, or less, and indicate that the process of mass loss from this star is subject to irregular activity.

$\delta$  Cen Observations of  $\delta$  Cen were made on six nights and a total of eight line profiles of H $\beta$  were obtained. The profile normally consisted of a single emission line superimposed on a shallow photospheric absorption line. Significant variations in the strength of the emission were found between the profiles for most nights and these intensity variations are listed in Table 5.7.

Figure 5.8 (c) shows the mean profile for April 22-23, when the emission was at its weakest, and for April 29-30, when the emission was strongest. The profile for April 29-30 shows the emission consisted of two components separated by a small central absorption, indicating the temporary

development of a shell spectrum. In addition to the changes in the emission strength, it was also found that as the emission became stronger, the underlying stellar absorption line became more filled-in (due to the emission wings) on both sides of the emission line.

$\chi$  Oph The strongest  $H\beta$  emission of the Be stars measured, was found in  $\chi$  Oph ( $\sim 2.2$  times the continuum intensity). Profiles measured on five nights again showed large variations in the emission strength. These variations are listed in Table 5.7. No variations were found in the structure of the line.

The mean profiles given in Figure 5.9 show the emission at its weakest (April 22-23) and at its strongest (May 25-26), the difference being  $\sim 15$  per cent (in units of the continuum intensity). The standard errors of these mean profiles are about  $\pm 2$  per cent.

#### Other Be Stars

Two of the remaining six Be stars which were observed showed no significant variations;  $\omega$  Car was measured on only two nights and  $\eta$  Cen was measured on four nights. Mean line profiles for these and the four other Be stars, each of which was measured on only one occasion, are shown in Figure 5.10.

These stars showed a variety of  $H\beta$  profiles. Only one star, HD 91465, had emission at  $H\beta$  which reached above the level of the adjacent continuum. The others showed different degrees of emission; HD 102776 merely had a small blue shifted emission hump near the core of the photospheric absorption;  $\lambda$  Cru showed definite filling-in on the blue side of the core of the absorption line;  $\zeta$  Pup showed some emission on the red wing and also had a very sharp, possibly shell, absorption core;  $\omega$  Car featured V and R emission components separated by a shell absorption; finally,  $\eta$  Cen did not show any evidence of emission. In addition to the various degrees of

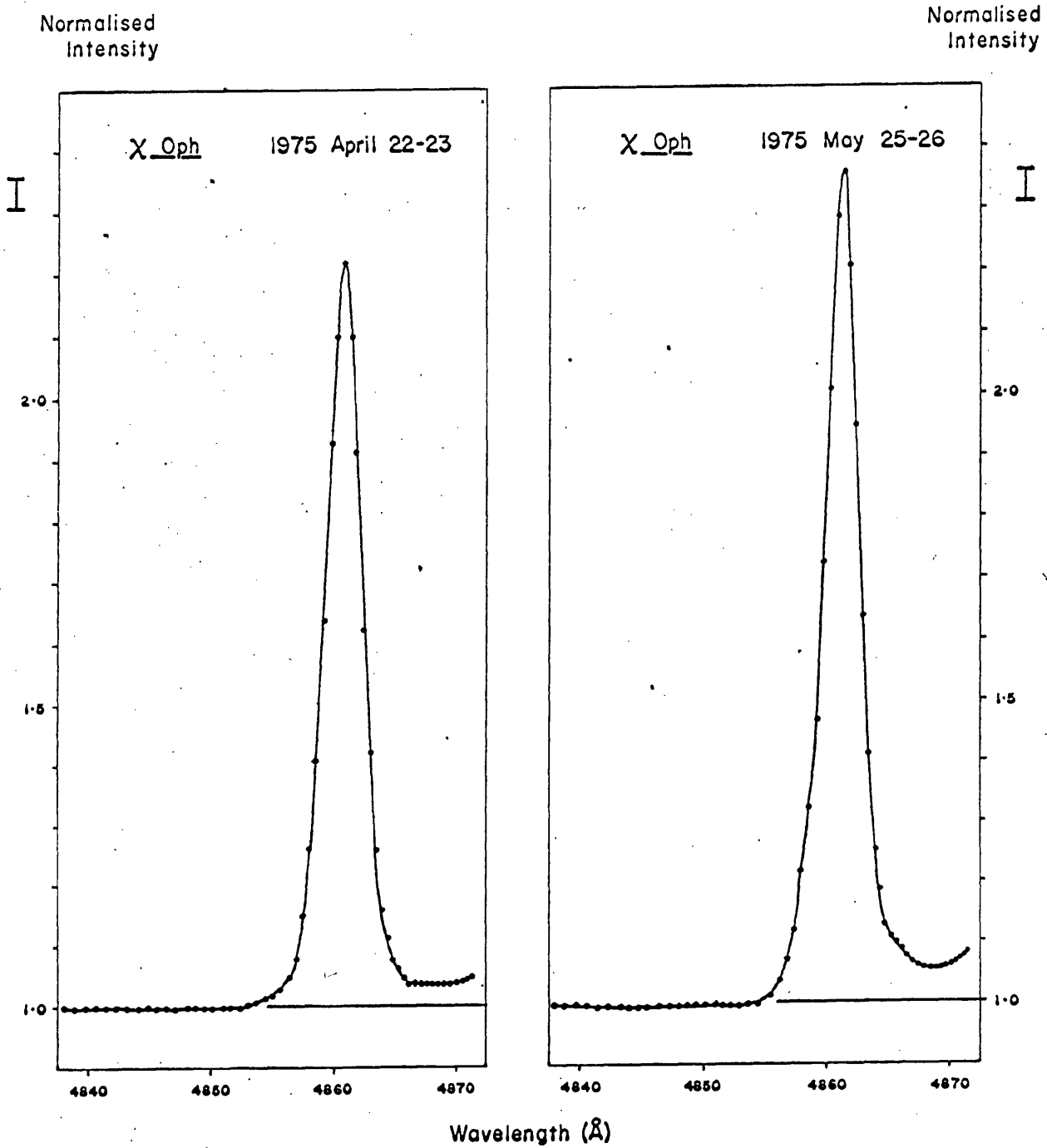


Figure 5.9

Variation of the strength of  $H\beta$  in  $X_{\text{Oph}}$

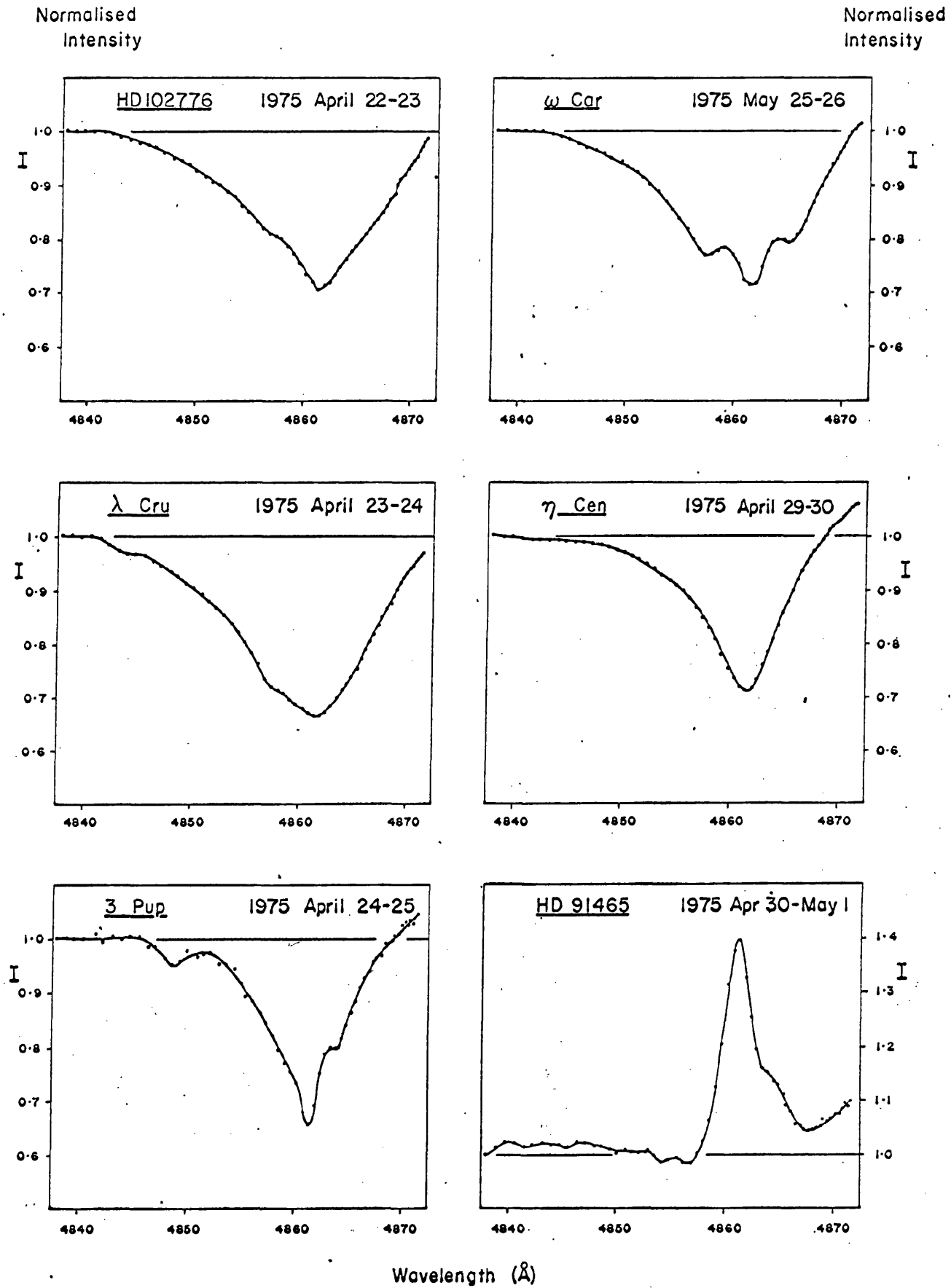


Figure 5.10  $H\beta$  profiles for the six remaining Be stars observed.

emission, there were also obvious differences between the underlying absorption lines of these six stars. The very broad lines of HD 102776,  $\omega$  Car and  $\lambda$  Cru contrasted with the sharper line of  $\eta$  Cen and the much sharper line of  $\zeta$  Pup while very little absorption was visible in the profile of HD 91465.

The different emission strengths of these stars are probably due to the variety of sizes, densities and shapes of their extended atmospheres, while the different widths of the underlying absorption lines probably indicate various rotation velocities and various aspects of their rotation axes.

### Summary

A wide variety of H $\beta$  line profiles was found in the Be stars which were observed and a high percentage of those stars which were observed on more than one night showed variability of the profiles on time-scales of days and longer.

The variations which were observed were found to take several forms such as simple changes in the emission strength (e.g.  $\chi$  Oph), changes in the V/R ratio (e.g.  $\alpha$  Ara, 48 Lib,  $\zeta$  Tau) and changes in the structure of the line (e.g.  $\gamma$  Cas,  $\delta$  Cen). Most of the stars were observed only once in a particular night and the measurements yield little information regarding variability on time-scales of less than a day. A few runs on  $\gamma$  Cas were of longer duration but indicate that there were no rapid fluctuations, between individual scans, which were larger than the expected levels of photon shot-noise.

### 5.3 Observations of $\epsilon$ UMa and $\gamma^2$ Vel

$\epsilon$  UMa Observations of the Ap star  $\epsilon$  UMa (A0 pv,  $m_v = 1.8$ ) have been made with the Glasgow telescope on only two nights since the scanner and observing techniques were sufficiently developed to allow reliable line profile measurements.

A series of 6 scans were obtained on 1975 March 24 between 22<sup>h</sup>.17 UT and 22<sup>h</sup>.46 UT. The integration time per spectral point per scan was 4 seconds and the scans consisted of 71 spectral points at single step intervals between  $\sim \lambda$  4837 Å and  $\sim \lambda$  4872 Å.

A further two series of scans were obtained on 1975 September 13-14. The first of these consisted of 22 scans obtained between 21<sup>h</sup>.33 UT and 22.44 UT on Sept 13 while another 10 scans were obtained several hours later, between 03<sup>h</sup>.40 UT and 04<sup>h</sup>.13 UT on Sept 14. The integration time for the Sept 13-14 observations was 3 seconds per spectral point per scan and 61 spectral points, at single step intervals, were measured.

The mean line profiles together with their associated errors were evaluated for the three sets of observations as before. For almost all spectral points, the intensity differences between the mean profiles were less than twice the sum of the standard errors, which were of the order of  $\pm 0.3 - 0.5$  per cent,  $\pm 0.2 - 0.4$  per cent and  $\pm 0.4 - 0.6$  per cent respectively for each series of scans. The conclusion reached, therefore, is that no long- or short-term changes of the H $\beta$  line in  $\epsilon$  UMa can be seen from the mean profiles for these dates, to within the accuracy of the observations (i.e.  $\sim \pm 0.5$  per cent). The fact that no evidence was found for rapid variations of the type reported by Wood (1964) is consistent with the observations of this star made at H $\alpha$  by Breger (1974). The mean profiles for 1975 March 24 and 1975 September 13-14 (21<sup>h</sup>.33 - 22<sup>h</sup>.44 UT) are shown in Figure 5.11.

The observed and the expected (photon) statistics have also been compared for these observations as a means of determining if rapid fluctuations were occurring. Ratios of  $\sigma_{\text{Obs}}/\sigma_{\text{Phot}}$  are shown in Figure 5.12. It can be seen that there is reasonable agreement between  $\sigma_{\text{Obs}}$  and  $\sigma_{\text{Phot}}$  and therefore there is no positive evidence of any rapid variations of greater amplitude than photon shot-noise. Although for March 24 there are some values

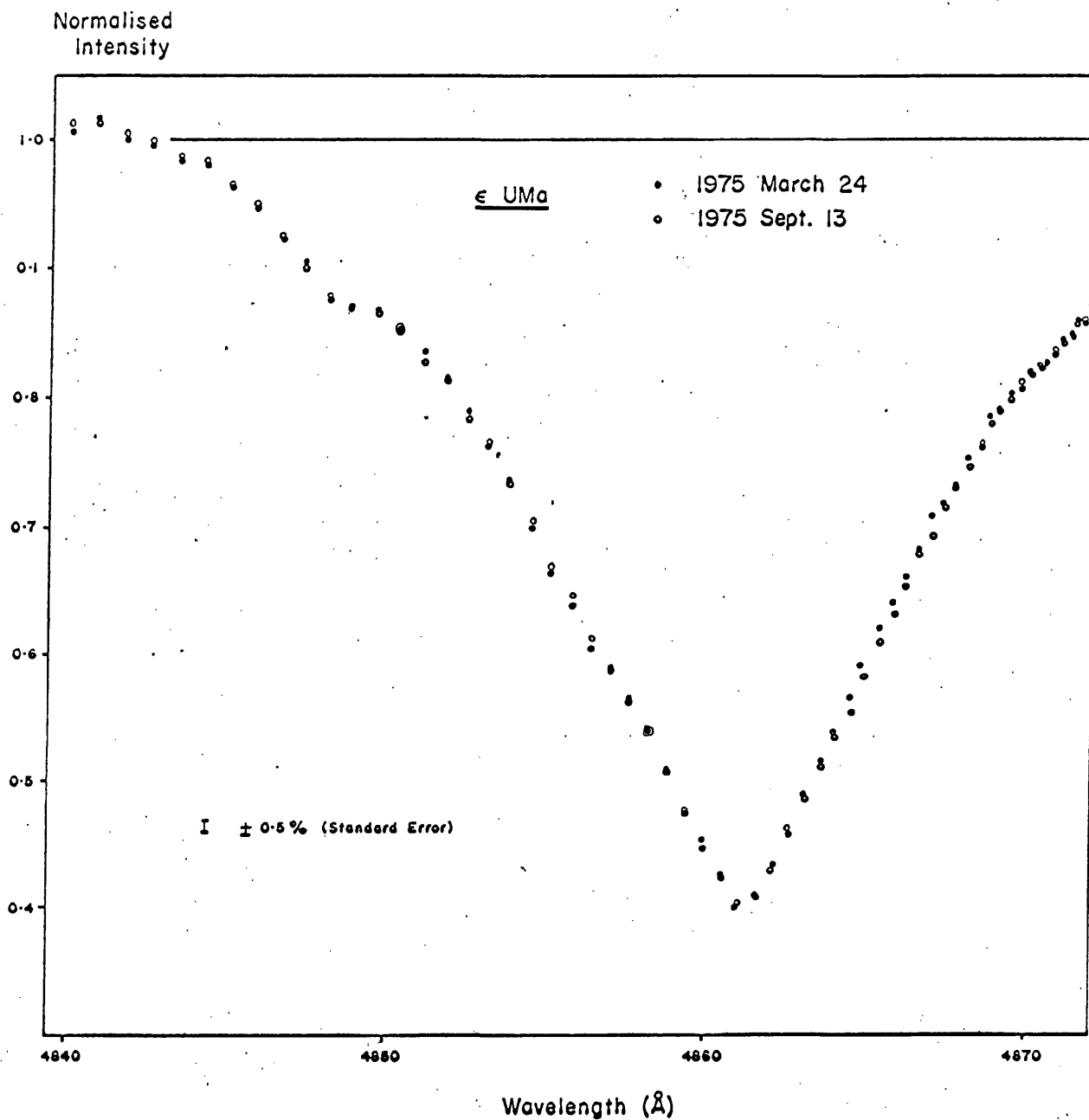


Figure 5.11

H $\beta$  profile for  $\epsilon$  UMa measured on 1975 March 24 (filled circles) and 1975 September 13 (open circles). No statistically significant variations can be seen.

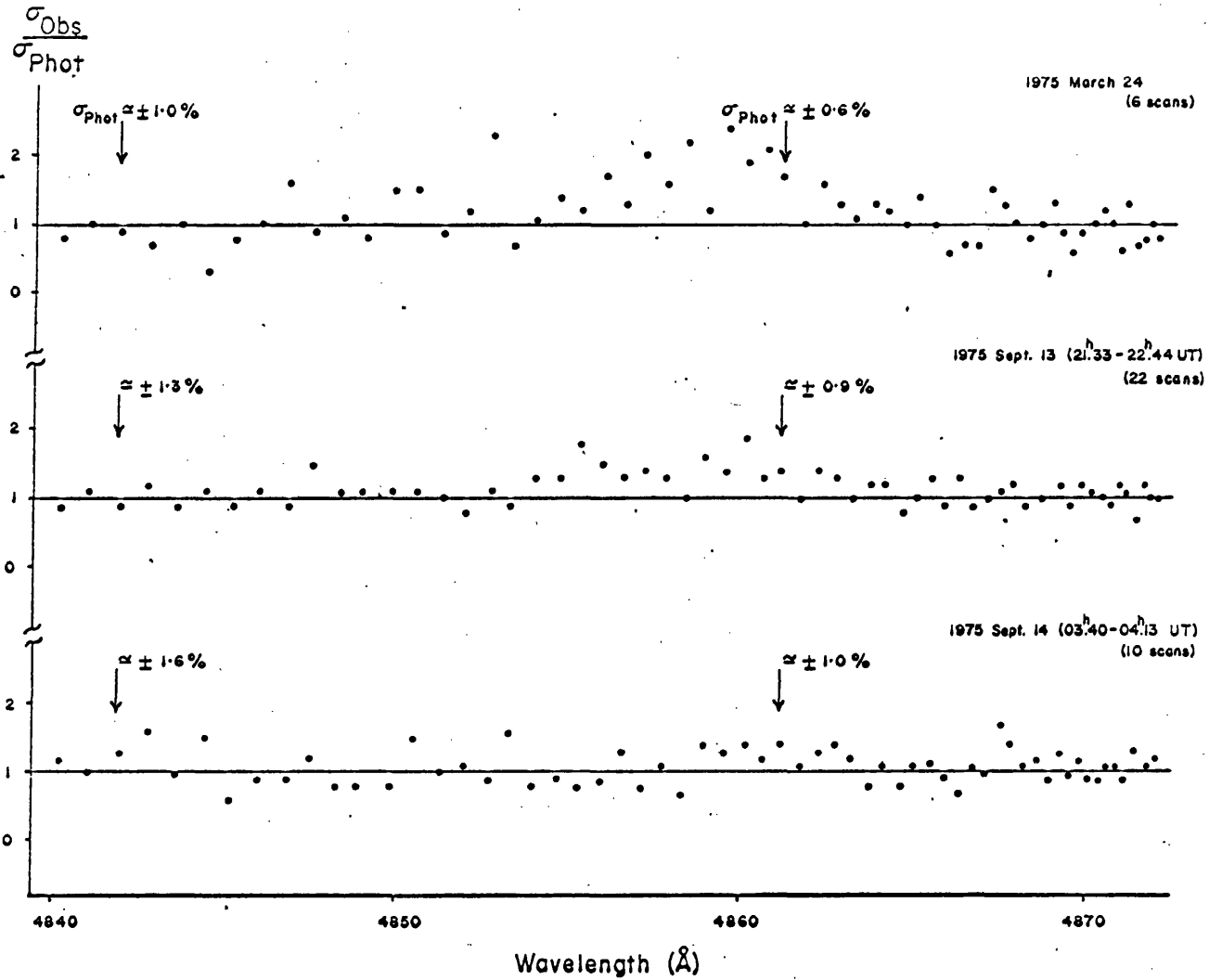


Figure 5.12

Ratios of the observed and ideal photon statistics for the observations of  $\epsilon$  UMa presented in Figure 5.11. There is no evidence of rapid variability; the slightly larger values of  $\sigma_{\text{Obs}}/\sigma_{\text{Phot}}$  for 1975 March 24 are probably the result of the small data sample for that date.

of  $\sigma_{\text{Obs}}$  which are more than twice  $\sigma_{\text{Phot}}$ , it seems likely that this is again caused by the small data sample. However, there may be a slight tendency for  $\sigma_{\text{Obs}}/\sigma_{\text{Phot}}$  on March 24 to be larger in the line core than in the wings and, since the expected standard deviation ( $\sigma_{\text{Phot}}$ ) was slightly smaller on this date, it is possible that  $\sigma_{\text{Obs}}$  was increased due to the presence of rapid fluctuations with amplitudes just below the level of the photon noise ( $\sim \pm 0.6$  per cent for a single measurement).

$\gamma^2$  Vel The brightest Wolf-Rayet star in the sky ( $m_v = 1.8$ ) is  $\gamma^2$  Vel (HD 68273). The spectral type is given by Conti and Smith (1972) as WC 8 + O9 I and it is a spectroscopic binary with an orbital period of 78.5 days (Ganesh and Bappu 1967).

Night-to-night variations in the strength of the C III - IV line ( $\lambda$  4650 Å) have been reported by Bahng (1975a) and by Lindgren, Lundström and Stenholm (1975) and there have been reports also of rapid periodic variations for this line (see Chapter 1).

Variations with phase have also been found in the V/R ratios of double emission lines, such as He I ( $\lambda$  3888 Å) and H. These V/R variations, first reported for H $\beta$  by Perrine (1918), have been discussed recently by de Monteagudo and Sahade (1970) and by Niemela (1973).

The observations presented here show night-to-night variations of the H $\beta$  emission. Variations of the V/R ratio have been observed and are found to be related to the orbital phase in the same way as found by Perrine; at phase 21 days (0.27P) V was found to be stronger than R and at phase 54 days (0.69P) R was stronger than V.

The observations, made with the 50 cm and 76 cm telescopes at the SAAO, are summarised in Table 5.8. Mean line profiles were derived for each night as before and are shown in Figure 5.13. The error bars adjacent to the

Table 5.8 Details of Observations and Variations of the H $\beta$  Emission Strength for  $\gamma^2$  Vel

Date (1975)	JD 2440000+	T (secs)*	Number of Scans	$\sigma_{\text{Phot}}$ $\approx \sigma_{\text{Obs}}$ (%)	Emission Strength		Phase (t)
					V	R	
April 22-23	2525.5	1	16	$\pm 0.8$	$1.160 \pm .002$	$1.140 \pm .002$	0.27
" 23-24	2526.5	1	10	$\pm 0.6$	$1.162 \pm .002$	$1.135 \pm .002$	0.28
" 24-25	2527.5	1	8	$\pm 1.5$	$1.146 \pm .005$	$1.130 \pm .005$	0.30
" 29-30	2532.5	1	16	$\pm 1.0$	$1.143 \pm .003$	$1.165 \pm .003$	0.36
Apr 30-May 1	2533.5	1	16	$\pm 1.2$	$1.149 \pm .003$	$1.160 \pm .003$	0.37
May 20-21	2553.5	2	10	$\pm 1.0$	$1.115 \pm .003$	$1.200 \pm .003$	0.63
" 25-26	2558.5	2	6	$\pm 1.2$	$1.096 \pm .005$	$1.185 \pm .005$	0.69

V  $\equiv$  Violet peakR  $\equiv$  Red peak

\* T is the integration time per spectral point per scan.

† Phases are derived from Ganesh and Bappu (1967).

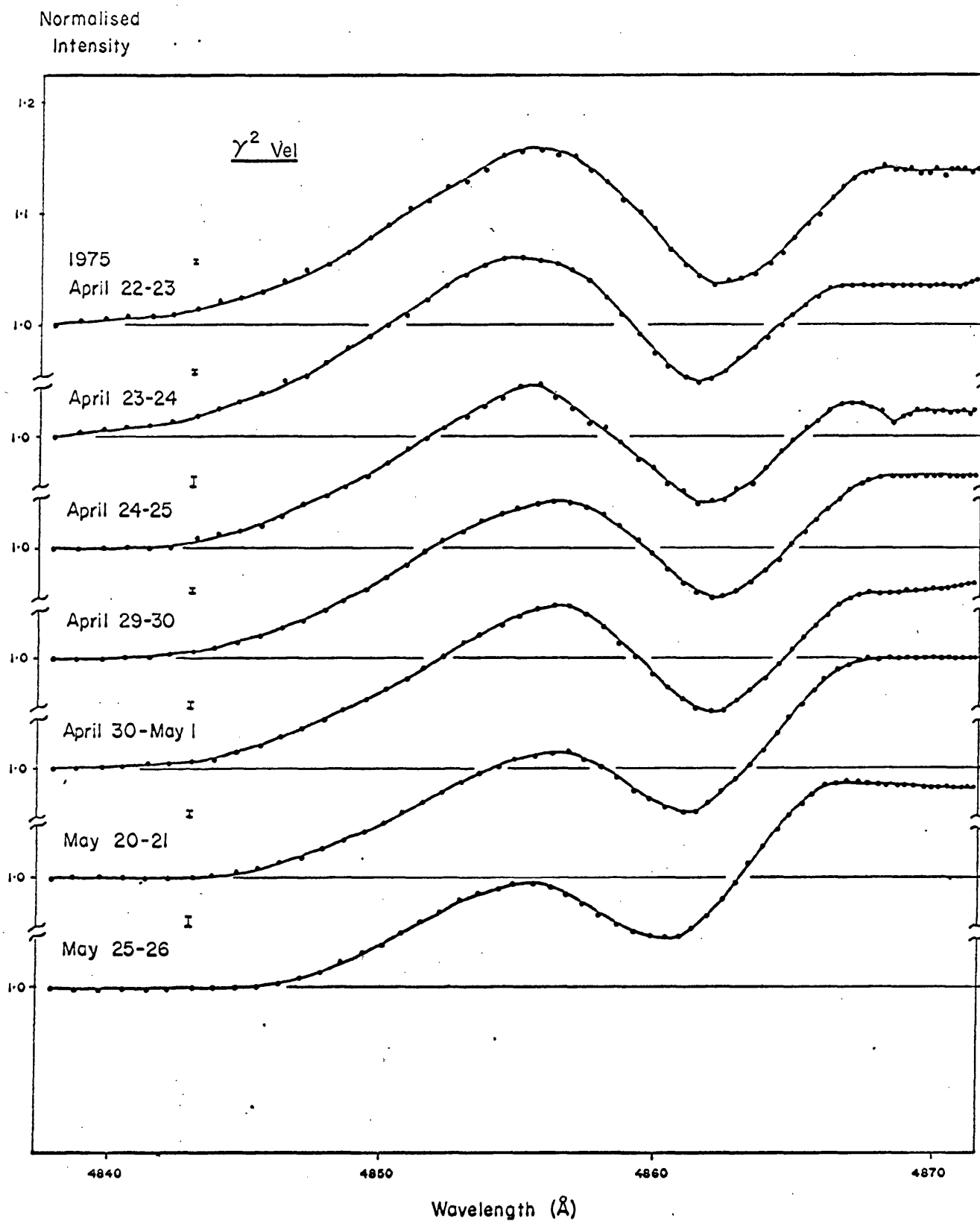


Figure 5.13

A series of H $\beta$  profiles for  $\gamma^2$  Vel showing systematic V/R variations. Notice also the differences between the appearance of the V and R components for April 23-24 and April 24-25.

dates of observation represent the standard errors of the mean intensities and any variations of these errors across the profiles are too small to be shown. In all cases, the observational errors were within a factor of two times the expected photon errors.

The variations in the V/R ratio can be seen clearly in Figure 5.13 and the strengths of the V and R components for each date are listed in Table 5.8. Magnitude differences between the intensity of each of the emission components and the intensity of the continuum at  $\lambda$  4838 Å have been evaluated and are plotted against phase in Figure 5.14. The differences in magnitudes between the intensities of the V and R components are also plotted. Although the observations cover less than half of one period of the spectroscopic binary, the variations of the V/R ratio with phase are in agreement with the relationship found by Perrine and the strengths of the V and R components can be seen (Figure 5.14) to vary in anti-phase with each other.

In addition to the V/R variations, there are also some small changes in the shapes of the individual emission components which can be seen in Figure 5.13. For example, on April 24-25 the violet component had a sharper peak than on the other dates and there was also a small absorption feature present on this date on the red side of the R component. On May 25-26, the V component was definitely narrower than on any other date, although this could be due partly to its decreased strength. Clearly, changes of the H $\beta$  line with phase do occur and the profiles for April 23-24 and April 24-25 seem to indicate that shorter term variations are also present. However, it has already been stated that the rms. scatter of the data from which the mean profiles in Figure 5.13 were derived, is not much larger than what would be expected from photon noise. Further observations are required to investigate if any rapid variations, such as those reported by Sanyal et al (1974) for the C III-IV line, are occurring at H $\beta$  in addition to the longer term V/R variations.

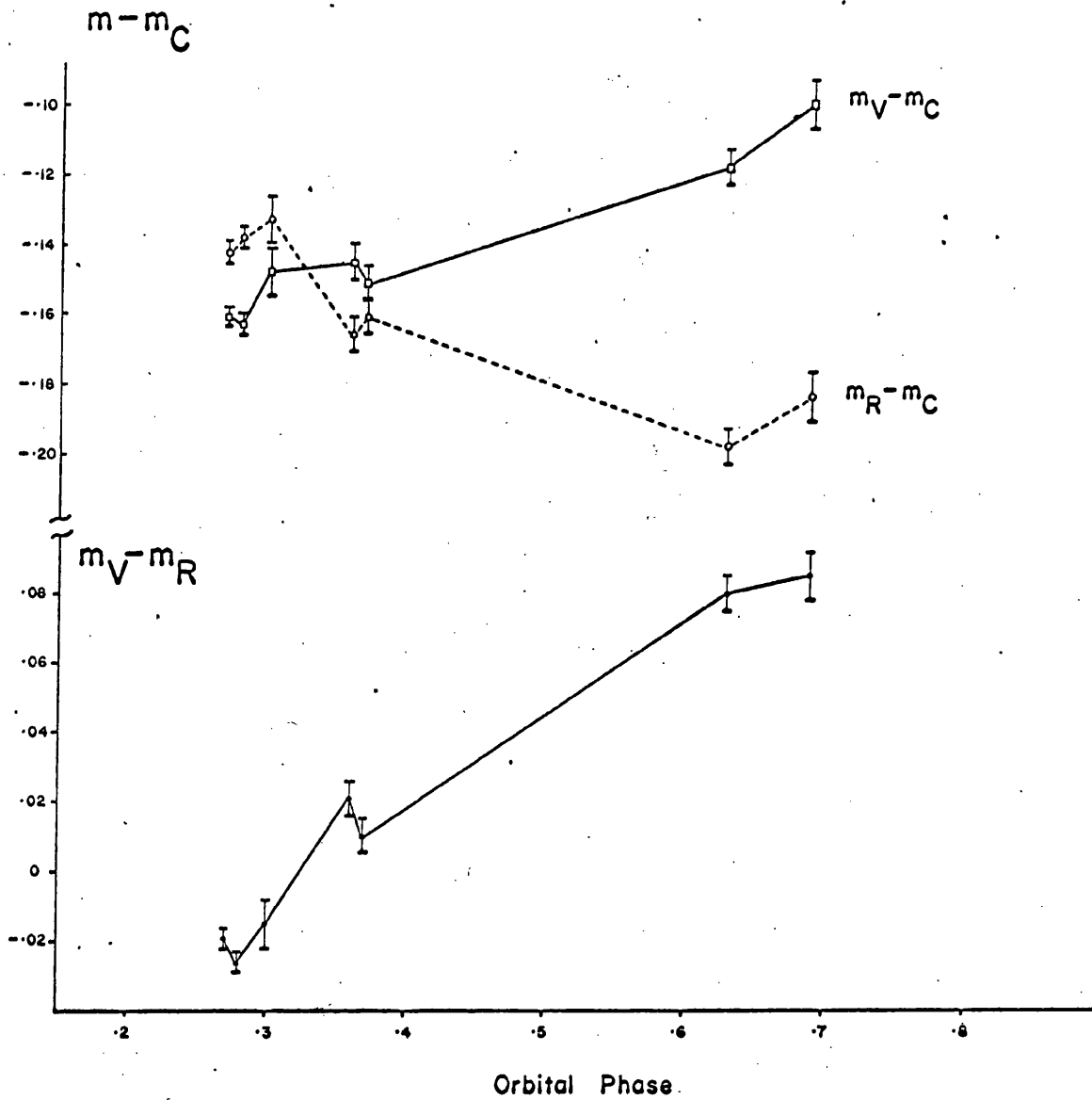


Figure 5.14

Variations of the emission strength with orbital phase for the V and R components of the  $H\beta$  line in  $\gamma^2$  Vel. Upper: brightness (in magnitudes) of the V and R components relative to the continuum intensity. Lower: relative brightness (in magnitudes) of the V and R components.

## 5.4 Conclusions

### Summary

The various chapters of this thesis have presented and discussed the design, performance and application of a novel line profile scanner.

The technique of tilt-scanning with narrow band interference filters has been studied in detail and applied with success to measurements of line profile variations in some early-type stars. Variations of the filter pass-bands brought about by tilting, illuminating with non-collimated light, variable seeing conditions and telescope tracking errors have all been considered.

Observationally, the emphasis has been mainly on Be stars and a large percentage of those observed have been found to show night-to-night variations of the H $\beta$  line profile. Although variability of the type found has been observed previously by others to be occurring on time-scales of months and years, the results of this study indicate that time-scales of days are not uncommon. No evidence has been found for the very rapid profile variations reported by Hutchings and Bahng, although only a short time interval has been covered by the observations. It is believed that for some of the observed Be stars (e.g.  $\alpha$  Ara,  $\delta$  Cen) night-to-night variations have not been previously reported.

A few observations were also obtained for the Ap star  $\epsilon$  UMa but no variations of the H $\beta$  profile were found. If the variations reported for this star by Wood were intrinsic, it is possible that they have since subsided.

Variations of the V/R ratio were observed for the H $\beta$  line in the Wolf-Rayet star  $\gamma^2$  Vel and these variations fit the known relationship between the V/R ratio and the orbital phase for this spectroscopic binary. Other less obvious night-to-night variations are also suspected for this star.

### Areas for Improvement

The performance of the scanner could be improved in a number of ways, most of which are related to the tilt-scanning technique. The effects of variable seeing conditions and of guidance errors have been discussed a number of times and several modifications could be made to lessen these effects.

The importance of the angular magnification of the telescope/collimator system has been mentioned in relation to the angular size of the seeing disc and its angular displacement from the optical axis as seen by the scanning filter. At present, the magnification is  $\sim 80/1$  (i.e.  $F_T/F_C$ ) for the Glasgow telescope and was even greater for the other telescopes used (see Table 5.1). However, since the filters are not fully illuminated, the magnification could be reduced by use of a longer focal length collimator, without suffering any light loss.

The adverse effects of variable seeing and guidance errors might be further reduced by physically imposing more stringent limits on the maximum size or displacement of the seeing disc by use of a smaller diaphragm, almost matching the size of a typical star image. There would, of course, be some light loss if the seeing disc became larger than the diaphragm or was allowed to drift partly out of the field and such variations of the illumination of the filters might be a source of noise. However, the monitor beam of the scanner would provide a good degree of compensation against these variations and it is felt that the resultant noise on the recorded profiles would be less than that produced by the larger movements and changes in the size of the seeing disc which can occur at present.

If a smaller diaphragm was used in the focal plane, very accurate guiding would be necessary. Because of difficulty in seeing both the cross-wires and the edges of the diaphragm with the dichroic viewer, it might be

necessary to replace this with a system of off-axis guiding on a nearby field star but care would be required to guard against differential image movement between the guide star and the programme star. With better equipped telescopes it would perhaps be possible to use an auto-guider system.

Improvements could also be made to the method of wavelength/tilt calibration. A smaller wavelength step-size would be useful when determining the positions of maximum intensity for the calibration spectrum lamps. There is also a possibility that the optical axis of the scanner will not be collinear with the axis of the telescope resulting in different wavelength/tilt relationships for stellar sources and for the piped calibration light. However, calibration with the laboratory lamps and the fibre optic pipe allows the wavelength of peak transmittance at normal incidence ( $\lambda_0$ ), the effective refractive index of the filter ( $\mu^*$ ) and also the fiducial of the tilt scale relative to the axis of the scanner to be determined. If measurements of the angles of tilt were then made on either side of normal incidence corresponding to the H $\beta$  line centre for a star having zero radial velocity (i.e. an undisplaced H $\beta$  line), the angle between the two optical axes could then be found by substitution in Equation 2.4. This equation could then be used for stellar wavelength/tilt calibrations since the values of  $\lambda_0$ ,  $\mu^*$ ,  $\phi$  and  $\alpha$  would be known (the latter two quantities defining the angle which the optical axis of the telescope makes with the optical axis of the scanner).

#### Future Studies

Be Stars: The observations which have been made in this study have shown that a large percentage of the Be stars measured show variations of the H $\beta$  line on time-scales at least as short as one day. Obviously, further observations of these stars should be made so as to determine the true time-scales of the variations. These future observations should be of longer duration and, if possible, should be made with larger collecting apertures

so that improved photometric accuracy can be achieved with higher time resolution. Use of larger telescopes would also allow the study to be extended to other, fainter, Be stars.

In its present form, the scanner can be used to obtain profiles of any other spectral lines, merely by using the appropriate interference filters, and future studies should also include measurements of  $H\alpha$  and  $H\gamma$  in addition to  $H\beta$ . Indeed, it would be desirable to obtain simultaneous scans of at least two lines so that correlations between any variations might be found. However, this would require constructing a completely new photometer head with perhaps three or four beams.

Ap Stars: The observations of Ap stars are very far from being complete since only one star has been observed. However, to extend the study to other Ap stars would require the use of larger telescopes. If any variations can be found at  $H\beta$  it would again be useful to obtain measurements of other lines, both by themselves and simultaneously.

Wolf-Rayet Stars: Further high time resolution observations of  $\gamma^2$  Vel should be made, in both a scanning mode and also in a non-scanning mode at particular wavelengths in the profile (e.g. the V and R peaks) or with perhaps a broader passband centred on the  $H\beta$  line, so that the rapid periodic variations reported for other lines in this star might be investigated at  $H\beta$ .

It has been proposed that many Wolf-Rayet stars of type WC might be spectroscopic binaries. Measurements should be made of the profiles of emission lines in these stars with the aim of detecting possible V/R variations. Any variations which were found to be periodic might provide evidence of the binary nature of these stars.

The entire study of rapid line profile variations is very important to our understanding of the evolutionary stages being witnessed in these

stars. The time-scales involved are very short in comparison to the stellar life times and yet many of the profile variations are probably the result of large scale changes in the atmospheres of these very active stars.

Although the measurement of rapid profile variations poses many technical difficulties, there is clearly a great deal of astrophysics to be learned from studies of these phenomena.

APPENDIX I

CONTROL ELECTRONICS - LOGIC DIAGRAMS

Logic symbols used:

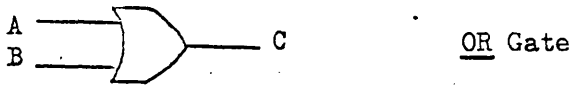
Truth Tables



A	B	C
0	0	0
0	1	0
1	0	0
1	1	1



A	B	C
0	0	1
0	1	1
1	0	1
1	1	0



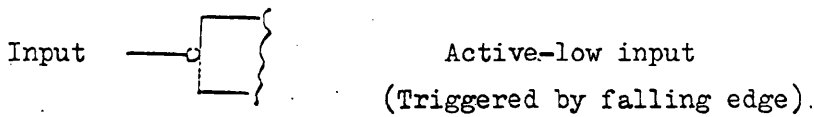
A	B	C
0	0	0
0	1	1
1	0	1
1	1	1



A	B	C
0	0	1
0	1	0
1	0	0
1	1	0

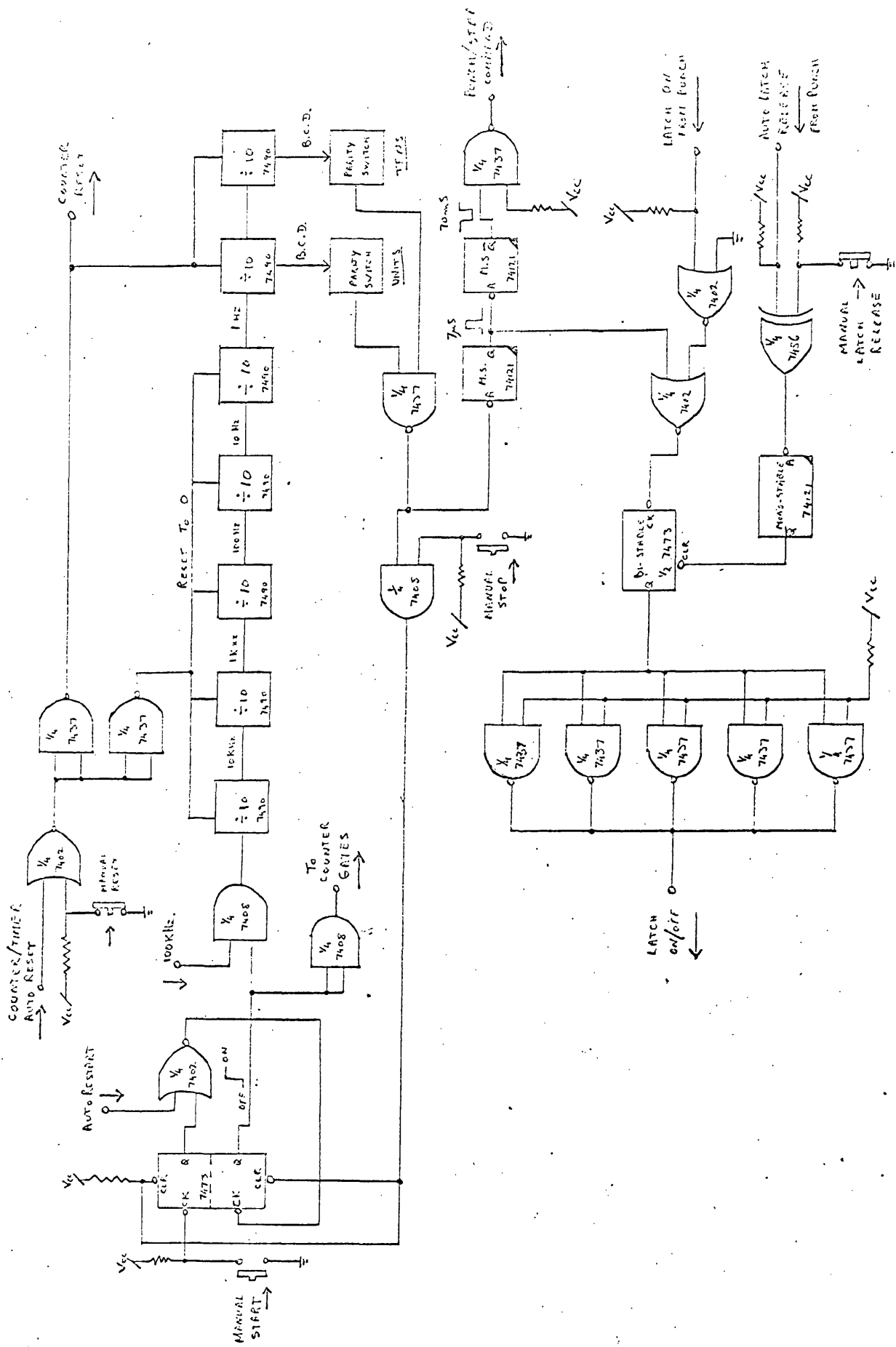


A	B	C
0	0	0
0	1	1
1	0	1
1	1	0



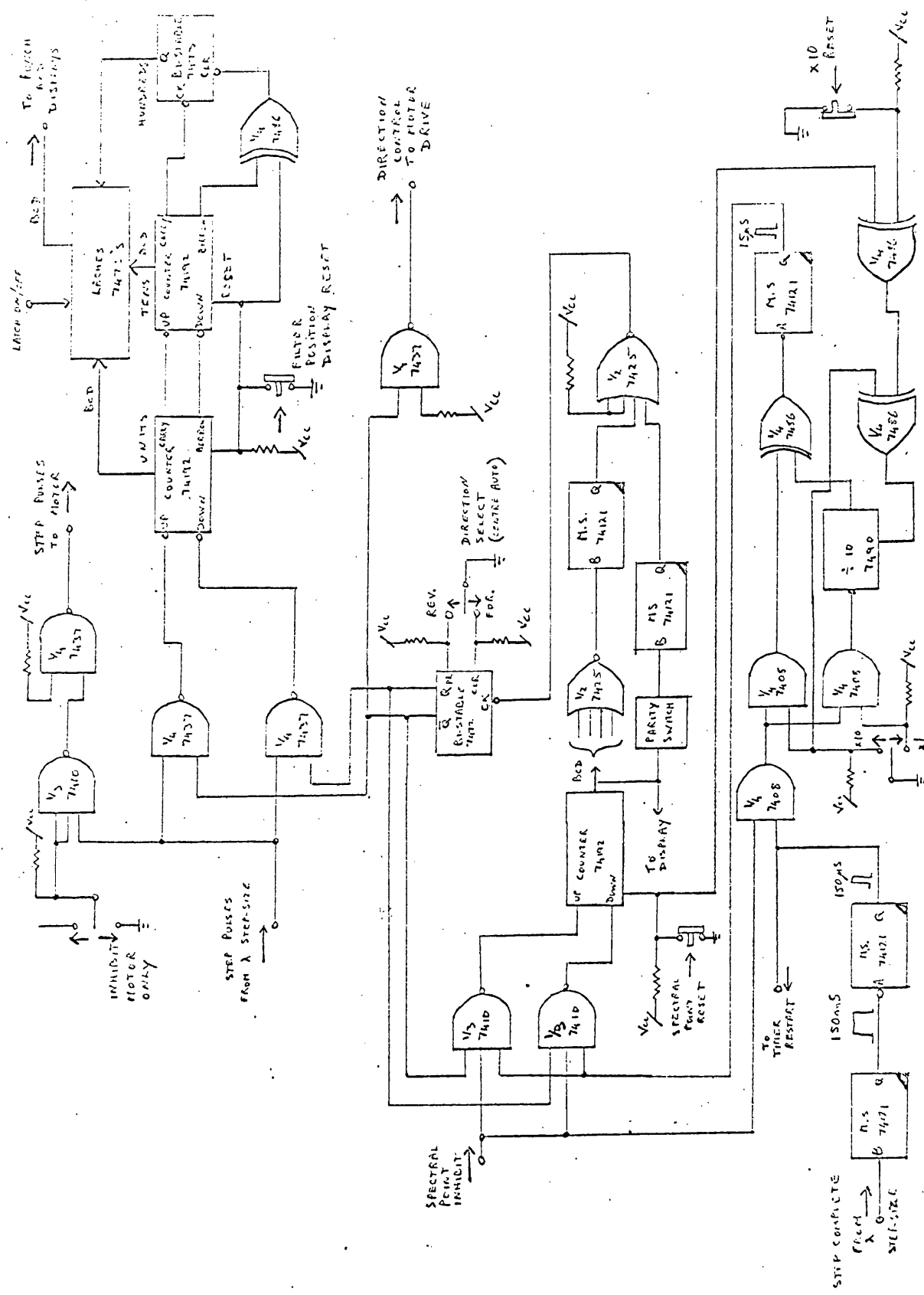
<u>I.C. Type</u>	<u>Function</u>
7400	Quad 2-input <u>nand</u> gate
7402	Quad 2-input <u>nor</u> gate
7404	Hex inverter
7408	Quad 2-input <u>and</u> gate
7410	Triple 3-input <u>nand</u> gate
7420	Dual 4-input <u>nand</u> gate
7425	Dual 4-input <u>nor</u> gate
7432	Quad 2-input <u>or</u> gate
7437	Quad 2-input <u>nand</u> buffer
7472	J-K Flip-flop (divide by 2)
7473	Dual J-K flip-flop
7475	4-bit Latch
7486	Quad 2-input <u>exclusive-or</u> gate
7490	Decade counter
7492	Divide by 6 / Divide by 12
7493	Hexa-decimal counter (4-bit binary counter)
74121	Monostable
74123	Dual monostable
74150	Data selector / multiplexer (1 from 16 lines)
74180	Parity generator
74192	Up/down counter



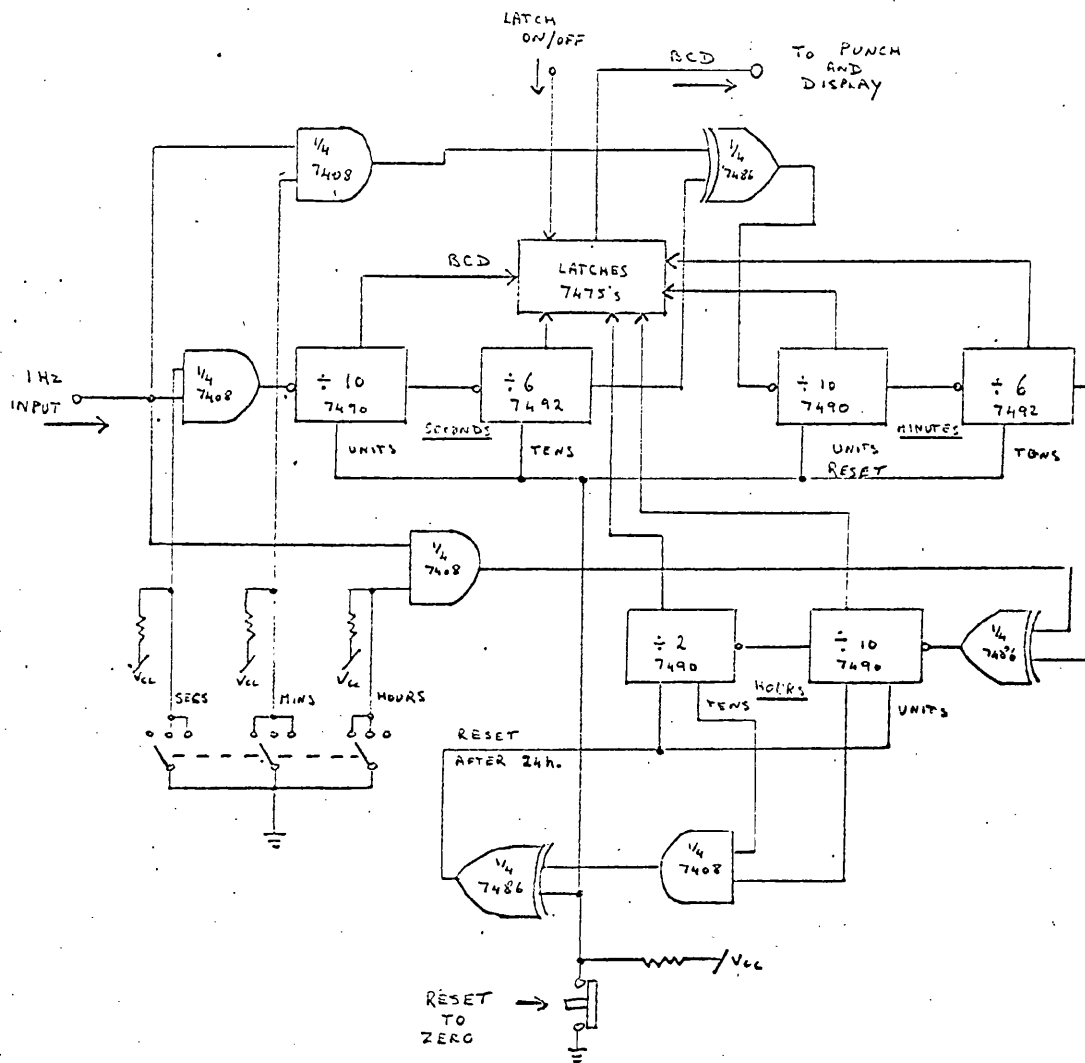


Integration Timer

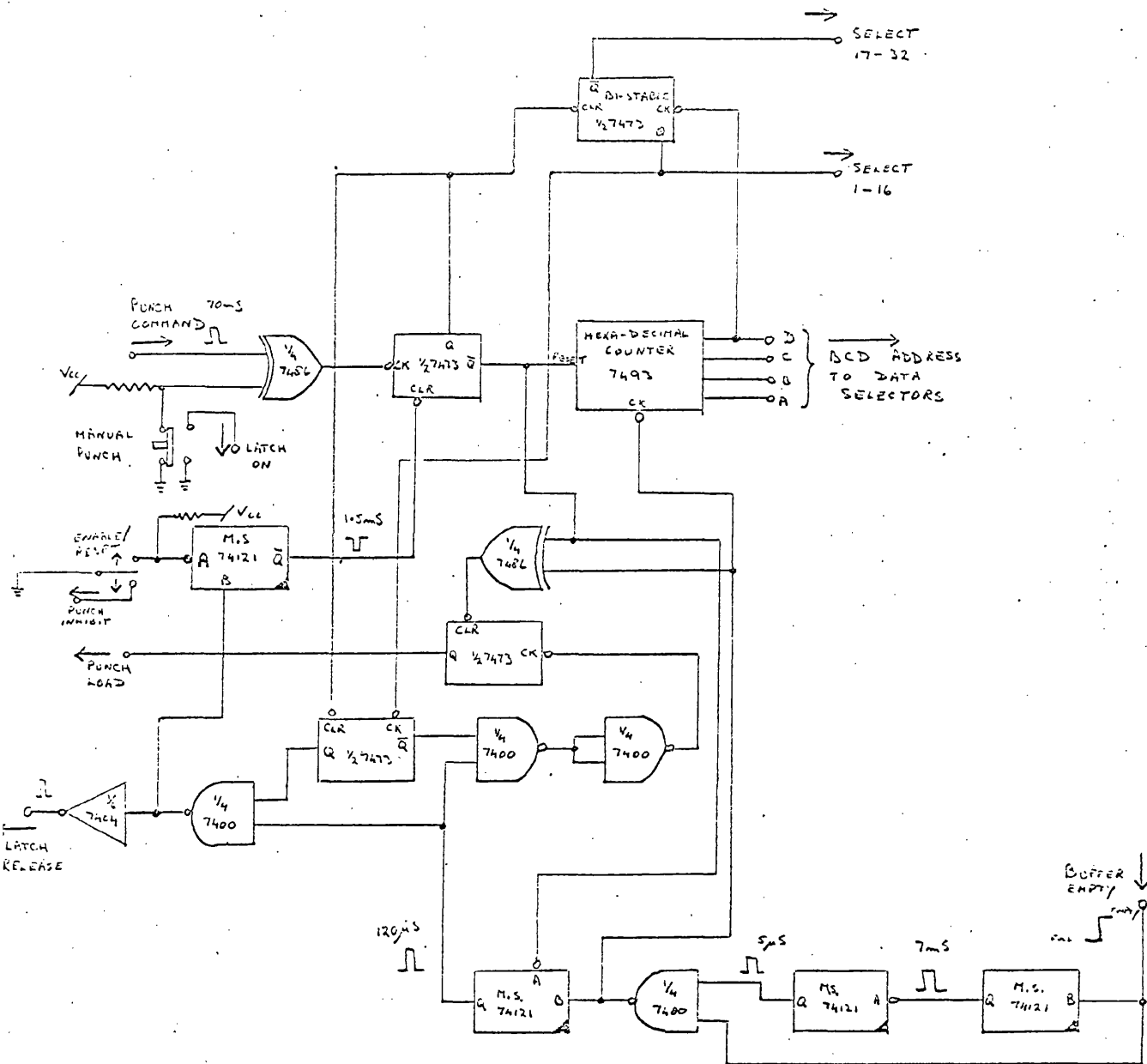




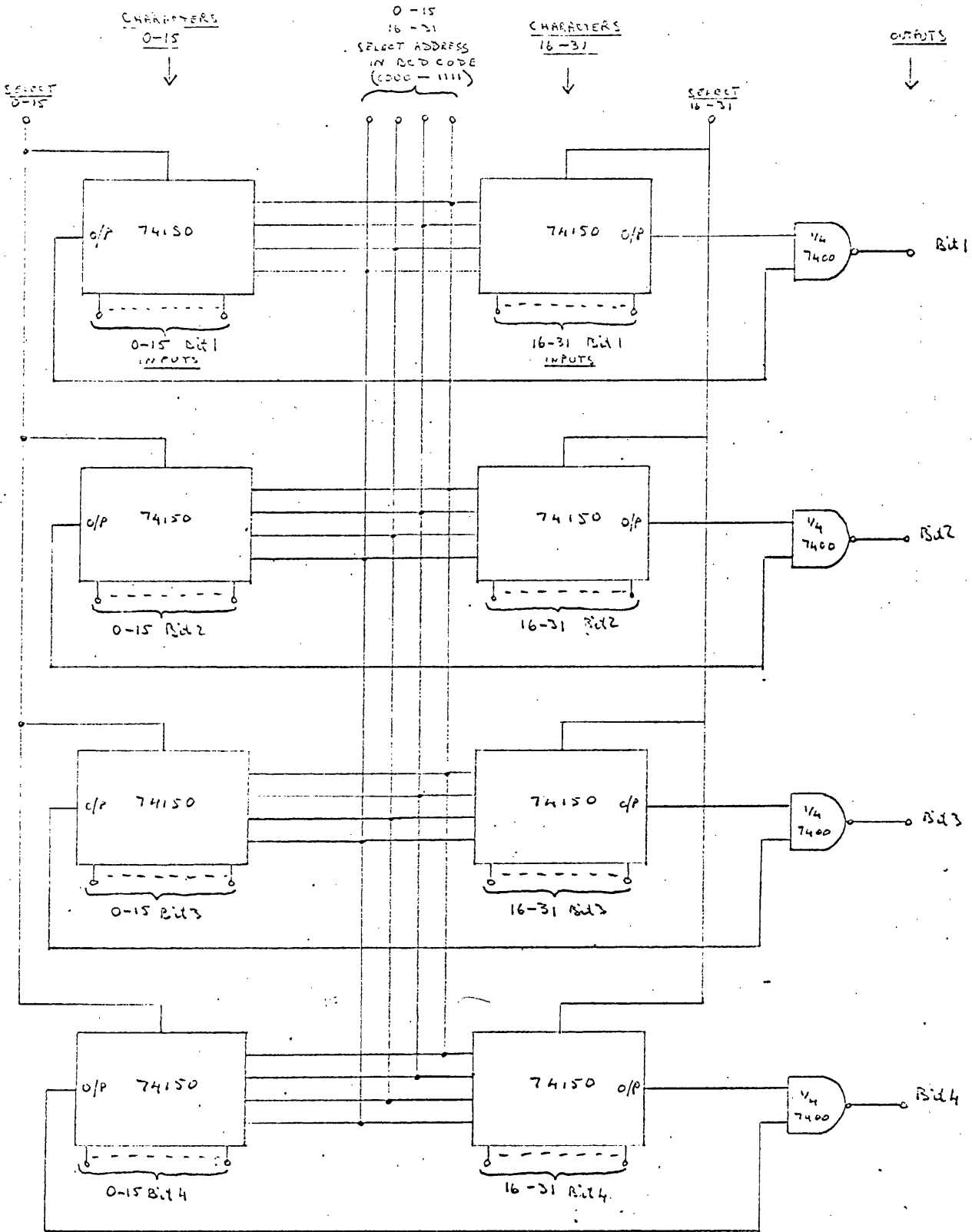
Filter Position Counter/ Spectral Point Control/ Direction Control



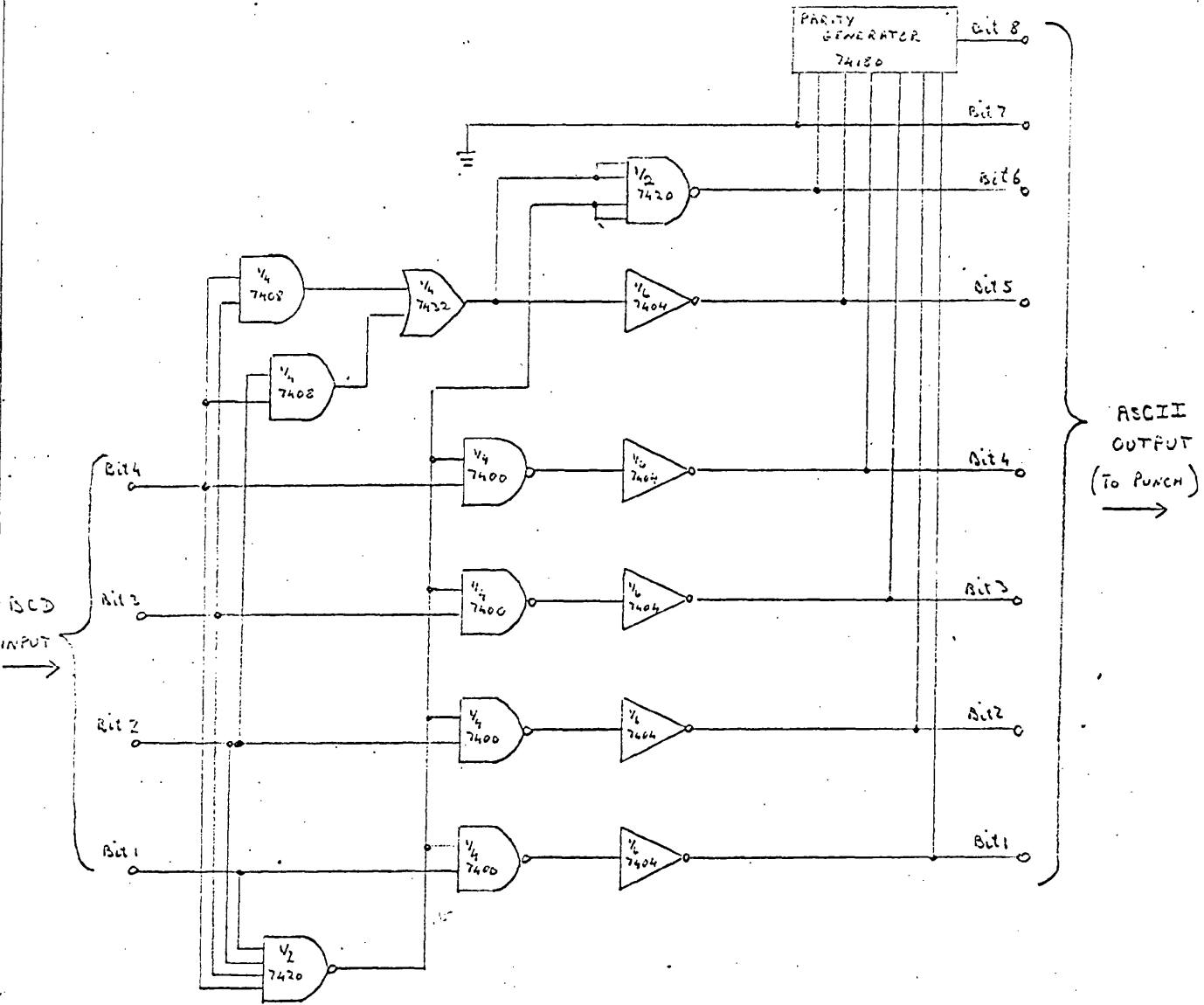
U.T. Clock



Punch Driver



Data Selector



BCD To ASCII Code Converter

APPENDIX II  
DATA FORMAT - FORTRAN PROGRAMME

Data Format:

	<u>code</u>	<u>beam 1</u>	<u>posn.</u>	<u>U.T.</u>	<u>beam 2</u>
Tape I.D. N <sup>o</sup> .	001610	00000	018	013538	00000
Date code	123040	00000	018	013607	00000
Background signal	500330	00022	018	013704	00002
"	500330	00024	018	013707	00002
"	500330	00027	018	013711	00002
"	500330	00023	018	013714	00002
"	500330	00022	018	013717	00002
"	500330	00025	018	013720	00002
"	500330	00025	018	013724	00002
"	500330	00024	018	013727	00001
"	500330	00024	018	013730	00002
"	500330	00026	018	013733	00002
"	500330	00024	018	013737	00003
"	500330	00023	018	013740	00002
Star signal	400330	02277	018	013816	25815
	400330	02268	019	013819	25779
	400330	02266	020	013822	25601
	400330	02249	021	013826	25876
	400330	02241	022	013829	25718
	400330	02258	023	013832	25888
	400330	02231	024	013835	25706
	400330	02207	025	013839	25590
	400330	02198	026	013842	25685
	400330	02189	027	013845	25710
	400330	02147	028	013848	25459
	400330	02181	029	013852	25571
	400330	02166	030	013855	25513
	400330	02149	031	013858	25606
	400330	02096	032	013901	25444
	400330	02123	033	013905	25682
Star signal	400330	02043	034	013908	25754
	400330	02009	035	013911	25457
	400330	02006	036	013914	25626
	400330	01977	037	013918	25689
	400330	01955	038	013921	25512
	400330	01876	039	013924	25443
	400330	01839	040	013927	25749
	400330	01785	041	013930	25524
	400330	01716	042	013934	25644
	400330	01635	043	013937	25449
	400330	01559	044	013940	25458
	400330	01491	045	013943	25508
	400330	01506	046	013947	25544
	400330	01557	047	013950	25492
	400330	01651	048	013953	25469
	400330	01728	049	013956	25658
	400330	01755	050	014000	25689
End of tape	900330	00000	050	014005	00000

↗ wave  
 ↘ star  
 ↖ plate  
 ↗ posn.

## Fortran Programme:

\*FORTRAN

```

C
C
C   AVERAGE DARK.
SUBROUTINE AVDARK(DATA,FLAG,ND,D1,D2)
INTEGER DATA(1000,7)
IF(FLAG.EQ.1.0)PRINT3
3  FORMAT(1H0,40HTOO MUCH DARK // AV. OF LAST 1000 VALS.)
PRINT 1
1  FORMAT(1H0,40X,10(1H*),2X,17HBACKGROUND SIGNAL,2X,10(1H*)/
11H0,9X,4HDATA,14X,5HBEAM1,4X,4HAV 1,4X,5HS.DEV,5X,5HS.ERR,
26X,5HBEAM2,4X,4HAV 2,4X,5HS.DEV,5X,5HS.ERR,6X,4HVALS/1H0)
ZIG1=0.0
ZIG2=0.0
ZIGSQ1=0.0
ZIGSQ2=0.0
SD1=0.0
SD2=0.0
DO 100 I=1,ND
ZIG1=ZIG1+DATA(I,1)
ZIGSQ1=ZIGSQ1+DATA(I,1)**2
ZIG2=ZIG2+DATA(I,6)
ZIGSQ2=ZIGSQ2+DATA(I,6)**2
IF(I.EQ.1) GOTO 101
SD1=SQRT((ZIGSQ1-(ZIG1*ZIG1/I))/(I-1))
SD2=SQRT((ZIGSQ2-(ZIG2*ZIG2/I))/(I-1))
101 SE1=SD1/SQRT(I*1.0)
SE2=SD2/SQRT(I*1.0)
D1=ZIG1/I
D2=ZIG2/I
PRINT2,(DATA(I,J),J=1,6),DATA(I,1),D1,SD1
1,SE1,DATA(I,6),D2,SD2,SE2,I
2  FORMAT(1H ,I5,1X,I2,1X,2(I2,1H.),I2,1X,I5,2(4X,I5,2X,F7.1,2X,
1F8.2,2X,F8.2),4X,I4)
100 CONTINUE
DO 200 I=1,ND
DO 201 J=1,7
201 DATA(I,J)=0
200 CONTINUE
RETURN
END

```

```

C   AVERAGE SIGNAL
*FORTRAN
SUBROUTINE AVSIG(DATA,NS,D1,D2,NORMP,BKSIZE)
INTEGER DATA(1000,7),BKSIZE,FTRPSN,VALS(200),WP
REAL MEANR,MEANB
DIMENSION BLOCK(100,2),FINAL(200,4)
LOGICAL NONE

C
C
DO 1000 NWP=1,10
WP=NWP-1
NONE=.TRUE.
EVALUATE MEAN RATIO FOR NORMALISING PT.
C
C
99  NVAL=0
RNORMP=0.0
DO 100 I=1,NS
IF(DATA(I,7).NE.WP)GOTO 100
NONE=.FALSE.
IF(DATA(I,2).NE.NORMP)GOTO 100
RNORMP=RNORMP+(DATA(I,1)-D1)/(DATA(I,6)-D2)
NVAL=NVAL+1
100 CONTINUE
IF(NONE)GOTO 1000
IF(NVAL.NE.0)GOTO 101
CALL NUNORM(DATA,NORMP,WP)
GOTO 99
101 RN=RNORMP/NVAL
PRINT1,WP,NORMP,RN,NVAL
1  FORMAT(1H0,19HWAVE PLATE AT POSN ,I1/1H0,21HRATIOS NORMD TO POSN ,
I13,10X,23HMEAN RATIO AT THIS PT ,F8.5,5X,I4,5H VALS)
C
C
C   PRINT TABLE HEADS
C   EVALUATE NORMD. RATIOS FOR EACH LAMBDA
C
DO 200 J=1,200
DO 199 JJ=1,4
199 FINAL(J,JJ)=0.0
VALS(J)=0
DO 201 K=1,100
BLOCK(K,1)=0.0
201 BLOCK(K,2)=0.0
NBLOCK=0
NVAL=0
FTRPSN=J-1
SUMR=0.0
SUMSOR=0.0
RB=0.0
SUMB=0.0
SUMSOB=0.0
MEANB=0.0
DEVB=0.0
ERRB=0.0
DO 202 I=1,NS
IF(DATA(I,2).NE.FTRPSN.OR.DATA(I,7).NE.WP)GOTO 202
R=(DATA(I,1)-D1)/(DATA(I,6)-D2)/RN

```

```

SUMR=SUMR+R
SUMSQR=SUMSQR+R**2
DEVR=0.0
NVAL=NVAL+1
IF(NVAL.EQ.1)GOTO 207
DEVR=SQRT(ABS((SUMSQR-(SUMR**2/NVAL))/(NVAL-1)))
207  ERRR=DEVR/SQRT(NVAL*1.0)
     MEANR=SUMR/NVAL
     IF(NVAL.EQ.1)PRINT3,FTRPSN,WP
3    FORMAT(1H0,22(1H*)/1H ,1H*,20X,1H*/1H ,1H*,10H  FILTER ,
110HPOSITION ,1H*/1H ,1H*,20X,1H*/1H ,1H*,7X,I3,10X,1H*/
21H ,1H*,16H  WAVE PLATE AT ,I1,3X,1H*/1H ,22(1H*),45X,5HBLOCK,44X,
35HTOTAL/1H0,9X,4HDATA,9X,6H1-DARK,3X,6H2-DARK,
44X,5HR 1/2,4X,4HVALS,3X,4HMEAN,5X,5HS.DEV,5X,
55HS.ERR,5X,5HR 1/2,4X,4HVALS,3X,4HMEAN,5X,
65HS.DEV,5X,5HS.ERR)
C    NEW HEADING AT EACH LAMBDA
C
C    AV. OF MOVING WINDOW
NBLOCK=NBLOCK+1
IF(NBLOCK.LE.BKSIZE)GOTO 203
DO 204 K=2,BKSIZE
KK=K-1
BLOCK(KK,1)=BLOCK(K,1)
204  BLOCK(KK,2)=BLOCK(K,2)
NBLOCK=BKSIZE
203  BLOCK(NBLOCK,1)=DATA(I,1)-D1
BLOCK(NBLOCK,2)=DATA(I,6)-D2
IF(NBLOCK.LT.BKSIZE)NB=0
IF(NBLOCK.EQ.BKSIZE)NB=NVAL+1-BKSIZE
IF(NB.EQ.0)GOTO 205
SUMB1=0.0
SUMB2=0.0
DO 206 J1=1,BKSIZE
206  SUMB1=SUMB1+BLOCK(J1,1)
SUMB2=SUMB2+BLOCK(J1,2)
RB=SUMB1/(SUMB2*RN)
SUMB=SUMB+RB
SUMSQB=SUMSQB+RB**2
IF(NB.EQ.1)GOTO 208
DEVB=SQRT(ABS((SUMSQB-(SUMB**2/NB))/(NB-1)))
208  ERRB=DEVB/SQRT(NB*1.0)
     MEANB=SUMB/NB
     GOTO 209
205  PRINT 7,DATA(I,1),(DATA(I,L),L=3,6),
1(BLOCK(NBLOCK,L),L=1,2),R,NVAL,MEANR,DEVR,ERRR
7    FORMAT(1H ,I5,1X,2(I2,1H.),I2,1X,I5,2X,F7.1,
12X,F7.1,47X,F8.5,2X,I3,3(2X,F8.5))
     GOTO 202
209  PRINT 4,DATA(I,1),(DATA(I,L),L=3,6),
1(BLOCK(NBLOCK,L),L=1,2),RB,NB,MEANB,DEVB,
2ERRB,R,NVAL,MEANR,DEVR,ERRR
C
4    FORMAT(1H ,I5,1X,2(I2,1H.),I2,1X,I5,2X,F7.1,
12X,F7.1,2(2X,F8.5,2X,I3,3(2X,F8.5)))
C
202  CONTINUE

```

```

IF(NVAL.EQ.0)GOTO 200
FINAL(J,1)=MEANB
FINAL(J,2)=DEVB
FINAL(J,3)=MEANR
FINAL(J,4)=DEV R
VALS(J)=NVAL
200 CONTINUE
C
C
C
PRINT5,WP
5 FORMAT(1H0/140,25HFINAL VALUES AT EACH POSN,
16X,19H WAVE PLATE AT POSN ,I1/1H0,17X,5HBLOCK,31X,5HTOTAL/1H0,
22HFP,7X,1HR,7X,5HS.DEV,5X,5HS.ERR,4X,4HVALS,6X,1HR,7X,
35HS.DEV,5X,5HS.ERR,4X,4HVALS)
DO 400 J=1,200
PSN=J-1
IF(VALS(J).EQ.0)GOTO 400
NB=VALS(J)+1-BKSIZE
ERR2=FINAL(J,4)/SQRT(VALS(J)*1.0)
IF(NB.LE.0)GOTO 401
ERR1=FINAL(J,2)/SQRT(NB*1.0)
PRINT6,PSN,FINAL(J,1),FINAL(J,2),ERR1,NB,FINAL(J,3),
1FINAL(J,4),ERR2,VALS(J)
6 FORMAT(1H ,I3,2(3X,3(F8.5,2X)),I4))
GOTO 400
401 PRINT8,PSN,FINAL(J,3),FINAL(J,4),ERR2,VALS(J)
8 FORMAT(1H ,I3,40X,3(F8.5,2X),I4)
400 CONTINUE
C
C
C
1000 CONTINUE
DO 300 M=1,NS
DO 301 N=1,7
301 DATA(M,N)=0
300 CONTINUE
C
RETURN
END

```

C TOO MUCH DARK

\*FORTRAN

SUBROUTINE XSDARK(DATA,ND,FLAG)

INTEGER DATA(1000,7)

ND=ND-1

DO 1 LL=2,ND

L=LL-1

DO 2 J=1,6

2 DATA(L,J)=DATA(LL,J)

1 CONTINUE

FLAG=1.0

RETURN

END

C

C

C TOO MUCH DATA

\*FORTRAN

SUBROUTINE XSDATA(DATA,NS,D1,D2,NORMP,BKSIZE)

INTEGER DATA(1000,7)

NS=NS-1

CALL AVSIG(DATA,NS,D1,D2,NORMP,BKSIZE)

NS=1

PRINT3

3 FORMAT(1H0,30HTOO MUCH DATA / MORE TO FOLLOW)

RETURN

END

C

C

C SELECT NEW NORM. POINT

\*FORTRAN

SUBROUTINE NUNORM(DATA,NP,WP)

INTEGER DATA(1000,7),WP

PRINT1,NP,WP

1 FORMAT(1H0,17HND DATA AT POSN ,I3,

111HWAVE PLATE ,I1/1H ,

227HNORM PT TAKEN AS FIRST POSN,

320H FOR THIS WAVE PLATE)

I=1

2 IF(DATA(I,7).EQ.WP)GOTO 3

I=I+1

GOTO 2

3 NP=DATA(I,2)

RETURN

END

```

C     MAIN ROUTINE
FORTRAN
      INTEGER BKSIZE,DATA(1000,7)
      DIMENSION LINE(12),STAR(9)
      LOGICAL NUDARK,NUSIG

C
      READ1,NTAPES
      DO 1000 NDONE=1,NTAPES

C
      READ1,NORMP,BKSIZE
1     FORMAT(80Z)
      NUDARK=.TRUE.
      NUSIG=.TRUE.
      DARK1=0.0
      DARK2=0.0
      XSD=0.0
      READ2,(STAR(I),I=1,9)
2     FORMAT(9A8)
      PRINT 50,(STAR(I),I=1,9)
50    FORMAT(1H1,9A8)

C
C     READ 1 LINE OF DATA
300   READ3,(LINE(I),I=1,12)
3     FORMAT(6I1,16,14,13,2I2,17)
      JUMP=LINE(1)+1
      GOTO(100,200,300,300,400,500,300,300,300,900),JUMP

C
C     TAPE I.D. CODE
100   PRINT51,(LINE(I),I=2,5)
51    FORMAT(1H,6HTAPE,4I1)
      GOTO 300

C
C     DATE CODE
200   PRINT52,(LINE(I),I=2,5)
52    FORMAT(1H,6HDATE,2(2I1,1H/),2H**)
      GOTO 300

C
C     DARK SIGNAL
500   IF(NUDARK)GOTO 502
      NDARK=NDARK+1
      IF(NDARK.GT.1000)CALL XSDARK(DATA,NDARK,XSD)
      DO 501 K=1,6
      KK=K+6
501   DATA(NDARK,K)=LINE(KK)
      GOTO 300

C
C     RESET DATA FOR NEW DARK AND AVERAGE PREVIOUS SIGNAL
502   IF(.NOT.NUSIG)GOTO 503
C     FIRST DARK NO PREVIOUS SIGNAL
      NDARK=0
      NUDARK=.FALSE.
      GOTO 500

C
C     AVERAGE PRECEEDING SIGNAL
503   CALL AVSIG(DATA,NSIG,DARK1,DARK2,NORMP,BKSIZE)
      NUDARK=.FALSE.
      NUSIG=.TRUE.
      NDARK=0
      GOTO 500

```

```
C
C
C   ACCUMULATE SIGNAL
400  IF(NUSIG)GOTO 402
      NSIG=NSIG+1
      IF(NSIG.GT.1000)CALL XSDATA(DATA,NSIG,DARK1,DARK2,NORMP,BKSIZE)
      DO 401 K=1,6
      KK=K+6
401  DATA(NSIG,K)=LINE(KK)
      DATA(NSIG,7)=LINE(2)
      GOTO 300

C
C
C   NEW SIGNAL      AV. ANY PREC. DARK
402  IF(.NOT.NUDARK)GOTO 403
C    NO PREVIOUS DARK
      DARK1=0.0
      DARK2=0.0
      NSIG=0
      NUSIG=.FALSE.
      GOTO 400

C
C   AV. PREC. DARK
403  CALL AVDARK(DATA,XSD,NDARK,DARK1,DARK2)
      NUDARK=.TRUE.
      NUSIG=.FALSE.
      NSIG=0
      GOTO 400

C
C   END OF DATA
900  CALL AVSIG(DATA,NSIG,DARK1,DARK2,NORMP,BKSIZE)
1000 CONTINUE
      CALL EXIT
      END
```

REFERENCES

- Babcock, H. W. : 1958, Ap. J. Suppl. 3, 141 (No. 30).
- Bahng, J. D. R. : 1971a, P.A.S.P. 83, 327.
- Bahng, J. D. R. : 1971b, Ap. J. Letters 167, L75.
- Bahng, J. D. R. : 1975a, Ap. J. 200, 128.
- Bahng, J. D. R. : 1975b, M.N.R.A.S. 170, 611.
- Barbieri, C., Cosmovici, C. B., Michel, K. W., Nishimura, T., and Roche, A. E.  
: 1974, Icarus 23, 568.
- Beer, A. : 1956, Vistas in Astronomy 2, Pergamon Press,  
London.
- Berg, R. A. : 1967, Publ. Leander McCormick Obs. 15,  
part IV.
- Bonsack, W. K., and Markowitz, A. H.  
: 1967, P.A.S.P. 79, 235.
- Breger, M. : 1969, Astrophys. Letters 3, 67.
- Breger, M. : 1974, Ap. J. 192, 71.
- Brucato, R. J. : 1971, M.N.R.A.S. 153, 435.
- Capps, R. W., Coyne, G. V., and Dyck, H. M.  
: 1973, Ap. J. 184, 173.
- Clarke, D., and Grainger, J. F.  
: 1971, Polarized Light and Optical Measurement,  
Pergamon Press, Oxford.
- Clarke, D., and McLean, I. S.  
: 1974a, Planets, Stars and Nebulae Studied with  
Photopolarimetry, ed. T. Gehrels, Univer-  
sity of Arizona Press, p. 752.
- Clarke, D., and McLean, I. S.  
: 1974b, M.N.R.A.S. 167, 27P.
- Clarke, D., and McLean, I. S.  
: 1975, M.N.R.A.S., in press.
- Clarke, D., McLean, I. S., and Wyllie, T. H. A.  
: 1975, Astron. Astrophys. 43, 215.
- Code, A. D., and Liller, W. C.  
: 1962, Stars and Stellar Systems 2, ed. W. A.  
Hiltner, University of Chicago Press.
- Conti, P., and Smith, L. F.  
: 1972, Ap. J. 172, 623.

- Coyne, G. V. : 1974, M.N.R.A.S. 169, 7P.
- Coyne, G. V., and McLean, I. S. : 1975, Astron. J. 80, 702.
- Crawford, D. L. : 1958, Ap. J. 128, 185.
- Crawford, D. L. : 1960, Ap. J. 132, 66.
- Crawford, D. L., and Mander, J. : 1966, Astron. J. 71, 114.
- Durham, G. E. : 1943, Ap. J. 98, 504.
- Eather, R. H., and Reasoner, D. L. : 1969, Applied Optics 8, 227.
- Faraggiana, R. : 1969, Astron. Astrophys. 2, 162.
- Faraggiana, R. : 1971, Astrophys. Letters 8, 45.
- Ganesh, K. S., and Bappu, M. K. V. : 1967, Kodaikanal Obs. Bull. 16, No. 183.
- Geuverink, H. G. : 1970, Astron. Astrophys. 5, 341.
- Golay, M. : 1974, Introduction to Astronomical Photometry, D. Reidel Publ. Co., Dordrecht.
- Gray, D. F., and Marlborough, J. M. : 1974, Ap. J. Suppl. 27, 121.
- Griffin, R. F. : 1968, A Photometric Atlas of the Spectrum of Arcturus, Cambridge Philosophical Society.
- Griffin, R. F. : 1970, The Observatory 90, 46.
- Gulliver, A. F., and Winzer, J. E. : 1973, Ap. J. 183, 701.
- Hack, M., and Struve, O. : 1970, Stellar Spectroscopy - Peculiar Stars, Osservatorio Astronomico di Trieste, p. 55.
- Hardie, R. H. : 1962, Stars and Stellar Systems 2, ed. W. A. Hiltner, University of Chicago Press.
- Hayes, D. P. : 1975, P.A.S.P. 87, 609.
- Hayes, D. P., and Illing, R. M. E. : 1974, Astron. J. 79, 1430.
- Hoffleit, D. : 1964, Catalogue of Bright Stars, Yale University, New Haven.
- Honeycutt, R. K. : 1966, P.A.S.P. 78, 153.
- Hubert, H. : 1973, Astron. Astrophys. Suppl. 9, 133.
- Hutchings, J. B. : 1967, The Observatory 87, 289.

- Hutchings, J. B. : 1968a, M.N.R.A.S. 141, 329.
- Hutchings, J. B. : 1968b, Non-periodic Phenomena in Variable Stars,  
IAU Colloquium of Commissions 27 and 42,  
Budapest (1968), p. 191.
- Hutchings, J. B. : 1968c, M.N.R.A.S. 141, 219.
- Hutchings, J. B. : 1970a, M.N.R.A.S. 150, 55.
- Hutchings, J. B. : 1970b, M.N.R.A.S. 147, 367.
- Hutchings, J. B. : 1971, M.N.R.A.S. 152, 109.
- Hutchings, J. B. : 1973, Contributions of the Dominion Astrophys.  
Obs., No. 180.
- Hutchings, J. B., Auman, J. R., Gower, A. C., and Walker, G. A. H.  
: 1971a, Ap. J. Letters 170, L73.
- Hutchings, J. B., Walker, G. A. H., and Auman, J. R.  
: 1971b, IAU Colloquium 15, Combined Colloquium  
of Commissions 27 and 42, Bamberg (1971),  
p. 279.
- Jacquinot, P. : 1954, J. Opt. Soc. Amer. 44, 761.
- Jaschek, C., Ferrer, L., and Jaschek, M.  
: 1971, Observatorio Astronomico De La Universidad  
De La Plata, Serie Astronomica XXXVII.
- Jaschek, M., and Jaschek, C.  
: 1973, P.A.S.P. 85, 127.
- Jeffers, S., Weller, W., and Sanyal, A.  
: 1973, Nature Phys. Sci. 243, 109.
- Johnson, H. L. : 1966, Ann. Rev. Astron. Astrophys. 4, 193.
- Kitchin, C. R. : 1970, M.N.R.A.S. 150, 455.
- Lacoarret, M. : 1965, Ann. Astrophys. 28, 321.
- Ledoux, P., and Renson, P. : 1966, Ann. Rev. Astron. Astrophys. 4, 293.
- Limber, D. N. : 1965, Ap. J. 140, 1391.
- Limber, D. N. : 1967, Ap. J. 148, 141.
- Limber, D. N. : 1969, Ap. J. 157, 785.
- Limber, D. N., and Marlborough, J. M.  
: 1968, Ap. J. 152, 181.
- Lindgren, H., Lundström, I., and Stenholm, B.  
: 1975, Astron. Astrophys. 44, 219.
- Maitzen, H. M., and Moffat, A. F. J.  
: 1972, Astron. Astrophys. 16, 385.

- Marlborough, J. M. : 1969, Ap. J. 156, 135.
- Marlborough, J. M. : 1970, Ap. J. 159, 575.
- Meaburn, J. : 1970, Astrophysics and Space Science 9, 206.
- Merril, P. W., and Burwell, C. G.  
: 1933, Ap. J. 78, 87.
- Merril, P. W., and Burwell, C. G.  
: 1943, Ap. J. 98, 153.
- Merril, P. W., and Burwell, C. G.  
: 1949, Ap. J. 110, 387.
- Merril, P. W., and Burwell, C. G.  
: 1950, Ap. J. 112, 72.
- Minnaert, M. G. J., Mulders, G. F. W., and Houtgast, J.  
: 1940, Photometric Atlas of the Solar Spectrum,  
Utrecht.
- McLaughlin, D. B. : 1957, Proc. Liège Symposium on Emission Line  
Stars, p. 231.
- McLean, I. S., and Clarke, D.  
: 1975, IAU Symposium No. 70, to be published.
- de Monteagudo, V. N., and Sahade, J.  
: 1970, The Observatory 90, 198.
- Morgan, W. W. : 1933, Ap. J. 77, 77.
- Niemela, V. : 1973, Wolf-Rayet and High Temperature Stars,  
IAU Symposium No. 49, D. Reidel Publ. Co.,  
Dordrecht, p. 222.
- Percy, J. R. : 1973, Astron. Astrophys. 22, 381.
- Perrine, C. D. : 1918, Ap. J. 47, 52.
- Peters, G. J. : 1972, P.A.S.P. 84, 334.
- Poekert, R. : 1975, Ap. J. 196, 777.
- Preston, G. W. : 1971, P.A.S.P. 83, 571.
- Rakos, K. D. : 1963, Lowell Obs. Bull. 6, 91.
- Rosendhal, J. D. : 1973, Ap. J. 182, 523.
- Sanyal, A., Weller, W., and Jeffers, S.  
: 1974, Ap. J. Letters 187, L31.
- Serkowski, K. : 1970, Ap. J. 160, 1083.
- Stępień, K., and Romaniuk, M.  
: 1973, Acta Astron. 23, 257.
- Struve, O. : 1931, Ap. J. 73, 94.

- Underhill, A. B. : 1960a, Stars and Stellar Systems 10,  
ed. J. L. Greenstein, University of Chicago  
Press.
- Underhill, A. B. : 1960b, Publ. Dominion Astrophys. Obs. 11, 353.
- Underhill, A. B. : 1966, The Early Type Stars, D. Reidel Publ.  
Co., Dordrecht.
- Underhill, A. B., and Geuverink, H. G.  
: 1969, Mass Loss from Stars, ed. M. Hack,  
D. Reidel Publ. Co., Dordrecht.
- de Vaucouleurs, G. : 1967, IAU Symposium No. 30.
- Wackerling, L. R. : 1970, Memoirs R.A.S. 73, part 3.
- Walker, G. A. H., Auman, J. R., Buchholz, V., Goldberg, B., and Isherwood, B.  
: 1971, Automation in Optical Astrophysics, IAU  
Colloquium No. 11, Publ. Roy. Obs. Edinburgh  
8, No. 11
- Williams, W. E., Frantz, R. L., and Breger, M.  
: 1974, Astron. Astrophys. 35, 381.
- Wood, H. J. : 1964, P.A.S.P. 76, 158.
- Wood, H. J. : 1965, Publ. Leander McCormick Obs. 15, Part II.
- Wood, H. J. : 1967, Magnetic and Related Stars, ed. R. C.  
Cameron, Mono Book Corp., Baltimore, p. 485.
- Wood, H. J. : 1968, Ap. J. 152, 117.
- Wood, H. J., and Hollis, J. M.  
: 1971, Astron. Astrophys. 12, 468.
- Wright, K. O. : 1962, Stars and Stellar Systems 2, ed. W. A.  
Hiltner, University of Chicago Press.

OBSERVATIONS OF  
LINE PROFILE VARIATIONS  
IN EARLY-TYPE STARS

Thesis  
submitted to the  
University of Glasgow  
for the degree of  
Ph.D.  
by  
T. H. ALAN WYLLIE

Department of Astronomy,  
University of Glasgow.

March 1976.

S U M M A R Y

During the past few years the literature has contained several reports concerning rapid line profile variations of some Be, Ap, Wolf-Rayet and other early-type stars. In some cases the time-scales of the variations have been reported to be as short as minutes or even seconds and clearly, if such variations are intrinsic to the stars, the processes giving rise to them must be accounted for by any future theories regarding the stellar structures and atmospheres.

However, some of the earlier observations are open to criticism and the reported variations may, in some cases, be the result of various instrumental errors which have not been fully appreciated. The work reported in this thesis was undertaken in order to investigate further the variations reported for the  $H\beta$  line in some of these stars.

A considerable amount of the work has been concerned with developing a novel stellar line profile scanner. By tilting a narrow band ( $\sim 2 \text{ \AA}$  half-width) interference filter in a collimated beam, a moderate resolution wavelength-scanning monochromator is achieved. The tilt-scanning technique has been explored in some depth and it is believed that this work is the first intensive application of the technique to the measurement of stellar line profiles at this wavelength resolution.

The indications are that the scanning range of one filter may be of the order of  $200 \text{ \AA}$ . Although there is a degree of distortion of the recorded profiles caused by the filter's transmittance decreasing and its pass-band broadening with tilt, the application for this study was concerned only with detecting line profile variations rather than making absolute measurements. However, over the smaller wavelength range normally scanned ( $\sim 30 \text{ \AA}$ ), the distortions of the recorded line profiles are sufficiently small as to be neglected.

More important, however, are the changes of the filter passband, and hence of the recorded profiles, brought about by variations in the angular size and movement of the stellar seeing disc in the telescope's focal plane due to unsteady seeing conditions and telescope tracking errors. Both of these topics have been considered as sources of photometric noise and it is felt that some of the variations of the Be stars reported previously by others may be the result of similar effects, especially since the extent of the noise becomes greater as the spectral gradients increase.

A special purpose double-beam photometer has been designed and built. One beam passes through a narrow band scanning filter while the other beam passes through a broader band ( $\sim 50 \text{ \AA}$ ) fixed interference filter whose passband is centred on the continuum adjacent to the scanned line. This second beam acts as a reference and after subtracting sky and dark contributions, the ratio of the signal in the two beams is largely free of atmospheric noise. The scanning filter is moved automatically along a series of discrete wavelength points by a stepping motor and both the step-size and the number of spectral points can be set on the electronic control. Pulse counting photometry is employed; the signals in both beams are recorded simultaneously and, after preset integration times, are punched on paper tape together with a record of the filter position and the Universal Time. Wavelength/tilt calibration is performed by piping light from laboratory lamps into the photometer by a fibre optic tube.

Observationally, the main emphasis of the work has been on measurements of the  $H\beta$  line in Be stars, several of which have been found to show night-to-night profile variations. Although variations of this type have been reported previously for some of the stars observed (e.g.  $\gamma$  Cas,  $\zeta$  Tau), it is believed that there are no previous reports of night-to-night variations for several of the others ( $\alpha$  Ara,  $\delta$  Cen,  $\mu$  Cen,  $\zeta^1$  Sco). No evidence of very rapid variability was found.

Other observations were made of the Ap star  $\epsilon$  UMa but these showed no signs of any of the variations reported earlier. The Wolf-Rayet star and spectroscopic binary  $\gamma^2$  Vel was also observed and in addition to the known variations of the H $\beta$  line with phase, night-to-night variations were also indicated.

The main advantages of the tilting-filter scanner over other line scanners with comparable resolution are its simplicity of design and its small physical size which, together with a high overall transmittance of the optical components, allows it to be used with small telescopes. Although the spectral purity of the recorded profiles is not as good as can be achieved with more sophisticated scanners, the technique clearly has a useful application for the detection of line profile variations.